Titre: Title:	Seismic performance of reinforced concrete bridge piers under simulted winter conditions
Auteur: Author:	Michael Holleran
Date:	1998
Type:	Mémoire ou thèse / Dissertation or Thesis
Référence: Citation:	Holleran, M. (1998). Seismic performance of reinforced concrete bridge piers under simulted winter conditions [Mémoire de maîtrise, École Polytechnique de Montréal]. PolyPublie. https://publications.polymtl.ca/6900/

UNIVERSITÉ DE MONTRÉAL

SEISMIC PERFORMANCE OF REINFORCED CONCRETE BRIDGE PIERS UNDER SIMULTED WINTER CONDITIONS

MICHAEL HOLLERAN
DÉPARTEMENT DES GÉNIES CIVIL GÉOLOGIQUE ET DES MINES
ÉCOLE POLYTECHNIQUE

MÉMOIRE PRÉSENTÉ EN VUE DE L'OBTENTION
DU DIPLÔME DE MAÎTRISE ÈS SCIENCES APPLIQUÉES
(GÉNIE CIVIL)
AOÛT 1998

UNIVERSITÉ DE MONTRÉAL

ÉCOLE POLYTECHNIQUE DE MONTRÉAL

Cette thèse intitulée :

SEISMIC PERFORMANCE OF REINFORCED CONCRETE BRIDGE PIERS UNDER SIMULTED WINTER CONDITIONS

Présentée par : HOLLERAN Michael

En vue l'obtension du diplôme de : Maîtrise ÈS Sciences Appliquées

a été dûment acceptée par le jury d'examen constitué de :

M. TREMBLAY Robert, Ph.D., président

M. FILIATRAULT André, Ph.D., membre et directeur de recherche

M. MASSICOTTE Bruno, Ph.D., membre et codirecteur de recherche

M. BISCHOFF Peter, Ph.D., membre

ACKNOWLEDGMENTS

I would like to sincerely thank my main research supervisor, Dr. André Filiatrault for his guidance, patience and expertise throughout this masters thesis. His support was immeasurable throughout the duration of this project and in accomplishing my master's degree. I would also like to express my appreciation to my co-supervisor, Dr. Massicotte, for his knowledge and advice during this project.

Acknowledgment is extended to the following organizations for their technical and financial assistance in this project : the Quebec Ministry of Transportation, the National Science and Engineering Research Council (NSERC) of Canada and the 'Fonds de formation des chercheurs et d'aide à la recherche (FCAR)' of Quebec.

Je remercie M. Gérard Degrange, directeur du laboratoire de structure de l'École Polytechnique de Montréal, les auxiliaires de recherche de l'été 1997, ainsi que les techniciens du laboratoire ; Denis Fortier et Patrice Bélanger, pour l'aide qu'ils m'ont fournie durant la partie expérimentale de ma maîtrise.

RÉSUMÉ

Les ponts en béton armé localisés dans des zones sismiques actives peuvent subir des tremblements de terre en hiver. Si un pilier est soumis à un chargement sismique à basses températures, les propriétés mécaniques de l'acier d'armature et du béton seront affectées par l'effet combiné du taux de chargement élevé et des basses températures. Ces changements des propriétés mécaniques peuvent altérer le comportement sismique de l'ouvrage.

Très peu de travaux de recherche ont été réalisés afin d'évaluer l'effet combiné des basses températures et des taux de déformation élevés sur le comportement mécanique du béton et de l'acier d'armature. Pour combler cette lacune, un total de 24 essais de traction furent réalisés sur des éprouvettes d'acier d'armature pour différentes combinaisons de basses températures et de taux de déformation. La plage de taux de déformation considérée est typique d'événements sismiques ($80x10^{-6}$/s, $5x10^{-3}$/s, 0.02/s et 0.1/s). La plage de température considérée est représentative des conditions hivernales et estivales au Québec (+20°C, -20°C, and -40°C). Les résultats des essais de traction montrent que l'effet combiné des basses températures et des taux de déformation élevés cause une augmentation de la limite élastique et de la contrainte ultime de l'acier d'armature. La déformation ultime ainsi que le module d'élasticité de l'acier d'armature, cependant, ne sont pas affectés de façon significative.

Un programme expérimental sur des cylindres en béton, incluant 24 essais de compression avec les mêmes combinaisons de taux de déformation et de températures que lors des essais de traction sur l'acier d'armature fut également réalisé. Les résultats des essais de compression montrent que l'effet combiné des basses températures et des taux de déformation élevés cause une grande augmentation de la résistance en compres-

sion et du module d'élasticité du béton. La déformation unitaire à laquelle se produit la résistance en compression ultime, cependant, n'est pas affectée de façon significative.

Quatre échantillons à échelle 1/3 d'un pilier de pont de la région de Montréal furent soumis à des essais sismiques sur le simulateur sismique de l'École Polytechnique. Le premier spécimen fut soumis à un essai quasi-statique normalisé. Les quatre autres échantillons furent soumis à des essais dynamiques à des températures de +20°C, -20°C et -40°C.

Une rupture prématurée du spécimen fut observée lors de l'essai quasi-statique pour un facteur de ductilité (μ) entre 1 et 2. Le mécanisme de rupture fut caractérisé par un glissement entre les barres longitudinales du pilier et les barres d'ancrage de la semelle. Ce glissement fut accompagné par une fissuration verticale et un écaillage du béton à la base du pilier.

Un mode de rupture par glissement fut également observé lors des essais dynamiques. La température n'a pas semblé influencer sensiblement le comportement de l'échantillon.

Finalement, les prédictions d'un modèle dynamique du pilier furent comparées aux résultats expérimentaux obtenus des essais dynamiques.

ABSTRACT

Reinforced concrete bridges located in seismically active regions can experience earthquakes during the winter season. If a bridge pier is subjected to seismic loading at low temperatures, the material behaviour of the reinforcing steel and the concrete are affected due to the combined effect of high strain rates and low temperatures and possibly, alter the seismic behaviour of these structures.

Knowledge on the combined effects of high strain rates and low temperatures on the behaviour of reinforcing steel and concrete are rather limited. Previous research focused on observed strength increases of either strain rate or temperature, with little or no attention given to the deformational behaviour of the combined effects of these variables. Therefore, monotonic tensile tests on reinforcing steel bars and compressive tests on concrete cylinders were performed under various combination of earthquake-type strain rates (quasi-static to 0.1/s) and temperature typical of Eastern North America (+20°C to -40°C), in order to evaluate the combined effects of these two parameters on the stress-strain curves of these materials. The results of the tensile tests indicate that the yield strength increases moderately as both the strain rates increase and the temperature decreases. The results of the compressive tests indicate that the compressive strength and the Young's modulus of the concrete significantly increase as the strain rate increases and the temperature decreases. From the test results, regression formulas are proposed to capture these behaviours for structural analyses.

Four 1/3 scaled concrete bridge piers were modelled from a typical bridge pier constructed in the 1960's (prior to recent seismic provisions) located in Eastern North

America. These specimens were experimentally tested to examine their seismic performance under simulated conditions.

A quasi-static test was performed on a reinforced concrete bridge pier specimen to obtain information concerning the resistance, rigidity and ductility of the specimen to help predict the structural behaviour of the prototype. The results of this test indicate that the governing failure mode is characterised by a slip between the longitudinal bars of the pier and the dowel bars at the foundation level due to the lack of confinement over the spliced region. The specimen suffered bond failure at a level less than the nominal flexural strength causing degrading pinched hysteric behaviour with very limited energy dissipation.

Three different ground motions (Adak, Atkinson and Morgan Hill) were used to perform seismic tests on the reinforced concrete bridge piers. General observations were made on the behaviour and the performance of the structures under seismic loadings and low temperatures. Results showed the governing mode of failure was due to slipping of the longitudinal bars with respect to the starter bars of the foundation. Testing also indicated that temperature had little effect on the response of the structure.

Numerical modelling was performed with the use of the RUAUMOKO computer program to validate the response of the structure. Comparisons between the measured values and the simulated computer model indicated that a realistic model could be obtained for the low intensity ground motions. According to the experimental results and the non-linear dynamic analysis results, it was demonstrated for the pier considered that the seismic design of reinforced concrete bridge piers in Eastern North America is adequate under seismic loading for the parameters which were studied.

CONDENSÉ EN FRANÇAIS

SOMMAIRE

Au Québec, un séisme peut se produire en hiver. Dans un tel cas, le béton et l'acier d'armature des piliers de ponts en béton armé seraient soumis à un effet couplé des basses températures et des taux de déformation élevés. Cette combinaison pourrait altérer le comportement sismique de ces ouvrages.

La première partie de ce rapport présente les résultats d'essais de traction sur des éprouvettes d'acier d'armature et des essais de compression sur des cylindres de béton. Ces essais furent réalisés pour différentes combinaisons de températures (+20°C à –40°C) et de taux de déformation typiques d'événements sismiques (quasi-statique à 0.1/s).

La deuxième partie de ce rapport présente les résultats d'un essai quasi-statique sur un modèle à grande échelle d'un pilier de pont typique du Québec.

Finalement, la troisième partie de ce rapport présente les résultats d'essais sismiques réalisés sur une série de modèles identiques à celui de l'essai quasi-statique. Ces essais furent réalisés à l'aide du simulateur sismique de l'École Polytechnique.

1. INTRODUCTION

Très peu de travaux de recherche ont été réalisés afin d'évaluer l'effet combiné des basses températures et des taux de déformation élevés sur le comportement mécanique du béton et de l'acier d'armature. Ce rapport discute des principaux résultats obtenus d'une étude expérimentale réalisée à l'École Polytechnique de Montréal visant à évaluer le comportement sismique de piliers de ponts en béton armé au Québec sous conditions hivernales.

2. PROGRAMME EXPÉRIMENTAL SUR L'ACIER D'ARMATURE

2.1 Portée

Un total de 24 essais de traction furent réalisés sur des éprouvettes d'acier d'armature pour différentes combinaisons de basses températures et de taux de déformation. La plage de taux de déformation considérée est typique d'événements sismiques ($80x10^{-6}$/s, $5x10^{-3}$/s, 0.02/s et 0.1/s). La plage de température considérée est représentative des conditions hivernales et estivales au Québec (+20°C, -20°C, et -40°C).

2.2 Éprouvettes et montage expérimental

Les figures 4.1 et 4.2 (dans le texte) montrent les dimensions des éprouvettes machinées ainsi que la machine utilisée pour les essais de traction sur ces éprouvettes. Toutes les éprouvettes furent machinées à partir de la même barre d'armature 15M (acier CSA G30.16).

Les essais furent réalisés à l'aide d'une machine d'essai servo-hydraulique d'une capacité de 100 kN (Instron, Ltd., U.K., Modèle 1350). Les deux extrémités des éprouvettes furent vissées directement dans les châssis de la machine d'essai.

2.3 Procédure expérimentale

La charge appliquée fut mesurée par une cellule de charge montée en série avec le vérin de la machine d'essai. La déformation unitaire moyenne fut mesurée sur une longueur de référence de 20 mm à l'aide de deux capteurs de déformation (clip gauge) montés sur la partie centrale de l'éprouvette.

Afin de maintenir la température constante pendant les essais, une chambre à température contrôlée fut installée autour de l'éprouvette. La température à l'intérieur de la chambre était maintenue constante à l'aide d'un débit d'azote liquide sous pression contrôlée. L'éprouvette d'essai était accompagnée dans la chambre d'une éprouvette témoin instrumentée par un thermocouple placé dans son noyau. L'essai débutait lorsque la température de l'éprouvette témoin atteignait la température désirée.

2.4 Résultats expérimentaux

Les résultats des essais de traction montrent que l'effet combiné des basses températures et des taux de déformation élevés est une augmentation de la limite élastique et de la contrainte ultime de l'acier d'armature. La déformation ultime ainsi que le module d'élasticité de l'acier d'armature, cependant, ne sont pas affectés de façon significative.

La figure 4.5 montre la variation de la limite élastique de l'acier d'armature en fonction du taux de déformation et de la température. La limité élastique augmente à mesure que le taux de déformation augmente et que la température diminue. La limite élastique augmente de 22% lorsque le taux de déformation passe de 80 x 10^{-6} /s à 0.1 /s et que la température passe de +20°C à -40°C.

Cette variation de la limite élastique de l'acier d'armature en fonction du taux de

déformation et de la température peut être estimée par l'équation de régression suivante:

$$\frac{F_{yDT}}{F_{yS20}} = [1.022 - 0.0011T]\left[1 + (0.0115 - 0.0001T)\ln\left(\frac{\dot{\varepsilon}}{80x10^{-6}}\right)\right] \quad (1)$$

Dans cette équation: F_{yDT} représente la limite élastique dynamique de l'acier d'armature pour un taux de déformation $\dot{\varepsilon}$ à une température donnée T, F_{yS20} représente la limite élastique de l'acier d'armature pour une condition de chargement statique (ε = 80 x 10^{-6} /s) à une température de 20°C, T représente la température en °C (-40 °C < T < +20 °C) et ε représente le taux de déformation en s^{-1} (80 x 10^{-6} /s < ε < 0.1 /s). Les prédictions de l'équation (1) sont aussi montrées sur la figure 4.5.

Le second terme de droite dans l'équation (1) représente le rapport entre la limite élastique dynamique, pour un taux de déformation ε et une température T, et la limite élastique statique à la même température T. Le premier terme de droite dans l'équation (1), tant qu'à lui, représente le rapport entre la limite élastique statique à une température T et la limite élastique à une température de 20°C.

La figure 4.6 montre la variation de la contrainte ultime de l'acier d'armature en fonction du taux de déformation et de la température. La contrainte ultime augmente aussi à mesure que le taux de déformation augmente et que la température diminue. La contrainte ultime augmente de 12% lorsque le taux de déformation passe de 80 x 10^{-6} /s à 0.1 /s et que la température passe de +20°C à -40°C.

Cette variation de la contrainte ultime de l'acier d'armature en fonction du taux de déformation et de la température peut être estimée par l'équation de régression suivante:

$$\frac{F_{uDT}}{F_{uS20}} = \left[1.03 - 0.0015T\right]\left[1 + (0.0064 + 0.00005T)\ln\left(\frac{\dot{\varepsilon}}{80x10^{-6}}\right)\right] \quad (2)$$

Dans cette équation: F_{uDT} représente la contrainte ultime dynamique de l'acier d'armature pour un taux de déformation $\dot{\varepsilon}$ à une température donnée T, F_{uS20} représente la contrainte ultime de l'acier d'armature pour une condition de chargement statique ($\dot{\varepsilon}$ = 80 x 10^{-6} /s) à une température de 20°C, T représente la température en °C (-40 °C < T < +20 °C) et ε représente le taux de déformation en s^{-1} (80 x 10^{-6} /s < ε < 0.1 /s). Les prédictions de l'équation (2) sont aussi montrées sur la figure 4.6.

3. PROGRAMME EXPÉRIMENTAL SUR LE BÉTON

3.1 Portée

Le programme expérimental sur le béton incluait aussi 24 essais de compression avec les mêmes combinaisons de taux de déformation et de températures que lors des essais de traction sur l'acier d'armature.

3.2 Cylindres d'essais

Afin de respecter la capacité de la machine d'essai (100 kN), des cylindres de béton ayant une diamètre de 38 mm et une hauteur de 76 mm furent choisis pour le programme expérimental. Un mélange de béton ayant une résistance en compression nominale de 20 MPa fut utilisé pour fabriquer les cylindres d'essais [1]. Tous les cylindres furent fabriqués à partir de la même gâchée. Le mûrissement des cylindres d'essais incluait un mûrissement en chambre humide pendant 30 jours et un mûrissement dans une chambre à humidité contrôlée (50% d'humidité relative) pendant 15 jours.

3.3 Procédure expérimentale

La même machine d'essai servo-hydraulique utilisée lors des essais de traction sur l'acier d'armature fut utilisée de nouveau pour les essais de compression sur les cylindres de béton. Chaque cylindre fut monté entre les deux châssis de la machine d'essais. Afin d'assurer un chargement axial pur, une bille fut insérée entre le châssis inférieur et le cylindre d'essai.

Encore une fois, la charge appliquée était mesurée par une cellule de charge montée en série avec le vérin de la machine d'essai. La déformation unitaire moyenne en compression était mesurée sur une longueur de référence de 50 mm à l'aide de deux capteurs de déplacement (LVDT). Ces capteurs étaient insérés entre deux anneaux circulaires qui étaient fixés à chaque extrémité du cylindre d'essai.

Afin de maintenir la température constante pendant les essais, la chambre à température contrôlée fut de nouveau installée autour du cylindre d'essai. Le cylindre d'essai était accompagné dans la chambre d'un cylindre témoin instrumenté par un thermocouple placé dans son noyau. L'essai débutait lorsque la température du cylindre témoin atteignait la température désirée.

3.4 Résultats expérimentaux

Les résultats des essais de compression montrent que l'effet combiné des basses températures et des taux de déformation élevés cause une grande augmentation de la résistance en compression et du module d'élasticité du béton. La déformation unitaire à laquelle se produit la résistance en compression ultime, cependant, n'est pas affectée de façon significative.

La figure 4.10 montre la variation du module d'élasticité du béton en compression en fonction du taux de déformation et de la température. Pour chaque cylindre d'essai, le

module d'élasticité fut mesuré sur une plage de contraintes entre 0 et 40% de la résistance en compression du béton. De façon générale, le module d'élasticité du béton en compression augmente à mesure que le taux de déformation augmente et que la température diminue. À 20°C, l'augmentation du module d'élasticité est minime sur toute la plage des taux de déformation. À -20°C et à -40°C, l'augmentation du module d'élasticité est significative pour des taux de déformation supérieurs à 0.02 /s.

Cette variation du module d'élasticité du béton en compression en fonction du taux de déformation et de la température peut être estimée par l'équation de régression suivante:

$$\frac{E_{DT}}{E_{S20}} = [1.06 - 0.003T]\left[1 + (0.0334 - 0.0009T)\ln\left(\frac{\dot{\varepsilon}}{80x10^{-6}}\right)\right] \qquad (3)$$

Dans cette équation: E_{DT} représente le module d'élasticité du béton en compression pour un taux de déformation ε à une température donnée T, E_{S20} représente le module d'élasticité du béton en compressions pour une condition de chargement statique ($\dot{\varepsilon} = 80 \times 10^{-6}$ /s) à une température de 20°C, T représente la température en °C (-40 °C < T < +20 °C) et ε représente le taux de déformation en s^{-1} (80×10^{-6} /s < $\dot{\varepsilon}$ < 0.1 /s). Les prédictions de l'équation (3) sont aussi montrées sur la figure 4.10.

La figure 4.11 montre la variation de la résistance en compression du béton en fonction du taux de déformation et de la température. La résistance en compression augmente à mesure que le taux de déformation augmente et que la température diminue. La résistance en compression augmente de 91% lorsque le taux de déformation passe de 80×10^{-6} /s à 0.1 /s et que la température passe de +20°C à -40°C.

Cette variation de la résistance en compression du béton en fonction du taux de

déformation et de la température peut être estimée par l'équation de régression suivante:

$$\frac{f'_{cDT}}{f'_{cS20}} = [1.159 - 0.008T]\left[1 + (0.0493 + 0.0007T)\ln\left(\frac{\dot{\varepsilon}}{80x10^{-6}}\right)\right] \qquad (4)$$

Dans cette équation: f'_{cDT} représente la résistance en compression du béton pour un taux de déformation ε à une température donnée T, f'_{cS20} représente la résistance en compression du béton pour une condition de chargement statique ($\varepsilon = 80 \times 10^{-6}$ /s) à une température de 20°C, T représente la température en °C (-40 °C < T < +20 °C) et $\dot{\varepsilon}$ représente le taux de déformation en s^{-1} (80×10^{-6} /s < $\dot{\varepsilon}$ < 0.1 /s). Les prédictions de l'équation (4) sont aussi montrées sur la figure 4.11.

4. ESSAI QUASI-STATIQUE SUR UN PILIER DE PONT COMPLET

4.1 Description du spécimen

La figure 5.3 montre les dimensions du spécimen de pilier de pont en béton armé qui fut soumis à un essai quasi-statique à température ambiante. Les dimensions du spécimen sont représentatives d'un modèle à l'échelle 1/3 d'un pilier de pont en béton armé typique au Québec. Le profilé en C permet à des tuyaux de drainage du tablier d'être installés dans l'ouverture. On considère qu'un point d'inflexion se produit à mi-hauteur du pilier et, par conséquent, seulement la moitié inférieure du pilier (853 mm de haut) est reproduite pour l'essai quasi-statique. La semelle de la fondation fut coulée en premier avec ses barres d'ancrage. Par la suite, le pilier fut coulé au dessus de la semelle, de sorte qu'une longueur de chevauchement de 245 mm fut introduite entre les aciers longitudinaux du pilier et les barres d'ancrage de la semelle.

4.2 Propriétés du béton

Un mélange de béton avec des agrégats de 6 mm fut utilisé pour couler le pilier. La résistance en compression du béton fut mesurée à 36 MPa juste avant l'essai quasi-statique.

4.3 Propriétés de l'acier d'armature

L'acier longitudinal du pilier était composé de barres #3 américaines d'un diamètre de 9.5 mm. La limite élastique de l'acier fut mesurée à 450 MPa et la contrainte ultime à 690 MPa. Des barres lisses de 3 mm de diamètre furent utilisées pour réaliser l'armature transversale. La limite élastique de ces barres lisses fut mesurée à 330 MPa.

4.4 Montage expérimental

Le chargement latéral quasi-statique fut simulé par un mouvement horizontal du simulateur sismique de haute performance de l'École Polytechnique. La semelle du spécimen fut ancrée à la table vibrante, alors que son extrémité supérieure fut fixée, par l'intermédiaire d'une rotule, à un support horizontal. Une charge de compression axiale de 120 kN, simulant le poids propre du pont, fut appliquée par deux barres de précontrainte entre l'extrémité supérieure du pilier et la table vibrante. Le montage expérimental pour l'essai quasi-statique est montré à la figure 5.9.

4.5 Résultats expérimentaux

Une rupture prématurée du spécimen est survenue à un facteur de ductilité (μ) compris entre 1 et 2. Le mécanisme de rupture fut caractérisé par un glissement entre les barres longitudinales du pilier et les barres d'ancrage de la semelle. Ce glissement fut accompagné par une fissuration verticale et un écaillement du béton à la base du pilier, comme le montre la figure 9.5.

La figure 9.6 montre les boucles d'hystérésis entre le cisaillement à la base et le déplacement relatif de la tête du pilier par rapport à sa base. L'effort de cisaillement maximal développé par le spécimen n'est que de 2/3 de l'effort de cisaillement correspondant à la résistance nominale en flexion du pilier. Le comportement du spécimen est médiocre avec une dégradation de sa résistance latérale et des boucles d'hystérésis très pincées.

La figure 9.14 montre deux séquences de déformation unitaire mesurées dans l'acier d'armature longitudinale, à une distance de 165 mm au dessus de la face supérieure de la semelle. La première séquence correspond à une barre longitudinale du pilier. La deuxième séquence correspond à une barre d'ancrage dans la semelle. Cette barre d'ancrage est adjacente à la barre longitudinale de la première séquence. On peut voir sur le graphique que jusqu'à une ductilité de 2, les deux séquences sont pratiquement identiques. Pour des ductilités supérieures à 2, cependant, les déformations unitaires dans l'acier longitudinale sont réduites considérablement. Ce résultat indique clairement que le mode de rupture du pilier est bien par glissement. Ce glissement se produit par le manque d'adhérence entre les aciers longitudinaux du pilier et les barres d'ancrage.

6. CONCLUSIONS

Les résultats d'essais de traction sur des éprouvettes machinées d'acier d'armature et d'essais de compression sur des cylindres de béton, sous différentes combinaisons de températures (-40°C à +20°C) et de taux de déformation (quasi-statique à 0.1 /s), ont permis de quantifier l'effet de ces deux paramètres sur les caractéristiques mécaniques de ces deux matériaux de construction. En se basant sur les résultats expérimentaux obtenus, on peut tirer les conclusions suivantes :

- La déformation ultime ainsi que le module d'élasticité de l'acier d'armature ne sont pas très affectés par le taux de déformation et la température.

- L'effet combiné des taux de déformation élevés et des basses températures est une augmentation de la limite élastique et de la contrainte ultime de l'acier d'armature. La limite élastique et la contrainte ultime augmentent de 22% et 12% respectivement, lorsque le taux de déformation passe de 80 x 10^{-6} /s à 0.1 /s et que la température passe de +20°C à –40°C.

- L'effet combiné des taux de déformation élevés et des basses températures est une forte augmentation du module d'élasticité et de la résistance en compression du béton. La résistance en compression du béton augmente de 91% lorsque le taux de déformation passe de 80 x 10^{-6} /s à 0.1 /s et que la température passe de +20°C à – 40°C.

Les résultats d'un essai quasi-statique sur un modèle à l'échelle 1/3 d'un pilier de pont en béton armé typique du Québec montrent que le comportement est caractérisé par un glissement entre les barres longitudinales du pilier et les barres d'ancrage de la semelle. La force de cisaillement maximale développée par le spécimen ne fut que de 2/3 de la force de cisaillement correspondante à la résistance nominale en flexion du pilier. Il est peut probable que les taux de déformation élevés et les basses températures puissent influencer sensiblement ce mode de rupture.

REMERCIEMENTS

Je remercie les organismes suivants pour leur support technique et financier dans le cadre de ce projet : le Ministère des Transports du Québec, le Conseil de Recherche en Sciences Naturelles et en Génie du Canada (CRSNG) et le Fonds de formation des Chercheurs et d'Aide à la recherche (FCAR) du Québec.

TABLE OF CONTENTS

LIST OF TABLES

LIST OF FIGURES

LIST OF SYMBOLES

α : parameter for the initial slope of the moment-curvature diagram

δ : deflection

δ' : logarithmic decrement

Δ : displacement

Δt : time step

ε : strain

ε' : *strain rate*

ε_{cu} : ultimate strain for the reduced section

ε_o : quasi-static strain rate (50×10^{-6}/s)

ϕ : curvature

ϕ_{cr} : cracking curvature

ϕ_y : yielding curvature

π : dimensionless products

σ : stress

ρ : mass density

ρ_{hc} : steel volume ratio of confinement to the volume of confined concrete

μ : ductility

μ_c : curvature ductility factor

ν : Poisson's ratio

ξ : damping ratio

b : width of the section

f : frequency

f' : mathematical function

f'_c : compressive strength of concrete

f'_{cDT} : dynamic compressive strength of concrete as a function of temperature

f'_{cS20} : quasi-static compressive strength of concrete at +20°C

f_{yh} : yield strength of the stirrups

g : acceleration

k_o : initial slope in Muto hysteresis model

k_u : yielding slope in Muto hysteresis model

l_c : distance between the critical section and the inflexion point

n : number of physical quantities

r : parameter for the post-yielding slope of the moment-curvature diagram

x : simulation characteristics of the prototype

EI_{cr} : after cracking stiffness in Muto hysteresis model

EI_g : initial stiffness in Muto hysteresis model

F : force

F_y : yield strength

F_{yd} : dynamic yield strength

F_{YDT} : dynamic yield strength as a function of temperature

F_{ys} : quasi-static yield strength

F_{yS20} : quasi-static yield strength at +20°C

F_{uDT} : dynamic tensile strength as a function of temperature

F_{uS20} : quasi-static tensile strength at +20°C

E : modulus of elasticity

E_{DT} : dynamic Young's modulus of concrete as a function of temperature

E_{S20} : quasi-static Young's modulus of concrete at +20°C

L : height of the column for the base to the center of mass

L_c : clear height of the column

M : moment

M_{cr} : cracking moment

M_{pb} : probable moment at the bottom of the column

M_{pt} : probable moment at the top of the column

M_y : yielding moment

P : load

PHA : peak horizontal acceleration

PHV : peak horizontal velocity

Q : force

S_l : length scaling factor

S_E : modulus of elasticity scaling factor

T : temperature

T' : time

T_1 : period of the structure

V : shear capacity

W : weight of the concrete blocks

LIST OF APPENDIXES

CHAPTER 1
INTRODUCTION

1.1 Earthquakes and Winter Conditions

Within the last 350 years, Eastern North America (ENA) has been faced with a number of significant earthquakes, with a magnitude of seven or greater on the Richter scale. These important seismic events, which occur in this region, have unique problem in that, there is a probability that an earthquake could take place during the winter season. During a twelve month period, it is not uncommon to have structures, like bridge piers, to be exposed to a large range of temperatures (+20 C to -40 C). Table 1.1 shows a lists of the major earthquakes which occurred in Eastern Canada having a magnitude greater than 5.5. It is evident that a large number of earthquakes had taken place during late autumn or winter. Therefore, the possibility of an earthquake occurring at low temperatures must be taken into account when engineers seismically design a structure. At very low temperatures, there is a change in the basic material properties of reinforced concrete. By changing the basic material properties of the reinforcing steel and of the concrete, the seismic response of the structure may be altered.

In other active seismic zones, with concentrated urban population, like regions around the Pacific Rim (i.e. California, Japan, New Zealand, etc.), temperature is not a major concern regarding the seismic response of a structure. Therefore, there has not been much research investigation on the combined effect of both, seismic loading and low temperatures.

Table 1.1 Earthquakes in Eastern Canada having a magnitude greater than 5.5

Location	Date	Year	Magnitude
La Malbaie region	February 5th	1663	~7
	February 24th	1665	~5.5
	December 6th	1791	~6
	May 7th	1831(2)	~5
	October 17th	1860	~6
	October 20th	1870	~6.5
	September 30th	1924	~5.5
	February 28th	1925	7
Montreal	September 16th	1732	~6
	September 9th	1816	~5.5
	March 23rd	1897(2)	~5.5
Ottawa	July 12th	1861	~5.5
Timiskaming	November 1st	1935	6.2
Cornwall-Massena	April 9th	1944	5.7
Grand Banks	November 18th	1929	7.2
Miramichi		1982	5.7
Saguenay	November 25th	1988	6.0

Its has been stated that low temperatures had a contributing factor in the brittle failures of structural members during the Hyogo-Ken Nanbu earthquake of 1995 [Park et al., 1995]. An example of this type of failure occurred in a complex of 50 high-rise apartments where there was a brittle fracture of the lower levels of the box columns forming part of the external concentrically braced frame system. Even though it was a relatively modern building (constructed in 1980), using 500 MPa yield strength steel for

the box columns, the lower levels suffered brittle failure in around 10% of the columns. Some inspectors thought a reason for these brittle failures may have been that these members were below their transition temperatures at the time of the earthquake. In ENA, this factor, as well as the large amount of structures constructed prior to modern seismic provisions in building codes, cannot be overlooked.

1.2 Objectives and Scope of the Research Project

The main objective of this research project is to investigate the seismic behaviour of reinforced concrete bridge piers in Eastern North America (ENA) under simulated winter conditions. Although the quasi-static response of bridge piers has been studied [e.g. Mitchell, 1991], qualification and seismic tests for these structures in ENA are lacking. In order to investigate the performance of these piers, a typical bridge pier from an existing bridge was chosen. This bridge was constructed during the 1960's, prior to recent seismic changes in the building codes. At that time the engineers' knowledge of the seismic performance of concrete was very limited, and as a result, these non-ductile reinforced concrete columns are considered vulnerable structural elements during earthquakes.

Another aspect of the seismic response of a bridge pier which is located in ENA, is the expected ground motion which is quite different than the ground motions commonly seen in other moderate to high seismic zones. Earthquakes in ENA generally have smaller amplitudes and a higher frequencies content, thus it is not representative to apply a western type earthquake to an eastern type structure. Being located in ENA, it is possible to experience an earthquake during the winter months, in which the temperatures can reach -40°C. Therefore, the combined effect of high strain rate and low temperatures can change the basic mechanical properties of the reinforced concrete and possibly, alter the seismic behaviour of these structures.

In this thesis, material tests were performed under various combinations of earthquake-type strain rates (quasi-static to 0.1/sec) and temperatures of summer and winter conditions in cold urban regions (+20°C to -40°C), in order to evaluate the combined effects of these two parameters on the stress-strain curves of concrete and reinforcing steel. Regression equations were constructed from the test results and formulas were developed.

Eight identical large-scale reinforced concrete bridge pier specimens, incorporating typical details found in ENA construction, were fabricated for this study. Four of the eight were tested experimentally under different earthquake ground motions (historical and artificial earthquakes). The other four specimens were used as a backup for the primary tests and/or for undertaking further studies, depending on the results of the initial experiments.

All the material and seismic testing was carried out on the Earthquake Simulator of the Structural Engineering Laboratory at Ecole Polytechnique, Montreal, Canada.

The experimental results were compared to the predictions of non-linear dynamic analyses obtained using the computer program RUAUMOKO [Carr, 1995].

1.3 Thesis Organization

The thesis is divided into eleven chapters, with the first chapter being the introduction. The second chapter presents the seismic performance and behaviour of bridge piers, in which different failure modes, observations and retrofit methods are discussed.

The third chapter is related to prior research that was completed relating the effect of strain rate and temperature on reinforcing steel and concrete. The fourth chapter discusses the experimental study on the stress-strain behaviour of these materials under seismic strain rate and low temperatures. Results from the regression formulas are developed to capture these behaviours for structural analysis.

In chapter five, the basic computer modelling of the test specimen, along with the description of the test set-up are discussed. First, there is a brief description of the prototype of which the model was scaled, as well as the scaling laws which were applied. Then, a comparison is made between the model and the prototype by implementing the simulation requirements.

Chapter six contains the preliminary analysis of the model specimen. The model was analysed with the computer programs RESPONSE and RUAUMOKO and the results are given. Also, the dimensioning of the test set-up, including the bridge pier, foundation and the steel testing frame, are discussed. Various earthquakes representative of different regions (East and West) of North America are used in non-linear analyses to determine the final selection of the earthquakes.

In the seventh chapter, the material properties are given for concrete and steel used in the experimental tests. The results of the tensile tests of the longitudinal and transversal reinforcement are given. A description of the concrete mix of the foundation and the column and their respective compressive strengths discussed.

Chapter eight introduces the fabrication methods of the specimens and the experimental set-up. Also, there is a brief description of the type and placement of the instrumentation used to obtain the test results. This chapter also describes the different

experimental set-ups which were used for the various seismic tests performed on the shake table.

Chapter nine and ten contain the experimental tests results. The results were separated by chapters, with the quasi-static test results in chapter nine and the seismic tests results in chapter ten. The performance of the shake table was verified with their corresponding input data. The performance and the behaviour of the specimen are discussed, including: maximum displacements, maximum accelerations, maximum base shear, variation of the mechanical characteristics (damping, stiffness and period). The different hysteresis curves comparing moment-curvature and base shear-relative displacements are also studied. A complete analysis was not completed on the each seismic test, rather general observations and comments were carried out and similarities discussed between the quasi-static and seismic tests.

Chapter eleven explains the final numerical modelling of the specimen. The RUAUMOKO computer model is described along with the choice of the hysteretic model. The final selection of the model and the type of non-linear analysis are also discussed. With the use of this model, analytical results were found and were compared to the experimentally found results. Several hysteresis and time-history curves are given and discussed.

Finally, the conclusion and recommendations on the material behaviour and the seismic performance of bridge piers in ENA are given in chapter twelve.

CHAPTER 2
SEISMIC PERFORMANCE AND BEHAVIOUR OF BRIDGE PIERS

2.1 Introduction

A large number of bridge structures were constructed in eastern Canada during the 1960's [Griezic et al., 1996]. At that time, the typical design of bridges did not incorporate the ability for energy absorption and ductility under lateral loads. The failure of a column, or a group of columns, can result in at least a partial collapse of the structure. Damage to bridge structures as a result of the 1971 San Fernando, 1987 Whitter Narrows, the 1989 Loma Prieta and the 1994 Northridge earthquakes have shown that the design and detailing methods of older concrete piers are not adequate and there is a need to assess the performance of bridge piers in moderate and high seismic regions.

It was found that the major problem with these older designs, was that the piers had inadequate ductility and shear strength. This led to different modes of failures, including : shear and flexural failures.

Considerable progress has been made with the use of retrofit techniques to upgrade the seismic resistance of bridge piers. Two of the most widely used retrofit techniques include the use of steel jackets and composite material jackets of fibreglass/epoxy or carbon fibre/epoxy. The use of these methods is becoming common and this retrofit technology has now developed to the stage that design approaches are available for enhancement of seismic performance.

2.2 Reinforced Concrete Bridge Piers

2.2.1 Assessment of Reinforced Concrete Bridge Piers

Two major problems are associated with the seismic performance of older non-ductile reinforced concrete columns.

- Insufficient transverse reinforcement or spiral ties within the column for adequate concrete confinement and seismic shear strength.
- Insufficient embedment and splice lengths of the column dowels to develop the strength of the reinforcement, which can lead to slippage.

These two major deficiencies limit the lateral strength and ductility of many older reinforced concrete piers.

In older design codes the shear resistance was not based on the shear force associated with the development of the flexural capacity of the columns. Therefore, there was inadequate shear strength of members due to insufficient transverse reinforcement. Furthermore, the transverse reinforcement was usually anchored into the concrete cover with 90° hooks, which tend to open after the concrete cover spalls off under severe cyclic loading. Such transverse reinforcement does not provide adequate ductility and shear strength of potential hinge regions of members, because the lack of transverse reinforcement does not provide sufficient confinement of compressed concrete [Park et al., 1993]. The failure to provide adequate transverse steel, as with the majority of piers constructed in the 1960's, gives inelastic cyclic response with poor energy dissipation, rapid strength, stiffness and physical degradation, which may lead to brittle shear failure with limited displacement ductilities [Chai and Priestly, 1992].

The other major deficiency is lap splice failure. During the 1960's lap splices of longitudinal reinforcement were typically designed with a length of about 20 bar diameters and were often located in potential plastic regions. Besides their length being short and located in a critical region, the lap splices were poorly confined by transverse reinforcement. There was also a possibility of bar buckling on load reversals and bond failure of the lap splice due to yielding of the reinforcement over a small length resulting in extremely high strains [Griezic et al., 1996]. It was observed that piers that were detailed with a splice length of 20 d_b (bar diameters) showed a significant pinching of the hysteresis loops beyond a displacement ductility of 1.5 as well as a rapid loss of lateral load carrying capacity and very little energy dissipation [Chai and Priestley, 1992].

2.2.2 Failure Modes of Reinforced Concrete Bridge Piers

One of the modes of failure that is often seen with older bridge piers is failure due to the lack of flexural strength and ductility. For columns with continuous reinforcement, flexural failure in the plastic hinge region was observed because of insufficient confinement. The column was unable to develop the necessary ductility at inelastic displacements caused by the seismic loading. The deterioration of the plastic hinge is followed by horizontal flexural cracks, spalling of the concrete cover, rupture of the stirrups, buckling of the longitudinal reinforcement and thus, crushing of the concrete core.

The ruptures of the plastic hinges generally occur during a certain level of ductility and displacement ($\mu = 4$), or large inelastic deformations. It is commonly seen that these failures occur at predictable locations in the column, but it is possible to have the migration of plastic hinges into non-designed regions of the column. This type of

failure is mainly seen in tapered columns or where there was a drastic change in the column profile, largely due to the loss of confinement in these regions.

For piers with dowel bars at the column-footing connection, flexural failure happens due to insufficient stirrup reinforcement, which leads to a lack of confinement within the plastic hinges. Thus, the ultimate flexural resistance of the column cannot be obtained due to slipping between the longitudinal and dowel bars. This slippage causes the formation of vertical micro-cracking in the concrete core. This phenomenon is amplified by the propagation of vertical cracks, which eventually leads to crushing of the concrete core. This loss of flexural strength usually occurs at low ductilities levels ($\mu \leq 2$). It should be noted that slipping could take place prior to yielding (i.e. $\mu \leq 1$).

Shear failure is another mode that has been noticed in many of the damaged bridge piers. This type of failure is mostly seen in short, stout columns with a high moment of interia. A shear failure is usually sudden due to the dramatic loss of strength. These columns are unable to reach inelastic shear deformations because of their poor ductility (lack of confinement). These short columns are particularly sensitive to shear failure because they have a higher resistance in flexure compared to shear for a given horizontal load.

There are two types of shear failures, one being a pure shear failure, while the other is a failure due to a combination of shear and flexure. Pure shear failure is usually observed when there is a large diagonal crack produced over the height of the column. On the other hand, the combination of shear and flexural failure is generally formed because of the migration of plastic hinges.

2.3 Ductility

2.3.1 Importance of Ductility

It is almost economically impossible to design a structure which can withstand the design lateral seismic forces in the elastic range of the material. Therefore, the practice which is generally used is to design for a lower force level and detail the structure so that it can undergo substantial inelastic deformation at nearly constant lateral force levels, without suffering any excess damage or loss of strength while the structure is seismically loaded during an earthquake.

For a bridge system, the substructure, which includes piers and foundations, must be stronger than the column. Figure 2.1 shows the designed plastic hinge regions in columns. For simple span structure the plastic hinge will usually be formed at the base, but if the structure is continuous, there is a possibility of plastic hinges to be formed also at the top of the column [Mitchell 1991].

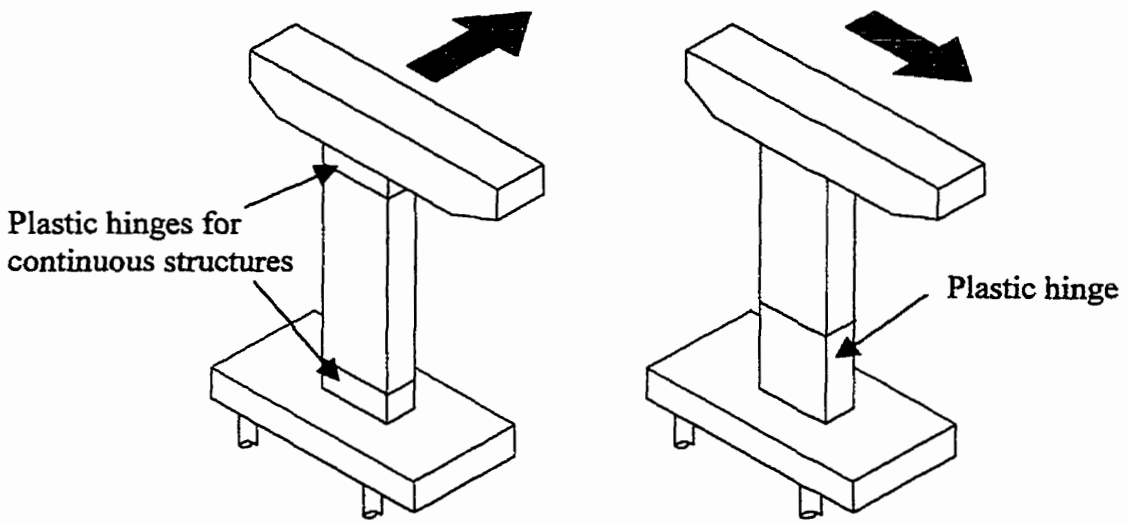

Figure 2.1 Plastic Hinge Region in Single Column (adapted from Mitchell, 1991)

2.3.2 Achieving Ductility in Bridge Columns

The design and detailing of the column is very significant in order to achieve the required ductility within the plastic hinge region. A number of important aspects are discussed below.

2.3.2.1 Buckling of Longitudinal Bars

The closer the transverse reinforcement is placed, the lower is the likelihood of buckling of the longitudinal reinforcement. The current Canadian specification states that the transverse reinforcement shall be spaced at a distance not exceeding [CSA Standards, 1994]:

- one quarter of the minimum member dimension;
- 100 mm;
- 6 times the diameter of the smallest longitudinal bar, or
- the requirement for shear design.

2.3.2.2 Confinement by Reinforcement

Priestley and Park [1987] have found that the behaviour of concrete columns under seismic loadings is related to the confinement of the concrete. It was discovered that, as the confinement improves, the compressive strength also increases and, thus, causing a significant improvement in the ductility of the concrete. Figure 2.2 shows a comparison between the stress-strain curves of confined concrete and the curve for identical, but unconfined concrete.

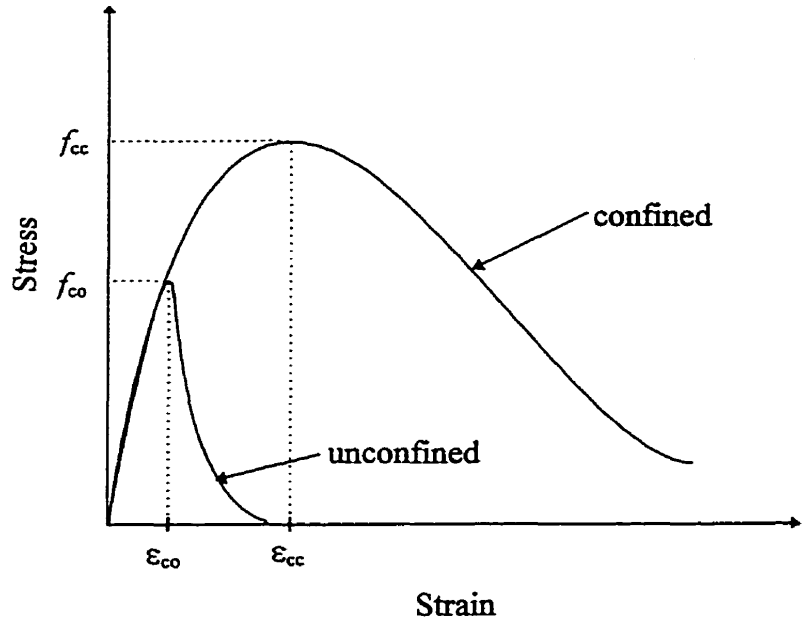

Figure 2.2 Compressive Response of Confined and Unconfined Concrete

Priestley and Park has also investigated the relationship between axial load and confinement. It was found that as the axial load increases, there was a need for more confinement [Priestly and Park, 1987]. This can be seen in figure 2.3, as the axial load increases the neutral axis depth also increases. The lack of confinement can cause the concrete cover to spall off and therefore the flexural strength and ductility becomes more dependent on the compression block within the core [Mitchell, 1991].

The spacing and geometry of reinforcement are important variables that influence the concrete confinement and hence the ductility of the column. As can be seen in Figure 2.4 as the spacing between the stirrups increases, it results in larger regions of unconfined concrete.

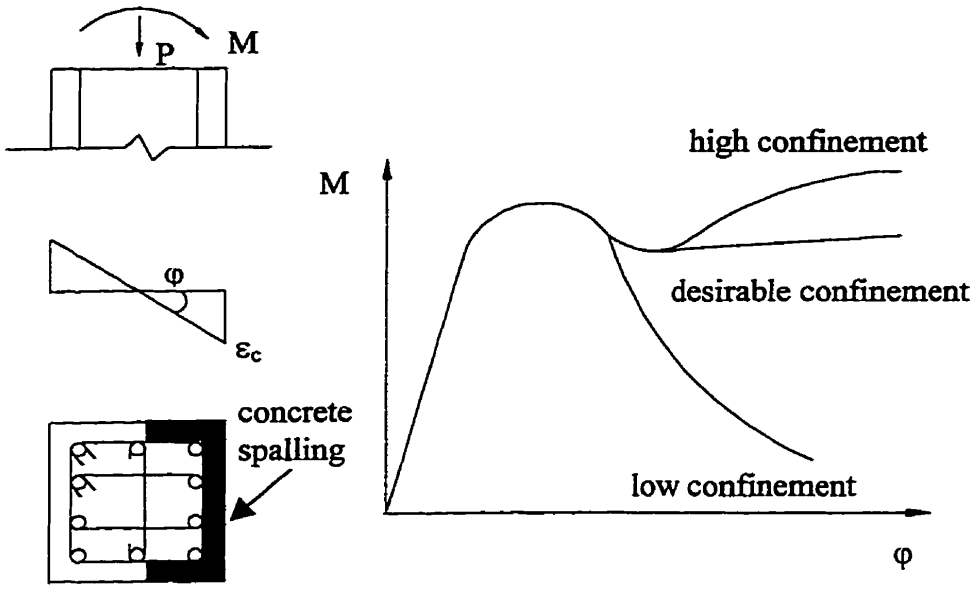

Figure 2.3 Influence on the Level of Confinement on the Flexural Response (adapted from Park, 1986)

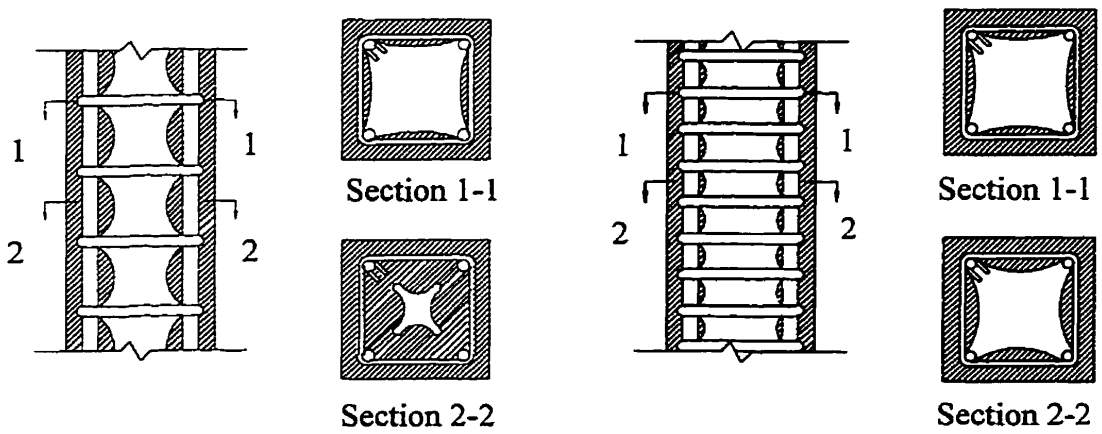

Figure 2.4 Influence of Hoop Spacing on the Confinement of the Concrete Core (adapted from Mitchell, 1991)

2.3.2.3 Shear Design

When flexural hinging develops in the column, it is necessary to ensure that the shear capacity exceeds the shear demand which corresponds to the flexural strength in order to prevent shear failures. The resulting shear capacities required are a function of the probable moment capacity at the hinges [Mitchell, 1991].
In the transverse direction:

$$V=\frac{M_{pb}}{L} \qquad [2.1]$$

In the longitudinal direction:

$$V=\frac{M_{pb}+M_{pt}}{L_c} \qquad [2.2]$$

In these equations M_{pb} and M_{pt} are the probable moments at the bottom and top respectively. Also, L is the height from the base to the centre of mass and L_c is the clear height of the column. The probable moments must take into consideration three governing criteria:

- The in-situ strength of concrete and reinforcing steel is greater than the specified level.
- The ability of the stress level of the reinforcement to increase due to strain hardening.
- The increase strength and ductility of the concrete due to the confinement.

There are equations given by Chai [Chai and Priestley, 1992] in which the shear strength of the existing column is calculated and the improvements given as a result of using different retrofit techniques. The shear strength depends on whether spiral reinforcement is used or normal ties and the spacing, axial load, and the length of the plastic hinge.

2.3.2.4 Hoop Anchorage

It is very important to effectively anchor the transverse reinforcement so that if the concrete cover spalls off, the hoops will give adequate confinement of the concrete. It is generally accepted, that the hoop reinforcement in a bridge column be made with 135° bend anchorages with the free end extensions having sufficient anchorage into the concrete core.

It has been found by CALTRANS (California Transportation Dept.) that spiral reinforcement provides greater efficiency in confinement when compared to hoop reinforcement. CALTRANS have developed equations to determine the amount of transverse reinforcement needed as a function of the axial load. More recently, the use of interlocking spiral reinforcement has been used for reinforcing bridge columns, to increase confinement within the column. In order to improve the composite action, there is a limit on the maximum spacing of the spirals and at least four longitudinal bars must be in the interlocking region of the spirals.

2.4 Retrofitting

There have been many research advancements in the concrete column design due to recent earthquakes. Due to the large number of columns which have inadequate transverse steel, as with the pre-1970 design, there is a high risk of brittle shear failure due to limited displacement ductilities. In order to reduce this risk, retrofit techniques were developed to provide confinement which enhances the shear strength of the column. A satisfactory retrofit of the column would increase the flexural response and increase the shear strength to avoid brittle shear failure. One of the most popular

methods of retrofitting is to place a cylindrical or elliptical jacket around the concrete columns. The most common techniques implemented on bridge columns to date have been steel jacketing and composite material jackets.

2.4.1 Steel Jackets

Steel jackets, either circular or elliptical are the most common type of column retrofit currently in use. A properly designed circular jacket can provide the confinement to sustain a displacement ductility of seven or eight, which easily meets a typical design requirement of four or five [Priestly and Park 1987; Chai and Priestley,1992]. The elliptical jackets commonly used for rectangular columns provides roughly the same ductility as a circular jacket. Circular jackets convert concrete confinement pressure into hoop stress in the jacket and thus are a very effective section for confinement. Also, because of their circular shape, the jacket provides equal confinement in all directions. For rectangular columns, it is recommended to use an elliptical jacket (rather than rectangular jackets) because it produces a continuous confining action similar to the circular jackets, but due to the varying curvature of the jacket, the confining stresses also vary around the circumference of the jacket. Figure 2.5 shows the confinement of the columns by steel jackets.

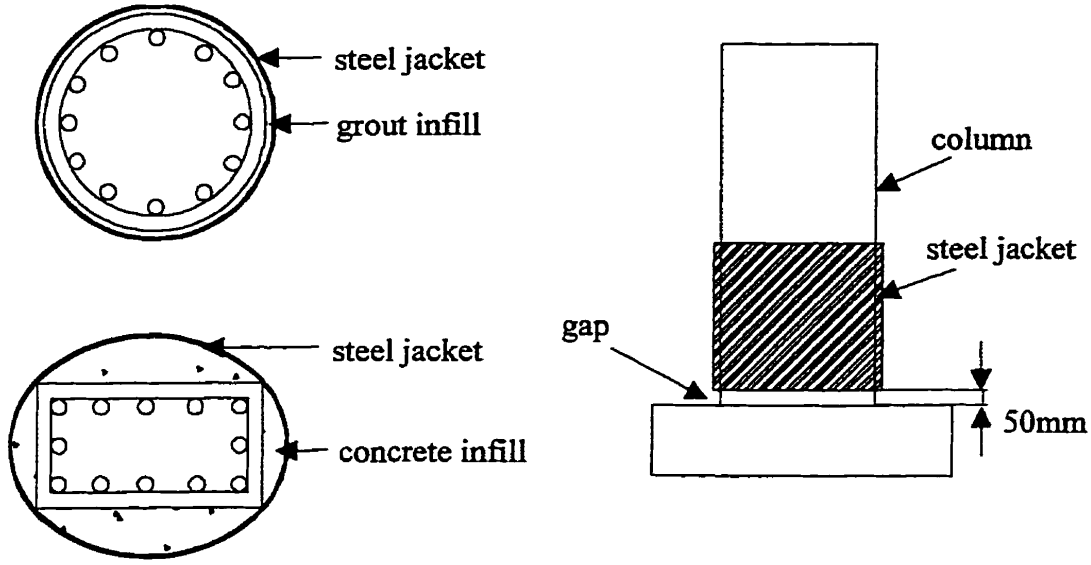

Figure 2.5 Confinement of Columns by Steel Jackets (Circular and Elliptical)

The steel jacket is placed over the potential hinge regions by welding two half shells of steel over the column on site. For ease of construction, the steel jacket is made slightly oversize, for the circular pier section. Later, the gap between the existing concrete and the steel shell (usually 25mm) is filled with a cement-based grout, after flushing with water. As for rectangular columns, the gap is filled with normal concrete, rather than grout. Typically, a vertical space of about 50mm is provided between the jacket and any supporting members (footing or cap beam) to ensure that only confinement is provided to the column concrete. Without leaving a gap at the base of the column, the jacket would increase the size of the critical section which may lead to an increase in the moment capacity and overload the footing and increase the shear demand. This gap is also provided to avoid the possibility of the jacket acting as compression reinforcement by contacting the supporting member at large drift angles. The length of the steel jacket is often determined by shear since in a ductile column the shear is constant (column plastic moment capacity divided by length).

Columns tested by Chai, [Chai and Priestley, 1992] comparing the lateral force-displacement response of an as-built column to steel-jacketed retrofitted column showed significant improvements in its flexural strength. The as-built columns did not reach their flexural strength due to bond failure. The peak lateral force was noted at μ=1.5 which corresponds to 97% of their theoretical ideal flexural capacity. After a μ=1.5 there was severe pinching of the hysteretic loops and a reduction in the shear force. On the other hand, the retrofitted column showed a ductile behaviour and did not experience bond failure. The response showed stable condition (hysteresis loops up to μ=7). By comparing the performance of the two specimens, it can be seen that the use of a grouted steel jacket greatly improve the seismic performance of the column.

2.4.2 Composite Material Jackets

Composite jackets are used in the same manner as the steel jackets. The composite (fibreglass/epoxy) jackets have proved to be particularly effective in shear retrofit applications for short columns, where flexural ductility requirements are secondary to the need for brittle failure. The jackets are manufactured with high strength fibreglass fibres in orthogonal directions, which allows for different strength properties in each direction. Confinement is induced in the reinforced concrete column by applying epoxy or cement based grout in the gap between the column and the jacket, with the epoxy being the most popular. Methods of application include the lay-up of a epoxy-impregnated fibreglass fabric, and machine winding with carbon fibre tows, also impregnated with epoxy. Commonly, for the cement based grout a pressure of between 0.7 and 1.4 MPa is used for this procedure.

Typical bridge columns were tested by Preistley [Priestley and Seible, 1991]. These tests compared the results of as-built columns to the results of retrofitted columns. The columns were tested for confined lap-splices in the vertical reinforcing steel at the

bottom flexural area of the bridge columns (typical pre-1970 design). The deflection curve before repair showed a μ=3 with the ductility decreasing after μ=2. With the retrofitted columns, a glass-polyaramide-epoxy was used and stressed by injecting cement grout into the gap. The results showed increased strength with ductilities of over 8 with no increase in stiffness.

2.4.3 Comparison Between Steel and Composite Material Jackets

Tests on circular columns retrofitted with composite materials jackets to improve ductility indicate that the confinement effectiveness is more efficient than with steel jackets [SEQAD Consulting Engineers]. The reason for this is thought to be because of the elastic nature of the composite material. During a seismic response the composite material has an essentially linear stress strain characteristics up to failure, therefore, with successive cycles of displacement there is no increases in hoop strain. On the other hand, with steel jackets, yield under hoop tension may occur early in seismic response. On unloading, residual plastic strains remain in the jackets, reducing its effectiveness for the next cycle and thus increasing the hoop strains. Another advantage of the composite material is that it increases the strength and ductility of the columns without increasing its stiffness. Tests have also proved that the composite material is non-corrosive, durable and there was no evidence of failure modes when tested at a temperature of -55°C. Also, because the composite material is more flexible compared to steel, it is possible to place the jacket in smaller places.

In the application of the jacket, the steel jacket does not need the same amount of expertise as compared to the composite material jackets therefore reducing the retrofitting time and expenditures. Also, because steel is a common material it has an economical advantage over the composite material and it can be easily produced.

2.5 Summary

Although in recent decades there have been a number of experimental studies and investigations on the seismic performance of columns constructed in the 1960's, further research is still needed to enhance their seismic loading and/or deformational capacities. The major findings, as to the failure of these columns, were their inability to deform beyond the elastic range and respond in a ductile manner. A main component to increase the ductility of concrete members is the amount of confinement, increasing the confinement increases the strength and the ductility of the concrete. New technologies and retrofit methods, such as jacketing, has proved to significantly improve the ductility of the concrete.

It has been seen that temperature has a direct effect on the ductility of material properties, therefore, questions have been raised about the seismic performance of bridge columns which are exposed to winter conditions. On account of the climate conditions found in ENA, information is needed on the behaviour of reinforcing steel and concrete subjected to high strain rates and low temperatures.

CHAPTER 3
PREVIOUS STUDIES ON STRAIN RATE AND TEMPERATURE EFFECTS

3.1 Introduction

Most engineering materials subjected to high rates of loading and low temperatures usually associated with ENA earthquakes, typically one hundred thousand times faster than the static loading case and -40°C, will exhibit some changes in their response. Material properties such as strength, stiffness and ductility can be affected by both, the loading rate and temperature. These changes usually enhance the material's strength behaviours, but may diminish the material's ductility response, thus changing the material's seismic response.

Knowledge on the combined effects of strain rates and low temperature on the behaviour of reinforcing steel and concrete is rather limited. Mainly, the research has been focused on observed strength increases of either strain rate or temperature, with little or no attention paid to changes to the deformational behaviour. Therefore, a thorough knowledge of the effects of strain rate and temperature are needed on material behaviour to properly design a structure for all types of loading likely to be encountered during the design lifetime.

3.2 Strain Rate Effects on Steel

As reported by Davis [Davis 1938], Ludwik in 1909, was possibly the first researcher to observe the effects of varying strain rates on the mechanical properties of metals. Manjoine [Manjoine, 1944] conducted a thorough investigation of the influence

of strain rates on the tensile behaviour of mild steel. Test results indicated that the yield stress increases with increasing strain rate, but to a lesser extent in higher strength steels.

Within the last few decades, a large number of research efforts have been devoted on the behaviour of steel members under earthquake-type strain rates [Wakabayashi et al., 1984 ; Udagavva et al., 1984 ; Kaneta et al., 1986 ; Nagataki et al., 1988 ; Suita et al. 1992 ; 1996]. Most of these investigations reported that the yield strength and tensile (ultimate) strength of steel increase linearly with logarithmically increasing strain rate. For example, the results of dynamic and quasi-static tests on round steel bars, conducted by Wakabayashi [Wakabayashi et al. 1984], have lead to the following expression to estimate the increase of yield strength with strain rate :

$$\frac{Fyd}{Fys} = 1 + 0.0473 \log\left(\frac{\dot{\varepsilon}}{\dot{\varepsilon}_o}\right) \qquad [3.1]$$

where F_{yd} is the dynamic yield strength for a strain rate $\dot{\varepsilon}$ and F_{ys} is the quasi-static yield strength under a strain rate $\dot{\varepsilon}_o = 50 \times 10^{-6}$ /s. Similar expressions were also proposed by others [Suita et al., 1996 ; Ammann and Nussbaumer, 1995 ; CEB 1988 ; Mander et al., 1984 ; Mirza and M^{ac}Gregor, 1979 ; Mahin and Bertero, 1972].

Wakabayashi [Wakabayashi et al., 1984] also recognised that the strain rate had negligible effect on the elastic modulus and the stiffness in the strain-hardening range. It was also observed that, as the strain rate increases, the ratio between the ultimate stress and the yield stress decreases, and higher strength steels are less susceptible to strain rate effects compared to lower strength steel [Restrepo-Posada 1993 ; Restrepo-Posada et al. 1994].

3.3 Low Temperature Effects on Steel

Structural steel materials are sensitive to temperature. As temperature decreases, the material behaviour migrates progressively from a ductile to a brittle behaviour. Loss of ductility in metal can be observed by examining the low temperature stress-strain relationship. As the temperature is lowered, both the yield point (where ductility begins) and ultimate strength point (where failure occurs) may shift to a higher stress value, but fracture may begin at a lower strain value. The temperature at which dramatic brittle failure is observed is described as the transition temperature. The Charpy notch-toughness test was developed to evaluate this transition temperature based on the energy absorbed by a standard notch steel specimen when it is impacted. A single blow is applied to the middle of the specimen, opposite to the notch ; as the impactor swings through, the specimen breaks and a recording dial indicates the absorbed energy. The majority of the research compiled on the effects of low temperature on steel have been related to the Charpy test. Therefore, the knowledge of the stress-strain behaviour of low temperate for steel is limited, with emphasis placed mainly on the observed notch toughness (energy).

The transition from a relatively ductile to a relative brittle mode of failure is believed to occur because of the very rapid rise in molecular viscosity with decreasing temperature. As with steel, the flow stress is low at high temperatures. On the other hand, at low temperatures, the molecular yield stress for slip is high so that deformation will start by microcracking and subsequent brittle fracture [Dutta, 1988 ; M^{c}Clintock and Ali, 1966].

A discussion on the mechanical properties of steel at temperatures colder than room temperature has been presented by Bruneau [Bruneau et al., 1997]. Results of monotonic tensile tests on ASTM A572 Grade 50 steel plates (approx. 25 mm thick)

indicated that, as temperature reduces, the yield and tensile strengths also increases, while the ultimate strain decreases. On the other hand, the elastic modulus of steel seems unaffected by a decrease in temperature. Furthermore, a large number of these investigations have been conducted by steel producers and are not readily available to the general public.

3.4 Combined Effects of Strain Rate and Low Temperature on steel

Very limited research has been carried out on the combined effects of strain rate and low temperature on steel. From the limited information available, it appears that the change in mechanical properties observed under high strain rates is accentuated at low temperatures. For example, an investigation on the Arctic grade steel [Faucher et al. 1987] has demonstrated that the yield strength between 400 and 700 MPa can be obtained from the following relationship :

$$F_y = 905.9 - 0.0942T \ln\left(\frac{2.7x10^8}{\dot{\varepsilon}}\right) \qquad [3.2]$$

for

$$2000 \le T \ln\left(\frac{2.7x10^8}{\dot{\varepsilon}}\right) \le 5500$$

where F_y is the yield strength expressed in MPa, T is the temperature in degrees Kelvin and $\dot{\varepsilon}$ is the strain rate in s^{-1}.

It was also proposed to model the combined effects of strain rate and low temperatures on the fracture behaviour of steel by using the results of standard Charpy tests with a transition temperature shifted towards higher temperatures as strain rate increases [Barsom, 1975 ; Roberts et al., 1974 ; Barsom and Rofle, 1970].

3.5 Strain Rate and Low Temperature Effects on Concrete

Despite the widespread use of concrete, there is a lack of knowledge concerning the strain-rate effects on the behaviour of concrete. Furthermore, most of these studies have been carried out for impact conditions, with strain rate several magnitudes above earthquake-type strain rates, thereby, these tests are not directly applicable. Most of the research completed followed the general trends of increase in elastic modulus, tensile strength, flexural strength and compressive strength with decrease in temperature. Bischoff and Perry [Bischoff and Perry, 1991 ; Bischoff and Perry, 1995] investigated the strain-rate effects on the behaviour of concrete, and showed significant differences between the impact and static behaviour of plain concrete in uniaxial compression. It was observed that the Young's modulus of concrete in compression increases with strain rate. The influence of strain rate on Young's modulus of concrete in tension is smaller than for compression. It was also found that the compressive strength of concrete increases with strain rate, but the influence of strain rate decreases for higher strength concrete. Furthermore, the ultimate compressive strain of concrete (strain which corresponds to the maximum stress) increases with strain rate.

Low temperature behaviour of concrete is related to the extent of curing, but more importantly, to the moisture content when the specimens are cooled [Berkovitch 1981]. Berkovitch also stated several general trends which were found for in-situ concrete cooled to low temperatures. It was observed that the compressive strength increased significantly, and the tensile strength increased marginally. This in turn, increases the flexural strength of the concrete. In addition, there was also an increase with respect to the Young's modulus.

Finally, information concerning the combined effects of strain rates and low temperatures on the compressive stress-strain behaviour of concrete is, to the author's knowledge, not available.

CHAPTER 4
EXPERIMENTAL STUDY ON THE STRESS-STRAIN BEHAVIOUR OF REINFORCING STEEL AND CONCRETE UNDER SEISMIC STRAIN RATES AND LOW TEMPERATURES

4.1 Introduction and Scope

Very limited research has been carried out on the combined effects of strain rates and low temperatures. Therefore, as part of this thesis, an experimental programme, aimed at studying the combined effects of earthquake-type strain rates and low temperatures on the mechanical properties of reinforcing steel and concrete, was conducted.

As shown in Table 4.1, a total of 24 different monotonic tensile tests were performed on reinforcing steel coupons for various combinations of strain rates and temperatures. The strain rates considered (80, 5 000, 20 000 and 100 000 microstrains/s) encompass the various loading rates typical of earthquake excitations, with 80 microstrains being representative of a quasi-static loading rate and 100 000 microstrains being an upper bound for earthquakes strain rates. Also, three different temperatures, +20°C, -20°C and -40°C, were considered to reproduce summer, moderate winter conditions and extreme winter conditions, respectively. For conformation of the testing results, two specimens were tested for each set of strain rate and temperature.

The test programme on concrete cylinders also included 24 different compressive tests, with the same combination of strain rates and temperatures used in the test programme for the reinforcing steel.

Table 4.1 Test Programme on Reinforcing Steel and Concrete

Temperature (°C)	Strain Rate (10^{-6} /s)	Number of Specimens
+20	80	2
	5 000	2
	20 000	2
	100 000	2
-20	80	2
	5 000	2
	20 000	2
	100 000	2
-40	80	2
	5 000	2
	20 000	2
	100 000	2

4.2 Test Programme on Reinforcing Steel

4.2.1 Test Coupons

Figure 4.1 shows the dimensions of the machined steel coupons tested in the experimental programme. In order to ensure that all of the steel specimen belonged to the same heat, the coupons were machined from a single 12 meter long, 15M (16 mm diameter) deformed reinforcing bar. The reinforcing steel was common commercial grade (CSA G30.16), typically used for construction in Canada. The machined specimens had a finished section diameter of 6 mm, with a length of 40 mm. The

specimens were fabricated with threads at each end, in order to facilitate mounting in the testing apparatus.

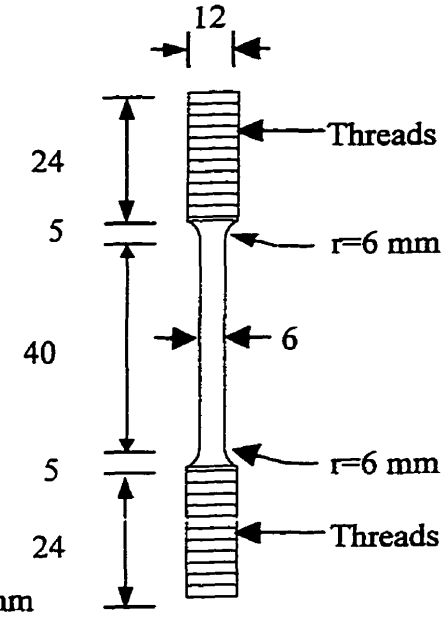

Note: All dimensions in mm

Figure 4.1 Dimensions of Machined Steel Coupons Tested

4.2.2 Experimental Set-up and Procedure

Figure 4.2 shows photographs of the loading frame used for testing the steel coupons. The tests were conducted on a 100 kN, self-contained, closed-loop, servo-hydraulic, dynamic testing machine (Instron Ltd., U.K., Model 1350). The two ends of the steel coupons were threaded directly in the cross-heads of the loading frame to eliminate slippage of the specimen during testing. A load cell was placed in series with the actuator and the testing machine, to allow for precise measurements of the applied load. Two clip gauges were placed on either side of the specimen to measure the

Figure 4.2 Experimental Set-up and Loading System

average tensile strain of the steel. The clip gauges were supported by two rings on the central portion of the specimen, giving a gauge length of 20 mm. These clip gauges had the ability to measure strain up to 25% in tension with acceptable resolution. For each test, the complete stress-strain curve of the steel was recorded by a high speed data acquisition system. The sampling rate was adjusted for the respective strain rates in order that approximately 500 points were obtained for each set of curves. Preliminary tests were performed in the elastic range of the steel to allow for calibration of the machine's speed in order to obtain the desired strain rate in the instrumented gauge length.

A temperature controlled chamber, approximately 0.5 m x 0.5 m x 0.5 m, was installed around the specimen to maintain a constant temperature for each test. The temperature was controlled by allowing liquid nitrogen to flow inside the chamber by the use of air pressure. Each steel coupon was accompanied in the chamber by a dummy coupon instrumented with a thermocouple placed in its core. The air temperature surrounding the specimen was measured by placing another thermocouple within the

chamber. The tests were performed when both, the temperature inside the dummy coupon and the chamber's internal air temperature, reached the desired thermal reading.

4.2.3 Test Results

Table 4.2 presents the results of the material properties for the various tests performed on the reinforcing steel. Figure 4.3 presents the tensile stress-strain curves of two steel coupons under the two most extreme conditions considered : one tested at a temperature of +20°C with a strain rate of 80 x 10^{-6}/s (quasi-static condition), and the other, tested at a temperature of -40°C with a strain rate of 0.1/s (extreme seismic condition). It was seen that the combined effects of strain rate and low temperature, caused an increase in both, the yield strength and the ultimate strength of the reinforcing

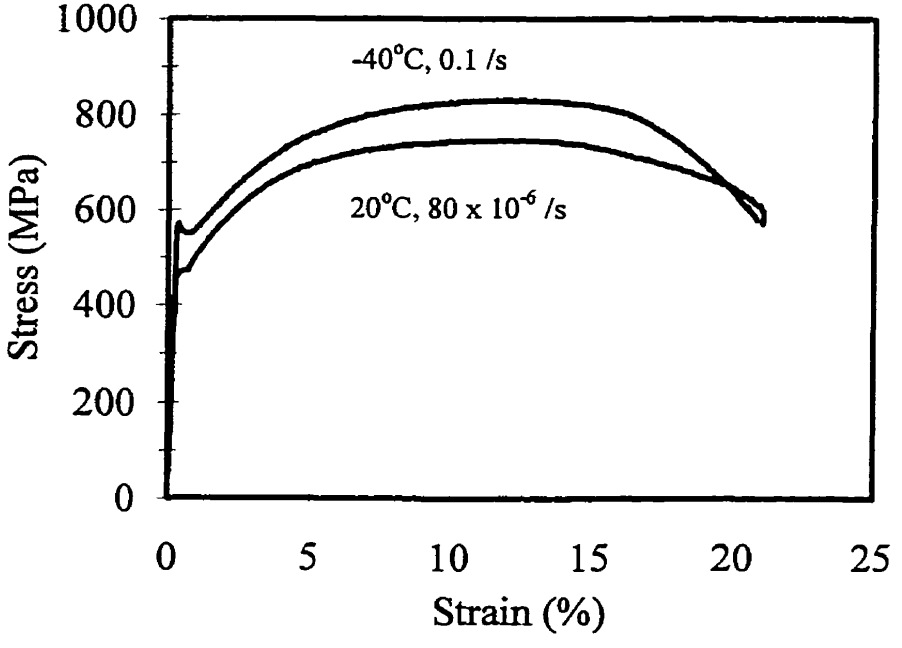

Figure 4.3 Tensile Stress-Strain Curves from two Tests on Steel Coupons

Table 4.2 Test Results on Reinforcing Steel

Temp. (°C)	Strain Rate $\dot{\varepsilon}$ ($x10^{-6}$/s)	Test No.	Young's Modulus E (GPa)	Yield Stress F_y (MPa)	Tensile Stress F_u (MPa)	Strain @ F_y (%)	Strain @ F_u (%)	Ult. Tensile Strain (%)
+20°C	80	1	190	464	741	0.26	13.3	24.4
		2	193	467	747	0.25	12.4	21.3
	5 000	1	197	492	780	0.30	12.9	21.1
		2	195	494	777	0.30	11.7	20.2
	20 000	1	196	490	768	0.31	12.2	20.3
		2	172	485	761	0.30	11.3	20.6
	100 000	1	166	496	778	0.31	11.2	20.7
		2	181	496	780	0.32	11.0	20.3
-20°C	80	1	193	492	782	0.32	11.6	21.6
		2	163	482	781	0.33	12.2	21.0
	5 000	1	178	505	813	0.29	13.9	21.9
		2	191	501	802	0.34	12.7	20.2
	20 000	1	191	525	821	0.31	12.1	20.6
		2	221	526	820	0.28	10.8	19.1
	100 000	1	201	545	820	0.30	15.8	21.2
		2	204	536	826	0.30	12.0	21.2
-40°C	80	1	200	499	823	0.29	11.6	20.0
		2	182	494	803	0.31	12.5	23.2
	5 000	1	183	517	819	0.33	12.0	21.3
		2	204	516	821	0.32	13.1	21.4
	20 000	1	204	539	819	0.32	11.5	20.0
		2	254	544	827	0.29	12.6	20.2
	100 000	1	198	574	840	0.32	11.9	20.1
		2	199	562	832	0.32	12.2	21.2

steel. On the other hand, the ultimate tensile strain and Young's modulus were not significantly affected by the strain rate and temperature.

The variation of Young's modulus of reinforcing steel with strain rate and temperature is shown in Figure 4.4 for the complete range of test variables. The Young's modulus was found by measuring the slope of the stress-strain curve, up to 50% of the yield stress for each test specimen. When comparing the Young's modulus to the change in strain rate and temperature, it was noticed that these variables had little affect, with the values remaining constant at about 200 000 MPa.

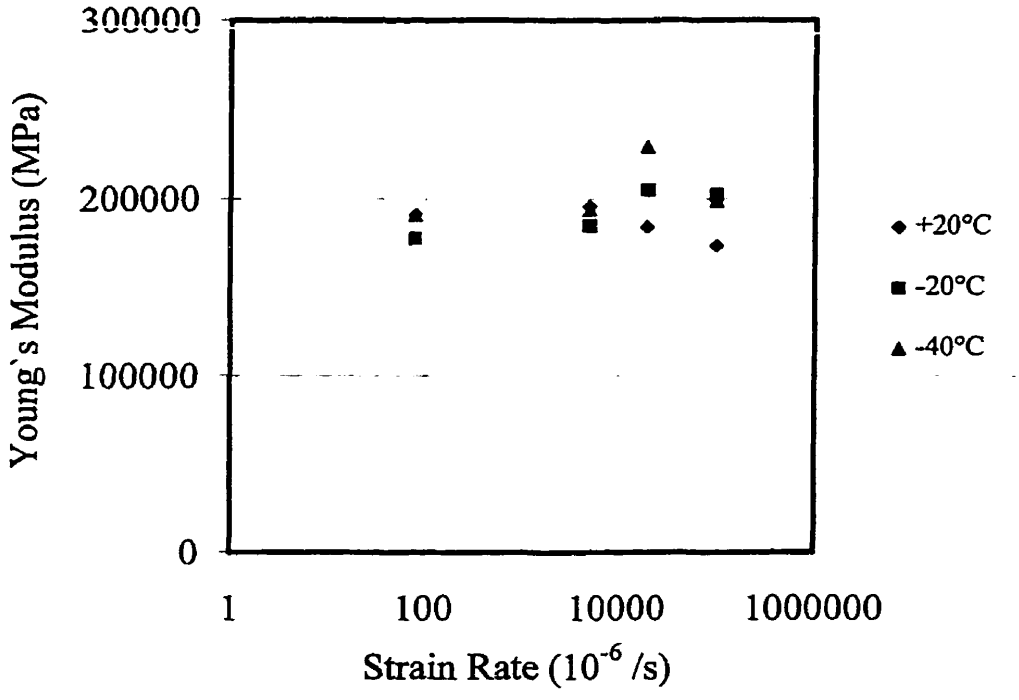

Figure 4.4 Variation of Young's Modulus of Reinforcing Steel with Strain Rate and Temperature (Mean Value of Two Tests at Each Temperature)

The variation of yield stress with strain rate and temperature is shown in Figure 4.5. It was seen, that as the temperature decreases the yield strength increases. A 22% increase in the yield strength was observed when the strain rate increased from 80 x 10^{-6} /s to 0.1/s and while the temperature decreased from +20°C to -40°C. This variation of the yield strength of the reinforcing steel can be modelled by the following formula based on a multiple regression analysis of the experimental results:

$$\frac{F_{yDT}}{F_{yS20}} = [1.022 - 0.0011T]\left[1 + (0.0115 - 0.0001T)\ln\left(\frac{\dot{\varepsilon}}{80x10^{-6}}\right)\right] \qquad [4.1]$$

where F_{yDT} is the dynamic yield strength of reinforcing steel for a strain rate $\dot{\varepsilon}$ at a given temperature T, F_{yS20} is the quasi-static yield strength of reinforcing steel ($\dot{\varepsilon}$=80 x 10^{-6} /s) at a temperature of +20°C, T is the temperature in °C (-40°C ≤ T ≤ +20°C) and $\dot{\varepsilon}$ is the strain rate in s^{-1} (80 x 10^{-6} /s ≤ T ≤ 0.1 /s). Equation [4.1] is plotted in Figure 4.5 for the different strain rates and temperatures. The first term on the right-hand-side of Equation [4.1] gives the ratio between the quasi-static strength at a given temperature to the quasi-static strength at +20°C. The second term on the right-hand-side of the equation represents the ratio of the dynamic yield strength for a strain rate $\dot{\varepsilon}$ and a temperature T, to the quasi-static yield strength at the same temperature, T.

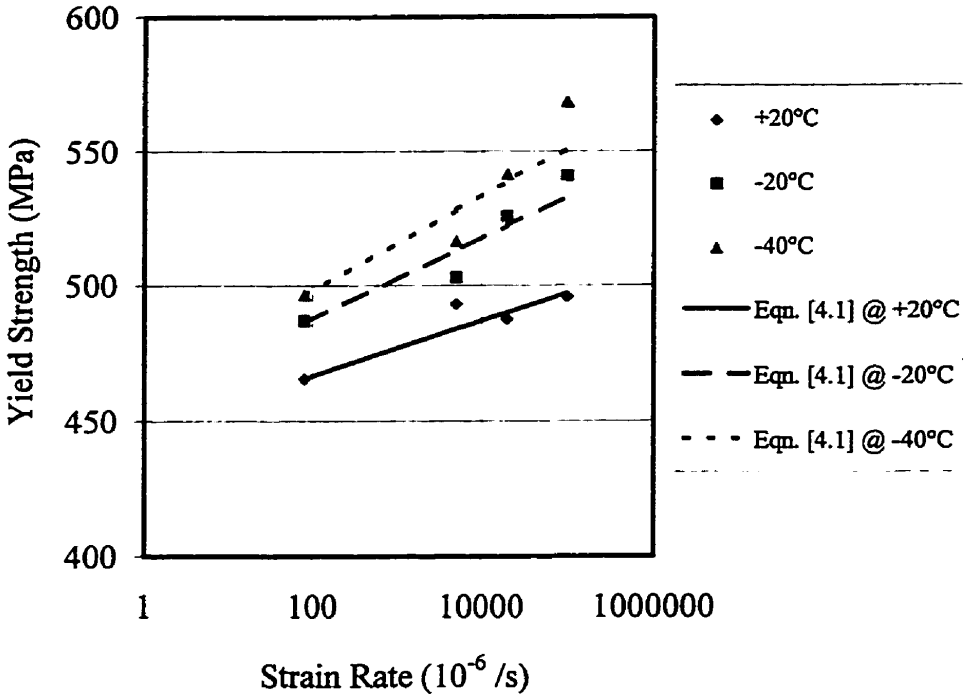

Figure 4.5 Variation of Yield Strength of Reinforcing Steel with Strain Rate and Temperature (Mean Value of Two Tests for Each Temperature and Strain Rate)

Figure 4.6 shows the variation of tensile strength of reinforcing steel with strain rate and temperature. The tensile strength of the steel increased as the strain rate increases and the temperature is lowered. Although there was an increase in the tensile strength, it was not as drastic compared to the yield strength. The tensile strength increased by 12% when the strain rate increased from 80 x 10^{-6} /s to 0.1 /s and the temperature fell from +20°C to -40°C. Again, as was seen above, this variation of the tensile strength of the reinforcing steel can be modelled by the following formula based on a multiple regression analysis of the experimental results :

$$\frac{F_{uDT}}{F_{uS20}} = [1.03 - 0.0015T]\left[1 + (0.0064 + 0.00005T)\ln\left(\frac{\dot{\varepsilon}}{80x10^{-6}}\right)\right] \qquad [4.2]$$

where F_{uDT} is the dynamic tensile strength of reinforcing steel for a strain rate $\dot{\varepsilon}$ at a given temperature T, F_{uS20} is the quasi-static tensile strength of reinforcing steel ($\dot{\varepsilon}$ = 80 x 10^{-6} /s) at a temperature of +20°C, T is the temperature in °C (-40°C ≤ T ≤ +20°C) and $\dot{\varepsilon}$ is the strain rate in s^{-1} (80 x 10^{-6} /s ≤ T ≤ 0.1 /s). The predictions of Equation [4.2] are shown in Figure 4.6.

Figure 4.7 shows the variation of the ultimate tensile strain of reinforcing steel with strain rate and temperature. The tensile strain reduces slightly when the strain rate increases ($\dot{\varepsilon}$ ≥ 0.02 /s). However, no correlation could be observed between the variation of the tensile strain of reinforcing steel and the temperature.

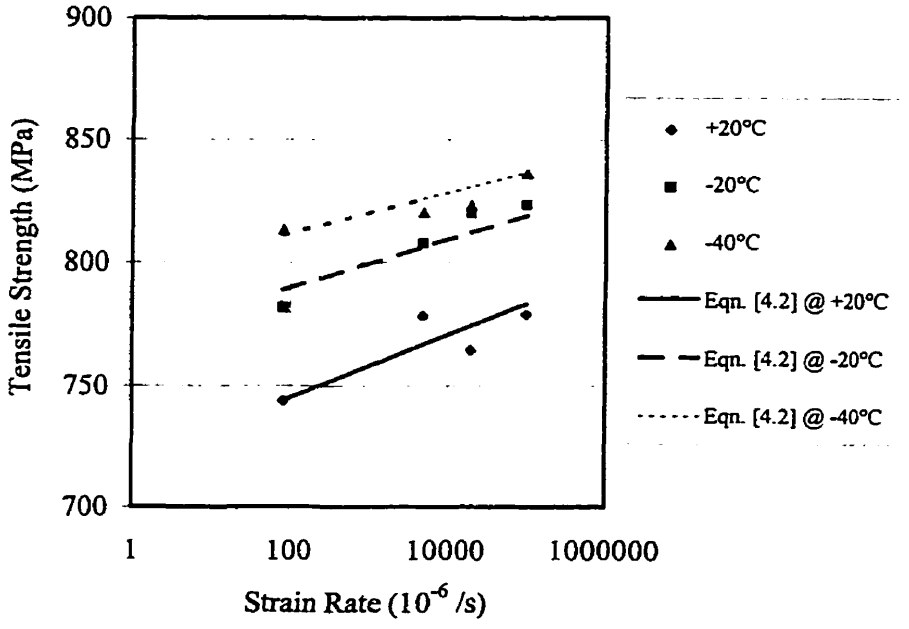

Figure 4.6 Tensile Strength of Reinforcing Steel with Strain Rate and Temperature (Mean Value of Two Tests for Each Temperature and Strain Rate)

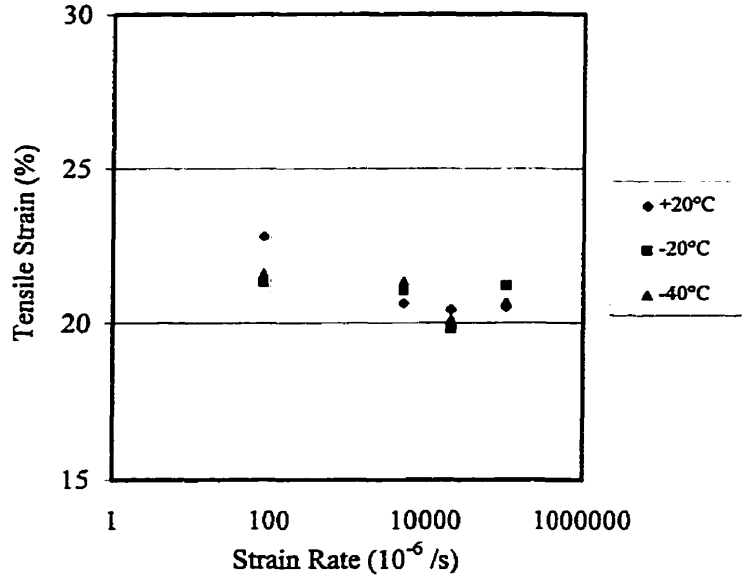

Figure 4.7 Ultimate Tensile Strain of Reinforcing Steel with Strain Rate and Temperature (Mean Value of Two Tests for Each Temperature and Strain Rate)

4.3 Test Programme on Concrete

4.3.1 Test Cylinders

The maximum capacity of the testing machine was 100 kN, therefore, the size of the concrete test cylinders were limited to a diameter of 38 mm and a height of 76 mm for the test programme. Table 4.3 presents the concrete mix (nominal compressive strength of 20 MPa) used to cast the cylinders. It should also be noted that all cylinders were cast from a single concrete batch to minimize the variations in material properties. The cylinders were cured in a moisture room (100% relative humidity) for 30 days, and then, they were placed in an environmentally-controlled room, at a relative humidity of 50%, for 15 days prior to testing.

Table 4.3 Concrete Mix Used for Test Cylinders

Material	Dosage
Type 30 cement	210 kg/m^3
Water	170 kg/m^3
Sand	1130 kg/m^3
6 mm aggregate	800 kg/m^3
Water/cement ratio	0.80

4.3.2 Experimental Set-up and Procedure

The test programme for the concrete cylinders followed the same outline as was used for the tensile tests for the reinforcing steel. The same loading frame was also used to perform the compressive tests. Prior to testing, each test cylinder were measured and their precise dimensions were recorded. To ensure that a pure axial compressive load was applied to each test cylinder, the specimens were centrally placed between the cross-heads of the machine. A spherical bearing was also inserted between two steel plates and placed under the cylinder to protect against uneven loading.

Again, the applied load was measured with the use of a load cell placed in series with the actuator of the testing machine. The tensile strain of the concrete was measured by two displacement transducers (LVDTs) on each side of the cylinder. Figure 4.8 shows a schematic of the test cylinder. The LVDTs had a gauge length of 50 mm and were inserted between two circular rings, which were attached at each end of the cylinder. Again for each test, the complete compressive stress-strain curve of the concrete was recorded by a high speed data acquisition system. The sampling rate was adjusted for each strain rate in order to obtain approximately 500 points for each set of curves. Preliminary tests, in the elastic range of the concrete (stress less than $0.4f'_c$) allowed for the calibration of the machine's speed to obtain the desired strain rate.

These preliminary tests also gave the ability to centre the cylinders, based on the readings of the two LVDTs.

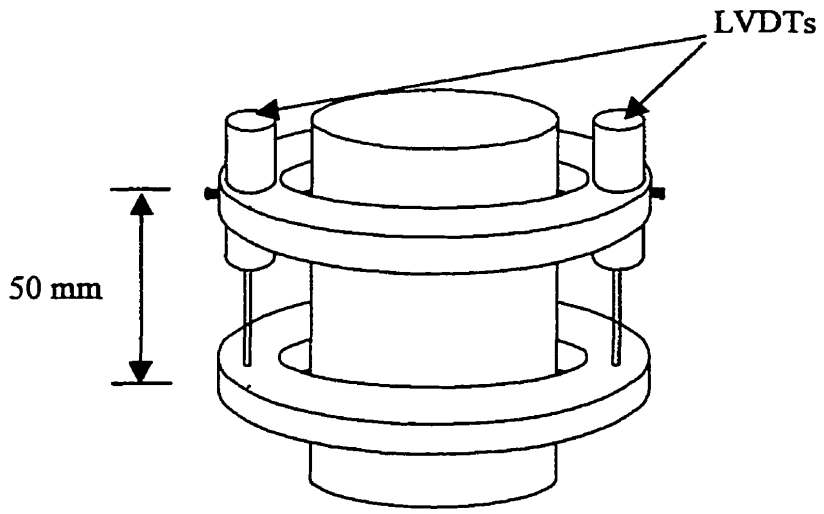

Figure 4.8 Concrete Test Cylinder

To maintain a constant temperature during each test, the temperature controlled chamber was again installed around the specimen. Each concrete cylinder tested was accompanied in the chamber by a dummy cylinder instrumented with a thermocouple in its core. Again, a thermocouple was placed within the chamber to measure its internal temperature. The tests were performed when both of the thermocouple readings were stabilized at the desired temperature.

4.3.3 Test Results

Table 4.4 presents the results of the material properties from the compressive concrete tests. Figure 4.9 presents the complete compressive stress-strain curves of two concrete cylinders obtained from tests under the two most extreme testing conditions : one tested at a temperature of +20°C and under a strain rate of 80 x 10^{-6} (quasi-static

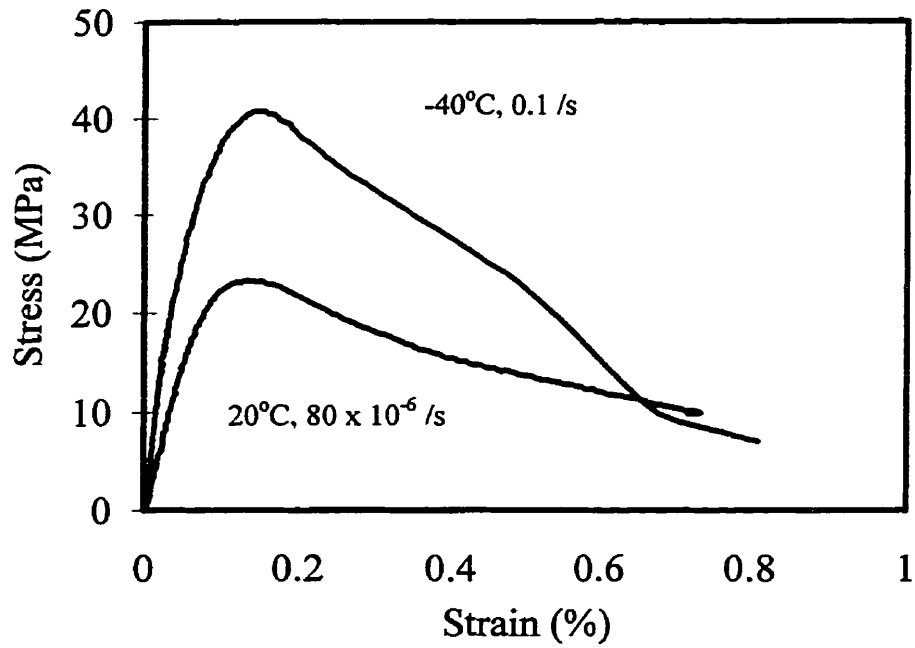

Figure 4.9 Compressive Stress-Strain Curves of Two Tests on Concrete Cylinders

condition), and the other, tested at a temperature of -40°C and under a strain rate of 0.1 /s (extreme seismic condition). The combined effects of strain rate and low temperature caused considerable increases in the compressive strength (f'_c) and Young's modulus of the concrete. On the other hand, there was no evidence that the ultimate compressive strain at peak stress (strain which occurs at maximum stress) is affected by combining strain rate and temperature. The peak stress occurred lower than the expected value of 0.2% strain, which can be explained due to the size effect of the concrete cylinders.

The variation of Young's modulus of concrete with strain rate and temperature is shown in Figure 4.10, for the complete range of test variables. For each test cylinder, the Young's modulus was found by measuring the slope of the stress-strain curve from 0

Table 4.4 Test Results on Concrete Cylinder

Temp. (°C)	Strain Rate $\dot{\varepsilon}$ ($x10^{-6}$/s)	Test No.	Young's Modulus E (GPa)	Compressive Strength f'_c (MPa)	Ultimate Compressive Strain (%)
+20°C	80	1	31.6	23.2	0.13
		2	32.8	17.6	0.19
	5 000	1	27.8	24.3	0.18
		2	33.9	20.9	0.16
	20 000	1	31.3	27.5	0.17
		2	37.7	29.0	0.17
	100 000	1	63.7	23.9	0.10
		2	34.0	32.1	0.13
-20°C	80	1	29.4	24.9	0.26
		2	37.2	25.5	0.11
	5 000	1	43.2	32.1	0.18
		2	29.5	23.4	0.19
	20 000	1	43.2	28.0	0.12
		2	30.9	26.6	0.14
	100 000	1	59.9	31.9	0.10
		2	64.6	36.4	0.18
-40°C	80	1	58.1	33.8	0.16
		2	38.8	28.8	0.13
	5 000	1	46.2	31.9	0.13
		2	38.3	28.7	0.15
	20 000	1	40.9	39.0	0.23
		2	55.6	35.3	0.15
	100 000	1	66.6	37.0	0.12
		2	61.8	40.8	0.14

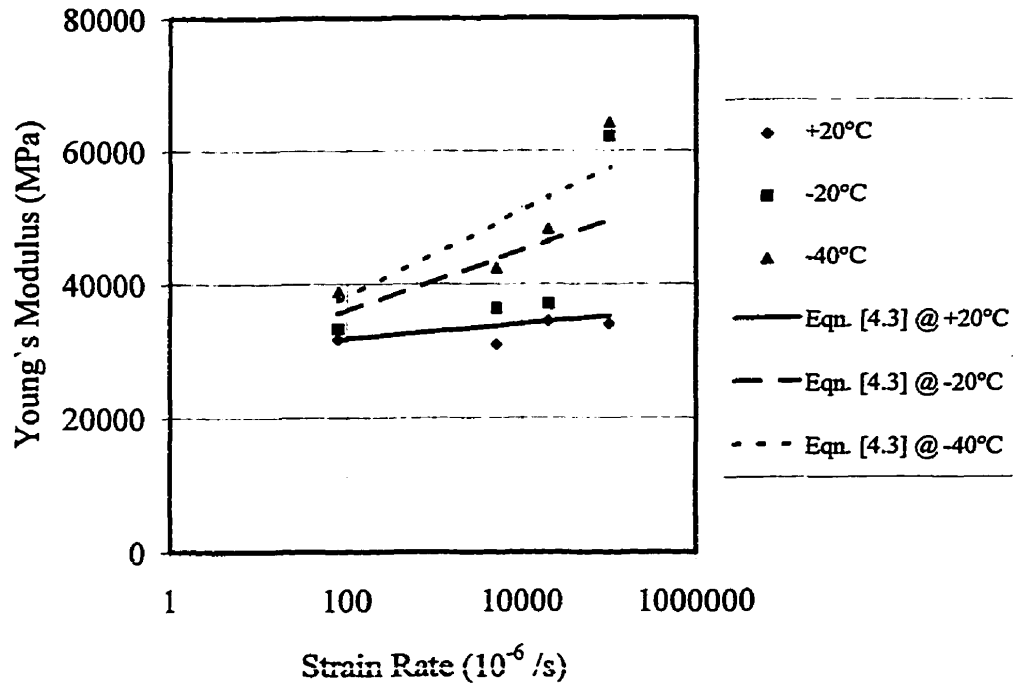

Figure 4.10 Variation of Young's Modulus of Concrete with Strain Rate and Temperature (Mean Value of Two Tests for Each Temperature and Strain Rate)

to 40% of the compressive strength of the concrete. It was seen that the Young's modulus generally increases as the strain rate increases and the temperature lowers.

The test results showed that, at +20°C, the Young's modulus increases marginally over the complete range of strain rates. However, at -20°C and -40°C, significant increases in the Young's modulus was seen when the strain rates were at 0.02 /s and higher. This variation of Young's modulus of concrete can be approximated by the following regression formula :

$$\frac{E_{DT}}{E_{S20}} = [1.06 - 0.003T]\left[1 + (0.0334 - 0.0009T)\ln\left(\frac{\dot{\varepsilon}}{80x10^{-6}}\right)\right] \qquad [4.3]$$

where E_{DT} is the dynamic Young's modulus of concrete for a strain rate $\dot{\varepsilon}$ at a given temperature T, E_{S20} is the quasi-static Young's modulus of concrete ($\dot{\varepsilon}$=80 x 10^{-6} /s) at a temperature of +20°C, T is the temperature in °C (-40°C ≤ T ≤ +20°C) and $\dot{\varepsilon}$ is the strain rate in s^{-1} (80 x 10^{-6} /s ≤ T ≤ 0.1 /s). Equation [4.3] is plotted in Figure 4.10 for the different strain rates and temperatures.

Figure 4.11 presents the variation of the compressive strength of concrete with strain rate and temperature. The compressive strength increases substantially as the strain rate increases and temperature decreases. A 91% increase was observed when the strain rate increased from 80 x 10^{-6} /s to 0.1 /s and the temperature was lowered from +20°C to -40°C. This variation of the compressive strength of the concrete can be modelled by the following formula based on a multiple regression analysis of the experimental results :

$$\frac{f'_{cDT}}{f'_{cS20}} = \left[1.159 - 0.008T\right]\left[1 + (0.0493 + 0.0007T)\ln\left(\frac{\dot{\varepsilon}}{80x10^{-6}}\right)\right] \qquad [4.4]$$

where f'_{cDT} is the dynamic compressive strength of concrete for a strain rate $\dot{\varepsilon}$ at a given temperature T, f'_{cS20} is the quasi-static compressive strength of concrete ($\dot{\varepsilon}$= 80 x 10^{-6} /s) at a temperature of +20°C, T is the temperature in °C (-40°C ≤ T ≤ +20°C) and $\dot{\varepsilon}$ is the strain rate in s^{-1} (80 x 10^{-6} /s ≤ T ≤ 0.1 /s). The predictions of Equation [4.4] are shown in Figure 4.11.

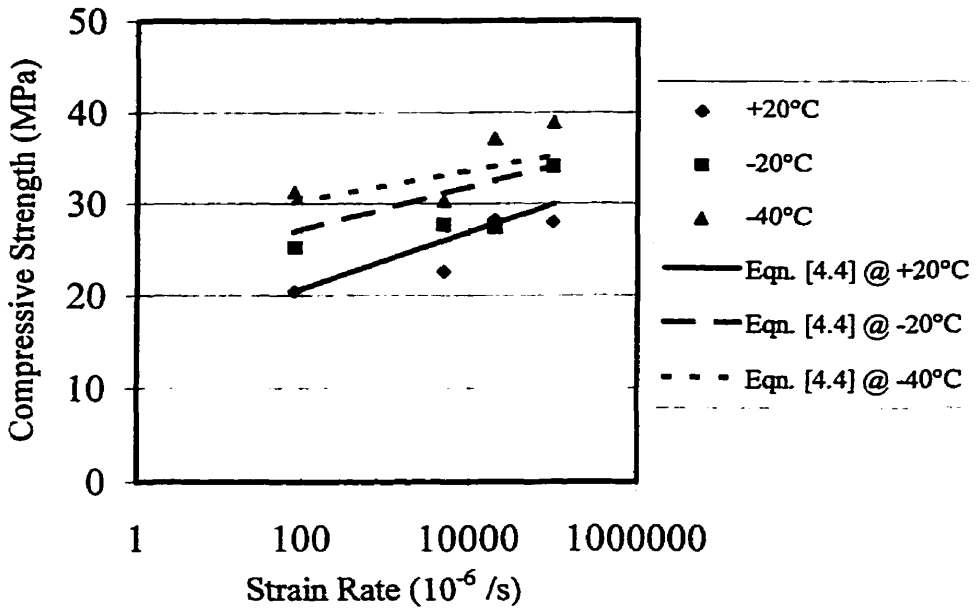

Figure 4.11 Variation of the Compressive Strength of Concrete with Strain Rate and Temperature (Mean Value of Two Tests for Each Temperature and Strain Rate)

4.4 Discussion

The results of tensile tests on machine reinforcing steel coupons and compressive tests on concrete cylinders, under earthquake-type strain rates (quasi-static to 0.1 /s) and at temperatures representative of winter and summer conditions in cold regions (-40°C to +20°C), gave the ability to quantify the combined effects of these two parameters on the basic stress-strain behaviour of these two construction materials. Based on the results obtained, the following observations can be made :

- The ultimate tensile strain and Young's modulus of reinforcing steel are not significantly influenced by the combined effect of strain rate and temperature.

- The combined effects of strain rate and low temperatures causes an increase in both, the yield and ultimate stress of the reinforcing steel. The yield and ultimate stresses increased by 22% and 12%, respectively, when the strain rate increased from 80 x 10^{-6} /s to 0.1 /s and the temperature decreased from +20°C to -40°C.
- The combined effect of strain rate and low temperature caused a substantial increase in the compressive strength and Young's modulus of the concrete. An increase of 91% was observed when the strain rate increased from 80 x 10^{-6} /s to 0.1 /s and the temperature decreased from +20°C to -40°C.

4.5 Recommendations

Although this experimental study helped to bring forth information concerning the combined effect of high strain rates and low temperature and cast some light on the material properties of reinforcing steel and concrete, more research is still warranted. In respect to the effect of strain rate and temperature on reinforced bridge structures located in active seismic cold regions, information is needed on the following :

- The size effects (aggregate size, cylinder diameter, concrete strength, bar diameter, etc.) on the results obtained in this study.
- The combined effects of strain rate and low temperature on the cyclic behaviour of reinforcing steel and concrete.
- The influence of moisture content in concrete.
- The extrapolation of the basic monotonic and cyclic stress-strain behaviours of reinforcing steel and concrete to the complete responses of reinforced concrete members under earthquake-type excitations at low temperatures.

CHAPTER 5
DESCRIPTION OF BRIDGE PIER SPECIMENS

5.1 Introduction

A large number of bridge piers in ENA were constructed during the 1960's, prior to recent seismic provisions in buildings codes. The majority of these columns were designed with flexure as their governing criteria, leaving them vulnerable to shear failures. The lack of transversal reinforcement is directly proportional to insufficient ductility of the columns. This, along with the column's behaviour at low temperatures, raised questions about the pier's seismic performance in an ENA environment.

In order to address these concerns, large scale reinforced concrete bridge pier specimens, typical of ENA construction, were fabricated at Ecole Polytechnique in Montreal, Canada, as part of this research project. These specimens were modelled from an existing bridge pier, so that the behaviour of the realistic bridge pier could be interpreted from experimental test results.

5.2 Description of Prototype Bridge Pier

The prototype bridge pier, shown in Figure 5.1 was provided by the Quebec Ministry of Transport, the column has a channeled cross-section (1320 mm x 813 mm) to allow for drainage pipes to be installed in the opening. The clear height of the column, from the foundation cap to the bridge deck was 6100 mm. The pier which was chosen, supports a bridge deck such that the tributary area gives a dead load of 1600 kN. The bridge pier was constructed in two distinct parts, the first being the foundation, and

the second being the column, attached to each other by dowel bars. The dowel bars and the longitudinal bars were connected with a lap splice length of 915 mm. The pier used No. 8 and No. 11, U.S. deformed bars for longitudinal reinforcement (25.4 mm and 35.8 mm diameter, respectively), and No. 4, U.S. deformed bars for the transversal reinforcement (12.7 mm diameter), with a spacing of 305 mm. The cross-section contains 35 longitudinal bars, with the two interior bars being No. 8, while the remaining bars are No. 11. The lap-splice contains 29 bars, all being of type No. 11. It was assumed that longitudinal and transversal reinforcement had a strength of 400 MPa and 350 MPa, respectively. The bridge pier also used a typical concrete mixture and despite the age of the column, the concrete strength was assumed to be 35 MPa.

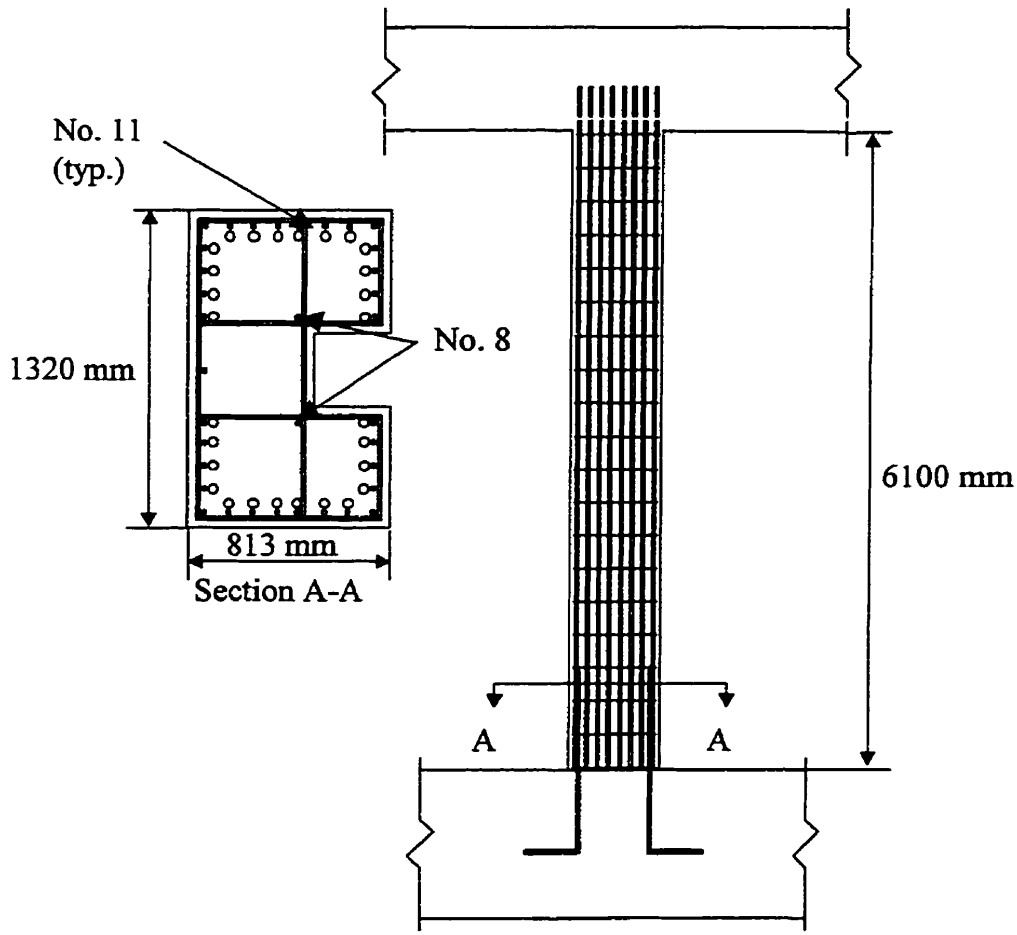

Figure 5.1 Schematic of existing bridge pier

5.3 Description of Model Pier

In the majority of the bridge piers which were damaged due to earthquakes, the principle area of failure was at the foundation-column connection, due to the presence of the lap-splice. Therefore, the lower section of the column was focused on for this research project.

Four columns in the transverse direction supported the prototype bridge pier deck. Therefore, it could be reasonably assumed that for seismic loading in the transverse direction, the presence of the bridge deck would act as a transfer beam, thus causing a fixed connection at the interface of the bridge deck and the column. It was assumed that the column would experience double curvature in the transversal direction, as shown in Figure 5.2. This would cause a zero moment to occur at the inflexion point (mid-height) of the column. To represent this phenomenon, and to make the model as close to reality, the model was scaled to portray half of the prototype, and a pin was place on top of the model to account for the zero moment.

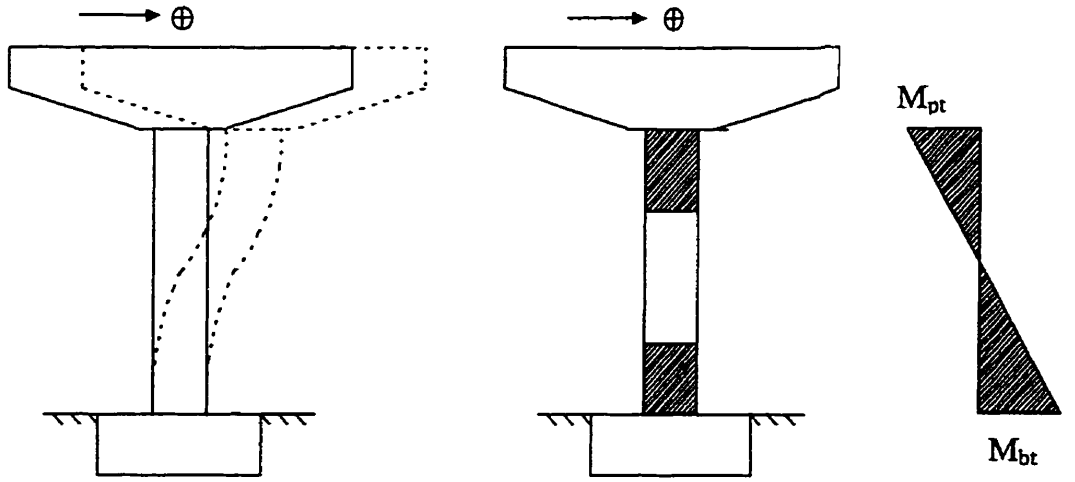

Figure 5.2 Curvature and Moment of Bridge Pier

From the limitations of the laboratory, a scale factor of 3.65 between the linear dimensions of the prototype and the model was selected. The modelled bridge pier, shown in Figure 5.3, also had a channelled cross-section (362 mm x 223 mm), with a square opening (83.5 mm x 83.5 mm). The clear height from the foundation to the centre of the pin was chosen as 853 mm. The specimen was cast in two sections, first being the foundation, and the second being the pier, connected together by dowel bars. A lap splice (250 mm long) was introduced between the dowel bars of the foundation and the longitudinal bars of the pier.

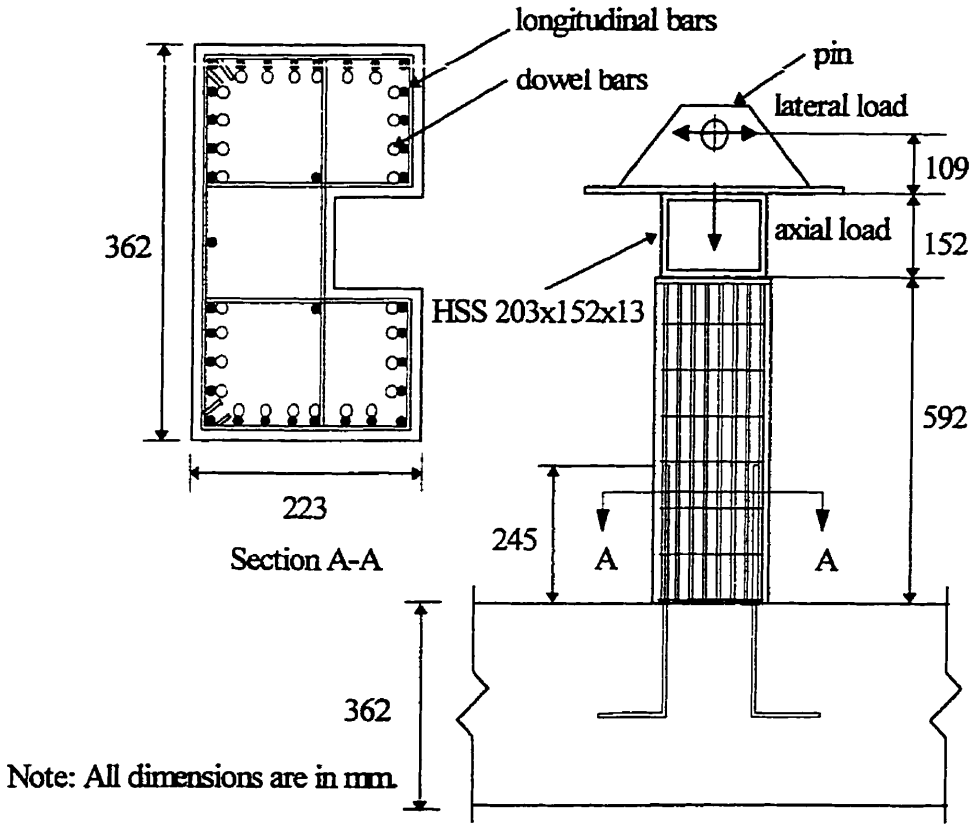

Figure 5.3 Modelled Bridge Pier Specimen

The layout for the reinforcement was the same as for the prototype. For the longitudinal reinforcement, No. 3 U.S. (diameter 9.5 mm) deformed bar, with a yield and ultimate strength of 450 MPa and 690 MPa respectively, were used. A plain 3.6 mm round bar was used for the transverse reinforcement, with a yield strength of 330 MPa. A concrete mix with a maximum aggregate size of 6 mm was used to cast the pier, with a compressive strength of 35 MPa at the time of testing.

A HSS beam (203 mm x 152 mm x 13 mm) was placed between the top of the concrete and pin, as part of the prestressing system. The HSS was used to support two high strength threaded rods, which simulated the dead load on the structure. By attaching these rods from the shake table to the HSS, it was possible to apply an compressive axial load of 120 kN, on the column.

5.4 Dimensional Analysis

Experimental investigations and techniques have always been a vital part of advanced engineering design. The ability to experimentally test a structural model, improves the existing knowledge and provides an alternative in the evaluation of the adequacy of proposed and existing designs. Model analysis in earthquake engineering gives the ability to predict the dynamic response of a prototype structure from laboratory tests on a physical model.

Modelling theory establishes the rules according to which the geometry, material properties, initial conditions, boundary conditions and environmental effects (loading) of the model and the prototype have to be related so that the behaviour of one can be expressed as a function of the behaviour of the other. Therefore, theories of similitude (commonly known as scaling laws) were developed, based on a complete set of correlation functions, which relates the model to the prototype. In general, most of the

structural modelling problems are mechanical ; thus the measures of length, force and time are the principle criteria used in structural modelling.

The theory of dimensions can be summarised by a general theorem stated by Buckingham in 1914, as the follows :

> ''Any dimensionally homogeneous equation involving certain physical quantities can be reduced to an equivalent equation involving a complete set of dimensionless products''.

In order to develop the necessary mathematical relationships between the characteristics of a prototype and the corresponding model must be constructed. This theorem states that the solution equation for some physical quantity of interest, can be written as :

$$F(x_2, x_3,...,x_n) = x_1 \qquad [5.1]$$

where F is a mathematical function and n is the total number of physical quantities involved in the phenomenon. It can also be seen in Equation [5.1], that the expressions x_2 to x_n are dependent upon x_1. According to the Buckingham Pi theorem, every dimensionally homogeneous equation can equivalently be expressed in the form ;

$$f(\pi_2, \pi_3,...,\pi_{n-N}) = \pi_1 \qquad [5.2]$$

where f is another mathematical function and the Pi terms are dimensionless products of the physical quantities x_1 to x_n. Generally , it can be stated that the number N represents the rank of fundamental measures, which is usually equal to the number of basic units needed to describe the physical quantities.

The main question to be resolved in applying the Buckingham Pi theorem pertains to the formation of the appropriate number of Pi terms. In order to correctly specify all of the important terms, insight is required into the physical problem which is to be studied. There are several methods and techniques used in the gathering the Pi terms, one of the less formal techniques involves the following steps:

- Choose the number of fundamental measures (n-N) which are dimensionally independent, required to express all variables of the problem. In other words, if a problem involves the dimensions of force F, length L, and time T, then the three variables chosen must collectively have dimensions which include F, L and T, but no two variables can have the same dimensions. Variables that are in themselves dimensionless (strain, Poisson's ratio, angles) cannot be chosen in the set of fundamental measures.
- Form the Pi terms by taking the remaining variables (N) and grouping them with the (n-N) variables such that all groups are dimensionless, thus producing a set of independent, dimensionless terms.

To investigate the performance of a vibrating structure, it is evident that in addition to length, L, and force, F, which are considered in static loading situations, time, T must also be included as one of the fundamental quantities in the dimensional analysis.

An excellent illustration is given in Filiatrault [1985] showing the determination of scaling laws, where the vibration conditions of an elastic structure constructed from a homogeneous isotropic material, is considered. A typical length in the structure is designated by ℓ and a typical force by Q. The materials for both the prototype and the model are defined by the material constants, which include : the modulus of elasticity E, the Poisson's ratio ν, and the mass density ρ. The important parameters to be determined from the structural shape are the deflected shape δ, the natural frequency f,

and the dynamic stresses, σ. The acceleration due to gravity g, is also considered because it is common in both model and prototype structure. The dimensions of the governing variables in both absolute and common engineering are shown in Table 5.1. This table shows the differences in the units by comparing the commonly used engineering units (F, T and L) to the absolute units (M, L and T)

Table 5.1 Dimensions of Governing Variables for Vibration of Elastic Structures (adopted from Sabnis et al., 1983)

Quantity	Dimensions	
	Absolute System	Engineering System
Length, ℓ	L	L
Force, Q	MLT^{-2}	F
Modulus of elasticity, E	$ML^{-1}T^{-2}$	FL^{-2}
Poisson's ratio, ν	----	----
Mass density, ρ	ML^{-3}	FT^2L^{-4}
Deflection, δ	L	L
Stress, σ	$ML^{-1}T^{-2}$	FL^{-2}
Frequency, f	T^{-1}	T^{-1}
Acceleration, g	LT^{-2}	LT^{-2}

Applying the Buckingham Pi theorem, the number of variables and dimensions are:

$$n = 9 \text{ variables } (\ell, Q, E, \nu, \rho, \delta, \sigma, f, g)$$

$$n\text{-}N = 3 \text{ dimensions } (F, L, T)$$

therefore, the number of Pi terms that can be formed is then:

N = 6 Pi terms

Then three variables are chosen which includes the three dimensions of the problem (F, L, T), hence ℓ (L), E (FL^{-2}) and g (LT^{-2}). Following the laws of the Buckingham Pi theorem, the remaining six variables (δ, σ, ν, ρ, Q, f) are grouped with the primary variables (ℓ, E, g), such that all groups are dimensionless. The dimensionless parameters that govern the behaviour for a true model is:

$$f\left(\frac{\delta}{l}, \frac{\sigma}{E}, \frac{f^2 l}{g}, \frac{\rho g l}{E}, \frac{Q}{El^2}\upsilon\right) = 0 \qquad [5.3]$$

By forcing the dimensionless variables in Equation [5.3] to be identical in the model and the prototype, it is possible to determine the dynamic characteristics of the modelled structure. In order to impose these restrictions on the model design, it is normal to relate the dimensional analysis with scaling factors, as a function of length and modulus of elasticity. A ratio is formed so that the unit of the model is divided by the unit of the prototype, as follows :

$$S_\ell = \frac{\text{length of model}}{\text{length of prototype}} = \frac{\ell_m}{\ell_p} \qquad [5.4]$$

$$S_E = \frac{\text{modulus of elasticity of model}}{\text{modulus of elasticity of prototype}} = \frac{E_m}{E_p} \qquad [5.5]$$

As is summarized in Table 5.2, the implied scale factors which govern these relationships, are expressed as a function of S_ℓ and S_E.

It is seen from this Table, that the density scale is equal to S_E/S_ℓ for a true elastic model and is usually different than one. Therefore, true replica models are extremely difficult to realise because of problems in material simulation. In practice this is usually very expensive, consequently models are often scaled without the effect of gravity forces. It should be noted that an exact replication of all parameters affecting the response of structures under dynamic actions can rarely ever be achieved. It is usually up to the model designer's judgement to decide whether or not the errors introduced by neglecting gravity effects are acceptable.

Table 5.2 Similitude Requirements for Vibration of Elastic Structure (adopted from Sabnis et al., 1983)

Group	Quantity	Dimension (Engineering Units)	Scale Factors	
			True Replica	Gravity Forces Neglected
Loading	Force, Q	F	$S_E S_\ell^2$	$S_E S_\ell^2$
	Gravitational accel., g	LT^{-2}	1	1
	Horizontal accel, g	LT^{-2}	1	S_ℓ
	Time, t	T	$S_\ell^{1/2}$	S_ℓ
Geometry	Linear dimension, ℓ	L	S_ℓ	S_ℓ
	Displacement, δ	L	S_ℓ	S_ℓ
	Frequency, f	T^{-1}	$S_\ell^{-1/2}$	S_ℓ^{-1}
Material properties	Modulus, E	FL^{-2}	S_E	S_E
	Stress, σ	FL^{-2}	S_E	S_E
	Poisson's ratio, ν	----	1	1
	Density, ρ	FL^{-3}	S_E/S_ℓ	Neglected

In the above table, the time scale is equal to $S_\ell^{1/2}$ for a true elastic model and to S_ℓ in the case of a model where gravity loading effects can be neglected. This means that an actual earthquake record should have a different time scale when used as the input for the test of a model. Furthermore, the frequency of vibration is inversely proportional to the period, will be $S_\ell^{-1/2}$ and S_ℓ^{-1} considering and neglecting gravity, respectively. Therefore, the model will have higher frequencies than the prototype structure.

5.5 Comparisons Between Prototype and Model

Due to the feasibility and time constraints, it was decided to neglect the gravity effects to simplify the model. This approach is acceptable since the gravity loads on the pier model is applied by external prestressing. By doing this, it enabled concrete to be used as the material for the model. This in turn forces S_E, the Young's modulus of the model divided by the Young's modulus of prototype, to be equal to one. Considering the laboratory limitations, a scale factor of 3.65 was selected for the length. Thus :

$$S_\ell = 0.274 \qquad [5.6]$$

$$S_E = 1 \qquad [5.7]$$

For a true replica model, the scaling factor for the density should be :

$$S_\rho = \frac{S_E}{S_\ell} = \frac{1}{0.274} = 3.65 \qquad [5.8]$$

Therefore, in theory, the density of the material should of had been 3.65 times of the normal density of concrete. Practically, this could be achieved by attaching a large

number of lumped mass to the specimen, but it was determined that the benefits would not be worthwhile for this project. Discussions found that it was not necessary to represent an exact model since the main goal of this study was to compare the performance of bridge piers at low temperatures.

Table 5.3 shows the differences between the prototype and the model for the various similitude requirements with gravity forces neglected. It can be seen from this table, that all of the quantities follow the scaling laws except for the natural frequency. Due to the laboratory constraints, the concrete blocks used to simulate the bridge deck had a mass of 30 kN/block, therefore, it was decided to used the closest amount of mass to achieve the best frequency, by following the similitude requirements. Although the frequency did not match the prototype exactly, the overall behaviour generally represents the prototype with tolerable differences. Also, in applying a time factor of 3.65, the strain rate is 3.65 higher than in the prototype. Figure 5.4 presents the increase due to increase strain rate. All values were below 2%, with the exception being the compressive strength of concrete, which varied from 8.2-5.7%. Therefore, by implementing the scaling laws, there is little influence on the structure.

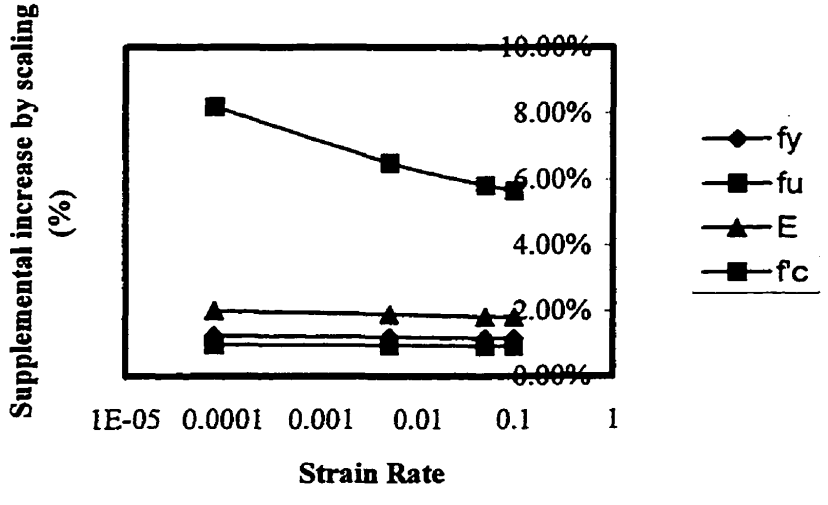

Figure 5.4 Increase Caused by Strain Rate Effects

Table 5.3 Comparison Between Prototype and Model

Quantity	Scaling Factors	Prototype Values	Theoretical Model Values	Actual Model Values	Percent Diff. (%) (theoretical-model)
Gravitational accel., g	1	1 g	1 g	1 g	0.0
Horizontal accel., g	S_ℓ	1 g	0.274 g	0.274 g	0.0
Column height, ℓ	S_ℓ	3048 mm	835 mm	853 mm	2.0
Column cross-section, ℓ	S_ℓ	1321 mm x 828 mm	362 mm x 223 mm	362 mm x 223 mm	0.0
Long, bar diameters, ℓ	S_ℓ	35.8 mm	9.8 mm	9.5 mm	3.2
Lap-splice length, ℓ	S_ℓ	913 mm	250 mm	250 mm	0.0
Stirrup spacing, ℓ	S_ℓ	305 mm	83.5 mm	83.5 mm	0.0
Dead load, ℓ	S_ℓ^2	1594 kN	120 kN	120 kN	0.0
Time, t	S_ℓ	1 s	0.274 s	0.274 s	0.0
Force, Q	$S_E S_\ell^2$	1 kN	0.075 kN	0.075 kN	0.0
Displacement, δ	S_ℓ	1 mm	0.274 mm	0.274 mm	0.0
Frequency, f	S_ℓ^{-1}	3.5 Hz	12.6 Hz	9.1 Hz	29.0
Modulus, E	S_E	26600 MPa	26600 MPa	26600 MPa	0.0
Density, ρ	Neglected	------	------	------	0.0

5.6 Dimensioning the Test Set-up

The test set-up includes three different aspects ; (1) the bridge pier (2) the foundation (3) the steel frame. Each component is discussed and the dimensioning requirements are explained.

5.6.1 Dimensioning the Bridge Pier

The experimental specimen is a 1:3.65 scale model of an existing bridge pier. Figure 5.5 shows the plan view of the cross section for the tested specimens. The column height was 853 mm, from the top of the foundation to the centre of the pin. Excluding the mechanical prestressing system and the pin, the concrete column had a height of 592 mm.

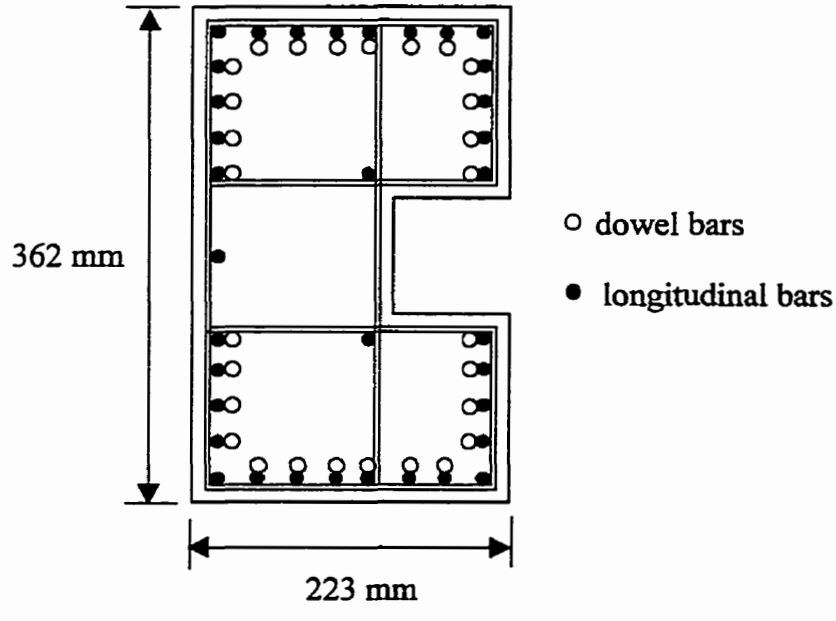

Figure 5.5 Cross Section and Dimensioning of the Bridge Pier Specimen

To respect the scaling laws, No. 3 U.S., deformed bars (9.5 mm diameter) were used for the longitudinal reinforcement, and 3.6 mm diameter plain bars were used for the transversal reinforcement. The stirrups spacing was equal to 83.5 mm, therefore, seven stirrups were placed in the column. The stirrups were tied to the longitudinal reinforcement by using typical tying wire. A 13 mm thick steel plate, with the dimensions corresponding to the column, was fixed to the top of the column. This allowed the longitudinal bars to be welded to the steel plate to ensure proper anchorage of the reinforcement, and to attach the HSS beam to the top of the column.

The dowel bars, which also used No. 3 U.S. deformed bars, had a scaled lap slice length of 245 mm from the base of the column. The compression development length had a length of 200 mm, and had an embedment length of 150 mm, which was in accordance with Clause 15.6 of CSA Standard A23.3-94. A 90° hook was used for the dowel bars to take into account the possibilities of tension and compression forces. The dowel bars were also attached to the longitudinal bars with tying wires. Figure 5.6 shows a photograph depicting the reinforcing cage of the column.

Figure 5.6 Column Reinforcing Cage and Foundation

5.6.2 Dimensioning the Foundation

Several parameters were considered when dimensioning the foundations. To ensure the possibilities of the formation of plastic hinges at the base of the pier, the column had to be properly anchored to the foundation. The width of the foundation beam was restricted to 584 mm, due to the placement of the anchorage keyholes in the shake table. The design must ensure that the foundation remains elastic throughout the experimental tests.

The foundation beam had a length of 1826 mm, a width of 584 mm and a height of 362 mm. The foundation was designed in agreement with CSA Standard A23.3-94, so that yielding would not occur under a maximum probable moment in the column of 215 kN-m. Figure 5.7 shows the detailing for the longitudinal and transversal reinforcment. Six 25M deformed reinforcing bars (three in the upper and lower halves) were placed in the foundation for tension and compression reinforcement, while 15M stirrups were used for shear reinforcements. Eleven stirrups were placed in each foundation at a spacing of 180 mm.

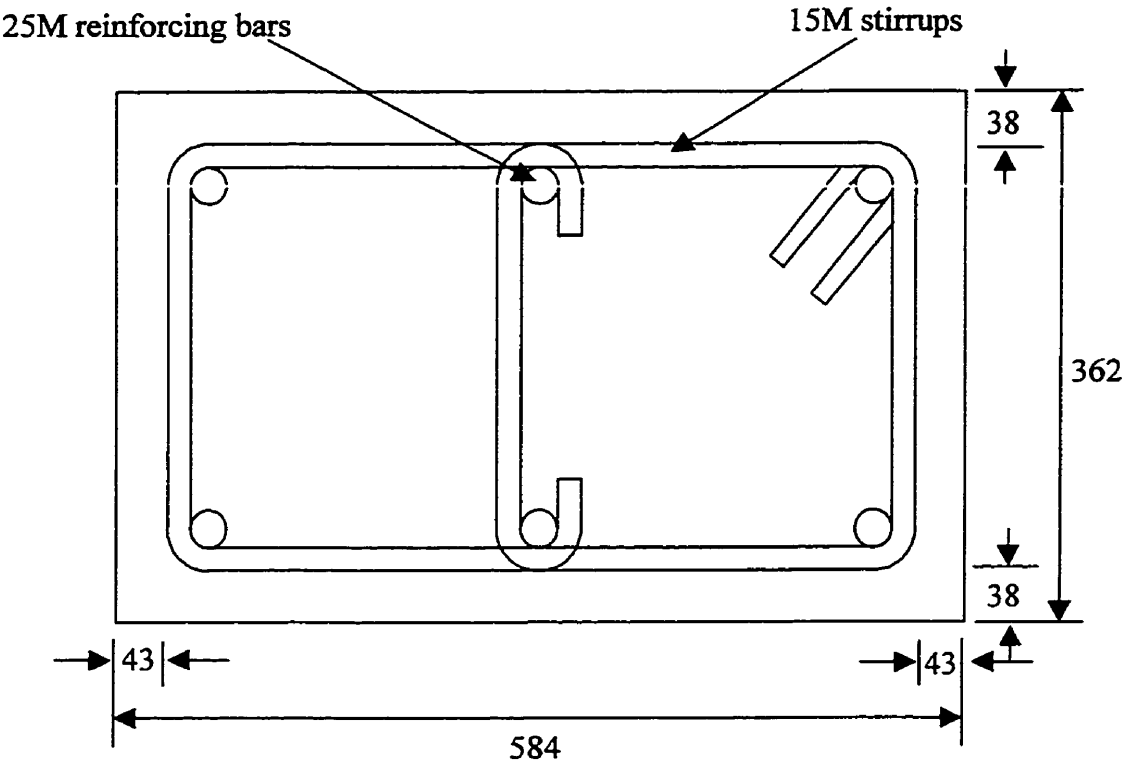

Figure 5.7 Cross Section and Dimensioning of the Foundation

The specimen was fixed to the shake table through the foundation. In order to ensure no slipping of the specimen, the normal force (N) multiplied by a coefficient of static friction (μ_s) must be greater than the maximum base shear (V_{max}). V_{max} is the sum

of the shear forces caused by the maximum probable moments of the column. The base shear was found to be 331 kN (increased by a factor of safety of 1.5). Therefore, N multiplied by the μ_s factor, must be grater than 331 kN, where μ_s equals 0.1 (conservative value for wood-concrete and wood-steel surfaces). It was found that eleven rods were needed to meet these requirements, and prevent yielding of the rods. Therefore, to reduce the size of the foundation, 3.4 m long angle sections (152 mm x 152 mm x 6.4 mm) were placed on either side of the foundation. By connecting these angles to the sides of the foundation, and to the surface of the shake table, it was possible to increase the number of rods to twenty-two, which greatly exceeds the specifications. A schematic of the bridge pier specimen with the corresponding dimensions are shown in Figure 5.8.

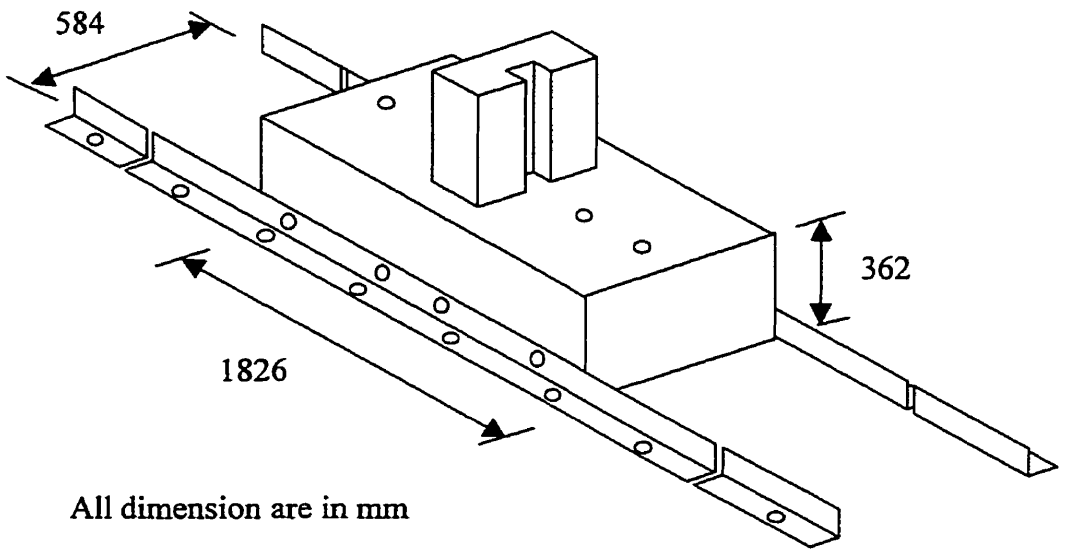

Figure 5.8 Connection System of Bridge Pier

5.6.3 Dimensioning of the Steel Frame

A previously constructed steel frame was modified to represent the bridge deck. The steel frame supported two concrete blocks (30 kN each) which simulated the mass of the superstructure. These concrete blocks were supported by a peripheral frame, which surrounded the pier specimen. The steel frame supported all the vertical loads from the concrete blocks, in such a manner, that the bridge pier carried only the lateral inertia loads. This peripheral frame was completely pinned in the direction of the shake table motion and braced in the opposite direction (perpendicular to the table motion) to prohibit any movement of the specimen in this direction.

To accommodate the scaled bridge pier specimen, HSS (127 mm x 64 mm x 6.4 mm) columns were fabricated for the peripheral frame, which brought the total height of the frame, including the masses to approximately 1600 mm. Security bracing with slotted holes were installed, in the direction of the table motion, to prevent against large unexpected displacements. Figure 5.9 shows a schematic of the steel frame set-up.

5.7 Description of the Bridge Pier Specimens

The final assemblage of the specimen and the experimental set-up on the shake table is shown in Figure 5.10. The threaded rod in the middle of the column shows the prestressing system. Pins were fabricated to be positioned at the base of the rods to minimise the bending during testing. The prestressing rods were supported at the top by a HSS section. To increase the stiffness of the HSS section, concrete was placed within its core. Strain gauges were placed on the rods and calibrated so that the correct amount of torque could be applied to the rods.

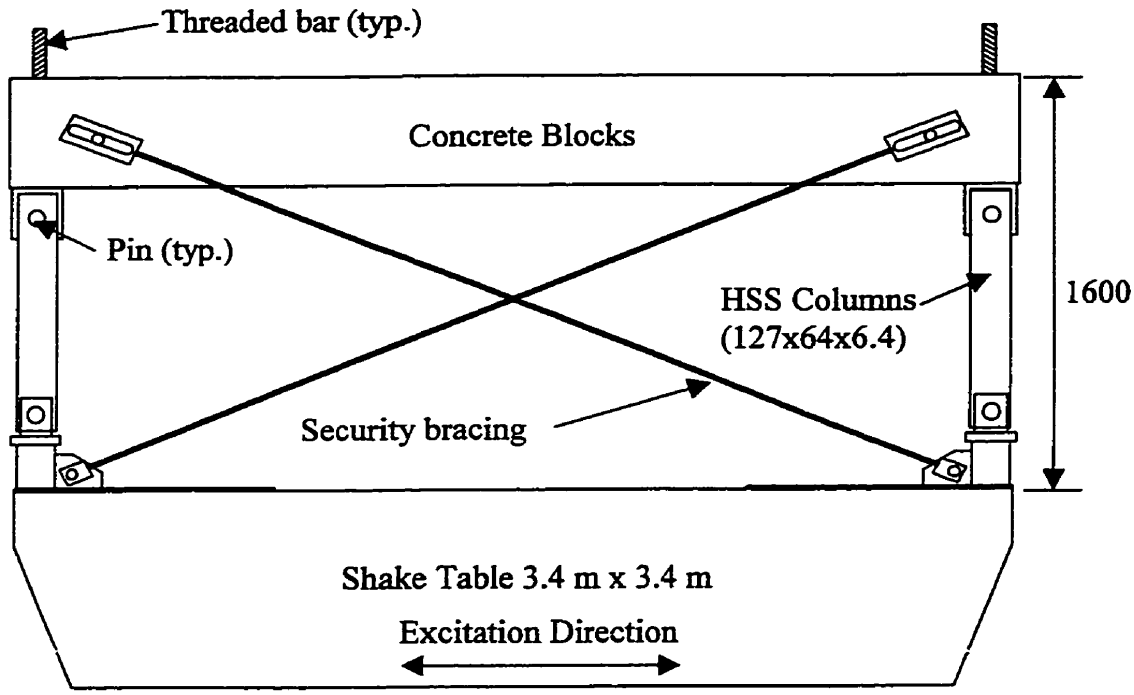

Figure 5.9 Steel Frame Set-Up

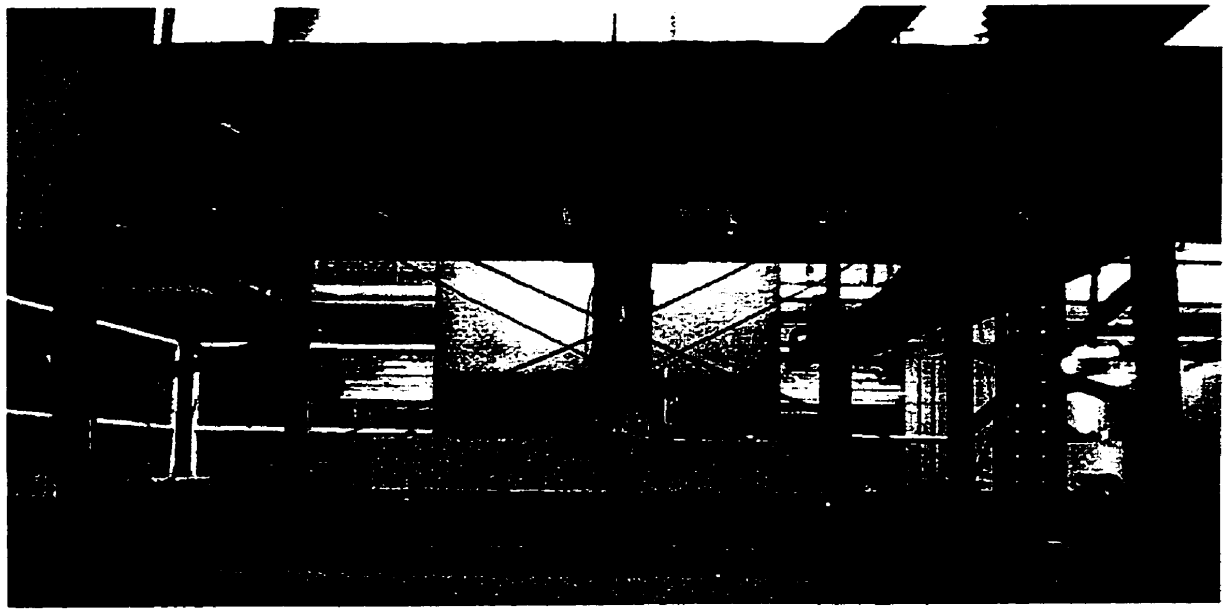

Figure 5.10 Photo of Specimen and Experimental Set-up

Figure 5.11 shows the prestressing system and the pin connection. The pin was connected on top of the HSS section with rods which were threaded into the steel plate at the top surface of the column. Two 25 mm thick steel plates were used to connect the upper portion of the pin to each of the concrete blocks. These concrete blocks were then attached to the steel frame.

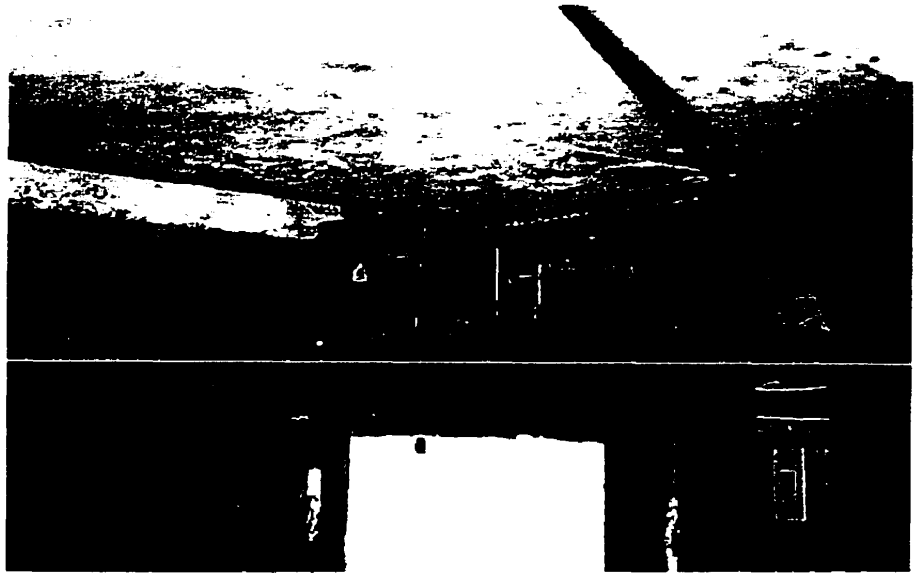

Figure 5.11 Assemblage of the Prestressing and Pin Connection

The experimental set-up was modified in order to perform the quasi-static tests. A reaction beam was designed and fabricated to inhibit the movement of the concrete blocks, thus fixing the pin position, but allowing the motion of the shake table. To ensure zero moment, a pin was placed between the reaction beam and the concrete blocks. The reaction beam was fabricated from a HSS member (152 mm x 152 mm x 13 mm) with a length of 1.2 m, which was then attached to a prefabricated reaction frame. A load cell was placed at the end of the HSS member to measure the force applied to the column. Figure 5.12 shows a photograph of the reaction beam attached to the steel frame and the reaction frame.

Figure 5.12 Assemblage of the Reaction Beam

CHAPTER 6
PRELIMINARY ANALYSES

6.1 Computer Modelling using RESPONSE

The computer program RESPONSE [Collins and Mitchell, 1991] was used to determine the moment-curvature response of a concrete cross section subjected to moment, axial load and shear. RESPONSE is a complex program compiled using TURBO C for personal computers. This program was developed as an educational tool, but due to recent upgrades, RESPONSE is now a popular program for an understanding of the behaviour of concrete structures. The program offers several options in the modelling of reinforced and prestressed concrete structures. The RESPONSE program provides the user the ability to combine different types of loading to find the theoretical response of the structure (i.e. axial and moment loading to find the curvature response). The program offers possibilities to configure several options, including concrete stress-strain (high-strength or parabolic model), shear model and strength reduction factors. Also the program allows the user to set convergence limits, thus setting the level of accuracy of the results. RESPONSE is accompanied with a graphics program which permits several displays of the model cross-section and graphical stress-strain behaviours of concrete and reinforcing steel.

The RESPONSE computer program was used in the preliminary analyses to find interaction curves (axial load-moment) and moment-curvature diagrams. In both cases, analyses of the prototype and the model were performed. By applying the scaling laws and comparing the results, it was possible to see the correspondence between properties of the model and the prototype.

6.1.1 Description of the Model Used with RESPONSE

Figure 6.1 illustrates the model of the cross section which was used in the RESPONSE program. The computer program is limited in its the capacity to model the geometry of the cross section by trapezoidal layers, therefore the RESPONSE model does not directly resemble the actual specimen. All of the layers are forced to be symmetrical around the vertical axis, therefore, the drainage opening was accounted for by placing the concrete for this section symmetrically about the y-axis, as shown in Fig 6.1. The placement of the reinforcing bars are again defined in terms of layers, therefore, the steel at a certain level were placed together. These minor changes in the model, caused some approximations in the final results, but these differences were insignificant and could be ignored.

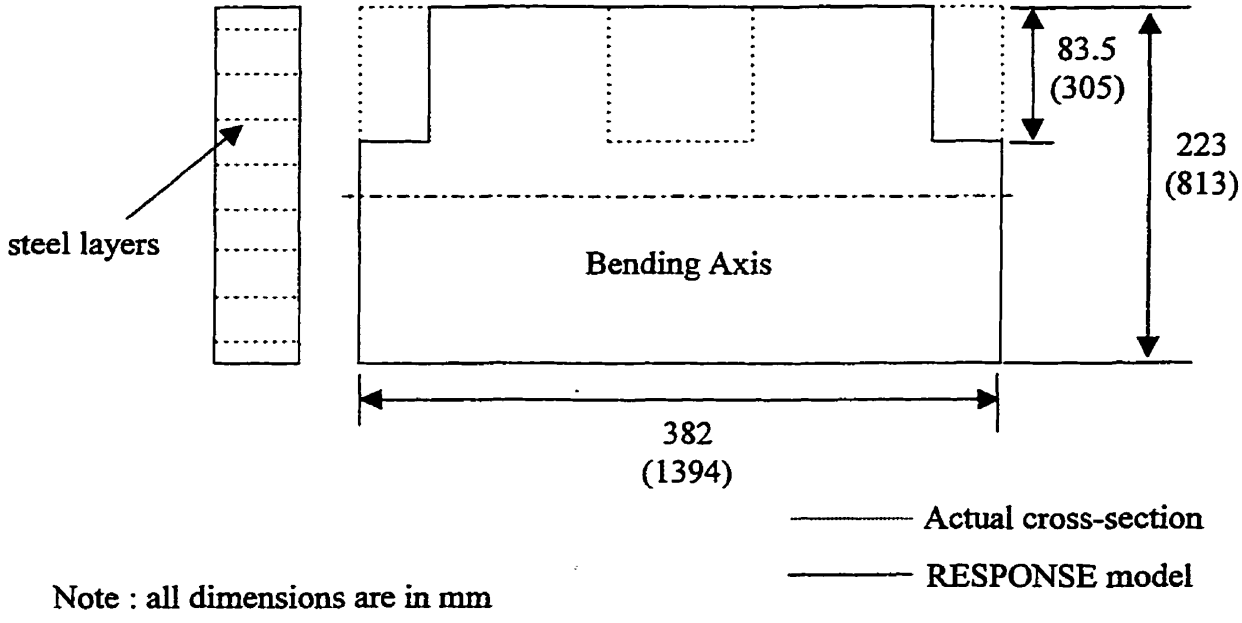

Figure 6.1 RESPONSE Computer Model

The same material properties for the prototype and the model were entered into the program. The Young's modulus used was equal to $E_c = 4500\sqrt{f'c} = 26600$ MPa which is given in Clause 8.6.2.3 from the CSA A23.3-94 Standard. Also, the steel was assumed of typical Grade 400 MPa with a corresponding yield strain of 2000 με.

6.2 Results Obtained from RESPONSE

Various aspects were analysed with the use of the RESPONSE program. Interaction diagrams (P-M) and moment-curvature analyses were carried out to find the strength capacity of the section. Analyses were computed in parallel with the prototype and the model, and by applying scaling laws, the results could be compared.

6.2.1 Interaction Diagrams

Interaction diagrams (P-M) were constructed for both the prototype and the model. For each column, two different cross-sections were analysed, one was within the lap splice region, which included the longitudinal and dowel bars, while the other was above the lap splice, which only accounts for the longitudinal bars. Three different resistance levels were also analysed by changing the material performance factors; factored (ϕ_c =0.6, ϕ_s = 0.85), nominal (ϕ_c =1.0, ϕ_s = 1.0), probable (ϕ_c =1.0, ϕ_s = 1.25). The factored moments are used to ensure that the flexural resistance of each member is equal or greater than the factored loads on the member. The nominal moments are used to ensure that in a beam-column connection, the columns are more resistant than the beams. The probable moments correspond to the maximum possible flexural resistance the element can obtain considering the uncertainty of the yielding limit, f_y, and the possibility of strain hardening in the reinforcing steel. Figures 6.2 and 6.3 show interaction diagrams of the scaled column model, one being above the lap-splice and the

other being within the lap-splice region. Figures 6.4 to 6.5 give a comparison between the model and prototype in the prototype domain.

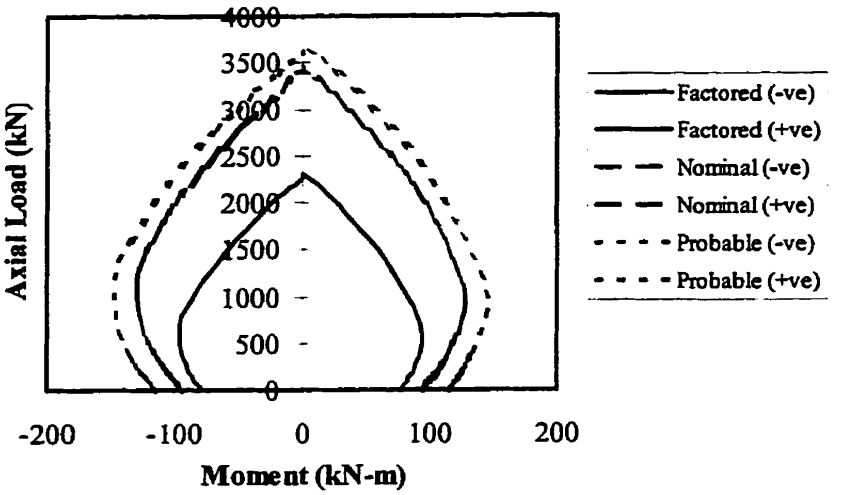

Figure 6.2 Interaction Diagram for Model Above Lap-Splice

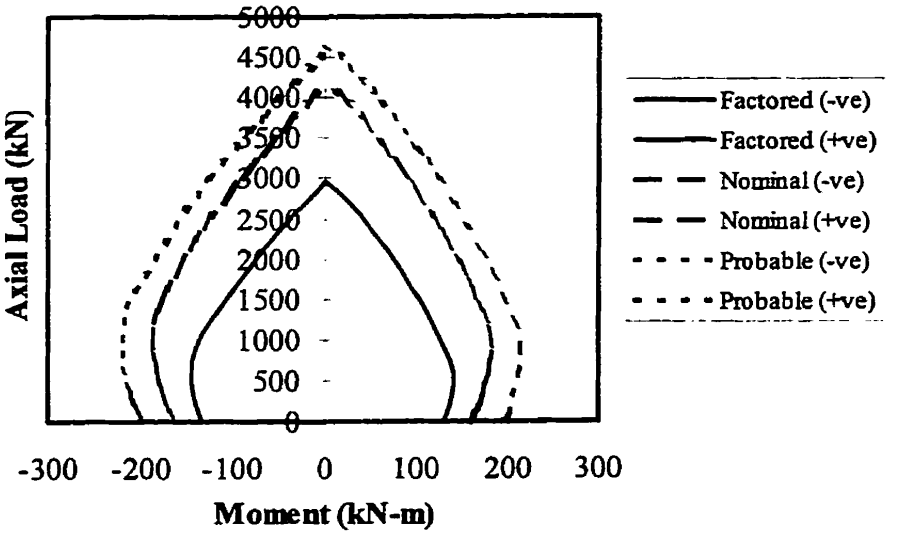

Figure 6.3 Interaction Diagram for Model Within Lap-Splice

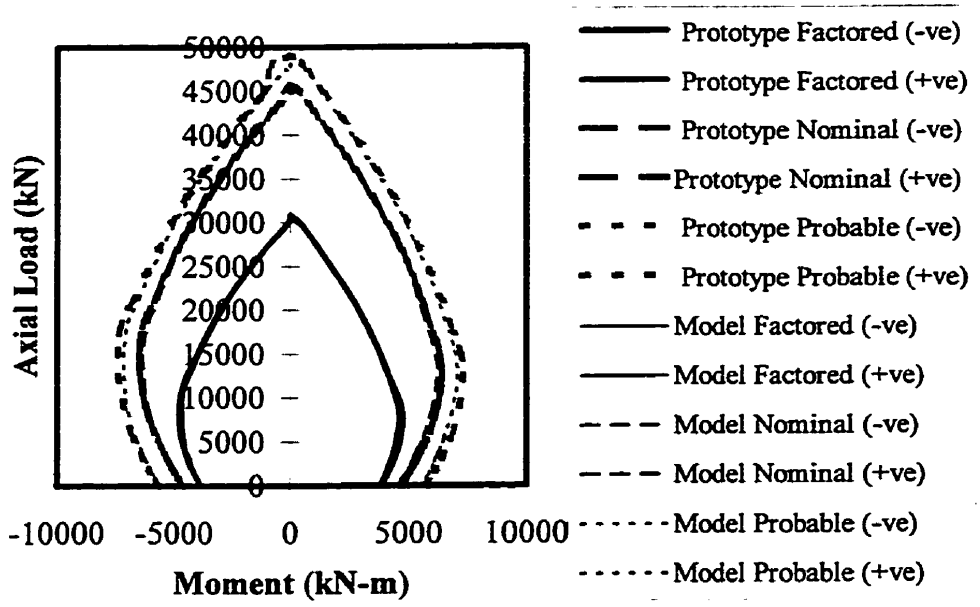

Figure 6.4 Interaction Diagram (P-M) Prototype and Model - Above Lap Splice in Prototype Domain

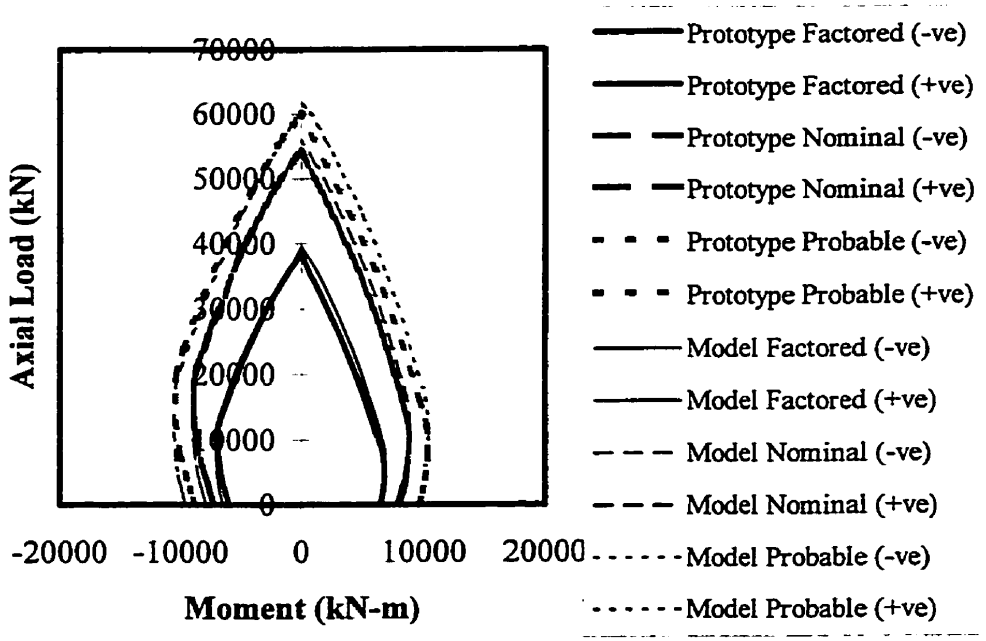

Figure 6.5 Interaction Diagram (P-M) Prototype and Model - Within Lap Splice in Prototype Domain

Table 6.1 presents the absolute values of the different flexural resistance, which correspond to the dead load on each of the respected structures (i.e. 120 kN for the model and 1600 kN for the prototype). Comparison are given between the prototype and the scaled model (multiplied by a factor of S_r^3) to show the close correlation of the two structures.

Table 6.1 Comparison Between prototype and Model at Different Loadings

Design Level	Model (P=120 kN)	Model scaled (P= 1600 kN)	Prototype (P=1600 kN)	Percent Difference
	Above Lap-Splice			
Factored	83 kN-m	4036 kN-m	4250 kN-m	5.3 %
Nominal	101 kN-m	4911 kN-m	5020 kN-m	2.2 %
Probable	122 kN-m	5932 kN-m	6080 kN-m	2.5 %
	Within Lap-Splice			
Factored	134 kN-m	6516 kN-m	6520 kN-m	0.1 %
Nominal	165 kN-m	8023 kN-m	7950 kN-m	0.9 %
Probable	200 kN-m	9725 kN-m	9420 kN-m	3.2 %

6.2.2 Moment-Curvature Diagrams

Moment-curvature diagrams for the model and prototype columns were also found with the use of RESPONSE. Due to the fact that the sections were not symmetrical about its x-axis, positive and negative moment analyses were performed. In each set of diagrams, the curves were plotted according to four different points (labelled A, B, C and D, originating from the centre).

Figures 6.6 and 6.7 presents two moment-curvature diagrams of the model above and within the lap-splice, respectively, with a axial dead load of 120 kN. To simplify the hysteresis model, the slopes of the post-cracking moment and the post-spalling moments were projected in order to locate an actual yielding co-ordinate. The two variables, α and r, correspond to the relation of these slopes as a function of the initial stiffness of the column. The variable α is the ratio between the post-cracking stiffness to the initial stiffness, while the variable r gives the ratio between the post-yielding stiffness to the initial stiffness.

The method used in finding the values of each of these points (A, B, C and D) is described as follows:

- Point A - the cracking moment of the section, analysed with RESPONSE when the concrete cover reaches a tensile strain of 75 $\mu\varepsilon$ corresponding to a concrete compressive strength of 35 MPa.
- Point B - the yield moment of the section, analysed with RESPONSE when the reinforcing steel (at a distance d from the face) reaches a tensile strain of 2000 $\mu\varepsilon$ corresponding to a steel stress of 400 MPa.
- Point C - the concrete spalling moment of the section, analysed with RESPONSE when the concrete at the face of the section reaches a compressive strain of 3500 $\mu\varepsilon$.
- Point D - the ultimate reduced section moment, analytically from empirical formulas when the compressed concrete at the core of the section reaches ε_{cu} for the confined section. The equation used for estimating the value of ε_{cu} [Corley, 1966] when the section is confined by rectangular reinforcement is;

$$\varepsilon_{cu} = 0.003 + 0.02\frac{b}{l_c} + \left(\frac{\rho_{hc} f_{yh}}{138}\right) \qquad [6.1]$$

where f_{yh} = yield strength of the stirrups (MPa)

l_c = distance between the critical section (maximum moment) and the inflexion point (zero moment)

b = width of the section

ρ_{hc} = steel volume ratio of confinement to the volumne of confined concrete

Figures 6.8 and 6.9 give a graphical comparison , where the model's values are related to the prototype's value in the prototype domain by the use of scaling laws.

Table 6.2 shows a summary of the various cracking, yielding and ultimate moments which corresponds to each of the different structures. Although both negative and positive moment analyses were performed, only the positive values are given due to the relatively close correlation between the two sets of data.

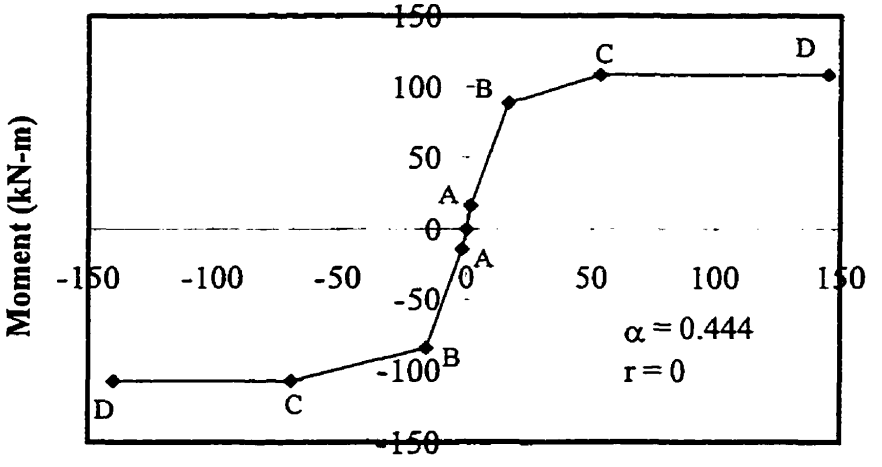

Figure 6.6 Moment-Curvature Diagram for Model Above Lap-Splice with Dead Load of 120 kN

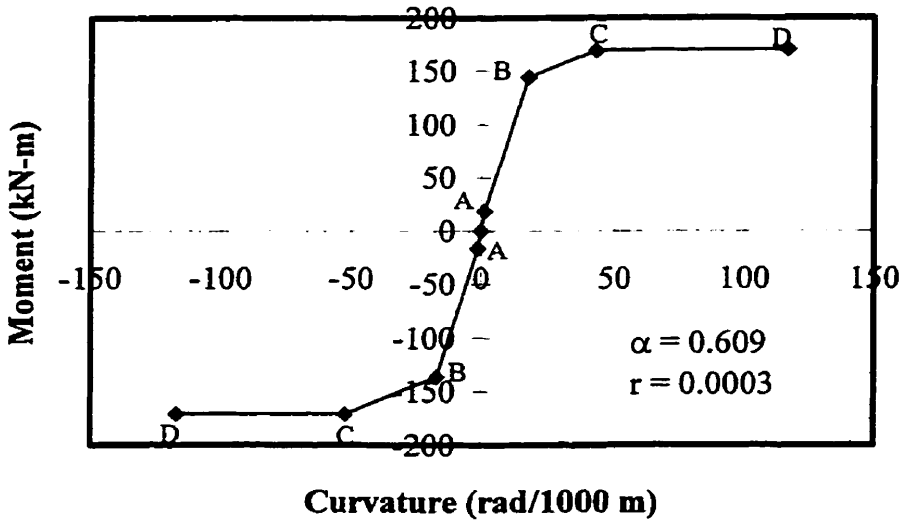

Figure 6.7 Moment-Curvature Diagram for Model Within Lap-Splice with Dead Load of 120 kN

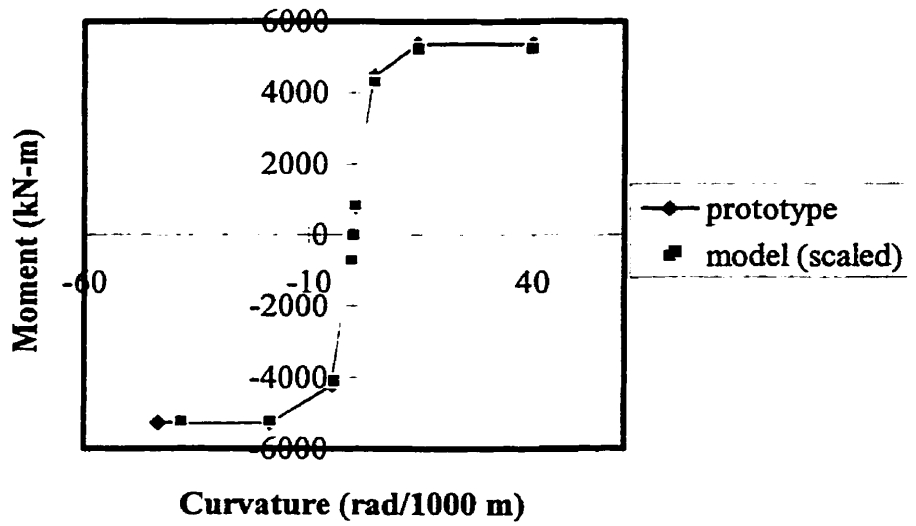

Figure 6.8 Moment-Curvature Diagram for Model and Prototype Above Lap-Splice with Dead Load of 1600 kN

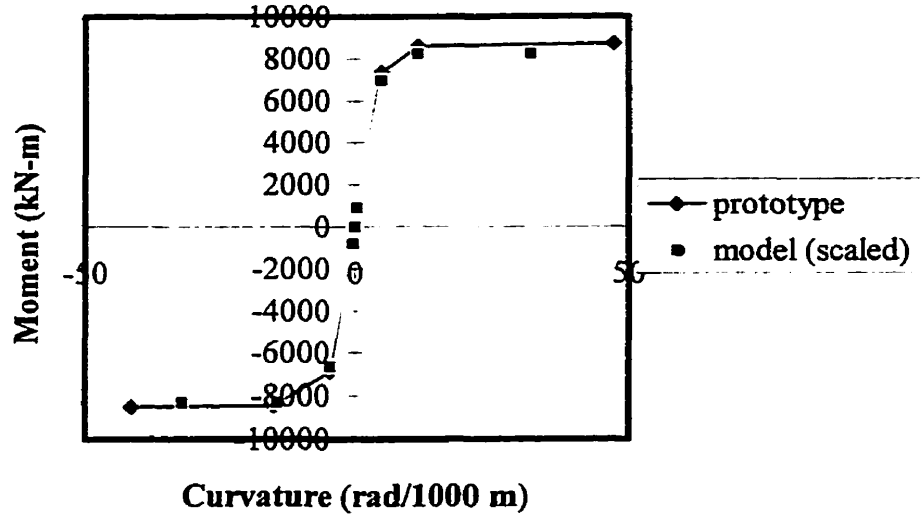

Figure 6.9 Moment-Curvature Diagram for Model and Prototype Within Lap-Splice with Dead Load of 1600 kN

Table 6.2 Summary of the Moments and Corresponding Curvatures

Moment	Model (P=120 kN)		Model scaled (P= 1600 kN)		Prototype (P=1600 kN)	
	Moment (kN-m)	Curvature (rad/km)	Moment (kN-m)	Curvature (rad/km)	Moment (kN-m)	Curvature (rad/km)
	Above Lap-Splice					
Cracking	16.6	1.54	807	0.42	803.1	0.43
Yielding	108.1	21.0	5257	5.8	5362	5.8
Ultimate	108.1	145.0	5257	39.7	5362	39.9
	Within Lap-Splice					
Cracking	18.5	1.44	900	0.39	921	0.40
Yielding	169.4	21.6	8237	5.9	8600	5.7
Ultimate	170.5	117.0	8291	32.1	8710	47.2

6.3 Computer Modelling using RUAUMOKO

The RUAUMOKO program [Carr 1995] is well recognized for non-linear dynamic analysis in earthquake engineering. RUAUMOKO is designed to produce a piece-wise time-history response of a non-linear, two-dimensional frame structure to ground accelerations or time varying force excitations. The program uses Newmark-Beta algorithms with $\beta = 0.25$. The program uses a modified Newmark scheme to ensure the maintenance of equilibrium at each time step. RUAUMOKO also allows the user the option to consider P-Δ effects in the analyses. Several damping models are available, including : Rayleigh and variation of the damping ratio (linear, constant and tri-linear damping). Many different hysteresis rules can be used within the RUAUMOKO program to represent the inelastic behaviour of frame and spring members. These hysteresis models range from simple elasto-plastic and bi-linear rules, to very complex models using large numbers of variables to represent the changing stiffnesses.

The program before the modal analysis considers the static loads so that the effects of the axial forces acting in the columns can be taken into account during the modal analysis. The static analysis is the starting point for the dynamic analysis as this ensures that all members start with the correct force distribution before starting the time-history analysis. For dynamic analyses, the loading of the structure is specified in terms of a ground acceleration history (in units of g), where the forces vary with respect to time. During the analysis, the relative displacements, velocities and accelerations are computed. Absolute accelerations can be generated by the post-processing program DYNAPLOT [Carr, 1995].

The RUAUMOKO program offers several practical modelling applications which can be applied to represent different realistic connection and construction methods,

including : four-hinge beam members, rigid links at ends of members, spring members, structural-wall members, constant force members, contact members, etc. The program also allows the user to perform pushover test by using a slow ramp loading function. The post-processing unit, DYNAPLOT, gives the user the ability to graphically visualise the displacements and the formation of plastic hinges during the dynamic analyses.

6.3.1 Hysteresis Models

Figure 6.10 shows the MUTO [Muto et al., 1973] degrading tri-linear hysteresis rule which was used as the moment-curvature model in the analyses of the bridge pier. The initial slope (k_o) corresponds to the stiffness (EI_g) of the section before cracking occurs. After cracking of the structure, the slope changes due to the decrease in the stiffness (EI_{cr}). The post-cracking slope is related to the initial slope by a factor α. The MUTO degrading tri-linear model follows an origin-centre philosophy, therefore, after cracking has occurred, the model comes back through the origin with a slope, k_u. The third slope corresponds to the post-yielding of the structure. Again, this post-yielding slope is related to the initial slope by a factor r. During the reverse loading, the model returns again with a slope, k_u. Once the loading crosses the abscissa, the slopes changes again according if opposite yielding has occurred. This model is suitable for reinforced concrete members because it follows a realistic understanding of the behaviour of loading and unloading with strength degradation. The envelopes of the first cycle (co-ordinates of the cracking and yielding moments and their corresponding stiffnesses) were obtained from results of moment-curvature analyses with the use of the RESPONSE program.

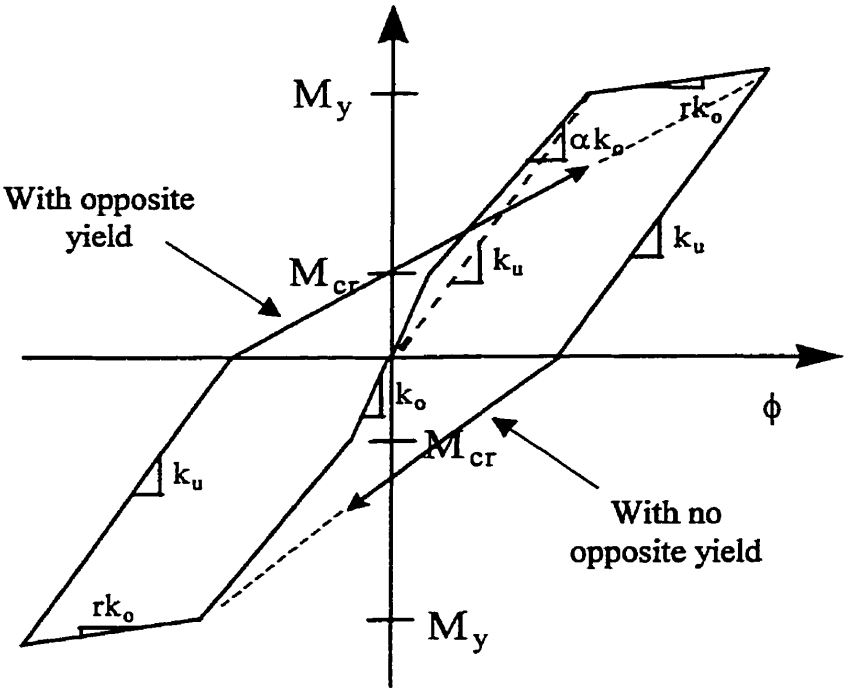

Figure 6.10 Muto Degrading Tri-linear Hysteresis

6.3.2 Description of the Initial Model

The structure was modelled in the RUAUMOKO program as shown in Figure 6.11. The model consisted of four nodes and three elements, with the total height of 835 mm and a fixed connection at the base. Node 3 represents the position of the lap-splice, while node 2 represents the mid-way point between the base of the column and the top of the dowel bars.

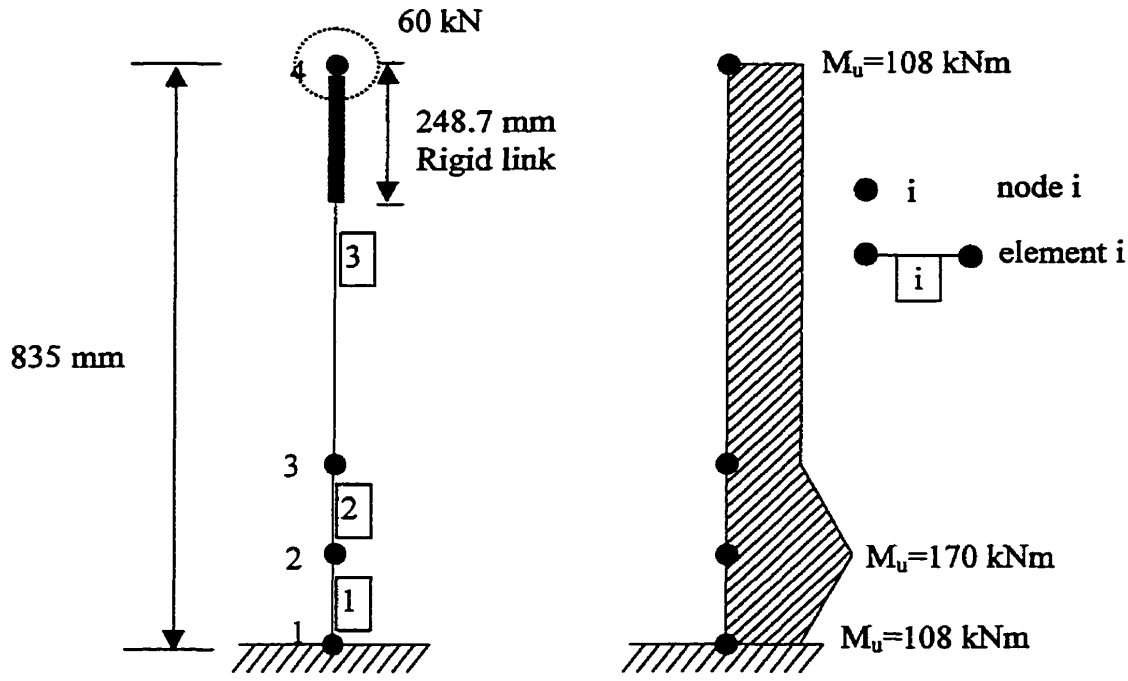

Figure 6.11 Initial Model of Column in RUAUMOKO

It was stated by Griezic [Griezic et al., 1996], that due to the detailing of the lap-splice, the predicted moment capacity of the column would follow a triangular distribution in this zone as shown in the above figure. It was assumed that presence of the dowel bars would increase the column's capacity at the middle of the lap-splice, while having little influence at the base or the top of the lap-splice. These assumptions were based on the flexural response of the member, therefore strength reduction caused by inadequate development length was not considered. Therefore, for the analyses performed with the RESPONSE program, yielding moments of 108 kN-m and 170 kN-m were found (see Table 6.2) as the values for sections with the effect of the lap-splice and without the effect of the lap-splice, respectively. Therefore, these values were used to determine the hysterical model. Table 6.3 gives a summary of the moment-curvature properties used in the RUAUMOKO program.

When considering the current code practices, the adequate development length is 386 mm. The length of the dowel provided in the specimen was equal to 245 mm, which

corresponds to a ratio of 63%. Therefore, only 63% of the flexural strength can be developed due to poor confinement of the lap-splice.

Plastic hinges were allow to form within the length of the member 1 and up to half-way within the length of member 2. This small predicted length of the plastic hinging was chosen due to the prediction of low ductility levels. A rigid link with a length of 248.7 mm, was also placed at the top of the column to represent the pin and the prestressing mechanisms. A typical volumetric density of 24 kN/m^3 for reinforced concrete was used to calculate the column's weight per unit length giving a mass distribution of 0.00183 kN/m. The RUAUMOKO model also incorporated the loading system that represented the actual loading, by applying an inertia mass of 60 kN and a compressive load of 120 kN at node 3, to reproduce the concrete block and the prestressing system, respectively.

Table 6.3 Summary of the Moment-Curvature Properties

Column	EI ($N-m^2$)	α	R	M_{cr} (kN-m)	M_y (kN-m)	ϕ_{cr} (rad/km)	ϕ_y (rad/km)
			Above Lap-Splice				
Model (+ve)	10.8×10^6	0.435	0	16.6	108.1	1.54	21.0
Model (-ve)	10.6×10^6	0.453	0	14.5	107.8	1.39	20.6
Prototype (+ve)	1867×10^6	0.462	0	803	5362	0.43	5.8
Prototype (-ve)	1864×10^6	0.437	0	708	5266	0.38	6.0
			Within Lap-Splice				
Model (+ve)	12.8×10^6	0.586	0.0005	18.5	169.4	1.44	21.6
Model (-ve)	12.5×10^6	0.632	0	16.4	170.8	1.31	21.3
Prototype (+ve)	2302×10^6	0.606	0.012	921	8600	0.40	5.7
Prototype (-ve)	2258×10^6	0.629	0	813	8440	0.44	5.7

6.3.3 Results Obtained from RUAUMOKO

Analyses were performed with the RUAUMOKO program to produce various time-histories responses from a non-linear two-dimensional model of the prototype and model columns. Numerous ground accelerations were used to excite the structure in order to examine the column's responses under different types of earthquake loadings. Different categories of Eastern and Western type earthquakes were also investigated, due to their distinct characteristics. Due to the lack of historical data for Eastern earthquakes, artificially generated ground motions, symbolic of typical accelerations from ENA were also examined. Table 6.4 gives a listing of the type and location of ground motions which were analysed, along with their corresponding PHA (peak horizontal acceleration) and PHV (peak horizontal velocity).

Table 6.4 Ground Motions and Locations

Region	E/Q Type	Event, Station and Component	PHA (g)	PHV (m/s)
Eastern	Historical	Whittier 1987, Hollywood Strg., LA 360	0.20	0.09
	Historical	Imeperial Valley Aftershock, 1979, El Centro 230	0.17	0.09
	Historical	Adak 1971, Navel Base West	0.19	0.08
	Historical	Saguenay 1988, Chicoutimi-North	0.44	0.13
Eastern	Artificial	Atkinson S32, M_L=5 @ 50 km	0.02	----
	Artificial	Atkinson S61 M_L=6 @ 50 km	0.05	----
	Artificial	Atkinson S81, M_L=7 @ 20 km	0.52	----
	Artificial	Atkinson S92, M_L=7 @ 50 km	0.13	----
	Artificial	Atkinson S102, M_L=7 @ 80 km	0.07	----
Western	Historical	Coalinga, Aftershock 1983, Oil Field Fire Sta., 270	0.22	0.16
	Historical	Whittier 1987, Union Oil Yard, 90	0.22	0.16
	Historical	Morgan Hill 1984, San Ysidro Sch. 270	0.22	0.19

Historical	Puget Sound 1949, Hwy Test Lab	0.16	0.21
Historical	San Fernando 1971, Hollywood St., S00W	0.17	0.17
Historical	San Fernando 1971, Hollywood St., N90E	0.21	0.21
Historical	Mexico City 1985, La Union, N90W	0.17	---

The ground motion accelerogram for each earthquake is presented in Appendix A. To respect the laws of similitude, each earthquake record was modified according to their appropriate scaling law, thus, the time was decreased, and the amplitude was increased by a factor of 3.65. For each of the historical ground motions, the unscaled acceleration was also normalized to a value of 0.21 g, which corresponds to the NBCC (National Building Code of Canada), design value for a 475-year return period. The related spectrums were calculated from the accelerograms with the use of RESAS program [Sarrazin and Filiatrault, 1993] (spectral acceleration, Sa (g) versus the natural periods) for a damping of 2 and 5%.

Each earthquake record was analyzed with the use of the RUAUMOKO program to determine which ground motion would be suitable for shake table testing. For each analysis, the pin displacement, pin acceleration and the moment-curvature at the base and at the top of the lap-splice were examined. Table 6.5 presents a summary of the maximum absolute values which were found during these analyses.

Table 6.5 Summary of Results from Preliminary Analyses with RUAUMOKO

Ground Motion	Drift at Pin Level (%)	Pin Accel. (g)	Curvature Ductility Factor μ_c (base)*	Curvature Ductility Factor μ_c (lap-splice)**
Whittier LA, 360	0.33	1.25	0.57	0.53
Imperial Valley	0.43	1.59	0.77	0.68
Adak	0.58	2.05	0.90	0.60
Saguenay	0.18	0.74	0.64	0.58
Atkinson M_L=5, 50 km	0.03	0.17	0.05	0.04
Atkinson M_L=6, 50 km	0.06	0.32	0.13	0.07
Atkinson M_L=7, 20 km	0.47	1.68	0.91	0.62
Atkinson M_L=7, 50 km	0.22	0.80	0.43	0.28
Atkinson M_L=7, 80 km	0.10	0.41	0.19	0.11
Coalinga	0.50	1.66	0.95	0.65
Whittier Union, 90	0.62	2.10	1.54	0.86
Morgan Hill	0.73	2.16	1.78	0.86
Puget Sound	0.79	2.11	2.40	0.82
San Fernando S00W	0.93	1.19	0.91	0.82
San Fernando N90E	0.74	2.16	1.11	0.89
Mexico City	0.68	2.10	1.52	0.84

* cracking and yielding occurs at a curvature ductility of 1.5 and 20.8 rads/km

** cracking and yielding occurs at a curvature ductility of 1.4 and 21.5 rads/km

Pushover tests were performed to obtain the maximum base shear and pin displacement of the experimental column. Pushovers tests involves applying a constantly increasing load to the top of the structure to find its flexural resistance. It was found that the model column had a base shear capacity of 124 kN, under a negative moment, with a relative displacement of 5 mm, giving a drift of 0.60 % at the pin level.

6.4 Final Selection of Ground Motions

To encompass all of the categories, Western and Eastern North America, and historical and artificial earthquakes, it was decided to select three different ground motions for shake table testing. These earthquakes included two from Eastern (a historical and an artificial), and one from Western North America.

For the Eastern historical earthquake, Adak, 1971 was chosen because the RUAUMOKO model experienced the greatest maximum pin acceleration and displacement compared to the other earthquake for this region. No yielding at the base of the column was seen for the analysis of eastern earthquakes. Although Adak is located in Alaska, it resembles an eastern type earthquake due to its high frequency, therefore it was classified in this region. For the artificial earthquakes produced by Atkinson, the ground motion with a magnitude 7 at a distance 20 km was retained. This earthquake was selected because it produced the greatest displacement and acceleration, and it was the only earthquake in which the column experienced yielding at the base.

Morgan Hill, 1984 was chosen as the ground motion to represent Western North America. Although Morgan Hill did not cause the column to experience the greatest maximum pin displacement or acceleration, it was chosen because the moment-curvature diagram at the base of the column experienced the most post-yielding cycles compared to other Western based earthquakes.

Figures 6.12, 6.13 and 6.14 give the scaled accelerograms for the three chosen earthquakes ; Adak 1971 (Eastern - historical), Atkinson M_L=7 at 20 km (Eastern - artificial) and Morgan Hill (Western - historical). The three graphs are given in units of g, and time in seconds.

There was a concern that due to the scaled ground motion (decreased time and increase amplitude), the shake table capabilities were not certain, therefore, preliminary tests were performed to determine the performance of the shake table. The acceleration feedback was recorded so that a comparison could be made between the true acceleration and the table's acceleration. A close correlation was seen between the spectra from the shake table's acceleration and the original input data, therefore, it was determined that the table's acceleration gave a reasonable representation of the actual recorded ground motion, as discussed in Section 10.2.

Figures 6.15, 6.16 and 6.17 represents the spectra for the corresponding earthquakes which were selected for the experimental testing. In each of the graphs, the spectra for both the model (scaled accelerogram) and the prototype (original accelerogram) are compared. For clarity, the graphs were plotted in the units of g and with a logarithmic time scale in seconds. The fundamental period of 0.0821 s, found with RUAUMOKO, is also plotted with the spectra to indicate the expected response the column would experience.

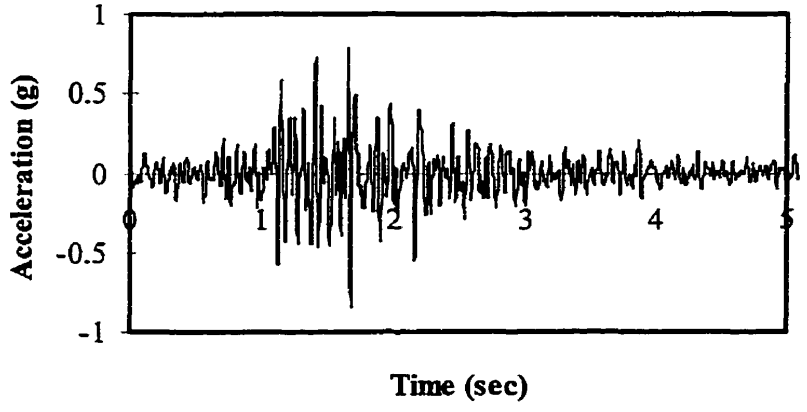

Figure 6.12 Scaled Ground Motion Accelerogram for Adak 1971

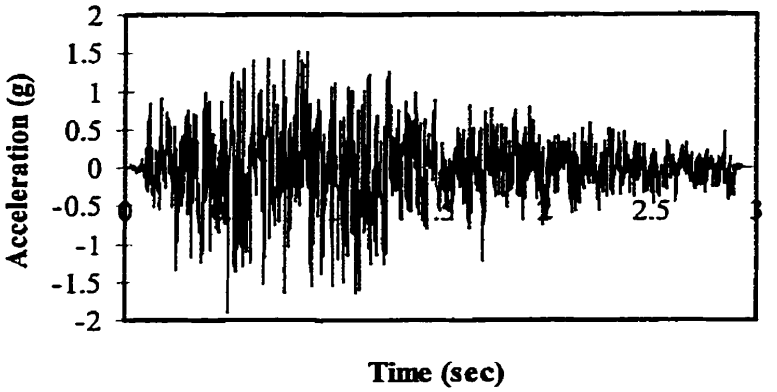

Figure 6.13 Scaled Ground Motion Accelerogram for Atkinson M_L=7 @ 20 km

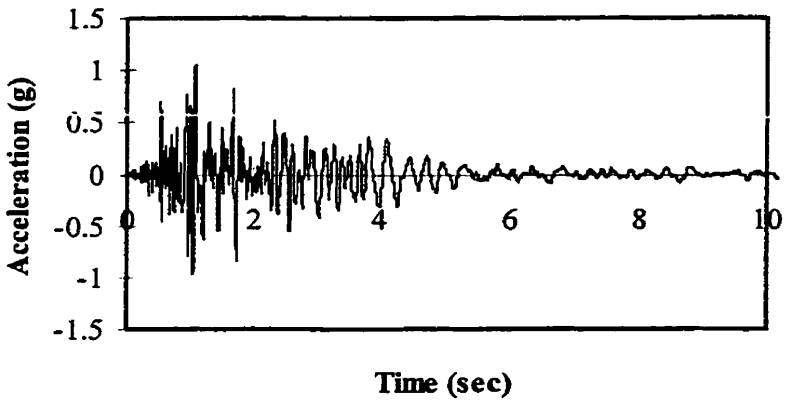

Figure 6.14 Scaled Ground Motion Accelerogram for Morgan Hill 1984

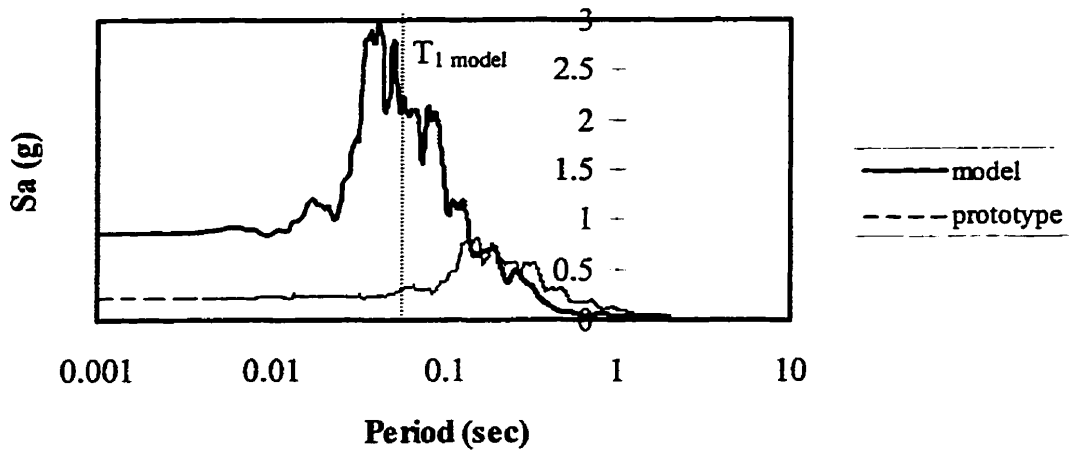

Figure 6.15 Model and Prototype Spectra for Adak 1971, 5% Damping

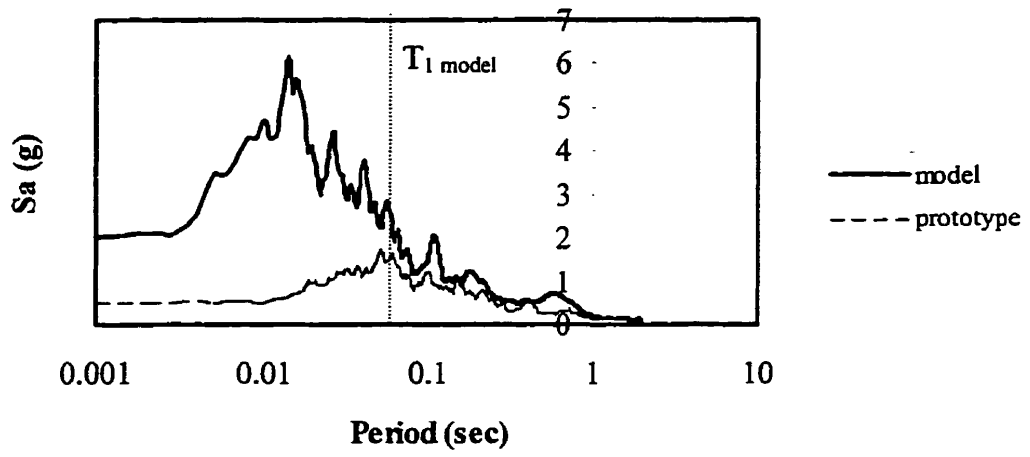

Figure 6.16 Model and Prototype Spectra for Atkinson M_L=7 @ 20 km, 5% Damping

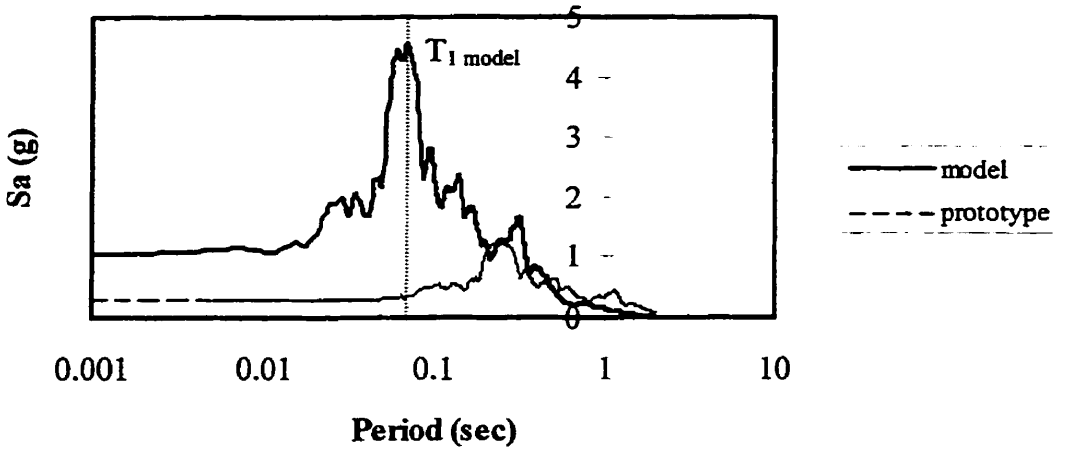

Figure 6.17 Model and Prototype Spectra for Morgan Hill 1984, 5 % Damping

CHAPTER 7
EVALUATION OF MATERIAL PROPERTIES

7.1 Tensile Tests on Steel Reinforcement

The properties of the steel reinforcement used in the fabrication of the specimens were determined by tensile tests which complied to the CSA G30.12-M77 standard [CSA, 1977]. The resistance of the 16 mm diameter threaded bar used in the prestressing system was also verified by tensile tests. The results of these test are described in the following sections. The mean values of the different test results were utilized for the non-linear dynamic analyses to be discussed in detail in later sections.

7.1.1 Longitudinal Reinforcement

In the fabrication of the specimens, the same reinforcement was used for the longitudinal and dowel bars. In order to respect the scaling laws, No. 3 US deformed bars were used for the column's reinforcement. Therefore, to determine the material properties of the reinforcing steel, tensile tests were performed on four 500 mm long samples randomly chosen from the given reinforcement. A hydraulic Amsler tensile testing machine was used for the testing of the samples. This machine was equipped with adaptable clamps designed to resist against slippage of the specimen samples. A dynamometer, attached to the testing apparatus, was used to record the stress-strain curves of each specimen during testing.

The yield strength (f_y) and the ultimate strength (f_u) of the dowel and longitudinal reinforcement were determined by computing the mean values obtained from the four tests. Initial and final measurements were recorded for each specimen, with the use of calipers, to ascertain the percentage of ultimate strain. The yield and ultimate loads were read directly from the loading dial on the testing apparatus for the longitudinal reinforcement.

Table 7.1 Properties of the Longitudinal Reinforcement (#3 US bars)

Sample No.	Yield Strength, f_y (MPa)	Ultimate Strength, f_u (MPa)	Initial Length (mm)	Final Length (mm)	Ultimate Strain, ε_u (%)
1	458	696	206.5	240.5	16.5
2	445	689	211.8	248.2	17.2
3	445	689	206.5	240.0	16.2
4	451	696	213.1	243.1	14.1
Mean	448	693	209.5	243.0	16.0

7.1.2 Transverse Reinforcement

For the transverse reinforcement, plain 3.6 mm diameter wires were used to represent the stirrups. Tensile tests were performed on two 300 mm long wire samples randomly selected from the supplied material. It was decided to test only two bars because the transverse reinforcement was used in lesser quantities compared to the longitudinal reinforcement. The small bar diameters prevented the use of the hydraulic tensile machine, therefore, a smaller electrical testing apparatus was used for the tensile tests. This machine was again outfitted with adaptable clamps to prevent slippage during testing.

Figure 7.1 shows a graph depicting stress versus displacement for one of the tested samples for the transverse reinforcement. A summary of the results is given in Table 7.2.

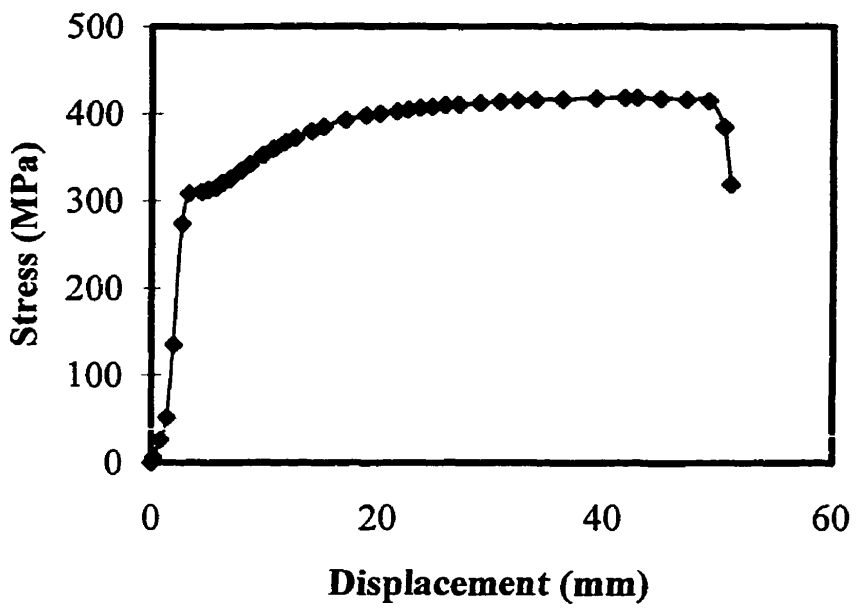

Figure 7.1 Stress-Displacement Curve for Transversal Reinforcement (3.6 mm diameter plain wire)

Table 7.2 Properties of the Transverse Reinforcement

Sample No.	Yield Strength f_y (MPa)	Ultimate Strength f_u (MPa)
1	315	417
2	331	422
Mean	323	420

7.1.3 Prestressing Bars

To minimize the effect of the prestressing bars on the lateral movement of the bridge piers, the smallest bar diameter was chosen so that the prestressing bars could bend with the least resistance during dynamic testing, but still remain elastic. Therefore, a preliminary tensile test was completed on a 16 mm diameter threaded rod to determine its yielding and ultimate strength capacities. The testing method followed the same procedure as was discussed for the longitudinal steel. The tensile tests followed a typical stress-strain behaviour with a yield strength 602 MPa and an ultimate strength of 719 MPa. These value were used to verify if the prestressing bars would remain elastic under the expected loading, in accordance with the CAN/CSA-S16.1-94 code [CSA 1994b].

7.2 Concrete Mix

Two similar concrete mixtures were used for casting the specimens, with the only exception being the amount of superplasticizer used in the mix. Both mixtures were designed to have a compressive seven-day strength of 35 MPa. Superplasticizer (WRDA 19) was added into the concrete mix for the column to produce a more fluidic mixture to ease in the placement of the concrete between the longitudinal reinforcement. Cement of type 30 was used to produce a high initial strength and crushed aggregate with a maximum diameter of 6mm was used in the mixture. The water to cement ratio was 0.56 for both mixtures. The concrete was mixed and cast in accordance with the CSA A23.1-M90 Standard [CSA, 1990]. Table 7.3 indicates the concrete mixture used for the foundations and the columns.

Table 7.3 Concrete Mixtures

Material	Quantity (kg/m^3)	
	Foundation	Column
Cement (type 30)	305	305
Water	170	170
Sand	1060	1060
Aggregate (6 mm)	800	800
Superplasticizer	--------	1000 ml / 100 kg cement

7.3 Compression Tests on Concrete Cylinders

Compression tests were completed on concrete cylinders from the concrete mix of the foundations and the columns. The tests were performed in accordance with the ASTM C-39 Standard [ASTM 1986]. The cylinders were cast in typical molds having a diameter of 150 mm and a height of 300 mm. A sulphur compound was used to cap both ends of the cylinders to ensure uniform axial stress. A hydraulic Amsler compressive testing machine, equipped with a dynamometer to measure the axial load, was used to test these cylinders. The testing apparatus had a precision of within ± 1% of the corresponding measuring scale. Once again, the mean values of these tests were used for the non-linear analyses.

7.3.1 Concrete of the Foundation

The compressive strength (f'_c) of the foundation was determined by calculating the mean strength values of six concrete cylinders which were cast along with the foundation. Since a similar mixture would be used for the columns, the results were used to foresee the compressive resistance of the more critical bridge pier. Two different

casts were performed to reduce the amount of formwork construction and to decrease the required casting area. The cylinders from each set of foundation were tested seven days after casting. Table 7.4 shows a summary of the given concrete resistance.

Table 7.4 Compressive Strength of Foundation Concrete

Cylinder	Batch No.	Compressive Strength, f'_c (MPa)
1	1	30.5
2	1	31.6
3	1	29.4
4	2	27.2
5	2	32.6
6	2	31.3
Mean	--------	30.4

7.3.2 Concrete of the Columns

The maximum compressive strength (f'_c) of the columns were also computed by calculating the mean strength value of two cylinders for each column. To reduce the strength variation between the columns, all eight specimens were cast together with their corresponding batch numbers for each column and cylinder recorded. Consequently, when the bridge pier specimens were tested, two corresponding cylinders were tested to determine the compressive strength of each particular column at the time of testing. Table 7.5 gives the compressive strengths for the various columns.

Table 7.5 Compressive Strength of Concrete Column

	Compressive Strength, f'_c (MPa)			
Cylinder	Specimen 1 Quasi-static	Specimen 2 Dynamic1 and 2	Specimen 3 Dynamic 3	Specimen 4 Dynamic 4
1	35.2	38.2	34.0	40.0
2	39.1	35.7	37.0	37.5
Mean	37.2	37.0	35.5	38.8

CHAPTER 8
DESCRIPTION OF THE SHAKE TABLE TESTS

8.1 Introduction

This chapter describes the fabrication of the model bridge pier specimens which includes the construction of the foundations and the columns. The type and placement of the instrumentation are explained and distinguished between the different tests. The experimental set-ups and the types of tests performed are also explained in the proceeding sections.

8.2 Fabrication of Specimens

Eight specimens in total were fabricated. As with realistic bridge pier construction, the model specimens were fabricated in two separate steps, first being the foundation and the second being the column. Dowel bars placed in the foundation connected the two sections, which were tied directly to the longitudinal bars of the column. Both sections are explained in detail in the following sections.

8.2.1 Fabrication of Foundations

The fabrication of the foundations were completed in several steps. First, the transversal reinforcement required were cut and bent to their correct dimensions. Due to the fact that 15M bars were used for the stirrups, the normal bar bender of the laboratory did not have the capacity to form the bars, therefore, a special apparatus was devised which used an electrical pump to bend the reinforcing bars to the correct shape.

Subsequently, the longitudinal bars were cut and the reinforcing cage was fabricated by attaching the stirrups at the correct locations. The transversal reinforcements were attached with the use of steel wires to resist movement during concrete placement. Dowel bars were then fabricated, with the correct scaling laws implemented above the surface of the foundation. A special template was designed and used to maintain the correct position of the dowel bars also during casting. Three strain gauges were placed on two dowel bars (six in total) to provide measurements during the experimental tests. The type and placement of these gauges will be further discussed in Section 8.3.1.

Subsequently, the formwork for the foundations were constructed. To reduce the amount of construction, four wooden forms were fabricated, which were to be used twice to provide the eight specimens. Furthermore, the casting area was confined, thus limiting the amount of foundations to be cast to four. Concrete with a compressive strength of 35 MPa was used to cast the foundation. Wooden braces were used to ensure against buckling of the side walls of the foundation forms. The formwork for the foundation and the reinforcing cage are shown in Figure 8.1.

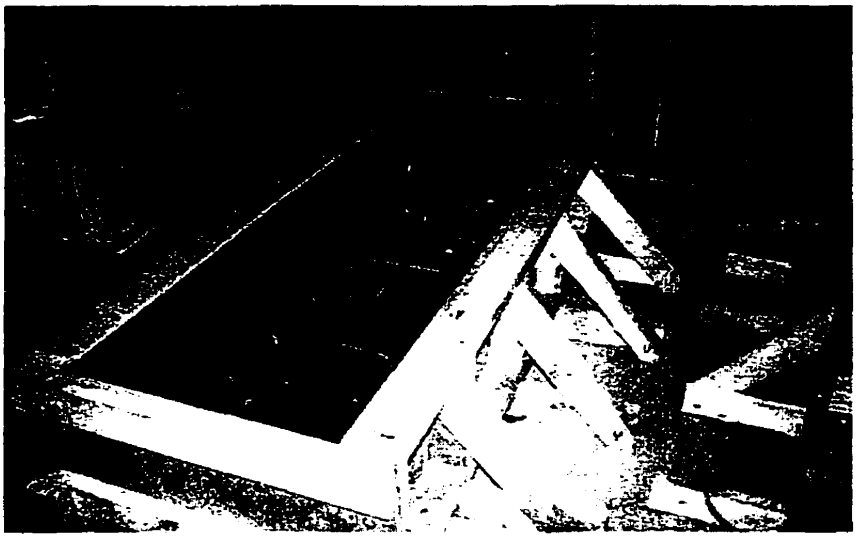

Figure 8.1 Formwork and Reinforcing Cage for the Foundations

8.2.2 Fabrication of Columns

The fabrication of the columns commenced by cutting and bending the transverse reinforcement. This was followed by cutting the longitudinal reinforcement to the desired length. Subsequently, a 13 mm thick steel plate, with the same dimensions as the columns, were fabricated for each column with four threaded holes in each plate to be used as part of the prestressing system, as shown in Fig. 5.5. The longitudinal bars were then welded to these steel plates to ensure proper anchorage. The reinforcing cages were completed by attaching the stirrups at their correct locations. The columns were anchored to the foundation by attaching the dowel bars from the foundation to the longitudinal bars of the column, with the use of steel tying wires. Figure 8.2 shows a photo of the assemblage of the reinforcing cage of the column section.

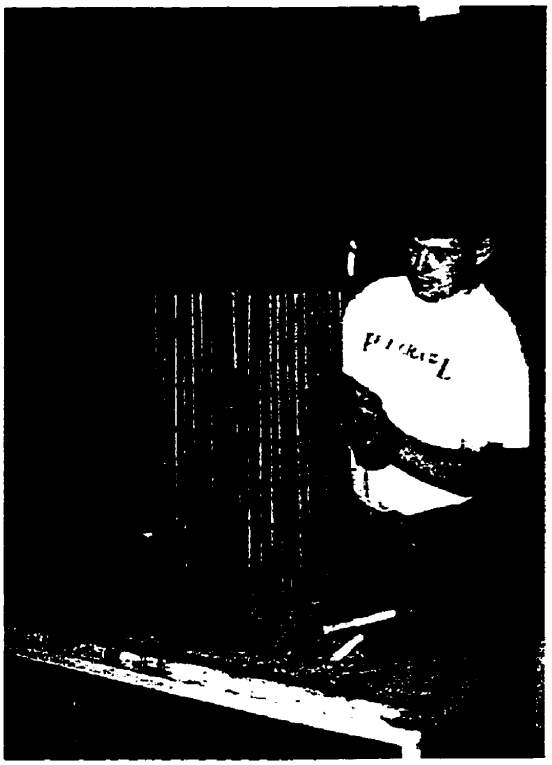

Figure 8.2 Construction of the Column Reinforcing Cage

To minimize the strength variances between the columns, all eight specimens were cast coincidentally. Consequently, eight separate forms had to be constructed. Since there was a steel plate placed on top of the columns, the conventional method of casting from the top had to be modified so that the concrete was placed though the side of the column. Again, concrete having a compressive strength of 35 MPa was used for casting the columns. Due to the close spacing between the longitudinal bars, vibration of the concrete was completed by external vibrators and by rodding the concrete by hand. Proper placement of the concrete was difficult to achieve due to the horizontal position of the column along with the large quantity of reinforcement. Minor patching of the concrete was performed after the removal of the forms.

8.2.3 Fabrication of the Cooling Chamber

A chamber was designed to encase the column, which would contain liquid nitrogen to allowed experimental test to be performed at low temperatures. The chamber was built in two separate sections to allow for accessible removal at the time of testing. To allow for proper distribution of the liquid nitrogen gas, the chamber was designed with a 50 mm air space around the circumference of the section. The chamber was constructed in three layers, with the outside being of 19 mm thick plywood, the center portion was packed with typical insulation material and then a 50 mm thick rigid industrial insulation material (R = 20) was used for the inner layer. With the use of air pressure, a controlled flow of liquid nitrogen could be achieved, thus allowing the regulation of the temperature. Thermocouples were used to measure and record the temperatures within the concrete core and the internal air temperature of the chamber. Preliminary tests were performed to monitor the chambers ability and it was seen that the chamber could maintain a temperature of -60°C, which was sufficient for the desired temperature of -40°C. The design of the chamber enabled enough time to decrease the

temperature and the quick removal of the box, so the specimen could be observed during testing at low temperatures. Figure 8.3 shows a photograph of the cooling chamber placed around the specimen.

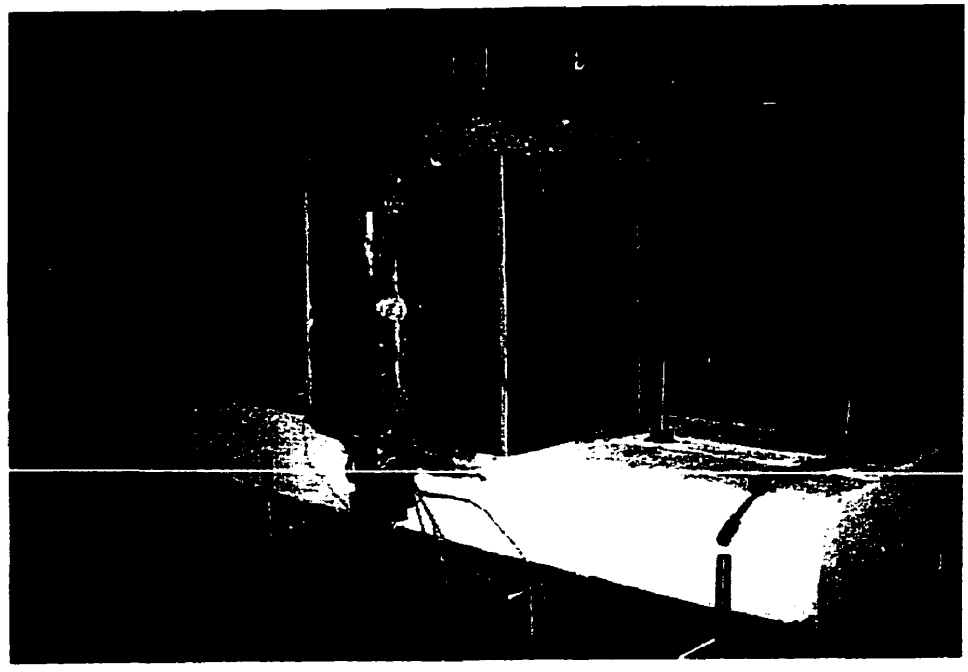

Figure 8.3 Cooling Chamber and Specimen

8.3 Instrumentation

8.3.1 Introduction

The model bridge pier was instrumented with electronic strain gauges, linear motion transducers, accelerometer, thermocouples and linear voltage displacement transducers (LVDTs). Figure 8.4 illustrates the instrumentation used throughout the different experimental tests. Three positions were instrumented with LVDTs, these instruments were located at 55 mm, 110 mm and 165 mm from the base of the column,

labeled Section 1, 2 and 3, respectively. Four positions were instrumented and measured with accelerometers and linear motion transducers, labeled A, B, C and D, which correspond to the concrete block, pin, top of the concrete column and the centre of the concrete column respectively. The control system of the shake table also had the capacity to measure the displacement feedback, acceleration feedback, force feedback and the base shear feedback of the table. These readings were used as the basis for sequencing the other two data acquisition systems.

The electronic strain gauges were placed at various positions to provide information pertaining to the strain levels of the different reinforcement. The locations were chosen based on various criteria, including; the probable plastic hinge region of the column, investigation of the possibility of slippage between the dowel and the longitudinal bars and the level of confinement of the stirrups. The recorded measurement of the strain gauges indicates the local deformation of the reinforcements during the experimental tests. Therefore, for a given section containing two strain gauges on two opposing bars, it is possible to evaluate the curvature of this region.

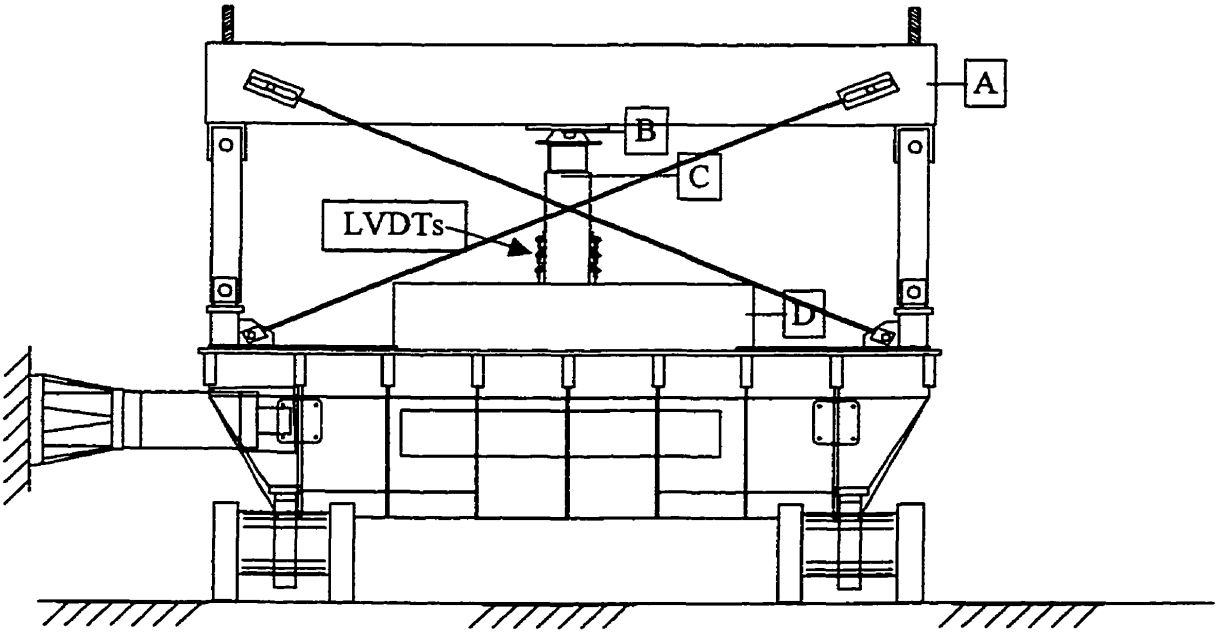

Figure 8.4 Layout for Instrumentation

8.3.2 Electronic Strain Gauges

Ten strain gauges were used in total for each of the specimens, with their positions as shown in Figure 8.5. Six strain gauges were attached to the dowel bars, one was placed on a longitudinal bar and the remaining three strain gauges were positioned on the lower two transversal reinforcements.

Strain gauges with the capacity for large deformation (± 20%) were used to ensure reliable results during the progression of the seismic tests. The positions of each strain gauge was carefully measured and the surface of the reinforcing bars were grinded and sanded to assure proper bonding. A protective coating was placed over each gauge to safeguard against possible damage during casting of the specimens.

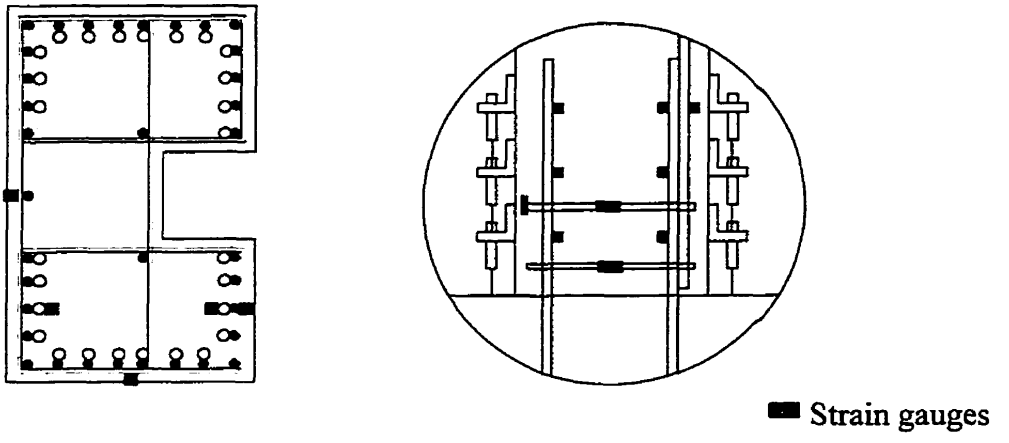

Figure 8.5 Placement of Strain Gauges

8.3.3 Linear Motion Transducers

The linear motion transducers served to determine the absolute horizontal displacements of the shake table, top of the concrete column, pin and center of the concrete blocks. These instruments are designed with spring loaded cords which measure the displacement at each selected time step. These cords were connected to the specimen with the use of concrete anchorage screws to ensure proper attachment. The base for each linear motion transducers was attached to a rigid anchorage system independent of the shake table to ensure reliable results. By using the table displacements as the base displacement values, the relative displacements for each recorded location could be evaluated.

8.3.4 Accelerometers

To evaluate the absolute horizontal acceleration of the specimens, the shake table, top of the concrete column, pin and the center of the concrete blocks were instrumented with accelerometers. The accelerometers were bonded to the faces of the concrete columns and blocks and to the center of the pin. An accelerometer was also placed at the center of the foundation which was considered rigidly fixed to the shake table. By doing this, the slippage of the foundation can be verified by comparing the acceleration of the shake table to the measurements recorded by the foundation accelerometer for a given ground motion. It was seen that these two accelerograms were virtually identical, therefore, it was stated that there was no evidence of slippage between the foundation and the shake table.

8.3.5 Thermocouples

Thermocouples were placed within the core of the concrete specimens to measure the interior temperature of the column. Three different positions were chosen to gauge the specimen's temperature, which are : within the foundation at the base of the column, center of the lap-splice and at the top of the lap-splice. During the low temperature seismic tests, the thermocouple readings allowed the specimen to be tested at the desired temperature.

8.3.6 Linear Voltage Displacement Transducers (LVDTs)

On each side of the concrete column, three 50 mm LVDTs were placed to measure the column's rotation during the experiment tests. The LVDTs were positioned through aluminum angles and bonded with epoxy on the concrete surface with a spacing of 55 mm which corresponds to d/4, d/2 and 3d/4, where d represents the distance from the extreme compression fibre to the centroid of the tension reinforcement. Each LVDT measured the change in displacement, relative to the lower LVDT, which was positioned directly below the other instrument. The curvatures of the specimen were able to be calculated by knowing the measurements and the position of two corresponding LVDTs. These curvatures were used to plot moment-curvature diagrams for each instrumented position.

8.4 Experimental Set-up

With the use of a forklift and a crane, the specimens were placed and fixed on the shake table. The foundation was securely attached to the table with threaded rods as described in Section 5.6.2. Due to the small variances in the height of each of the

columns, the pin-block connection was designed such that small adjustments could be made by placing small shims between the upper portion of the pin and the steel plates. Therefore, the connection system could be adapted for each specimen to be properly fastened to the inertia mass.

The strain gauges, LVDTs, accelerometers and linear motion transducers were then attached to two data acquisition systems. Video and photographic cameras were positioned to record the behaviour of the column during the experimental testing.

The following sections describe in detail the shake table and the data acquisition systems which were used for the tests. Figure 8.6 shows a photograph of the complete experimental set-up.

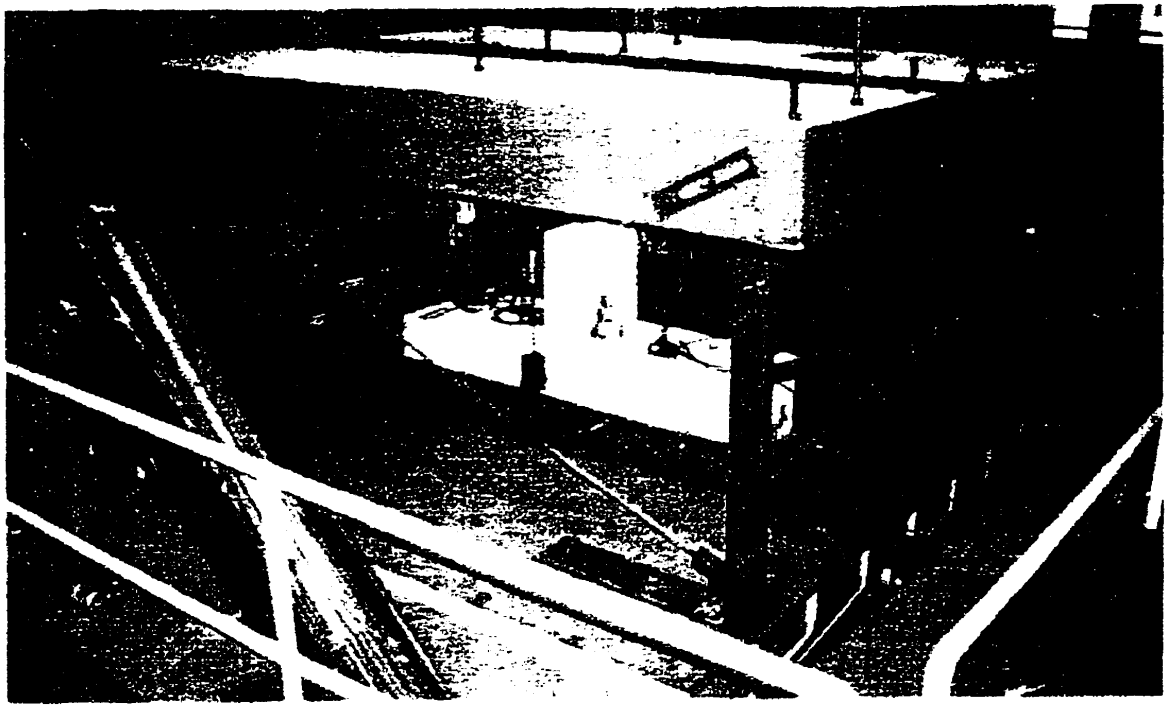

Figure 8.6 Experimental Set-up on the Earthquake Simulator

8.4.1 Shake Table Description

The earthquake simulator at Ecole Polytechnique has the ability to reproduce different excitations including seismic, harmonic or random vibrations. The shake table gives researchers the ability to seismically test large scale structural systems, thus giving better insight into their behaviour and performance. The earthquake simulator was designed such that the input data could be expressed in either displacements or accelerations. The shake table is capable of producing frequencies within the range of 0 to 50 Hz. The maximum limitations for the acceleration and velocity are 3 g and 800 m/s, respectively, with a maximum stroke of ± 125 mm. The structure of the table is composed of several steel components, with its base connected to a strong floor, allowing for a maximum payload capacity of 15 tons.

The surface of the shake table has a plan dimension of 3.4 m x 3.4 m. Ten shear keys are located within the table along with a grid of 25.4 mm diameters threaded keyholes at 406 mm o/c, allowing the specimens to be securely anchored to the table's surface, with high strength threaded rods.

The shake table is powered by a hydraulic jack having a dynamic capacity of 300 kN and a static capacity of 400 kN, with a stroke of 250 mm. Hydrostatic bearing supports ensure a horizontal movement of the table with a maximum friction of 0.6 kN. The hydraulic supports are equipped with two 200 hp (150 kN) and a 40 hp (30 kN) overload motor, producing an oil discharge of 730 liters/minute at a pressure of 3000 psi.

The shake table is accompanied with a digital control system. The control system is designed with three variable control, giving favorable responses for displacement for low frequencies, acceleration for high frequencies and velocity for intermediate frequencies. The system also uses two methods for compensating the dynamic influence

of the system (table and specimen) : by using the dynamic influence of the system (table and specimen) or, by using adaptive filters for compensation and an on-line time iteration method [Filiatrault et al., 1996].

8.4.2 Data Acquisition Systems

Two high speed data acquisition systems were used to record the readings form the quasi-static and dynamic tests. Each of the data acquisition system could record information with twelve bit resolution. A frequency of 50 Hz was chosen for the acquisition system to ensure a proper sampling rate during the tests. Both the two systems relied on personal computers and specialized software programs to record the data at these high speeds. The ten strain gauges, the six LVDTs and the velocity meter were connected to one data acquisition system (17 channels), while the other accelerometers and the linear motion transducers were connected to another data acquisition system (8 channels).

The first data acquisition system had a precision of the deformation for the strain gauges of ± 25 με, and a precision of ± 0.01 mm for the LVDTs. The second data acquisition system recorded the linear motion transducers had a precision of ± 0.03 mm. The accelerations were also recorded with a precision of less than 0.005 g.

8.5 Types of Tests

Several tests were performed to find certain mechanical properties and observe the seismic behaviour of the reinforced concrete bridge pier specimens. A quasi-static test was performed on the first of the four specimens to determine the basic lateral load - displacement hysteretic behaviour of the pier - footing assembly, including the column's strength, stiffness and ductility. A total of 16 seismic tests were performed which encompassed three different ground motions of varying intensities and two different temperatures (+20°C and -40°C). White noise tests were completed prior to each test to determine the natural frequency of the structure before testing. Also, foregoing testing, damping tests were performed to calculate the amount of damping within the structure. The extent of cracking of the column was recorded prior to testing and after each seismic test. During the quasi-static testing, the loading cycle was interrupted at the end of each cycle in order that photographs and cracking patterns could be documented before the recommencing of the loading cycles. These properties are used in the modelling of the non-linear dynamic analyses, which will be discussed in later sections. Each type of testing is explained in detail in the following sections. Table 8.1 present a summary of the shake table test, ground motion, specimen number and the temperature at which the specimen was tested.

8.5.1 White Noise Tests

White noise tests were performed to evaluate the fundamental periods of the structures. The shake table was programmed to carry out white noise tests, in which the table outputs a uniform power spectral density function of intensity over the entire frequency range between 0 and 50 Hz for a duration of approximately three minutes. The displacements, accelerations and deformation of the strain gauges were measured by the data acquisitions systems as a provision against excessive loading during the

preliminary tests. The testing parameters included a Nyquest frequency (f_{NYQ}) of 50 Hz which corresponds to a sampling rate (Δt) of 0.01 seconds.

Table 8.1 Summary of Shake Table Tests

Ground Motion	Specimen No.	Temperature (°C)
Quasi-static	1	+20
Adak 100%	2	+20
Adak 200%	2	+20
Morgan Hill 100%	2	+20
Morgan Hill 200%	2	+20
Morgan Hill 400%	2	+20
Atkinson 100%	3	+20
Atkinson 200%	3	+20
Atkinson 300%	3	+20
Atkinson 400%	3	+20
Adak 100%	4	-40
Adak 200%	4	-40
Atkinson 100%	4	-40
Atkinson 200%	4	-40
Atkinson 300%	4	-40
Atkinson 400%	4	-40
Atkinson 500%	4	-40
Atkinson 600%	4	-40

The recorded readings were analyzed with the use of the U2 program [EDI, 1993]. This program divides the recorded signal into several intervals with equal time steps, and produces a Fourier spectrum for each given interval. Subsequently, the power spectral density is determined by calculating the average of the Fourier spectra, thus

indicating the fundamental frequency of the structure to be tested. The U2 program used 2048 points per interval to obtain an average accuracy. Eight intervals of 20.48 seconds were used which corresponds to a frequency resolution of $\Delta f = 0.0488$ Hz.

To record the degradation of the structure's stiffness, white noise tests were performed before each test. During these tests, the accelerometer was positioned at the top of the concrete to enhance the instrument's response. Table 8.2 gives a summary of the natural periods of the four specimens tested under dynamic conditions along with their corresponding lateral stiffness ratio. The ratio represents the column's stiffness calculated from the relationship between the specimen's stiffness to the initial specimen's experimental stiffness, expressed as a percentage. Appendix B gives the power spectral density graphs for each test performed. In several plots, a second mode of approximately 28 Hz could be observed.

Furthermore, the mean value of the measured natural period of the initial specimens was found to be 0.120 s (8.3 Hz), compared to the theoretical natural period of 0.083 s (12.0 Hz), obtain from the preliminary RUAUMOKO analysis. The decrease in the frequency was considered to be from the lack of stiffness in the pin connection. Also, the specimen was theoretically modelled with a fixed link to represent the prestressing system which may not be entirely accurate.

Table 8.2 Summary of the Fundamental Periods of the Structure

Specimen No.	Sequence	Period (sec) (± 0.001)	Lateral Stiffness Ratio
2	Before 100% Adak	0.124	100
	After 100% Adak	0.126	97
	After 200% Adak	0.136	83
2	after 100% Morgan Hill	0.138	81
	after 200% Morgan Hill	0.149	69
	after 400% Morgan Hill	not measured	N/A
3	Before 100% Atkinson	0.117	100
	after 100% Atkinson	0.123	90
	after 200% Atkinson	0.141	69
	after 300% Atkinson	0.164	51
	after 400% Atkinson	0.230	26
4	Low temperature	not measured	N/A

8.5.2 Damping Tests

The level of equivalent viscous damping for the structure was determined by free vibration tests. Each specimen was excited with a sinusoidal input at its fundamental natural frequency. Once the specimen reached resonance, the input from the shake table was interrupted and the decrease of the specimen's acceleration was recorded with respect to time. The shake table was programmed with a sinusoidal harmonic motion to produce a peak acceleration of 0.2 g at the top of the specimen, which was calculated to be less than the cracking moment of the structure. The damping ratio (ζ) was calculated by using logarithmic degradation (δ) which is obtained from the natural logarithmic

relation between the amplitudes of two concurrent cycles (x_n-x_{n+1}/x_{n+2}-x_{n+3}), as seen in Equation [8.2]. The calculation is illustrated in Figure 8.7. This figure shows the results from the initial white noise test for specimen # 2 after the readings were analyzed with a low-pass filter between the range of 0-25 Hz. Subsequently, the damping of the structure was determined from the average of the calculated damping for all the cycles. Table 8.3 gives a summary of the calculated damping ratios. Appendix C gives the damping ratio graphs and the calculations for each test performed.

$$\zeta = \frac{\delta}{2\pi\sqrt{1+\left(\frac{\delta}{2\pi}\right)^2}} \qquad [8.1]$$

where

$$\delta = \ln\left(\frac{x_n - x_{n+1}}{x_{n+2} - x_{n+3}}\right) \qquad [8.2]$$

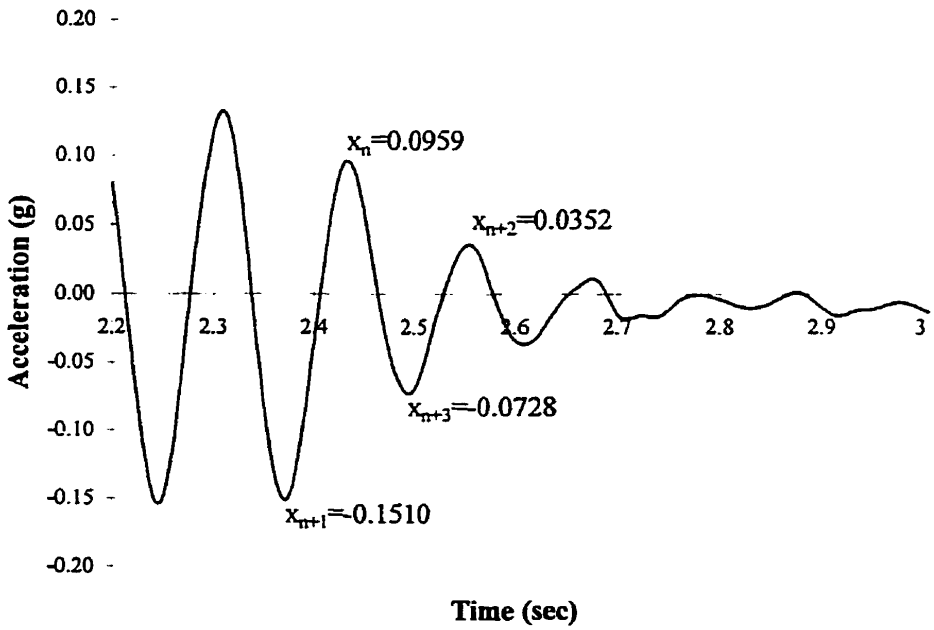

Figure 8.7 Evaluation of the Damping

Table 8.3 Summary of the Damping Ratios of the Structure

Specimen No.	Sequence	Damping Ratio
2	before 100% Adak	13.2
	after 100% Adak	13.8
	after 200% Adak	11.1
2	after 100% Morgan Hill	12.8
	after 200% Morgan Hill	12.5
	after 400% Morgan Hill	N/A
3	before 100% Atkinson	16.7
	after 100% Atkinson	10.3
	after 200% Atkinson	10.4
	after 300% Atkinson	8.9
	after 400% Atkinson	7.7
4	low temperature	N/A

8.5.3 Quasi-Static Test

A quasi-static test was performed on one of the specimens to obtain information concerning the strength, rigidity and the ductility of the specimen to help predict the structural behaviour of the prototype. The quasi-static test replaces the inertia forces generated on a structure by an earthquake with equivalent static forces. A reaction beam was used to resist the movement of the steel frame, thus fixing the position of the pin as described in Section 5.7 and shown in Fig. 5.11. The New Zealand protocol [Cheung et al., 1984], as seen in Figure 8.8, was used as the loading procedure during the quasi-static test with a loading rate of $\dot{\Delta} = 0.05$ mm/s. Preliminary results with the RESPONSE program allowed for the calculation of the nominal yield moment and a

yield displacement (Δ_y) of 7 mm, which corresponds to a displacement ductility factor (μ) of 1.

Due to the displacement of the top of the column during the quasi-static test, the threaded rods were consequently stressed, therefore the prestressing load was adjusted to maintain the predetermined load of 120 kN on the column.

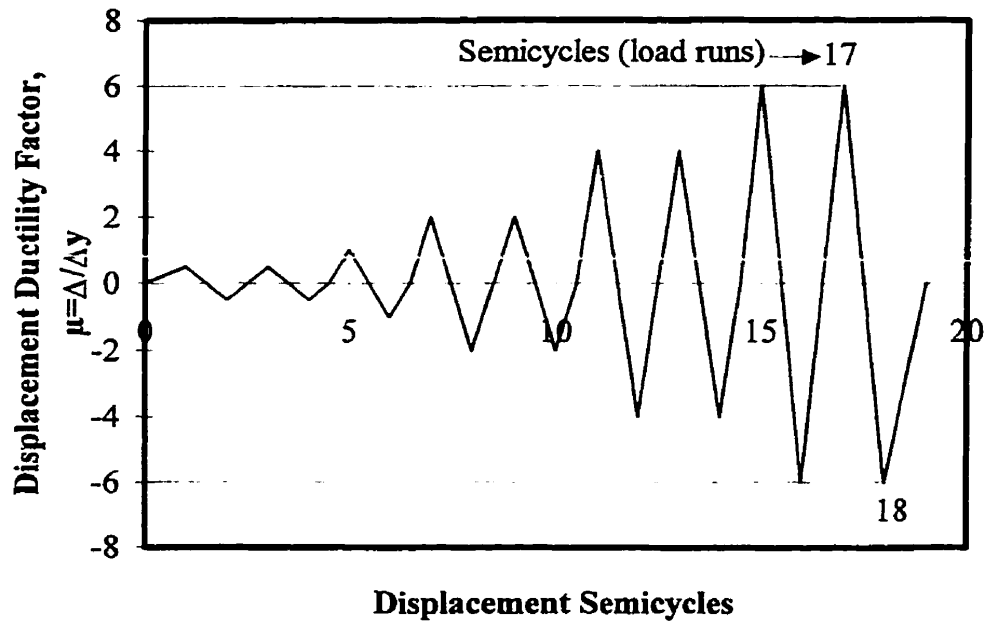

Figure 8.8 New Zealand Quasi-Static Loading Procedure

8.5.4 Seismic Simulations

Experimental tests were performed on the earthquake simulator to directly simulate the seismic forces on the bridge specimens. The shake table was programmed to reproduce historical and artificial ground motions. Sixteen seismic tests were

performed in total on the bridge pier specimens to reproduce three different ground motions at varying intensities and temperatures. The obtained results permitted the evaluation of the non-linear behaviour and modes of failure of the structural system in a realistic seismic environment.

8.5.5 Crack Identification

For crack identification purposes, each specimen was painted with a coat of a water based, white latex paint. Subsequently, all of the apparent cracks were identified after the specimens were placed in position and the prestressing forces were applied to the column. During the quasi-static testing, the loading was briefly interrupted at the end of each cycle in order that the progression of cracking could be documented. Different colours were used to indicate if the cracking was observed prior to testing and to signify the direction of force applied to the column. After each seismic test, the level of cracking was noted and the cracking pattern was traced and photographed.

CHAPTER 9
QUASI-STATIC TEST RESULTS

9.1 Introduction

A quasi-static test was performed on the first of the four specimens to determine the basic lateral load - displacement hysteretic behaviour of the pier - footing assembly, including the column's strength, stiffness and ductility. The test column was subjected to the same lateral displacement pattern as described in Section 8.5.3 until a ductility of 6 was reached. An experimental relative yield displacement (Δ_y) between the center of the hinge and the top of the foundation was assumed at 7 mm based on the results of an analysis using the RESPONSE computer program [Collins and Mitchell, 1991]. This yield displacement corresponded to a nominal flexural resistance of 124 kN.

All applied loads were measured by a calibrated load cell, while linear motion transducer were used to measure the deflections. In additions, vertical LVDTs were placed on each side of the column which allowed for curvature measurements within the plastic hinge region. Strains in the reinforcement were measured by means of electrical resistance strain gauges. The placement and characteristics of the instrumentation are described in Section 8.3.

In this section, the characteristics of the reinforced concrete bridge pier under quasi-static condition are described. Various parameters including base shear-relative displacement, moment-curvatures, strain gauge measurements and bond failures were investigated and are discussed in the proceeding sections.

9.2 General Observations

Diminutive amounts of cracking were observed during the first four semi-cycles at a ductility (μ) of 0.5. Important slippage and flexural cracks were first observed at the base of the column during the fifth semi-cycle at 70 kN and subsequently vertical slippage cracks were observed and spread to the total height of the column when the load reached 80 kN (μ=1.0), as shown in Figure 9.1. The flexural cracks were formed at near-regular intervals of 80 mm and appeared to be influenced by the transverse stirrup spacing. Slippage cracks were closely spaced at the base of the column indicating slippage between the longitudinal bars and the starter bars. At the end of semi-cycle 6-7 (ductility (μ) of 1 - 1.5), large vertical cracking propagated from the base of the column signaling bond failure. As loading continued (ductility (μ) of 2 and 4), the vertical cracking advanced from the base of the column shown in Figures 9.2 and 9.3. A vertical gap of approximately 15 mm was also noticed under the longitudinal bars as a results of slipping of the bars. Spalling of the cover concrete occurred on the tension faces during a ductility (μ) of 4. Throughout the loading there was no observed cracking in the foundation. Failure of the column was caused by slippage between the longitudinal reinforcement and the starter bars in conjunction with spalling of the cover concrete in the lap-splice region due to large displacement reversals, as seen in Figures 9.4 and 9.5.

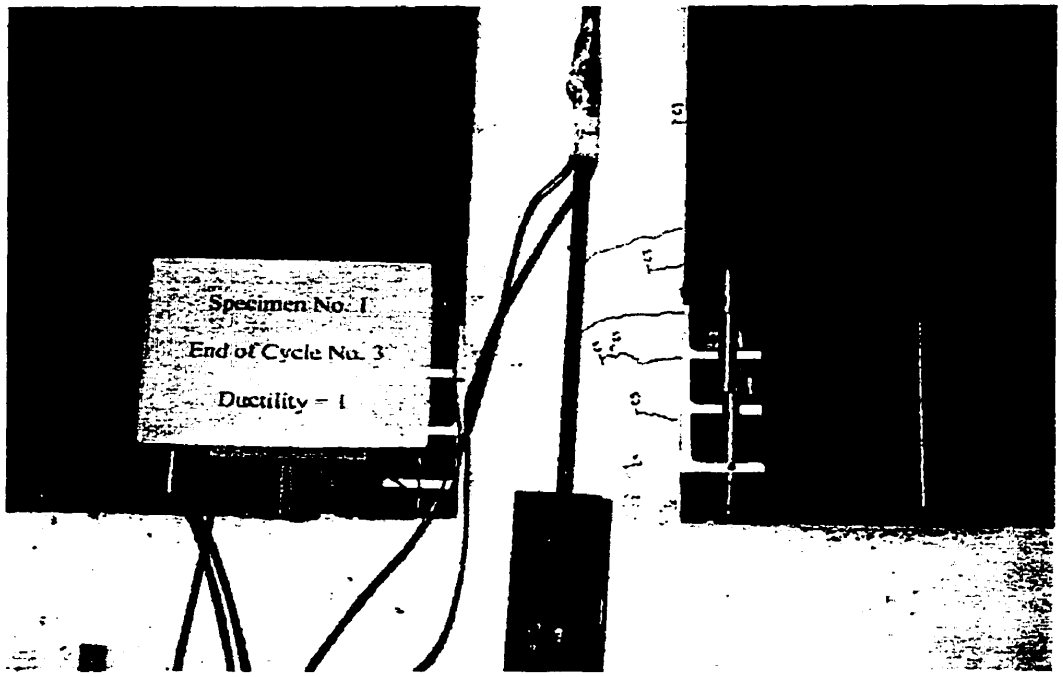

Figure 9.1 Photograph of Specimen at Ductility (μ) = 1

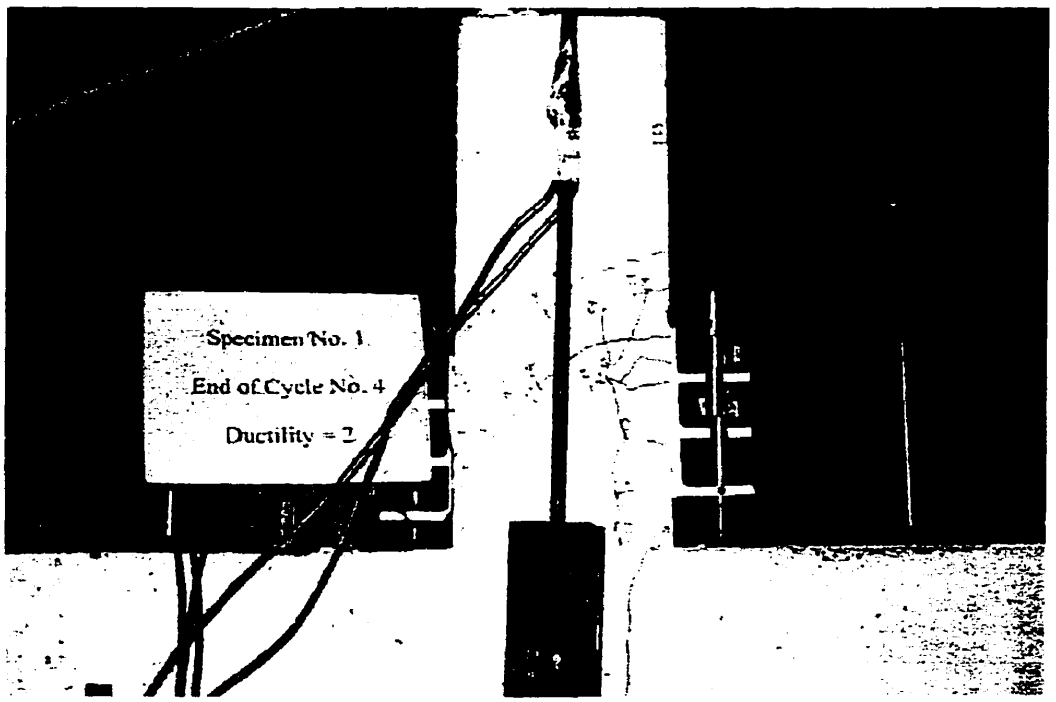

Figure 9.2 Photograph of Specimen at Ductility (μ) = 2

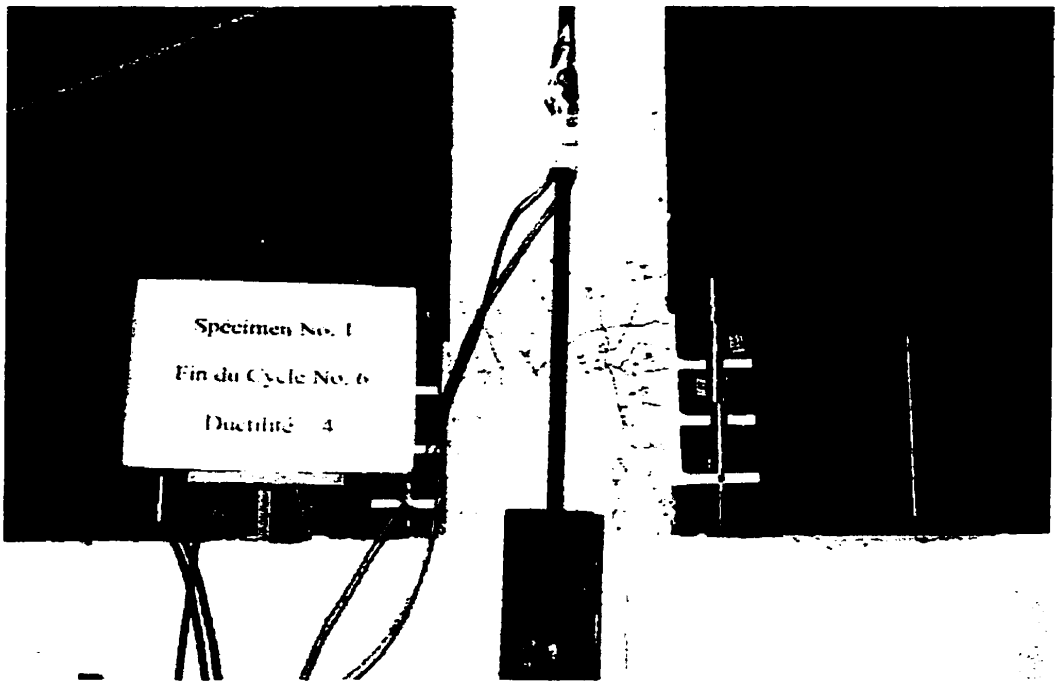

Figure 9.3 Photograph of Specimen at Ductility (μ) = 4

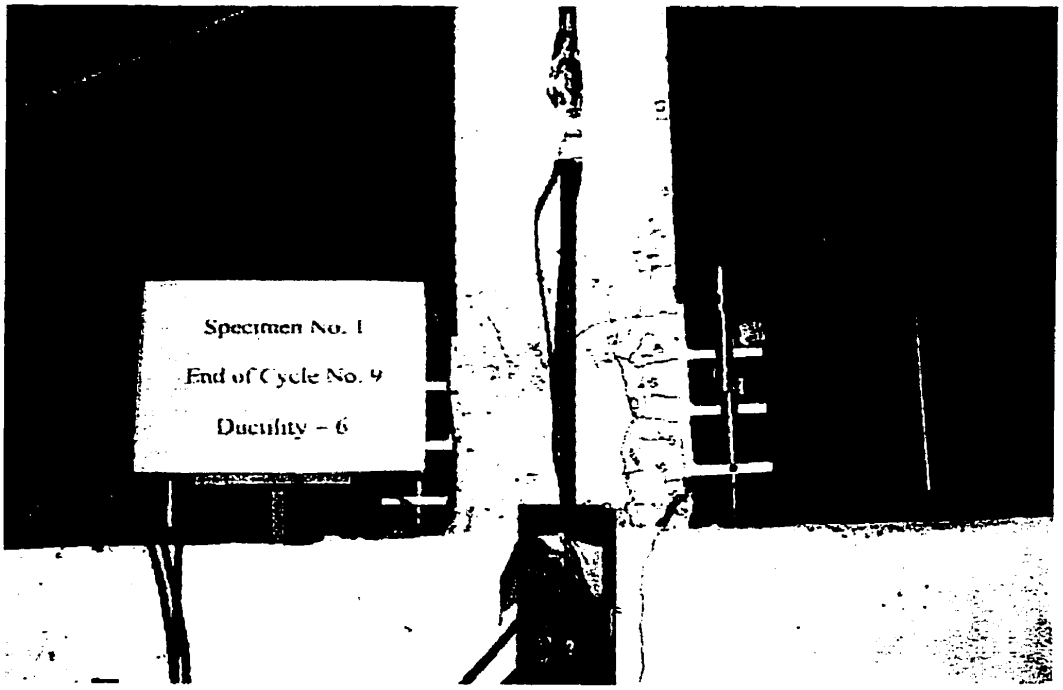

Figure 9.4 Photograph of Specimen at Ductility (μ) = 6

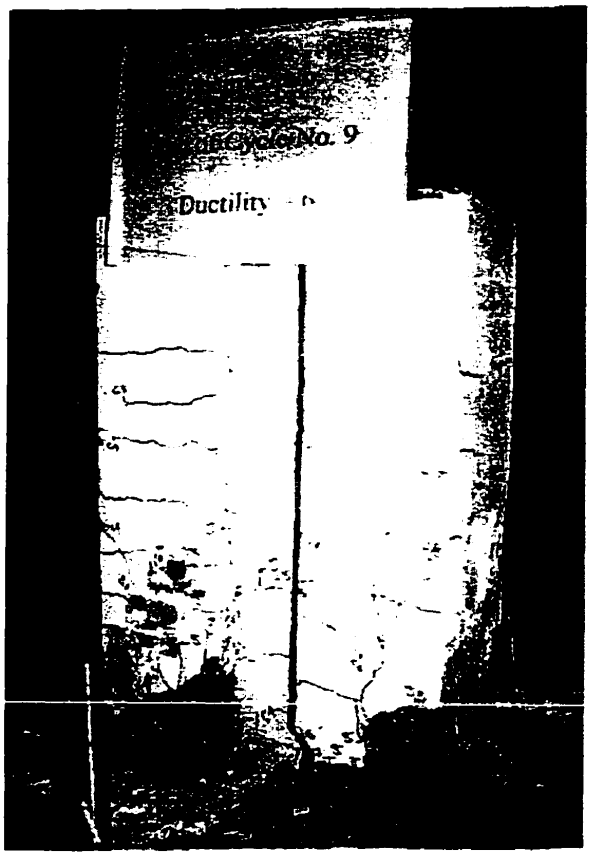

Figure 9.5 Photograph of Specimen after Testing (Ductility (μ) = 6)

9.3 Base Shear - Relative Displacement

The base shear versus relative displacement hysteresis loops of the concrete column obtained from the quasi-static test are shown in Figure 9.6. In this plot, the theoretical ideal flexural capacity of the column is represented by the dashed line. This figure shows that the column's hysteresis loops degrade rapidly between a ductility ratio (μ) of 1 and 2. A maximum lateral load of 80 kN was noted at a ductility (μ) of 1.0 which corresponds to approximately 2/3 of the nominal flexural resistance of the reinforced concrete section, which corresponds to 63% of the adequate development length. The strength envelope is seen to degrade asymptotically after μ = 1.5. The

degradation followed a common pinched hysteretic behaviour with very poor energy dissipation capacities.

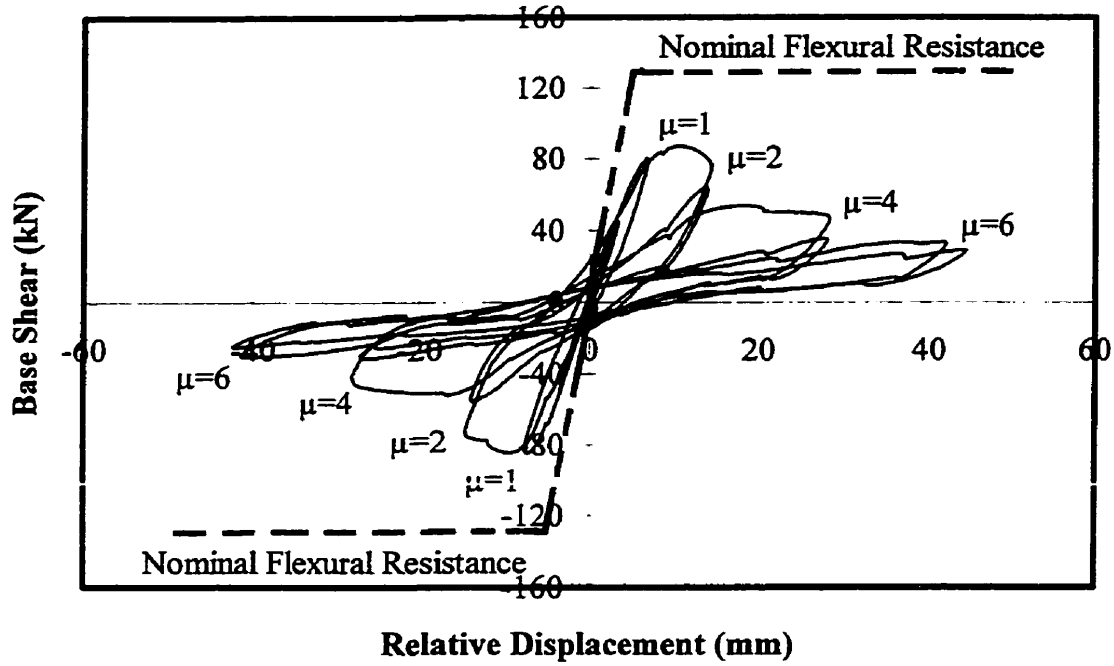

Figure 9.6 Global Shear Force - Relative Displacement Hysteresis Loops from Quasi-Static Test.

9.4 Moment-Curvature

Figure 9.7, 9.8 and 9.9 present moment-curvature plots for three sections within the lap-splice region of the concrete column. The applied moment was calculated from the load cell placed at the end of the reaction beam. The placement of the LVDTs on the extreme tension/compression faces of the column allows an average curvature at the section to be estimated as given in Equation [9.1] by :

$$\phi = \frac{\Delta_N + \Delta_S}{h_c l_c} \qquad [9.1]$$

where Δ_N and Δ_S are relative vertical displacements between adjacent curvature readings on the extreme faces on opposite sides of the column. The variable h_c, corresponds to the vertical displacements between the adjacent LVDTs, and l_c is the horizontal distance between the pair of LVDTs (325 mm).

Three sections were investigated, 55 mm, 110 mm and 165 mm from the base of the column which corresponds to d/4, d/2 and 3d/4, where d is the distance from the extreme compression fibre of the concrete face to the centroid of tension reinforcement. In comparing the three graphs (figures 9.7, 9.8 and 9.9), it can be seen that the curvatures are distributed over the plastic hinge region, with a noticeable reduction at 110 mm from the base which approximately corresponds to the mid-height of the lap-slice. A maximum absolute curvature of 423 rad/km, 122 rad/km and 69 rad/km were observed for each of the three sections at 55, 110 and 165 mm from the base of the concrete column, respectively. Therefore, resulting in a decrease of 71% and 69% of the curvature for sections 2 and 3 when comparing their respective values to those corresponding to section 1. The increased curvatures at the base of the column were due to the appearance of the main flexural cracks, which occurred at that point. Furthermore, the dowel bars in the plastic hinge region suffered bond failure prior to reaching their nominal flexural strength causing rapid strength degradation, as seen in the decrease in the curvature between section 1 and 2.

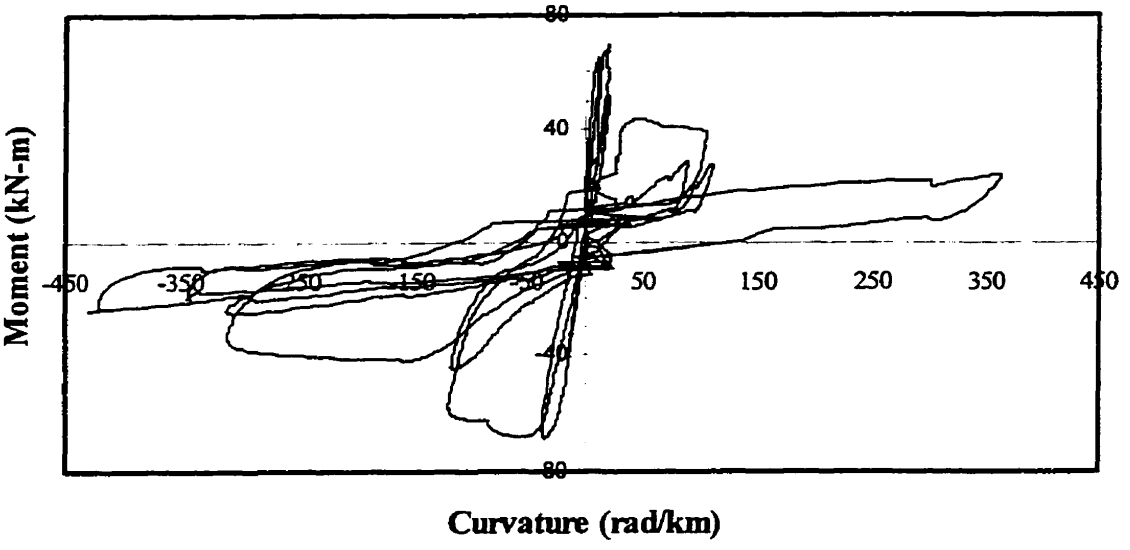

Figure 9.7 Moment-Curvature Diagram for Section 1 (55 mm from the Base of Column)

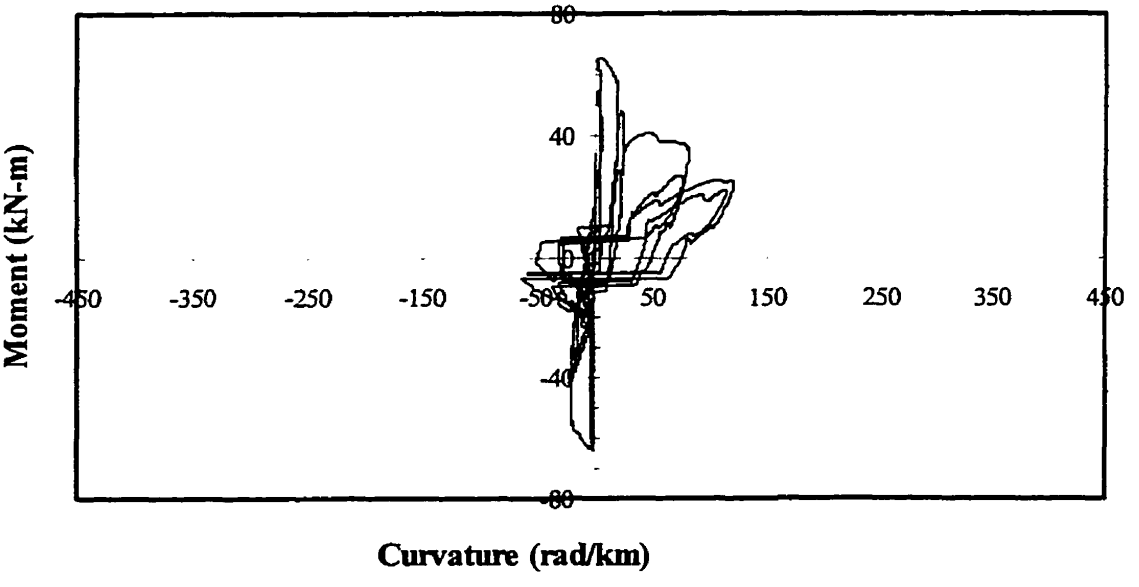

Figure 9.8 Moment-Curvature Diagram for Section 2 (110 mm from the Base of Column)

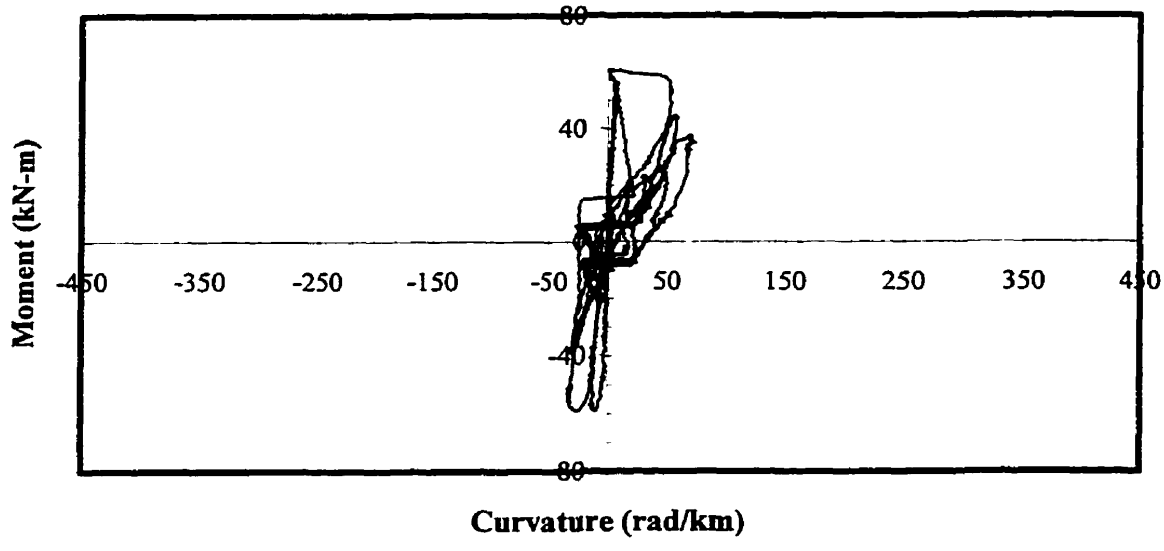

Figure 9.9 Moment-Curvature Diagram for Section 3 (165 mm from the Base of Column)

9.5 Strain Gauge Measurements

Strain gauges were placed on reinforcing bars giving the ability to monitor the level of strains at various positions within the structure during the quasi-static test. Figures 9.10, 9.11 and 9.12 compare maximum strains recorded during the test with respect to the corresponding ductility sequence. Although each specimen was instrumented with ten strain gauges as described in Section 8.3, only seven strain gauges functioned properly. Figure 9.10 represents four strain gauges, three placed on the dowel bars in sections 2 and 3 (110 mm and 165 mm above the base of the column), one placed on the longitudinal bar at 165 mm. For clarity, the strain gauge measurements from section 1 (55 mm from the base of the column) are presented in Figure 9.11. Figure 9.12 represents the results from a strain gauge placed on a stirrup, 83.5 mm from the base of the column, perpendicular to the direction of motion.

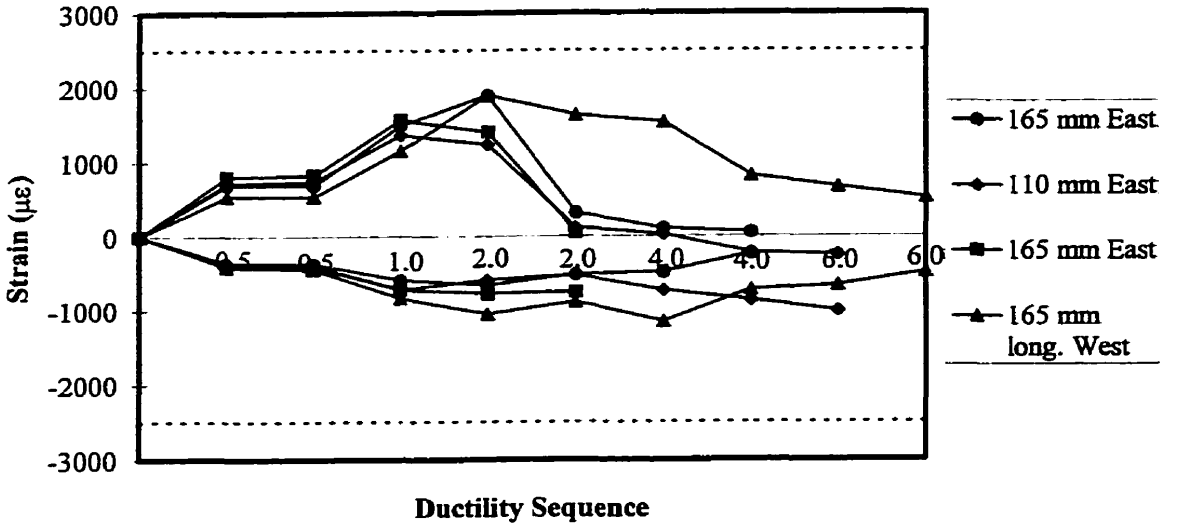

Figure 9.10 Strain Gauge Measurements from Section 2 and 3 (110 mm and 165 mm from the Base of the Column)

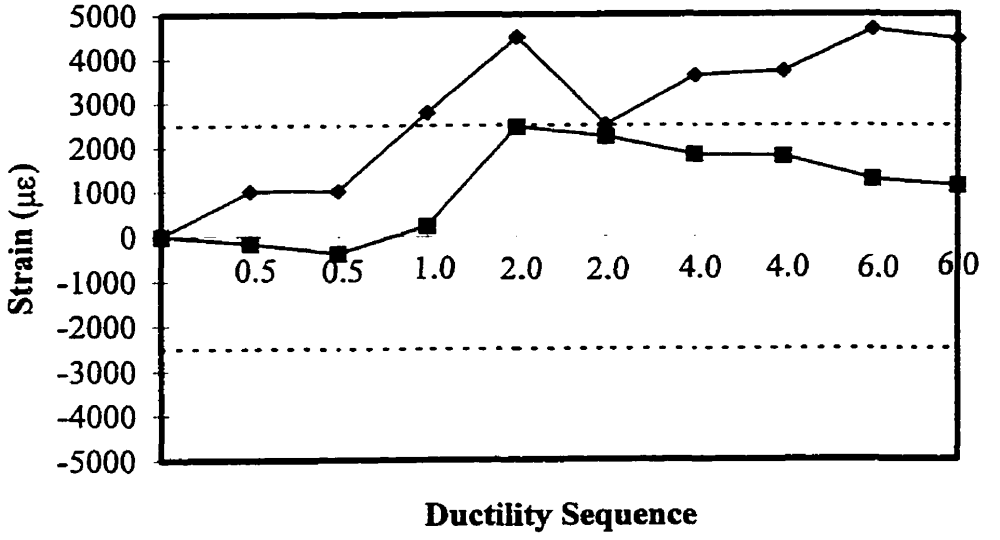

Figure 9.11 Strain Gauge Measurements from Section 1 (55 mm from the Base of the Column)

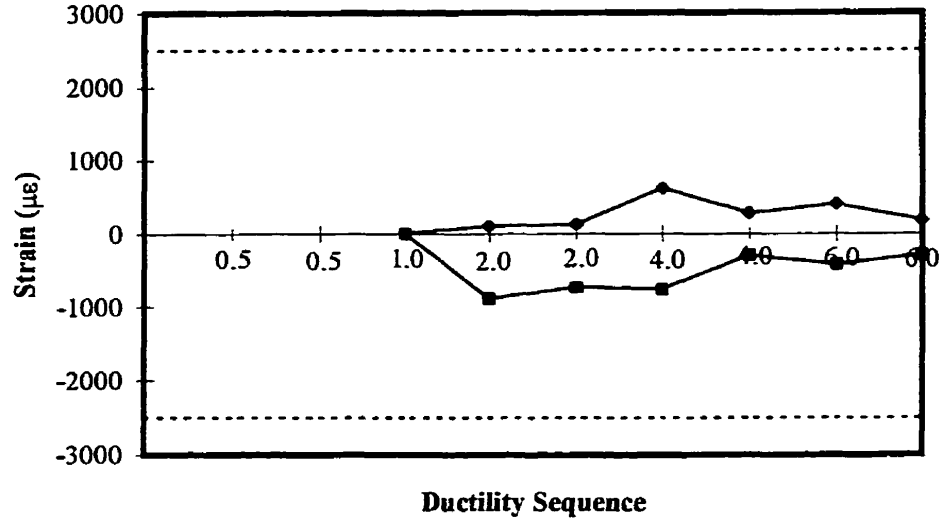

Figure 9.12 Strain Gauge Measurements from Base Stirrup (83.5 mm from the Base of the Column, Perpendicular to the Direction of Motion)

For each plot, an ascertained yield limit of 2500 με was presented as a dashed line to demonstrate the possibility of yielding within the reinforcement. It was evident that slight yielding occurred at section 1 (d/4 or 55 mm) from the base of the column, while other strain gauge measurements recorded at d/2 and 3d/4 (110 mm and 165 mm, respectively) showed lower strain levels. Therefore, indicating high stress concentrations at the base of the lap-splice. In the majority of the readings, the maximum value occurs at a ductility level of 1.5, which corresponds to the bond failure of the reinforcement. Furthermore, higher levels of strains were observed in tension compared to the equivalent compression readings because of the cracked section of the column, thus causing the neutral axis to be shifted from the center, generating higher strains at the opposite extreme face.

Figure 9.13 presents the average of the maximum strains measured in tension over the height of the dowel bar. The graph clearly illustrates the increase stresses at the lower portion of the dowel bars with a maximum tensile strain of 4700 με compared to 1400 με and 1700 με for section 2 and 3, respectively.

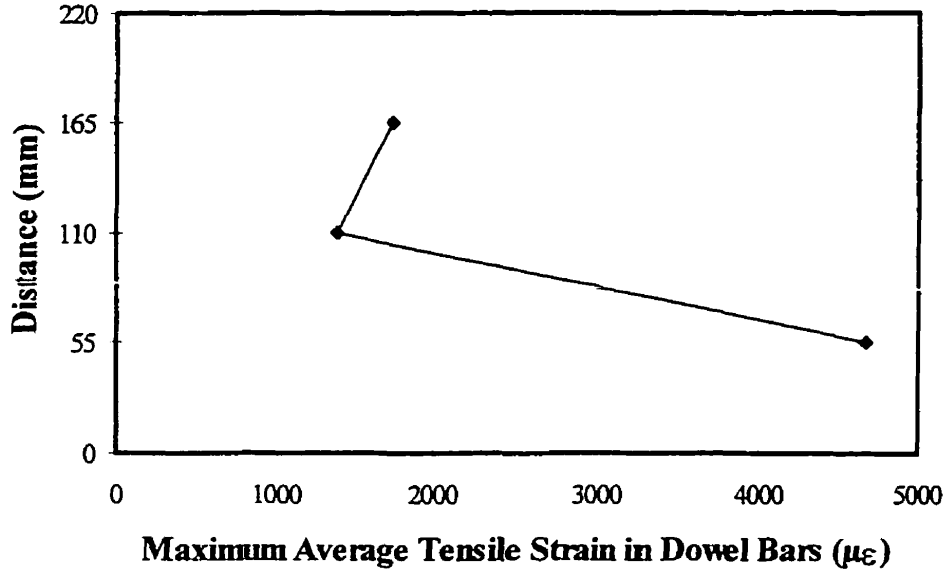

Figure 9.13 Maximum Average Tensile Strain in Starter Bars

9.6 Bond Failure

In order to examine the response of the dowel and longitudinal bars during the quasi-static loading, a strain gauge was placed on the longitudinal bar located adjacent to the instrumented dowel bar, as described in Section 8.3. Both strain gauges (dowel and longitudinal bar), were located at 3d/4 (165 mm) from the base of the column, allowing for direct comparisons between the reinforcement. Figure 9.14 presents the strain

sequences from the strain gauge reading of the longitudinal bar and dowel bar. This figure demonstrates that the specimen with lapped dowel bars in the plastic hinge region suffered bond failure, by the drastic decrease in the strain levels of the dowel bar at a ductility (μ) of 2. During the first three cycles of the loading pattern, the starter bar followed the same pattern and level of strain as the longitudinal, but during the forth cycle (ductility (μ) of 2), a decrease in the level of strain was observed indicating slippage between the two bars.

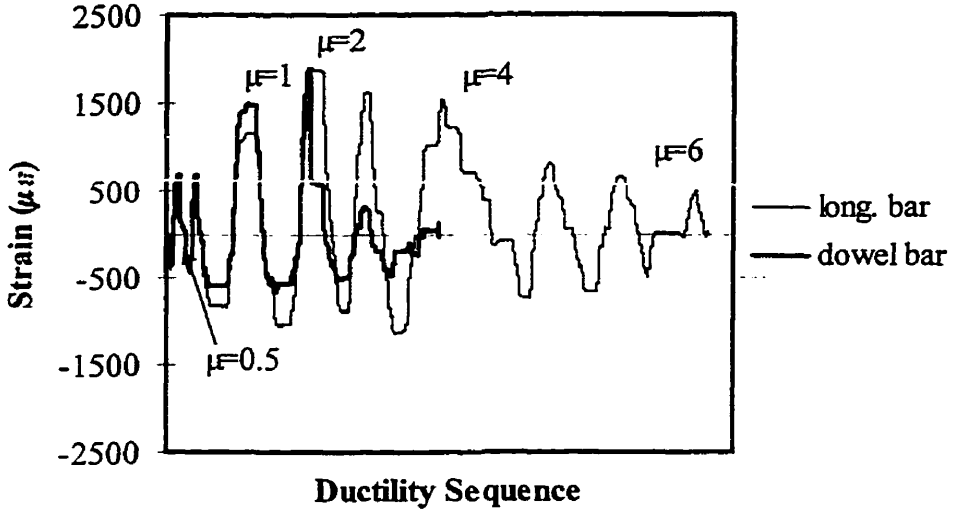

Figure 9.14 Strain Histories of Strain Gauges from Longitudinal Bar and Dowel Bar

9.7 Discussion

The quasi-static test results indicated that failure of the pier specimen was characterized by bond failure of the longitudinal reinforcement of the concrete column relative to the starter bars of the foundation. As a consequence, the maximum shear

force of the specimen was only 2/3 of the shear force corresponding to the nominal flexural strength with rapid flexural strength degradation under cyclic loading. This value corresponds to the value of 63% of the adequate development length, as described in Section 6.2.2. Furthermore, moment-curvature plots showed large curvatures at the base of the column, with decreasing curvatures for sections farther from the base. A high strain level at the base of the column implies yielding of the dowel bars at a ductility of 1.5 which corresponds to the bond failure of the reinforcement. Lack of confinement was also observed over the spliced region due to insufficient transverse reinforcement. As a result, the ultimate curvature developed within the plastic hinge region was limited by the strain at which the cover concrete begins to spall (0.5% strain).

CHAPTER 10
DYNAMIC TEST RESULTS

10.1 Introduction

In this chapter, the results from the seismic tests are presented. General observations are made on the behaviour and performance of the structure under seismic loading and low temperatures. Complete analyses were not carried out on each test due to the limitations of this project, rather a general overview was performed on the general behviour of the columns under seismic loading and comparisons were drawn between the failure modes of the quasi-static test and the seismic tests. Also, unforeseen problems in the experimental set-up caused slippage at the pin connection causing uncertain results from the higher intensity ground motions. Appendix D presents tables giving the peak recorded values for each seismic test. Time-histories of all recorded channels are also given in Appendix D for each seismic test.

For each completed test, the results from the two different data acquisition systems were synchronized to correspond to the recorded data from the shake table's control system. The recorded readings were subsequently filtered with a low-pass filter at 25 Hz with the use of the U2 computer program [EDI, 1993], thus removing all the frequencies which appeared higher than 25 Hz. This process was performed to eliminate the low-level noise produced by the measuring instruments, to give more representative results.

10.2 Performance of the Shake Table

With the use of the RESAS computer program [Sarrazin and Filiatrault, 1993], the spectral accelerations of the three ground motions (Adak, Atkinson and Morgan Hill) were obtained for the 100% intensity. The shake table's spectral accelerations were also analyzed with RESAS from the input accelerations for each of the three ground motions. In order to verify the performance of the shake table, comparisons were made between two spectra (the given ground motion spectrum and the shake table spectrum). Figures 10.1, 10.2 and 10.3 present these spectra for each ground motion at an intensity of 100% and with 5% critical damping. These ground motions plotted below are scaled with a scaling factor equal to 3.65 in the time domain. In each figure, the specimen's measured fundamental period is plotted by a vertical line.

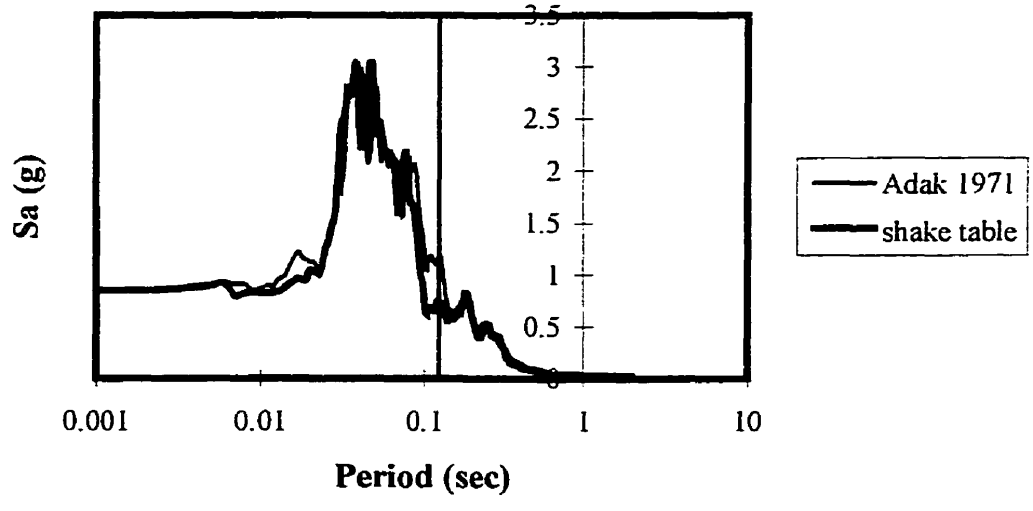

Figure 10.1 Spectral Acceleration for Shake Table and Adak (1971) at 100% with 5% Critical Damping

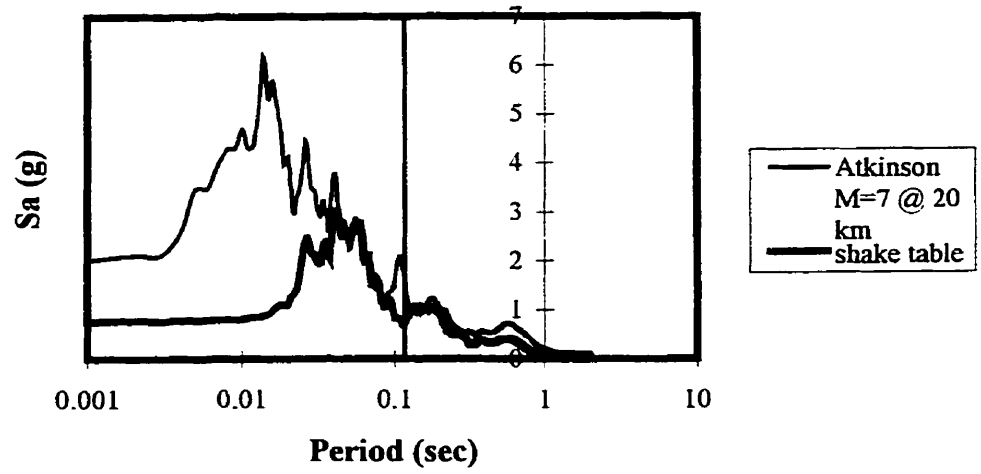

Figure 10.2 Spectral Acceleration for Shake Table and Atkinson (M=7 @ 20 km) at 100% with 5% Critical Damping

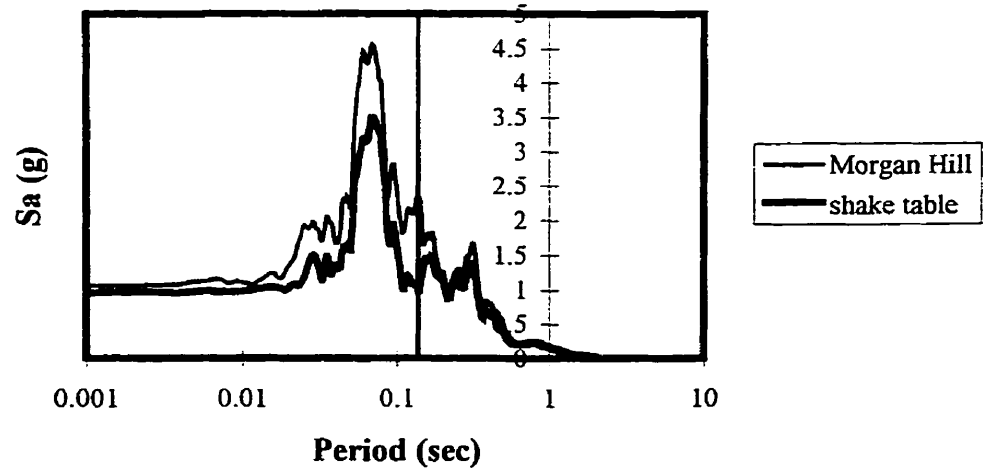

Figure 10.3 Spectral Acceleration for Shake Table and Morgan Hill (1984) at 100% with 5% Critical Damping

The comparison of the above spectra shows that the earthquake simulator has the ability to reproduce the registered ground motions with satisfactory accuracy, with the exception being the high frequencies of the artificial earthquake from Atkinson. For the Atkinson ground motion, the implementation of the scaling laws produced high frequencies beyond the capacity of the earthquake simulator which resulted in deviation between the given ground motion and the shake table results. The lateral stiffness of the specimen decreases from one test to another, causing the specimen's fundamental period to increase. As the level of intensity increases, the structure's fundamental period subsequently increases, therefore resulting in a closer correlation between the two different spectra.

10.3 General Behaviour of Specimens

In this section, the behaviour during simulated loading of a typical pre-1971 reinforced concrete bridge pier is investigated by experimental tests on the earthquake simulator. Various parameters were examined, including : maximum slip at the block - pin connection, drift ratio, pin acceleration, measured curvatures, maximum tensile strain in the stirrups and tensile strain in the starter bars. Furthermore, comparison between ambient and low temperatures (+20°C and -40°C) are discussed. Hysteresis curves are also presented demonstrating the observed behaviour of the specimens during testing, which were latter used in the numeric modelling of the structures.

Table 10.1 give a summary of the seismic tests and the basic observation and comments which correspond to each test.

Table 10.1 Seismic Test Summary

Specimen No.	Ground Motion (Temperature)	Comments and Observation
2	Adak 100% (+20°C)	No cracking noticed and small amount of slippage at connection (2 mm).
	Adak 200% (+20°C)	Diminutive amounts of cracking (horizontal) at the base of both faces, little effect on the frequency (decrease of 17%), therefore decide to use Morgan Hill with same specimen.
	Morgan Hill 100% (+20°C)	Minor amount of crack propagation from the base (vertical cracking), small amount of slippage at pin connection (5 mm).
	Morgan Hill 200% (+20°C)	Enlargement of vertical cracks in the lap-splice and at the base, horizontal crack at the perimeter of column at the base, slippage at pin connection increased (8 mm).
	Morgan Hill 400% (+20°C)	Total structural failure, large amounts of vertical cracking over entire lap-splice, large amounts of spalling of the concrete at the base, vertical gap between longitudinal and dowel bars (15 mm), large amount of slippage at the pin connection (12 mm).
3	Atkinson 100% (+20°C)	No noticeable cracking, small amounts of slippage at the connection (4 mm).
	Atkinson 200% (+20°C)	Diminutive amounts of cracking (horizontal) at the base of both faces and at mid-height of lap-splice.
	Atkinson 300% (+20°C)	Crack propagation, small flexure cracks appear through out lap-splice on both faces, increasing amounts of slippage at pin connection (6 mm).
	Atkinson 400% (+20°C)	Total structural failure, large amounts of vertical cracking over entire lap-splice, small amount of spalling of the concrete at the base, vertical gap between longitudinal and dowel bars (15 mm), decrease in the amount of slippage at the pin connection (5 mm).
4	Adak 100% (-40°C)	No cracking noticed, large amount or slippage at connection was noticed (6 mm).
	Adak 200% (-40°C)	Minor amount of crack propagation from the base (vertical and horizontal cracking), decrease in the amount of slippage at pin connection (3 mm).
	Atkinson 100% (-40°C)	No advancement in crack propagation, amount of slippage at pin connection remained constant (3 mm).
	Atkinson 200% (-40°C)	No advancement in crack propagation, errors in data acquisition.
	Atkinson 300% (-40°C)	Little increase in cracking, large amounts of slippage at the pin connection (10 mm).
	Atkinson 400% (-40°C)	No increase in cracking, large amounts of slippage at the pin connection (10 mm).
	Atkinson 500% (-40°C)	Small vertical cracks formed at the base of the column, little increase in crack propagation, very large amounts of slippage at the pin connection (16 mm).
	Atkinson 600% (-40°C)	Extreme amount of slippage at pin connection (17 mm), no major cracking or failure noticed.

10.3.1 Drift Ratios

Linear motion transducers measuring the horizontal displacement of the table and at the center of the pin allowed the calculation of the maximum relative displacement for each seismic test. As a result, a peak drift ratio expressed as a function of the percentage of the column's height was calculated and plotted with respect to the measured peak table acceleration, as shown in Figure 10.4. The two specimens tested to failure, Morgan Hill +20°C and Atkinson +20°C, both tested at an intensity of 400%, experienced the greatest drift ratio with values of 7.3% and 4.7%, respectively. The drift ratios corresponding to the high intensity seismic tests from Atkinson -40°C ground motions, indicated with circled data points, had values that were less than expected as a result of the slipping of the block - pin connection during the seismic tests, thus biasing the true percentage of the drift ratios.

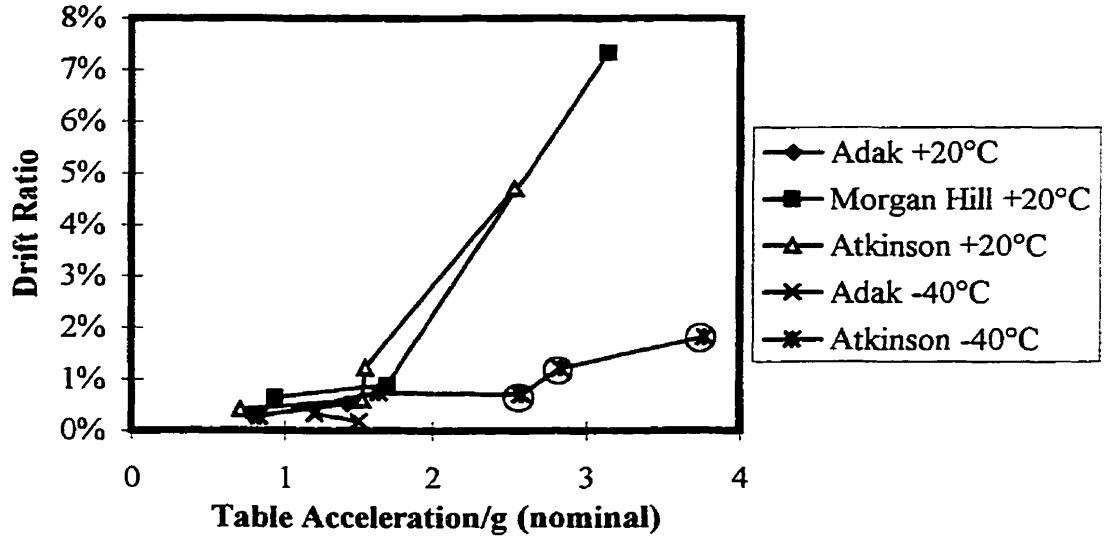

Figure 10.4 Maximum Peak Drift Ratios for Seismic Tests

An indication of the effect of temperature was evident in the comparisons between the two Adak tests performed at +20°C and -40°C. It was observed that drift ratios corresponding to the sequence of tests performed at -40°C were lower than the similar sequence of tests performed at +20°C. An explanation of this trend can be given from the discussion made in Section 4.3. Within the graph, each point on the line represent a specific intensity of their respective earthquake. Also, due to variations in measuring, the peak values from two different tests are not identical (i.e Adak +20°C and –40°C). In this section, the results from experimental tests performed on concrete cylinders indicated a substantial increase in the Young's modulus and the unconfined compressive strength of concrete under the combined effects of high strain rates and low temperatures. These results indicated that at a temperature of -40°C and under seismic loading, the concrete column would experience an increase of the Young's modulus in the order of 50%, compared to the concrete specimens tested at +20°C, subsequently resulting in an increase in the stiffness of the column, thus resulting in lower drift ratios for the specimens tested at low temperatures.

10.3.2 Pin Acceleration

An accelerometer placed at the pin center allowed for the measurement of the acceleration during each of the seismic tests. From these results, the maximum absolute pin acceleration was plotted as a function of the measured peak table acceleration for each temperature and ground motion. The results from these measured readings are normalized and plotted in Figure 10.5. A dashed line at 45° is plotted to indicate acceleration amplification of the pin. In this figure, the Morgan Hill series of tests represents a reasonably linear line of increasing pin acceleration, as expected. In comparing the effect of temperature, there is a general trend of increased pin acceleration for the series of tests performed at low temperatures. An explanation of this trend could

be offered from the results found from the experimental tests, described in Section 4.3, on concrete cylinders at high strain rates and low temperatures. As the Young's modulus of the concrete increases, the stiffness of the specimen consequently increases, resulting in higher frequencies at lower temperatures. Also, as the f'_c increases due to low temperature and high strain rates, the concrete would have a better bond capacity. These phenomenon explains the increase seen in the pin acceleration in the series of tests performed at -40°C compared to the similar tests performed +20°C for the Adak ground motion.

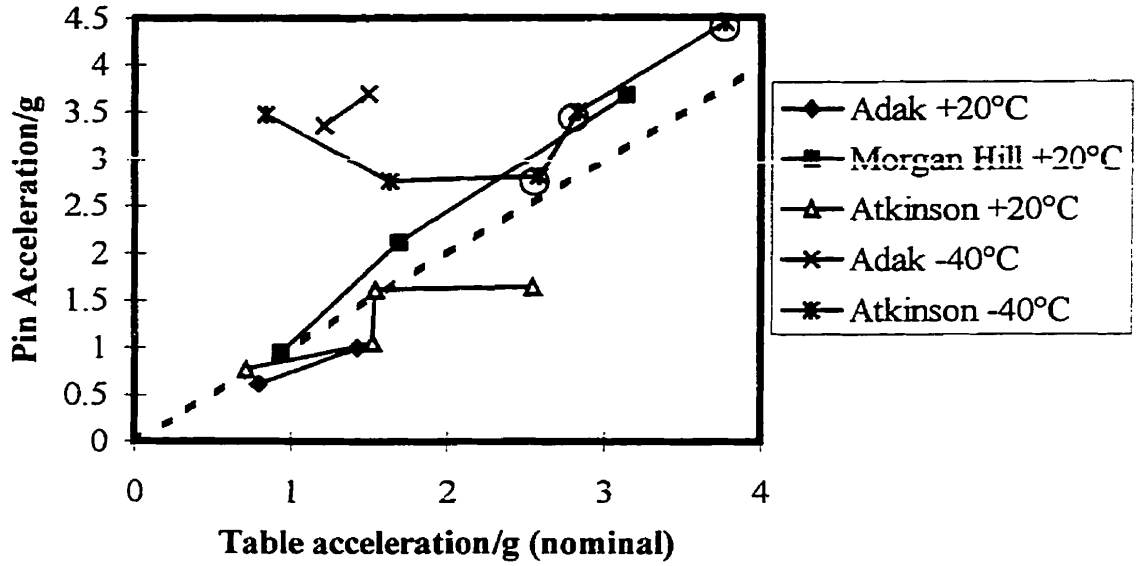

Figure 10.5 Measured Pin Acceleration for Seismic Tests

10.3.3 Maximum Tensile Strain in Dowel Bars

Three strain gauges were placed on two adjacent dowel bars to record the induced forces in the reinforcement during the seismic tests. For each bar, strain gauges were placed at d/2, d/4 and 3d/4, corresponding to 55 mm, 110 mm and 165 mm from the base of the column as explained in section 8.3. The maximum tensile strain was

plotted with respect to the gauge's position, expressed as a percentage of the total height of the column, as shown in Figure 10.6. A dashed line plotted at 2000 $\mu\varepsilon$ gives an assumed level of yielding for the reinforcement. This graph demonstrates that only three ground motions, Morgan Hill 400% (+20°C), Atkinson 400% (+20°C) and Atkinson 600% (-40°C), produced yielding in the dowel bars, which corresponds to the seismic tests in which the specimens were tested to failure. This figure clearly illustrates that outside from these three seismic tests, insignificant amounts of strains were recorded for the remaining tests. The results from this figure indicates that the governing failure mode is characterized by a slip between the longitudinal bars of the pier and the dowel bars at the foundation level due to the low level of strains in the reinforcement. Furthermore, in the majority of the tests, the level of strains were fairly consistent over the measured height of the starter bars, indicating that there was no concentration of stresses, also indicative of a bond failure of the specimens.

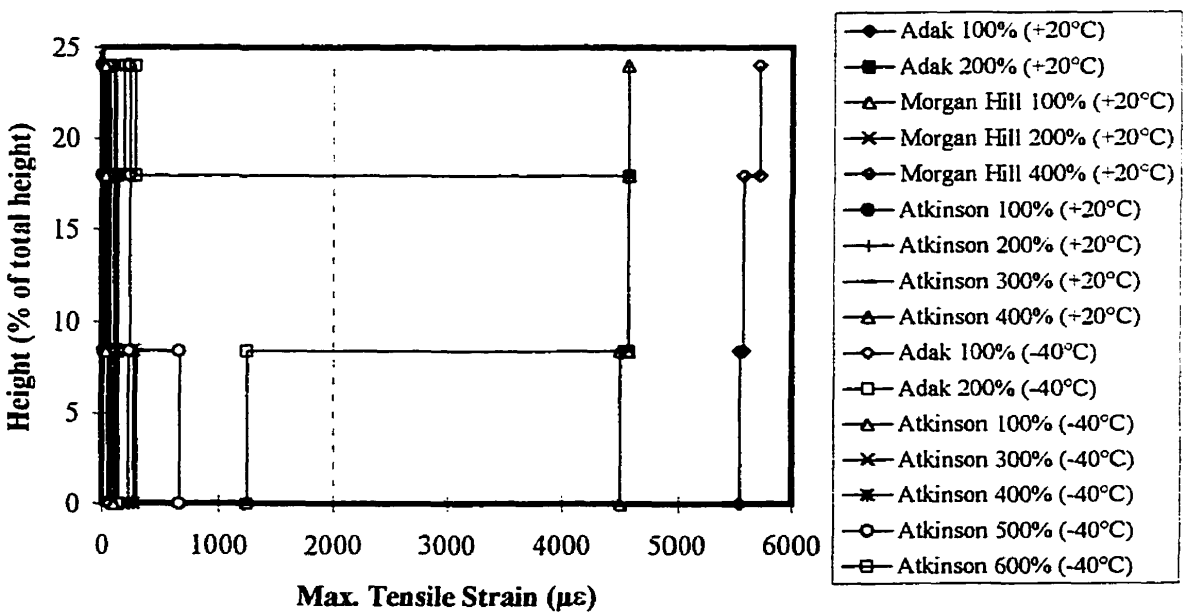

Figure 10.6 Maximum Tensile Strain of Dowel Bars

10.3.4 Maximum Tensile Strain in Stirrups

Three strain gauges were positioned on two separate stirrups to measure the strain levels during the seismic tests. Two gauges were placed on the stirrup located at 83.5 mm from the base, while the other was placed on the above stirrup, positioned at 167 mm from the base, as described in Section 8.3. The maximum recorded tensile strains in the stirrups were plotted against the table acceleration for each of the seismic tests, as shown in Figure 10.7. A dashed line located at 2000 $\mu\varepsilon$ indicates the assumed level of yielding for the transversal reinforcing. This graph clearly illustrates the low levels of strains measured in the stirrups with the exception being Atkinson 400% (+20°C) in which the column experienced total structural collapse. These measurements indicate the little influence and effectiveness of lateral confining steel in the plastic hinge region to increase the columns ductility. The insufficient transverse reinforcement caused a lack of confinement which consequently lead to bond failure of the reinforcement at levels less than their nominal flexural strength.

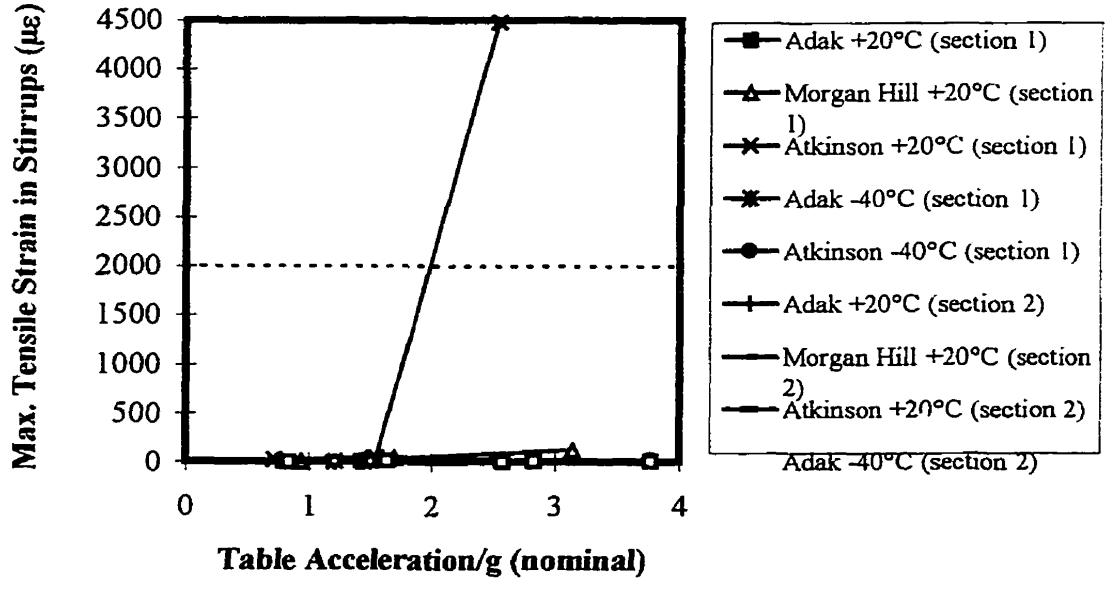

Figure 10.7 Maximum Tensile Strain in Stirrups

10.3.5 Curvature

Curvatures within the plastic hinge region were measured at three locations using pairs of LVDTs which were mounted on the extreme tension/compression faces of the concrete column. The LVDTs were located at d/4, d/2 and 3d/4 which corresponds to 55 mm, 110 mm and 165 mm from the base of the column, as described in Section 8.3. A separate graph for each of the different ground motions displays the measured curvatures plotted against the LVDT's position expressed as the percentage of the total column height. Figures 10.8, 10.9 and 10.10 present the measured curvatures for Adak, Morgan Hill and Atkinson ground motions, respectively. The same scale was used for each of the three ground motions to better compare the level of curvature recorded during testing.

In each case, it is evident that little or no curvature was recorded above section 1, which corresponds to 55 mm from the base of the column. The recorded strains levels were similar (less than 0.005 rad/km) for all three ground motions, with the exception being Morgan Hill at 400% and Atkinson at 400%, where the specimens experienced total structural failure. Also, the values recorded at high intensities tests for the Atkinson tests at –40°C were less than expected due to the slipping at the concrete block – pin connection. In all the seismic tests, the recorded curvatures between the tests conducted at +20°C and -40°C were consistent, concluding that the temperature had little influence in the curvature response. The recorded curvature values coincide with the strain distribution seen in the quasi-static tests, with higher strain levels recorded in section 1 of the dowel bars with respect to sections 2 and 3, thus proving bond failures of the reinforcement as the mode of failure during the seismic tests. The lower curvatures values above section 1 indicate that the column did not bend as an end loaded cantilever column with a fixed base connection. Rather, the column behaved approximately as a

rigid structure indicating the presence of slipping of the longitudinal bars with respect to the starter bars during the seismic tests.

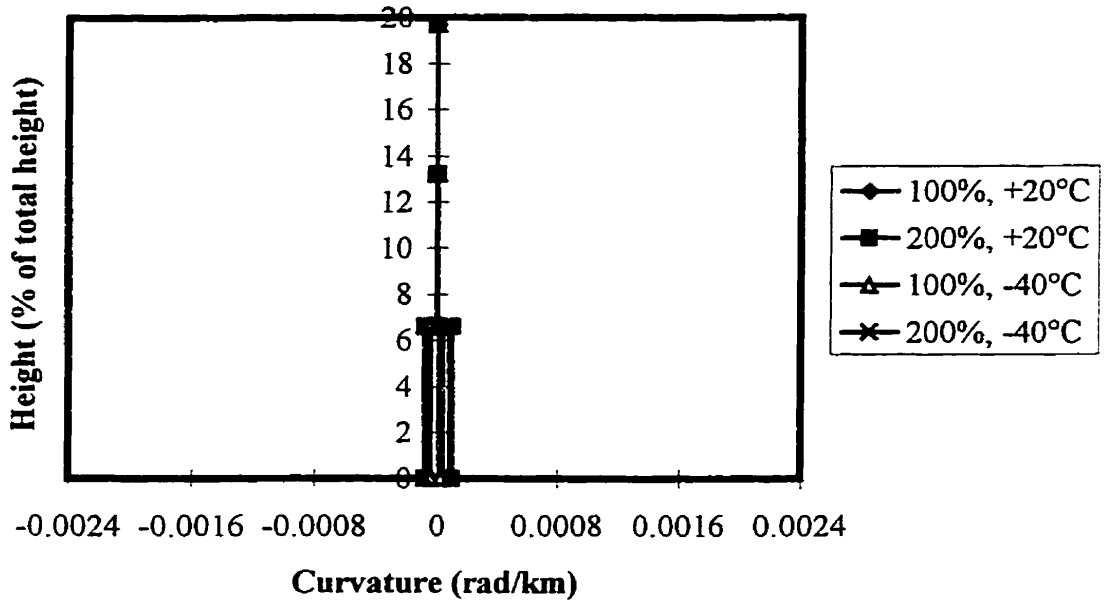

Figure 10.8 Measured Curvature for the Adak Ground Motions

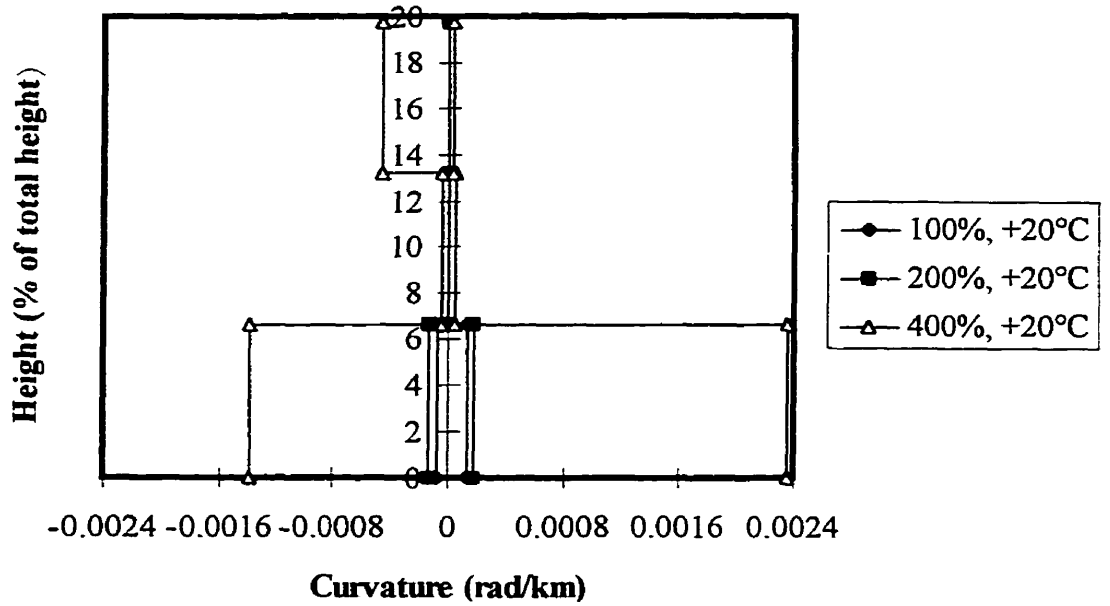

Figure 10.9 Measured Curvature for the Morgan Hill Ground Motions

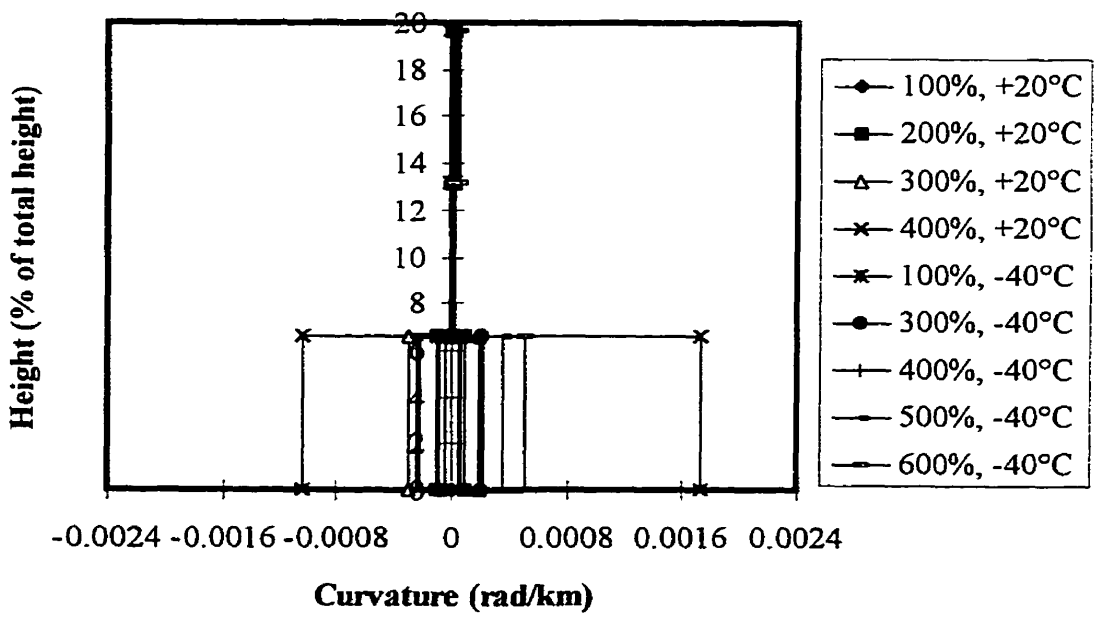

Figure 10.10 Measured Curvature for the Atkinson Ground Motion

10.3.6 Block - Pin Slippage and Measurements

To accommodate the pre-existing assemblages, the concrete blocks were connected to the pin by means of two steel plates (710 mm x 420 mm x 25 mm) which transmitted the forces from the concrete blocks to the pin. Although steps were taken to ensure proper fixed connections which would allow realistic modelling characteristics, unforeseen slipping occurred between the concrete blocks and the pin connection. This movement was most likely caused by the improper tightening of bolts which connected the concrete blocks to the pin. The positioning of linear motion transducers gave the ability to monitor and record the level or relative horizontal movement of these components during testing. By having instruments positioned at the top of the column, the pin and the concrete blocks, it was possible to measure the level of displacement with respect to the applied force, giving the ability to numerically model this phenomenon. Figure 10.11 presents the maximum slip observed for each of the seismic tests corresponding to the measured peak table acceleration. In comparing the maximum slip with the calculated drift ratios, the results from seismic tests with a maximum slip greater than 7 mm (μ=1) are suspect to their validity, principally the Atkinson -40°C tests performed at intensities of 400%, 500 % and 600%, which are identified with a circle around the data point. Although general trends can be observed, it must be recognized that the values from these tests may have skewed results due to the amount of slipping in the experimental set-up.

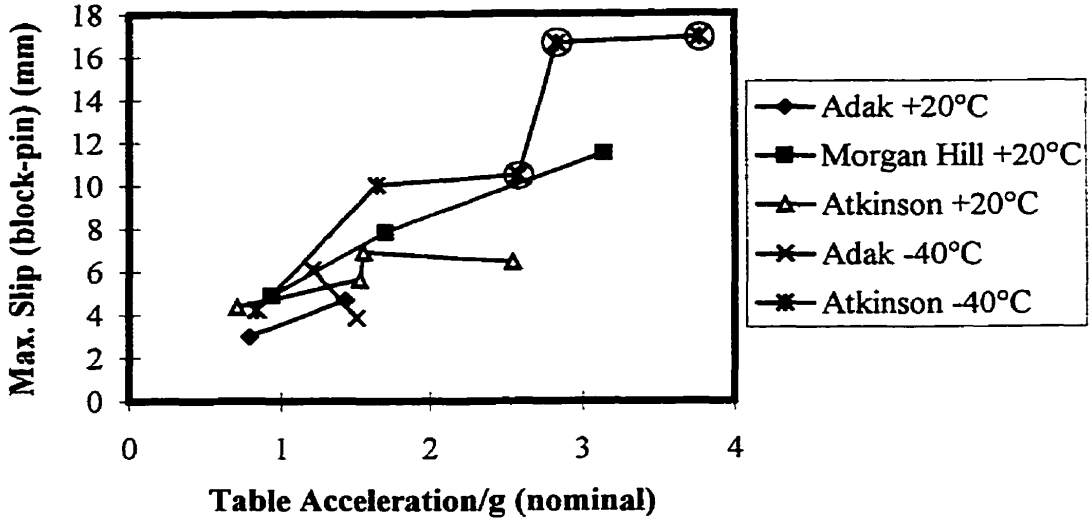

Figure 10.11 Maximum Slip Between the Block and Pin for Seismic Tests

The slippage (movement) of the connection was able to be measured by placing linear motion transducers at the top of the concrete column and at the center of the pin, thus allowing the relative displacement between these two components to be measured. When these values are plotted against the base shear, as seen in Figures 10.12 and 10.13, a calculation of the stiffness of the connection can be made. The base shear was calculated from the pin acceleration which was measured during each test. Figures 10.12 and 10.13 presents the hysteresis curves of the relative displacement between the pin and the top of the concrete for Morgan Hill for intensities of 100% and 200%, respectively. In order to determine the stiffness of the connection, a regression line going through the origin was estimated from the data. For the seismic tests, a stiffness of 27 kN-mm was calculated by interpolating the slope of this line. In figures displayed below, base shear value of 54 kN corresponded to a relative displacement of 2 mm. Therefore, this stiffness value of 27 kN enabled the pin connection to be numerically modelled and the validation of the results to be performed. Chapter 11 discusses the numerical modelling procedure.

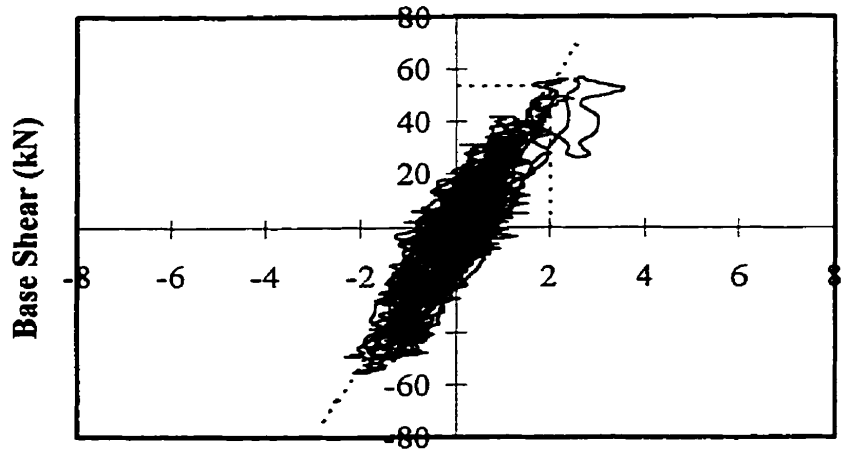

Figure 10.12 Hysteresis Curve of the Relative Displacement Between the Pin and the Top of Concrete for Morgan Hill 100%

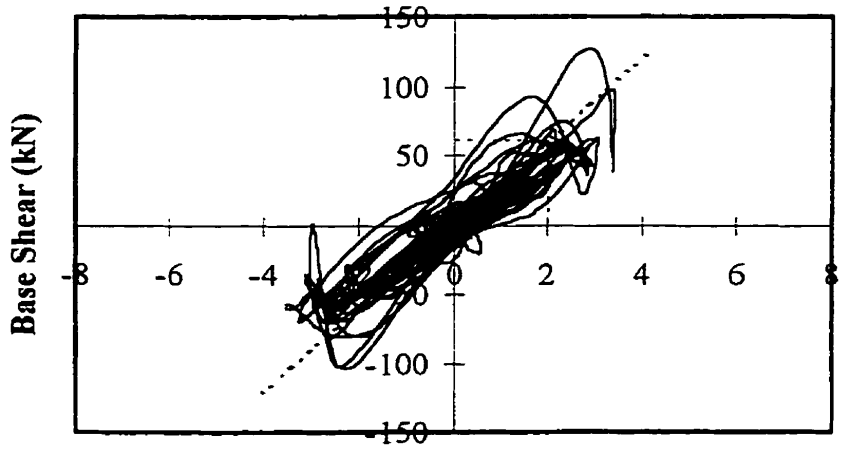

Figure 10.13 Hysteresis Curve of the Relative Displacement Between the Pin and the Top of Concrete for Morgan Hill 200%

CHAPTER 11
NUMERICAL MODELLING

11.1 Introduction

Numerical modelling was performed with the use of the RUAUMOKO computer program [Carr, 1995] to validate the seismic response from the experimental results of the reinforced concrete bridge piers. In this chapter, the methodology and the development of the final models that were considered in the numerical analyses are discussed. Furthermore, the results from the computer models are investigated and compared to the corresponding measured values of the tested specimens. By performing numerical modelling, a better understanding of the behaviour of the reinforced concrete bridge column can be drawn. Numerical modelling also gives researchers an ability to realistically simulate the existing structures.

11.2 Non-linear Dynamic Analyses

In this section, a description of the numerical modelling performed on the reinforced concrete bridge pier is described which best represented the experimentally tested structure. The modifications used in the RUAUMOKO model are briefly described and the hysteresis model used is presented. The parameters used in the hysteresis model including moment, curvature and initial stiffness factors are also given. Furthermore, the different modifications that were introduced from the existing model are explained and discussed. Changes, in regard to the measured natural frequency of the structure, are described and the numerical values used in the model are justified.

11.2.1 Hysteretic Model

The RUAUMOKO computer program was used to investigate the non-linear response of the reinforced bridge pier specimen. By using the recorded table acceleration as the excitation, a piece-wise time-history response of a non-linear, two dimensional frame structure could be calculated which simulated the experimental results. Figure 11.1 shows the MUTO [Muto et al., 1973] degrading tri-linear hysteresis rule which was used for the non-linear analyses. The Muto degrading tri-linear hysteresis rule, shown below, is the equivalent of the moment – curvature model used in the preliminary analysis, as described in Section 6.2.1.

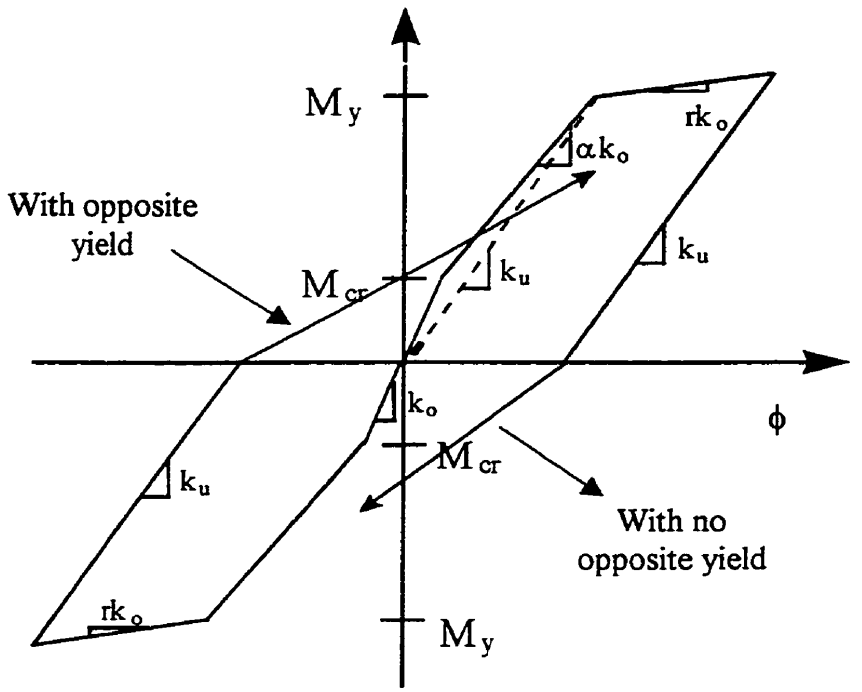

Figure 11.1 Muto Degrading Tri-linear Hysteresis Model

The envelope for the hysteresis model was adapted from the base shear – relative displacement hysteresis loops from the quasi-static test. Verification of the initial

from LVDTs positioned at the three various section on the column's surface and from preliminary push – over analyses. The moment – curvature relationship of the column are simplified by the tri-linear model and adapted to the Muto hysteresis rule.

Table 11.1 gives the values for the moment, curvatures and the stiffness coefficients, which corresponds to the hysteresis model. The Muto model is limited with one numerical input value for the cracking and the yielding stiffnesses, therefore, an average was calculated between the positive and negative stiffness coefficients and inputted into the data file. The post-yielding stiffness, r, was unable to have a negative slope, as seen in the quasi-static hysteresis loop, therefore, a value of zero was used. The hysteresis model gives the ability to input positive and negative values for the cracking and yielding moments. Therefore, a closer simulated model could be achieved my inputting the different moments from the unsymmetrical section. The actual section properties were used as the initial stiffness. The cracking moment could not be clearly identified from the quasi–static tests, therefore, the analytical values were used in the numerical modelling. The yielding moments and the corresponding curvatures were calculated directly from the base shear – relative displacement hysteresis loops from the quasi-static tests. The post-cracking stiffness coefficients were subsequently calculated from the cracking and yielding moments co-ordinates.

Table 11.1 Summary of the Muto Hysteresis Modelling Parameters

	M_{cr} (kN-m)	M_y (kN-m)	α post-cracking	r post-yielding
Positive	16.6	70.3	0.007	0.00
Negative	-14.8	-68.4	0.007	0.00

11.2.2 Computer Modelling

Modifications were done on the existing model to best represent the actual response of the tested specimens. Minor adjustments were made in the height of the column and the length of the fixed link from the existing model. Due to the availability of the HSS section needed in the prestressing system, the length of the fixed link was therefore increased by 12 mm to correspond with the actual length.

The recorded table accelerations were used at excitations for the RUAUMOKO modelling to generated the same seismic loadings as applied to the specimens. The input had an time step of 0.002 seconds and was filtered with the use of the U2 program [EDI, 1993].

In order to model the slipping which was experienced at the pin connection, a spring was introduced into the model as seen in Figure 11.2. This spring was placed between the top of the column (above the prestressing system) and the concrete blocks. To represent the lateral inertia loads, the concrete blocks (mass of 60 kN) were modelled with roller connection in the horizontal direction. A stiffness of 27 kN/mm for the pin connection was determined by calculating the slope of the hysteresis curves of the relative displacement between the pin and the top of the concrete versus the base shear, as described in Section 10.3.7. By placing a spring into the model to

represent the slipping at the pin connection, it was possible to reduce the frequency of the system. The original model which was used for the preliminary analyses had a frequency equal to 12.5 Hz, which assumed a fixed connection between the pin and the top of the concrete. Therefore, by introducing a spring with a stiffness of 27 kN-mm, the frequency reduced to 8 Hz, which corresponds to the measured values of the specimens determined from the white noise tests (see Section 8.5.1).

The damping ratio was also modified from the value of the initial model. The damping ratio was increased from the original value of 5% to a value of 12%, which corresponds to the average value of the damping tests performed prior to each seismic tests.

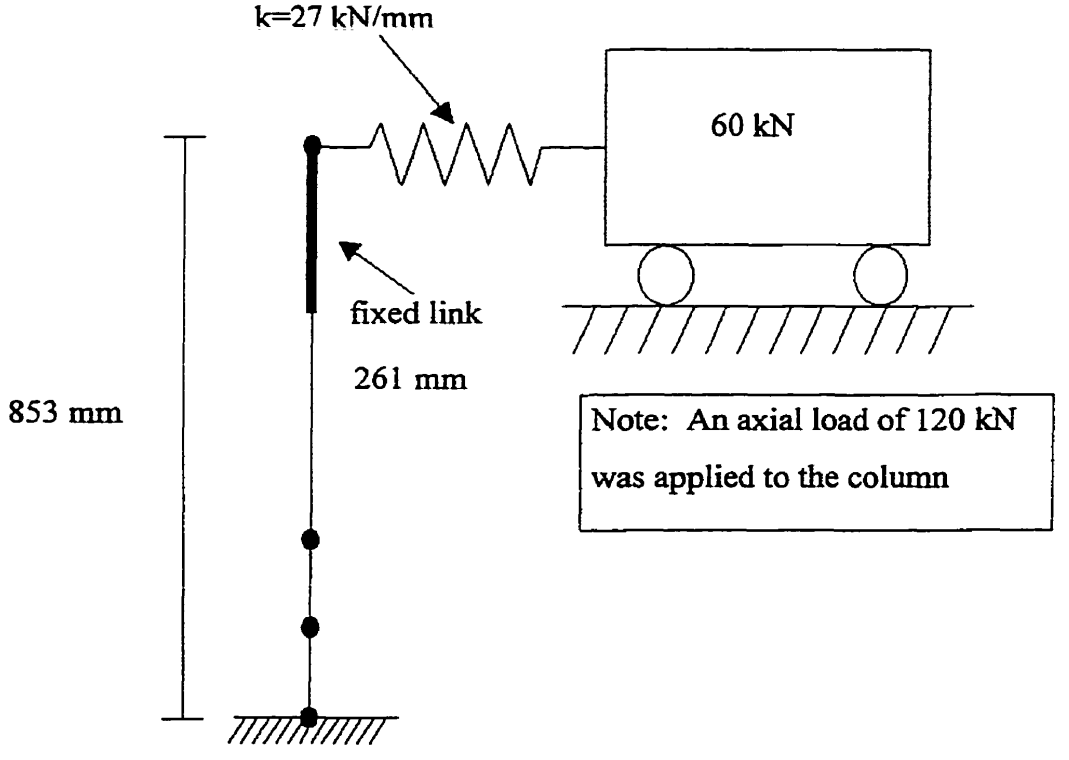

Figure 11.2 Computer Model

Two models were developed for the non-linear analysis. The first one, identified as "Ruaumoko", is the final model in which a spring was introduced with a stiffness of 27 kN-mm (frequency of 8 Hz) and a damping ratio of 12%. The second model resembled the model used in the preliminary analyses, entitled "Ruaumoko (5% damping, no spring)" in which the spring was not introduced (frequency of 12 Hz) and a more realistic damping of 5% was used, with modifications to the column height and the length of the fixed link.

11.3 Comparison of Final Model to Experimental Results

In this section, the models are compared to the experimental results by investigating the results of their corresponding pin acceleration and displacements. The comparisons are illustrated by the seismic loading for the two specimens tested at +20°C (specimen # 2 and specimen # 3). The time histories for specimen # 2 were plotted for 60 seconds, which included the Adak and the Morgan Hill series of tests (Adak 100%, 200% and Morgan Hill 100%, 200% and 400%). The time histories for Specimen # 3 were plotted for 30 seconds and included the Atkinson series of ground motions (Atkinson 100%, 200%, 300% and 400%). To realistically model the loading applied to the specimens, the models which were used in the non-linear analyses were consecutively loaded with an appropriate lap time given between each ground motion, as performed in the experimental tests.

Figures 11.3 and 11.4 display the comparisons between the experimental results and the results from the two non-linear models of the pin acceleration and displacement, respectively, for specimen # 2 (Adak and Morgan Hill). Figures 11.5 and 11.6 present the comparisons between the experimental results and the results from the two non-

linear models, for the pin acceleration and displacement, respectively, of specimen # 3 (Atkinson).

In each of the figures, little difference can be seen between the two non-linear computer models, the first model, which had a frequency of 8 Hz and a damping of 12% and the second model, which had a frequency of 12.5 Hz and a damping of 5%. The similarities between the time histories from the two models resulted from the high frequencies of the inputted ground motions. The change in the damping ratio (12% to 5%) and the column's natural frequencies (12.5 Hz to 8 Hz) caused little effect on the computer results due to the high frequencies levels of the chosen earthquakes.

When comparing the three time-histories from each of the figures, it is evident that as the intensity of the ground motion increases, the correlation between the measured values and the values generated from non-linear analysis deviate from each other. The explanation for this trend is that the RUAUMOKO model was unrealistic in the modelling for the failure modes experienced by the specimens. The failure of the column seen in both the quasi-static and seismic tests, was bond failure of the reinforcement. The RUAUMOKO computer program could not adequately model this phenomenon. Various features in the computer program, such as strength degradation, were used to reproduce the slipping which occurred at the higher intensity tests, but unfortunately, improvements in the correlation between the non-linear model and the experimental results could not be made. At the lower intensities, Adak 100 % and 200%, Morgan Hill 100% and Atkinson 100%, a closer correlation was seen because the slipping of the reinforcement was not as predominate, as was the case with the higher intensities. For the lower intensity ground motions, the percent differences between the measured values and the values produced by numerical modelling were in the range between 25% – 35%.

For the overall behaviour of the specimens, major structural failure did not occur at the intensities as predicted, due to the fact that the unforeseen slipping occurred at the pin connection. Therefore, the true lateral inertia load was not applied to the specimen as anticipated. Due to the slipping which occurred at the pin connection, the pre-calculated frequencies of the column was decreased, thus changing the energy level the column would experience.

The overall failure of the specimens coincided with the behaviour seen in the quasi-static tests. The performance of the reinforced concrete columns was governed by bond failure of the longitudinal reinforcement, due to the lack of confinement of transversal reinforcement. The large stirrup spacing, with respect to the height of the lap-splice, did not produce enough confinement, which in turn, lead to failure of the specimens at only 2/3 of their nominal flexural resistance.

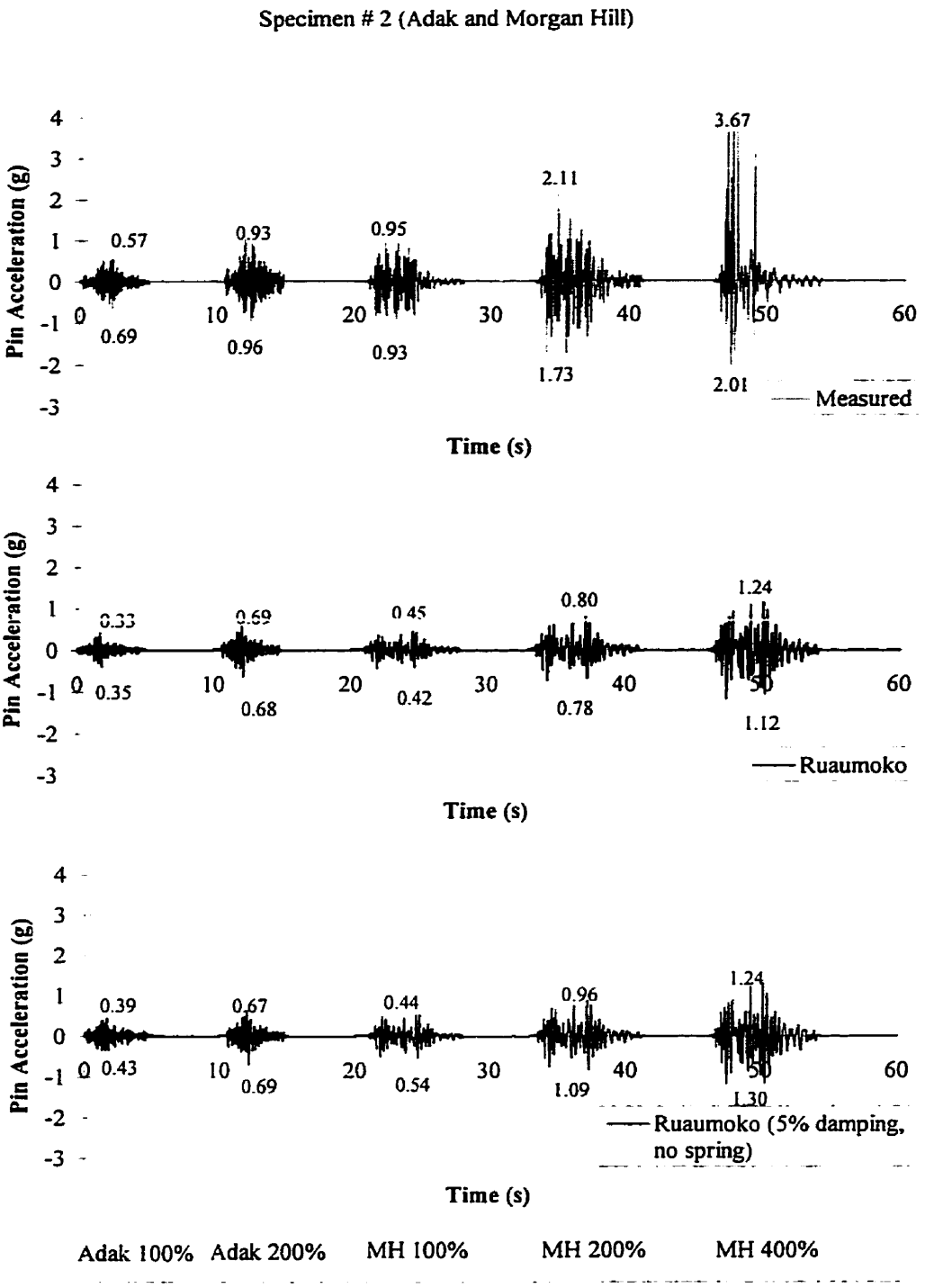

Figure 11.3 Pin Acceleration (g) for Specimen #2 (Adak and Morgan Hill)

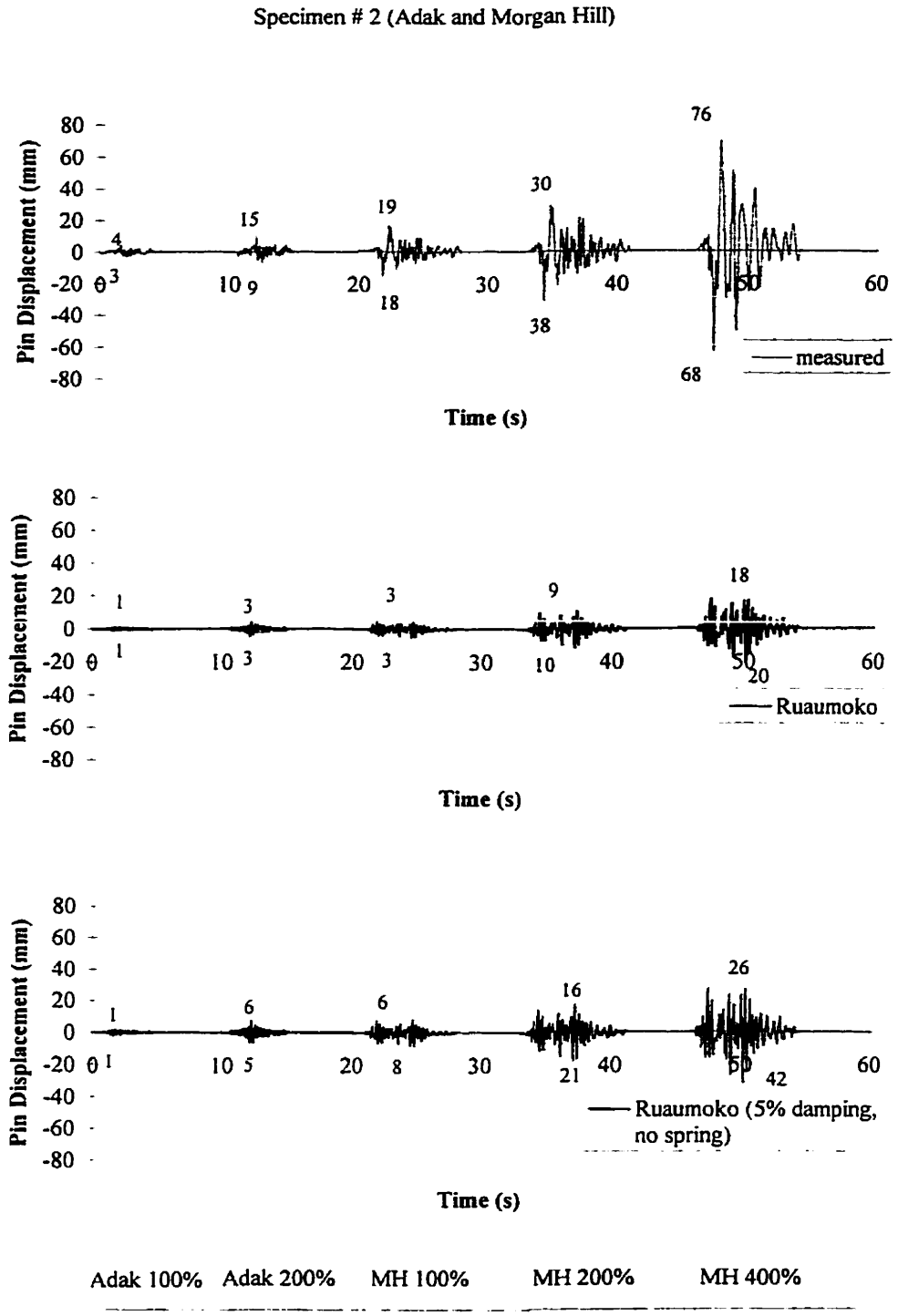

Figure 11.4 Pin Displacement (mm) for Specimen #2 (Adak and Morgan Hill)

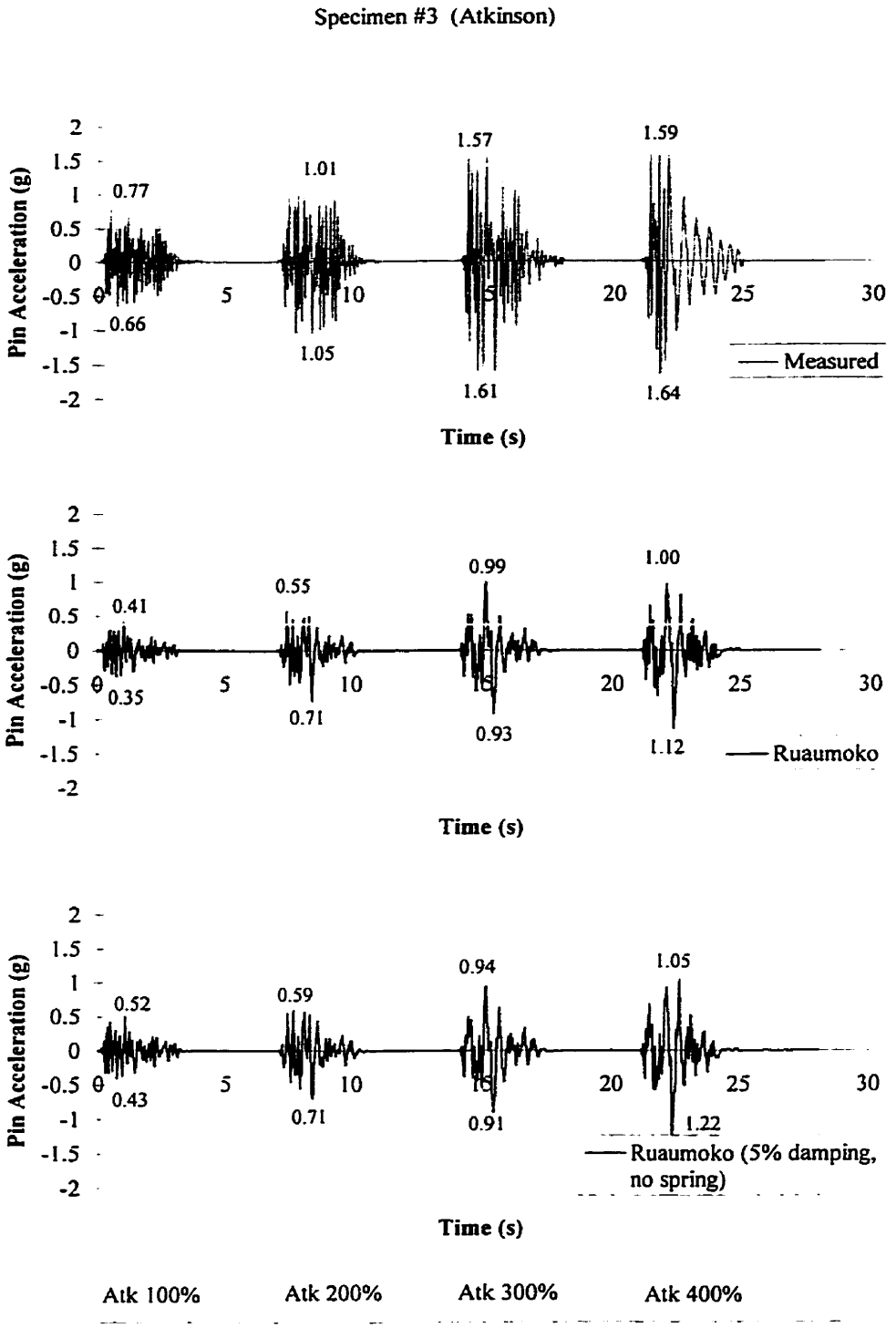

Figure 11.5 Pin Acceleration (g) for Specimen #3 (Atkinson)

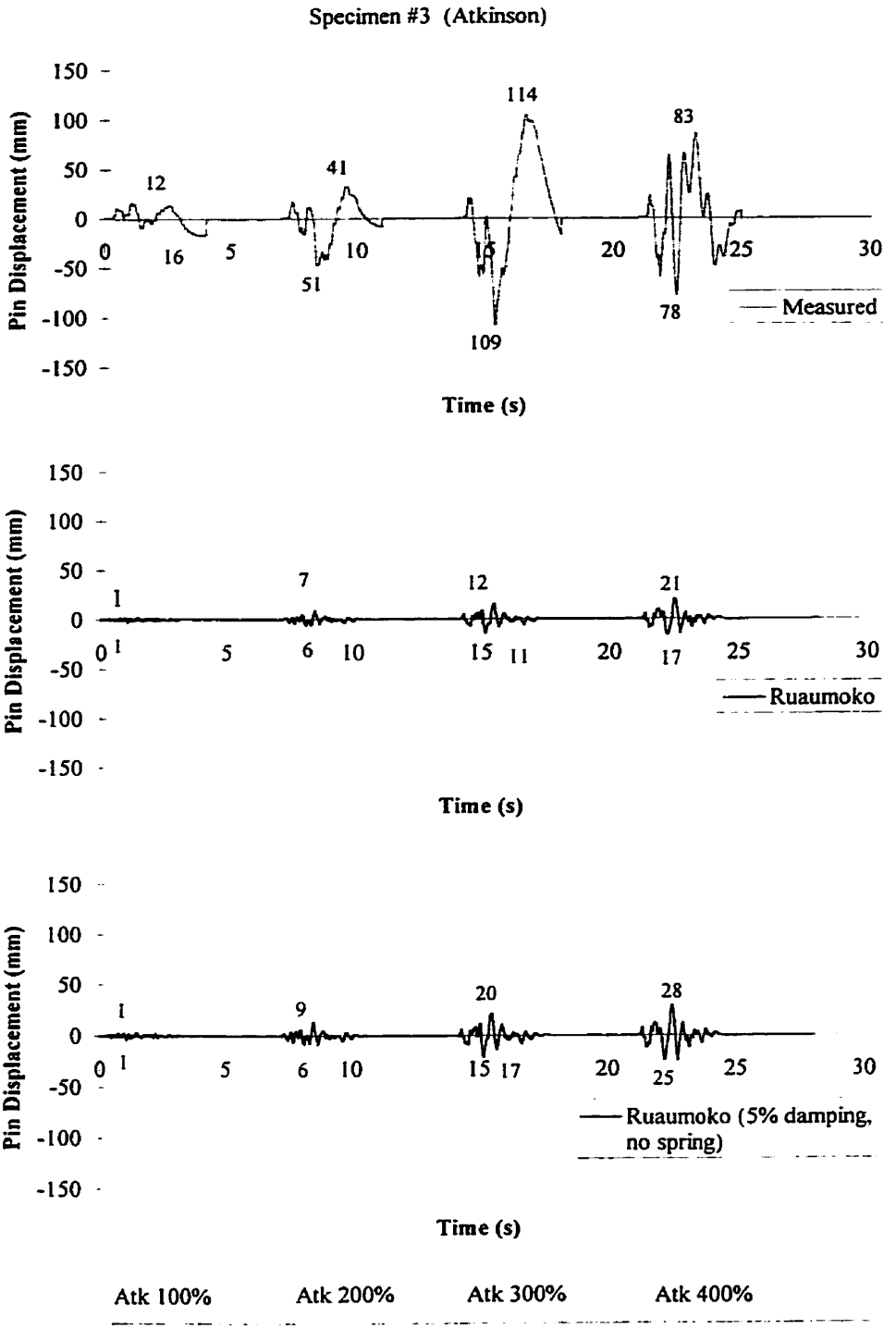

Figure 11.6 Pin Displacement (mm) for Specimen #3 (Atkinson)

CHAPTER 12
CONCLUSIONS

12.1 Introduction

In this research project, experimental modelling and testing were performed to better understand the seismic behaviour of reinforced concrete bridge piers under simulated winter conditions associated with Eastern North America. In order to address the various concerns which accompany reinforced concrete structures which are seismically loaded at low temperatures, the research project was divided into two distinct sections. The first being focused on the material characteristics of concrete and reinforcing steel under the combined effects of high strain rates and low temperatures. The second section involved the fabrication of eight bridge piers which were dimensioned following simulation requirements. Four of these specimens were subsequently tested under seismic loadings to determine their behaviour and to give the ability to draw comparisons between the model specimens and the existing structures.

12.2 Material Characteristics

Investigations were carried out to determine the material characteristics of concrete and reinforcing steel when they are subjected to high strain rates similar to earthquake loading and low temperature common to Eastern North America. Twenty-four different monotonic tests were conducted on concrete and reinforcing steel specimens, which encompassed the various loading rates typical of earthquake excitations and temperatures, which represented summer and winter conditions. With the use of data acquisition systems, completed stress-strain curves were plotted, which allowed for comparison between tests performed under different parameters. Equations

developed from the test results using multi-linear regression formulas to model the governing tends.

From the results of the tensile tests performed on reinforcing steel coupons, it was seen that the combined effects of strain rate and low temperature is an increase in both, the yield strength and the ultimate strength of the steel. The yield and ultimate stresses increased by 22% and 12%, respectively, when the strain rate increased from 80 x 10^{-6} /s (quasi-static) to 0.1 /s (upper limit for earthquake excitation) and the temperature decreased from +20°C to -40°C. Contrary to these results, the ultimate tensile strain and Young's modulus of the reinforcing steel was not significantly influenced by the combined effects of strain rate and temperature.

Compression tests performed on concrete cylinders proved an increase in both the compressive strength and the Young's modulus when subjected to both, high strain rates and low temperatures. As the strain rate increased from a quasi-static condition to an extreme seismic condition and the temperature decreased from +20°C to -40°C, the compressive strength of the concrete increased significantly by 91%. The Young's modulus of the concrete also showed increases when the strain rates were at 0.02 /s and higher and the temperature was below -20°C. On the other hand, there was no evidence that the ultimate compressive strain (strains which occurs at maximum stress) is affected by combining strain rate and temperature.

12.3 Recommendations for Material Testing

Although the results for monotonic tests on concrete and reinforced steel proved to introduce new information on the combined effects of strain rate and temperature, more research is still warranted in this field. Investigations should be focused on the size

effects (aggregate size, cylinder diameter, concrete strength, bar diameter, etc.) of the results obtained in this study. Also, the influence on the moisture content within the concrete should be further studied. Procedures other than monotonic tests, such as cyclic loading, can also be performed to determine if similar behaviours can be observed. Furthermore, the extrapolation of the basic monotonic and cyclic stress-strain behaviours of reinforcing steel and concrete should be performed on the complete responses of reinforced concrete members under earthquake-type excitations at low temperatures.

12.4 Testing of Model Specimens

The vast majority of reinforced bridge piers in Eastern North America were constructed prior to recent seismic provisions in design standards, resulting in inadequate transverse reinforcement in the plastic hinge regions of these columns. The fact that these columns were susceptible to shear failures, coupled with the uncertainty of the column's behaviour at low temperatures, lead to experimental testing of modelled specimens to better interpret the response of an existing bridge pier under realistic conditions.

Reinforced concrete bridge piers were modelled following simulation requirements and experimentally tested under quasi-static and seismic conditions. Three different ground motions were selected for the seismic tests from preliminary analyses to represent eastern and western earthquakes. The seismic tests were conducted at both +20°C and –40°C to investigate the influence of temperature on structure during earthquake excitations. With the use of numerous instrumentation devices, an accurate response of the column was recorded during each test.

The experimental results from the quasi-static tests indicated that the governing failure mode was due to a bond failure of the longitudinal reinforcement of the concrete

columns relative to the dowel bars of the foundation. As a consequence, a maximum shear force of 80 kN was recorded at a ductility (μ) of 1.5, which corresponds to approximately 2/3 of the nominal flexural resistance of the reinforced concrete section. Vertical cracks, indicating slipping of the reinforcement appeared at ductility (μ) of 1.5, which coincided with the maximum base shear value. Subsequently, rapid strength degradation was observed under cyclic loading after the maximum shear force was reached. The degradation followed a common pinched hysteretic behaviour with very poor energy dissipation capacities. Data from strain gauges positioned at various position on the dowel and longitudinal bars demonstrated bond failure from the significant decrease in the strain level of the dowel bar compared to the longitudinal bar at a ductility (μ) of 2. Results from moment-curvature analyses showed large curvatures at the base of the column, with decreasing curvatures for sections farther from the base, which also indicates slippage of the bars. Lack of confinement was also observed over the splice region due to insufficient transverse reinforcement. As a result, the ultimate curvature developed within the plastic hinge region was limited by the strain at which the cover concrete began to spall (0.5% strain).

Three specimens were seismically loaded with three different ground motions and at two temperatures, +20°C and –40°C. Test results proved that the columns, which were seismically loaded, followed similar failure modes as were seen with the quasi-static tests. The results from the strain measurements of the dowel bars indicates that the governing failure mode was characterized by a slip between the longitudinal bars of the column and dowel bars at the foundation level due to the low level of strains in the reinforcement. Low strain levels measured in the stirrups indicates the insignificant influence of the lateral confining steel in the plastic hinge region to increase the column's ductility. Furthermore, an influence of the change in temperature was also observed between similar tests. The test results showed an increase in the pin acceleration and lower drift ratios at -40°C, compared to the results at +20°C. An explanation of this

trend could be offered from the results found from the material tests on concrete cylinders at high strain rates and low temperatures. At lower temperatures, the Young's modulus of the concrete increases, consequently increasing the stiffness of the specimen, thus, resulting in a decrease in the drift ratio and higher frequencies at these lower temperatures.

Numerical modelling was performed with the use of the RUAUMOKO computer to validate the seismic response of the experimental results. Although various aspects within the computer program were used to simulate the specimen's actual response, close correlation between the measured and the numerically modelled results could not be generated. It was seen that as the intensity of the ground motion increased, the measured values and the values produced from computer program began to deviate from each other due to increase slipping which occurred at the pin connection at the top of the pier specimen.

The overall behaviour of the specimens coincided with the behaviour of the quasi-static tests, with the governing failure occurring due to bond failure of the longitudinal reinforcement. Furthermore, major structural failure did not occur at predicted intensities, largely due to the unforeseen slipping at the pin connection. Also, the columns did not have the capacity to reach the nominal flexural resistance due to the lack of confinement in the plastic hinge region. The insufficient transverse reinforcement was also a contributing factor in the bond failures of the reinforcement. Also, when considering the change of the temperature parameter, little influence on the behaviour of the column was observed during the seismic tests when the temperature decreased from +20°C to -40°C.

When interrupting the results obtained from the quasi-static and seismic tests, correlation between the model and the prototype: the response of the existing bridge pier

would behave similar to the response of the model and the major mode of failure of the prototype would be bond failure of the reinforcement. By applying the scaling laws to the reinforcement, the behaviour of the rebar due to the complexity of the bond mechanism (chemical adhesion, mechanical bond, etc.) would be improve in the model, therefore, resulting in bond failure in prototype at an earlier level of loading. Also, at low temperatures, the compressive strength of the concrete increases causing improved bond of the reinforcement. Although there is some uncertainty about the level of increase of the bond stress in the model, it was ascertained that the similar failure modes would occur in the prototype at lower loading levels as was seen in the model.

12.5 Bridge Pier Recommendations

Although information on the seismic behaviour of reinforced concrete bridge piers is advancing, knowledge on the effects on these structures under actual earthquake loadings are still rather limited. Many aspects are still unknown with respect to the effect of temperature on behaviour of bridge piers.

Further tests should be carried out with similar specimens and set-ups, but an increase effort should be taken to ensure a proper connection between the top of the column, the pin and the concrete blocks. Although numerous seismic tests were performed on the specimens, many of the measured values were skewed due the slipping from the improper pin connection, therefore, further testing is warranted.

Experimental tests should be conducted to determine the performance of reinforced concrete columns designed with recent seismic provisions (such as, increased concrete confinement) and compare the results to similar structures designed without these provisions to see if coinciding failure modes are observed

Further information is needed on the comparisons between models and prototype. Experimental tests should be performed to verify the validity of the experimental values when a direct scaling of the prototype is not used (i.e. reinforcing bar diameters and type, concrete aggregate size, etc.).

An investigation on the retrofitting techniques should also be studied. Various techniques, such as steel and composite jacketing and increasing the columns section over the lap-splice proved to be viable solutions in improving the confinement of the concrete section. Tests should be performed to better understand the response of these techniques under earthquake excitations and at low temperatures.

REFERENCES

ABOUTAHA, R.S., ENGELHARDT, M.D., JIRSA, J.O. and KREGER, M.E. (1994). Seismic retrofit of R/C columns using steel jackets. Seismic Rehabilitation of Concrete Structures, American Concrete Institute, SP-160.

AMMANN, H., and NUSSBAUMER, H. 1995. Behavior of concrete and steel under dynamic actions. Vibrations problems in structures practical guide. Chapter F. H. Bachmann et al., Birkhäuser Verlag, Boston, 177-183.

BARSOM, J.M. 1975. Development of the AASHTO fracture-toughness requirements for bridge steel. Engineering Fracture Mechanics, 7(3), 605-618.

BARSOM, J.M., and ROFLE, S.T. 1970. The correlations between K_{IC} and Charpy V notch test results in the transition-temperature range. Impact Testing of Metals, ASTM STP466, American Society for Testing and Materials, 281-302.

BERKOVITCH, I. 1981. Using concrete to store liquefied gases. Civil Engineering. August 1981, 27-29.

BISCHOFF, P.H., and PERRY, S.H. 1991. Coompressive behaviour of concrete at high strain rates. Material and Structures, **24**(144), 425-450.

BISCHOFF, P.H., and PERRY, S.H. 1995. Impact behavior of plain concrete in uniaxial compression. ASCE Journal of Engineering Mechanics **121**(6), 685-693.

BRUNEAU, M., UANG, C-M., and WHITTAKER, A. 1997. Ductile design of steel structures. M^{c}Graw-Hill, New York.

CANADIAN STANDARDS ASSOCIATION (CSA). 1994a. Design of concrete structures for building. CAN3-A23.3-M95. CSA, Rexdale, ON.

IDEM. 1990. Concrete mixtures and placement. Standard CAN3-A23.1-M90. Canadian Standards Association, Rexdale, ON.

IDEM. 1977. Billet-steel bars for concrete reinforcement. Standard CSA-G30.12-M77. Canadian Standards Association, Rexdale, ON.

CANADIAN STANDARDS ASSOCIATION (CSA). 1994b. Limit states design of steel structures. CAN/CSA-S16.1-94. CSA, Rexdale, ON.

CARR, A.J. 1995. RUAUMOKO (The Maori God of Volcanoes and Earthquakes) - Inelastic Frame Analysis. Department of Civil Engineering, University of Canterbury, New Zealand.

CEB. 1988. Concrete structures under impact and impulsive loading. Bulletin d'information No. 187, Comité Euro-International du Béton. Lausanne, Switzerland.

CHAI, Y.H. and PRIESTLY, N. 1992. Retrofit of bridge columns for enhanced seismic performance. Seminar Proceedings of the Seismic Design and Retrofit of Bridges, University of California at Berkley.

COLLINS M.P. and MITCHELL D. 1991 Prestressed Concrete Structures. Preentice Hall. Englewood Cliffs, NJ, USA.

CORLEY, W.G. 1966. Rotational capacity of reinforced concrete beams. ASCE, Journal of the Structural Division. **91**, ST5, p. 121-146.

DAVIS, E.A. 1938. The effect of speed of stretching and the rate of loading on the yielding of mild steel. Journal of Applied Mechanics, 5(4), A137-A140.

DUTTA, P.K. 1988. Behavior of materials at cold regions temperatures. Special Report 88-9. US Army Corps of Engineers, Cold Regions Research & Engineering Laboratory.

EDI. 1993. U2 & V2 manual. Experimental Dynamic Investigations Ltd., Vancouver, Canada.

FAUCHER, B., WANG, K.C., and BOUCHARD, R. 1987. Relationship between strain-ratesensesitivity of yield stress and transition temperature for an arctic grade steel. Physical Metallurgy Research Laboratories, Canada Centre for Mineral and Energy Technology (CAMNET), Report No. 87-50.

FILIATRAULT, A. and CHERRY, S. 1985. Performance evaluation of friction damped braced steel frames under simulate earthquake loads. Report No. EERL 85-01. Department of Civil Engineering. University of British Columbia.

FILIATRAULT, A., HOLLERAN, M. and MASSICOTTE, B. 1998. Stress-strain behaviour of reinforced steel and concrete under seismic strain rates and low temperatures. ASCE Journal of Cold Regions Engineering. (under review).

GRIEZIC, A., COOKE, W.D., and MITCHELL, D. 1996. Seismic retrofit of bridge of bridge-footing connections. Proceedings of the 11th World Conference on Earthquake Engineering. Acapulco, Mexico.

KANETA, K., KOHZU, I., and FUJIMURA, K. 1986. On the strength and ductility of steel structural joints subjected to high speed monotonic tensile loading. Proceedings on the 8th European Conference on Earthquake Engineering, Lisbon, Portugal, **4**, 7.2/17-7.2/24.

MAHIN, S.A., and BERTERO, V.V. 1972. Rate of loading effects on uncracked and repaired reinforced concrete members. Report No. EERC 72-9., Earthquake Engineering Research Center, University of California, Berkley, CA.

MANDER, J.B., PRIESTLY, M.J.N., and PARK, R. 1984. Seismic design of bridge piers. Research Report No. 84-2, Department of Civil Engineering, University of Canterbury, Christchurch, New Zealand.

MANJOINE, M.J. 1944. Influence of rate of strain and temperature on yield stress of mild steel. Journal of Applied Mechanics. **11**, 211-218.

M^{C}CLINTOCK, F.A. AND Ali, S.A. 1966. Mechanical behavior of materials. Reading, Addison-Wesley, MA., 546-561.

MITCHELL, D. 1991. Detailing for ductility in concrete bridge column. Proceedings of the Bridge Design Seminar, Vancouver, Canada, January 25 and 26, 1991.

MIRZA, S.A., and M^{AC}GREGOR, J.G. 1979. Variability of mechanical properties of reinforcing bars. ASCE Journal of the Structural Division, **105**(5), 921-937.

MUTO, K., OHMORI, N., SUGANO, T., MIYASHITA, T and SHIMIZU, H. 1973. Non-linear analysis of reinforced concrete buildings. Theory and Practice in Finite Element Structural Analysis. Yamada, Y. and Gallagher, R.H. Eds. University of Tokyo Press, Toyko, 1973. p 399-421.

NAGATAKI, Y., KITAGAWA, Y., MIDORIKAWA, M., and KASHIMA, T. 1988. Dynamic response analysis with effects of strain rate and stress relaxation. Proceedings of the 9th World Conference on Earthquake Engineering, Tokyo-Kyoto, Japan IV, 693-698.

PARK, R. BILLINGS, I.J., CLIFTON, G.C., COUSINS, J., FILIATRAULT. A., JENNINGS, D.N., JONES, L.C.P., PERRIN, N.D., ROONEY, S.L., SINCLAIR, J., SPURR, D.D., TANAKA, H. and WALKER, G. (1995). The Hyogo-ken Nanbu Earthquake of 17 January 1995. Bulletin of the New Zealand National Society for Earthquake Engineering, **28**(1), March 1995.

PARK, R., RODRIGUEZ, M.E., and DEKKER, D.R. 1993. Assessment and retrofit of a reinforced concrete bridge pier for seismic resistance. Earthquake Spectra, **9**(4): 781-801.

PRIESTLEY, N. and PARK, R. 1987. Strength and ductility of concrete bridge columns under seismic loading. ACI Structural Journal, **84**(1):61-76, Jan.-Feb., 1987.

PRIESTLEY, M.J.N. and SEIBLE, F. 1991. Design of retrofit measure for concrete bridges. Seismic Assessment and Retrofit of Bridges. University of California, San Diego, Structural System Research Project Report No.91/03, July 1991, 197-250.

RESTREPO-POSADA, J.I. 1993. Seismic behavior of connections between precast concrete elements. Research Report No. 93-3, Department of Civil Engineering, University of Canterbury, New Zealand.

RESTREPO-POSADA, J.I., DODD, L.L., PARK, R., and COOKE, N. 1994. Variables affecting cyclic behavor of reinforcing steel. ASCE Journal of Structural Engineering, **120**(11), 3178-3196.

ROBERTS, R. 1974. Fracture toughness of bridge steels. Phase II Report. FHWA-RD-74-59, Federal Highway Administration.

SABNIS, G,M., HARRIS, H.G., WHITE, R.N., and MIRZA, M.S. 1983. Structural modeling and experimental techniques. Prentice-Hall Civil Engineering and Engineering Mechanics Series.

SARRAZIN, M and FILIATRAULT, A. 1993. Manuel d'utilisation du programme RESAS (version 1.03) - réponses spectrales des accélérogramme séismique. Rapport no. EPM/GCS - 1993 - 05. Section Structures, Département de génie civil, École Polytechnique de Montréal, Canada.

SAQAD Consulting Engineers. 1993. Seismic retrofit of bridge columns using high strength fiberglass/epoxy jackets. Design Recommendations. August, 1993.

SMITH, W.E.T. 1962. Earthquakes of eastern Canada and adjacent areas, 1534-1927. Publications of the Dominion Observatory, Ottawa, **26**:271-301.

SUITA, K., KANETA, K., and KHOZU, I. 1992. The effect of strain rate in steel structural joints due to high speed cyclic loading. Proceedings of the 11th World Conference on Earthquake Engineering, Madrid, Spain, 2863-2866.

SUITA, K., KOHZU, I., and YASUTOMI, M. 1996. The effect of strain rate in restoring force characteristics of steel braced structures under high speed cyclic loading. Proceedings of the 11th World Conference on Earthquake Engineering, Acapulco, Mexico, Paper No. 1220 (on CD Rom)

UDAGAVVA, K., TAKANASHI, K., and KATO, B. 1984. Effects of displacement rates on the behavior of steel beams and composite beams. Proceedings of the 8th World Conference on Earthquake Engineering, San Francisco, CA, IV, 177-184.

WAKABAYASHI, M., NAKAMURA, T., IWAI, S., and HAYASHI, Y. 1984. Effects of strain rate on the behaviour of structural members. Proceedings of the 8th World Conference on Earthquake Engineering, San Francisco, CA, IV, 491-498.

APPENDIX A

SCALED GROUND MOTION ACCELEROGRAMS

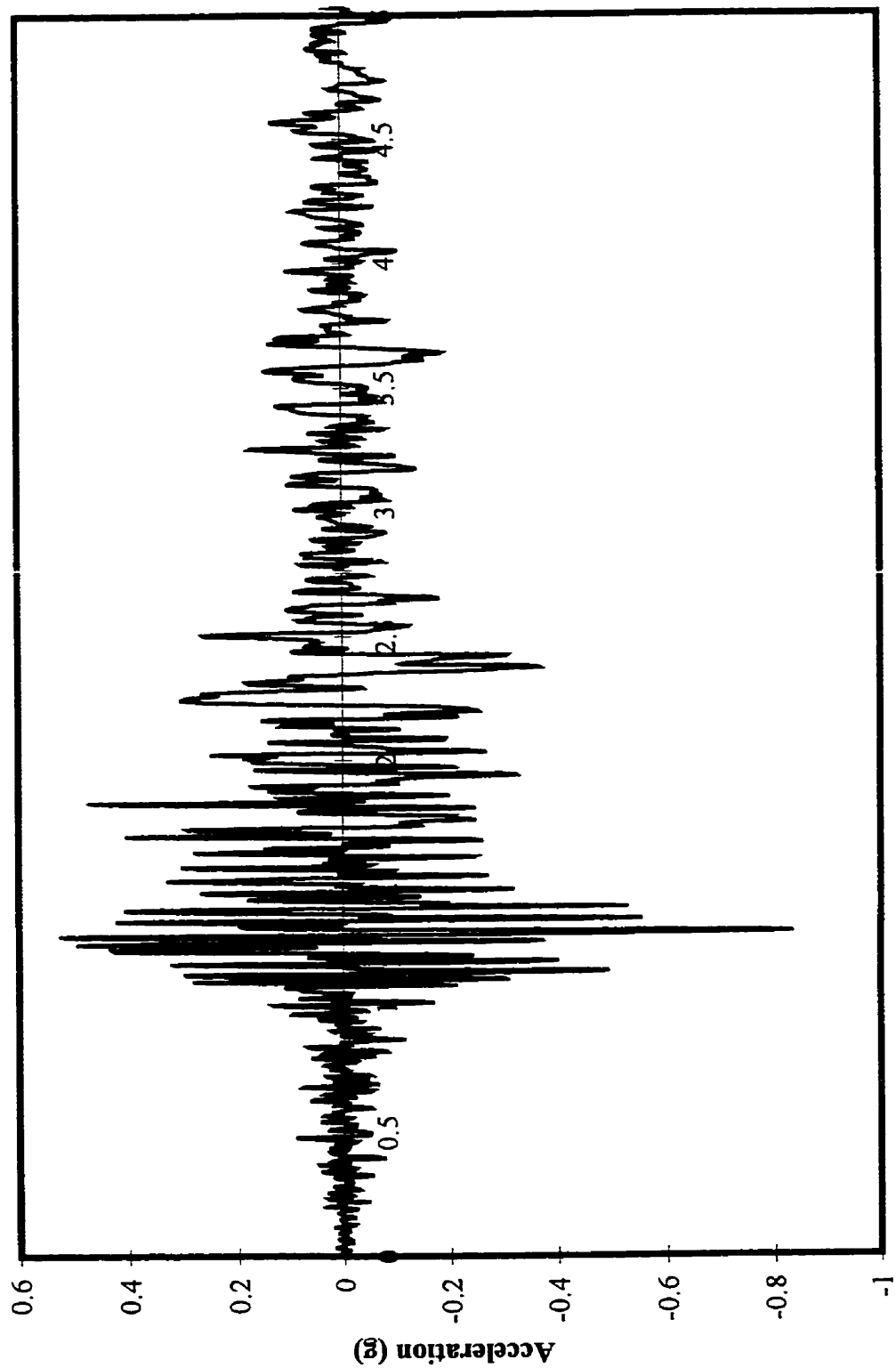

Figure A.1 Ground Motion Accelerogram for Whittier 1987, LA - Scaled at 3.65

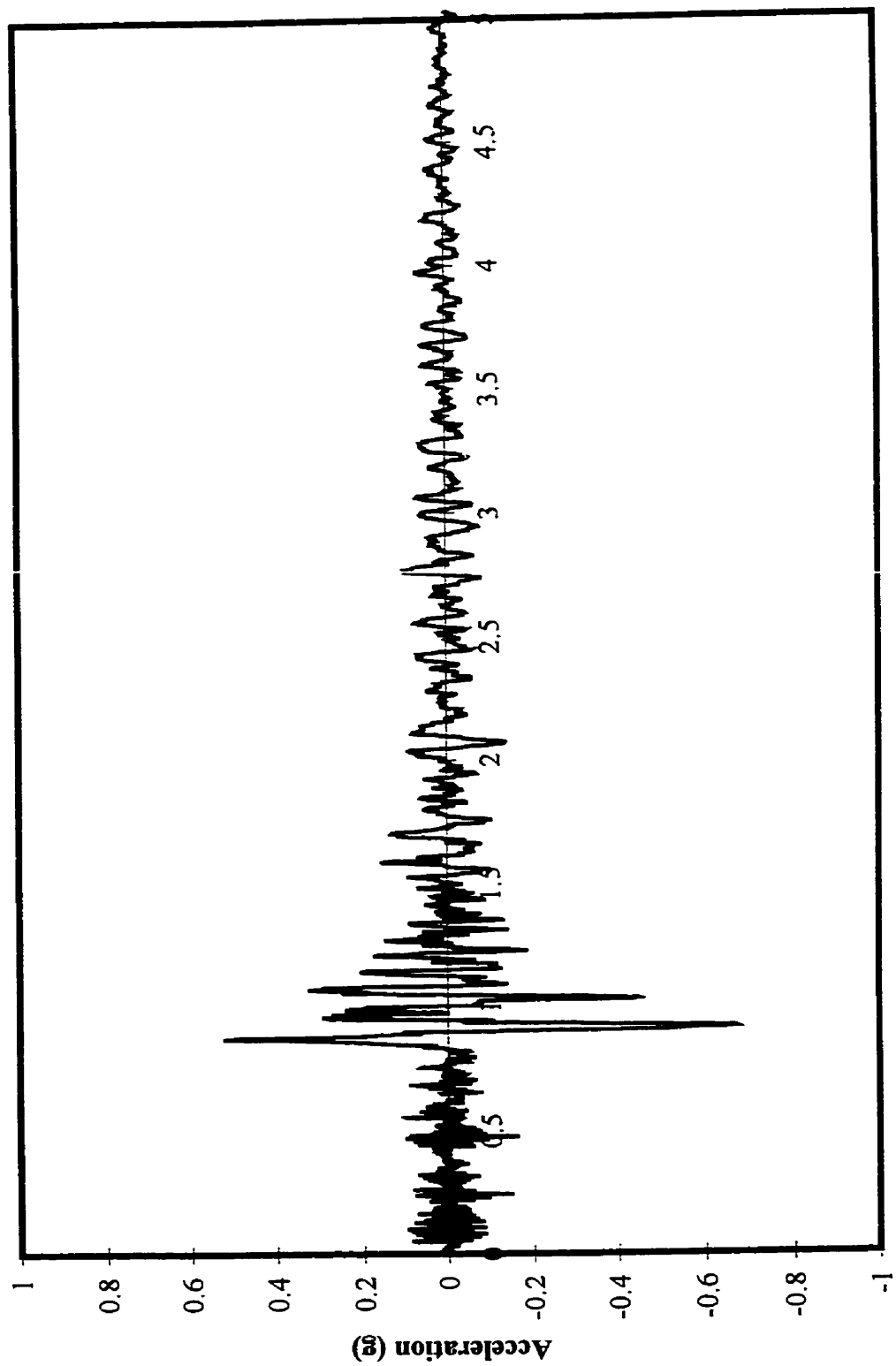

Figure A.2 Ground Motion Accelerogram for Imperial Valley Aftershock, 1979 - Scaled at 3.65

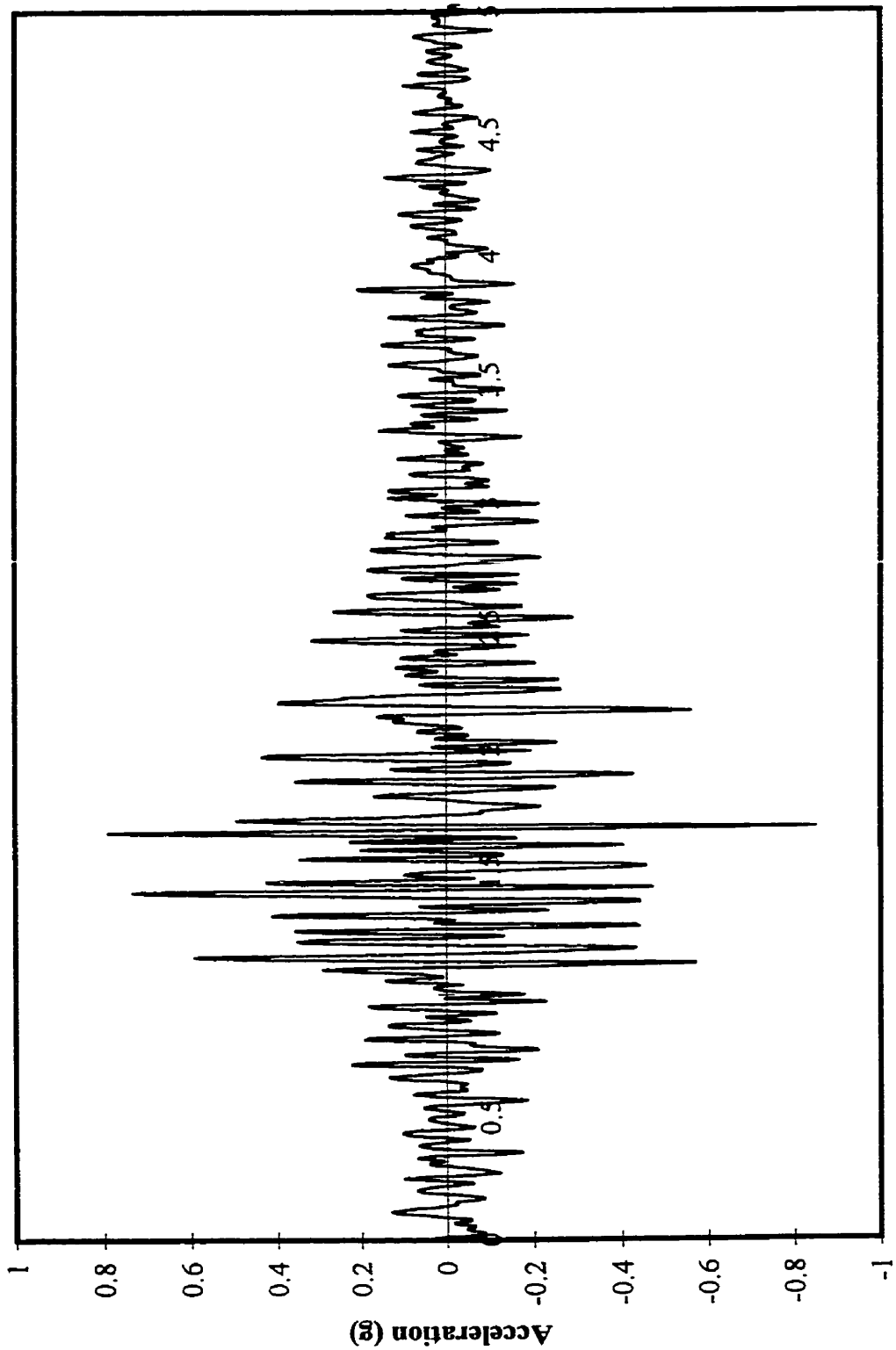

Figure A.3 Ground Motion Accelerogram for Adak 1971 - Scaled at 3.65

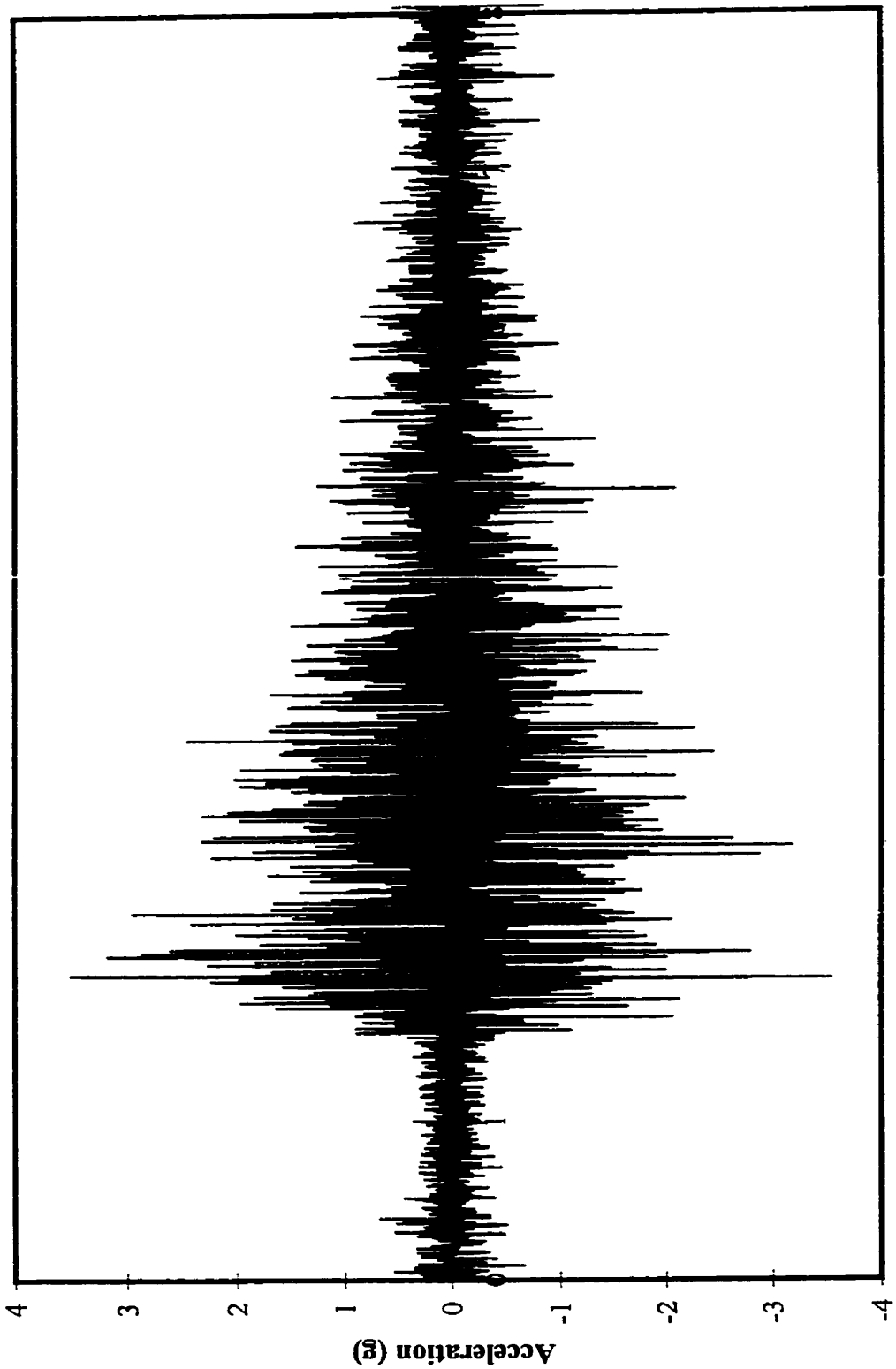

Figure A.4 Ground Motion Accelerograms for Saguenay - Scaled at 3.65

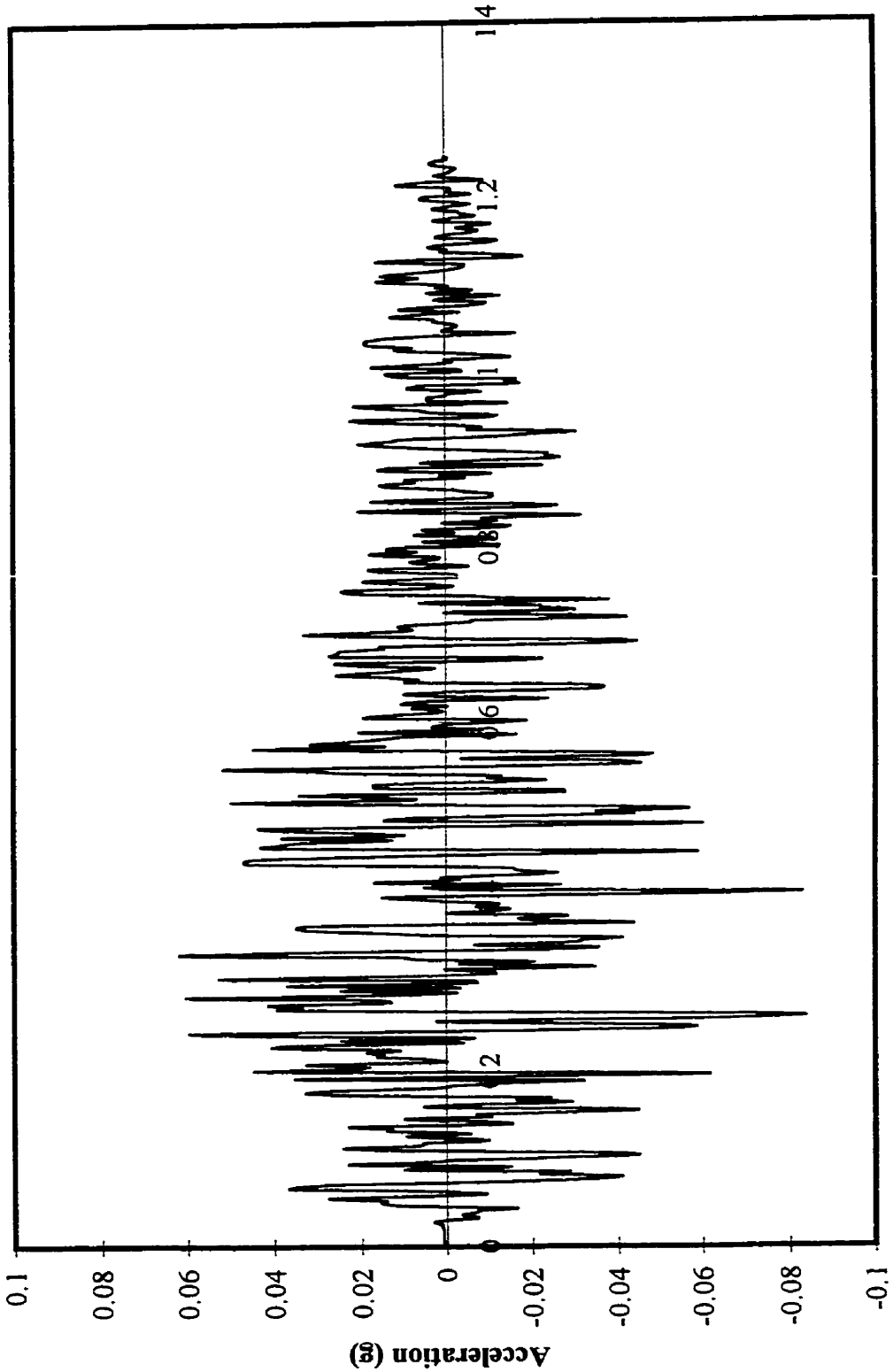

Figure A.5 Ground Motion Accelerogram for Atkinson M=5 @ 50 km - Scaled at 3.65

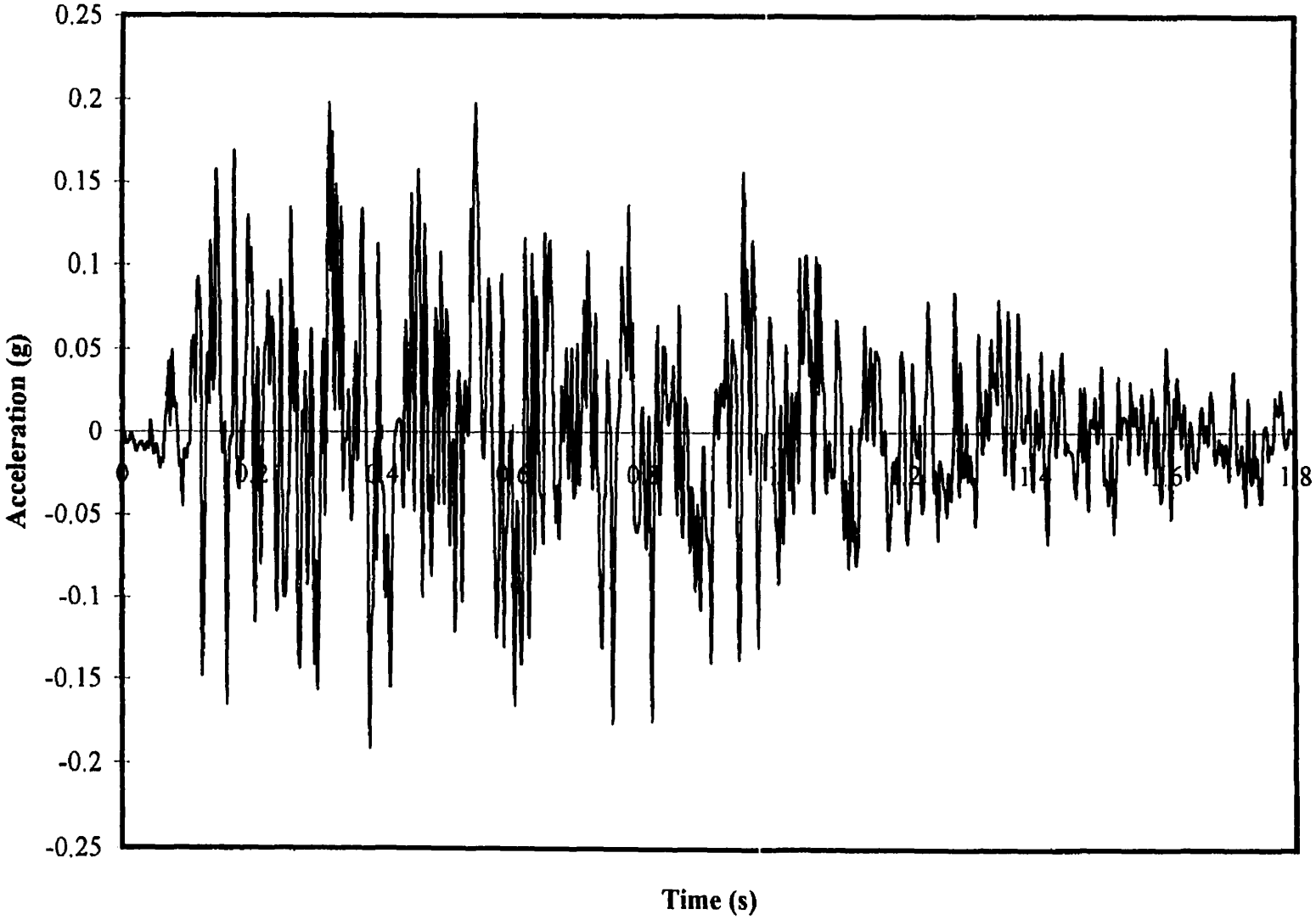

Figure A.6 Ground Motion Accelerogram for Atkinson M=6 @ 50 km - Scaled at 3.65

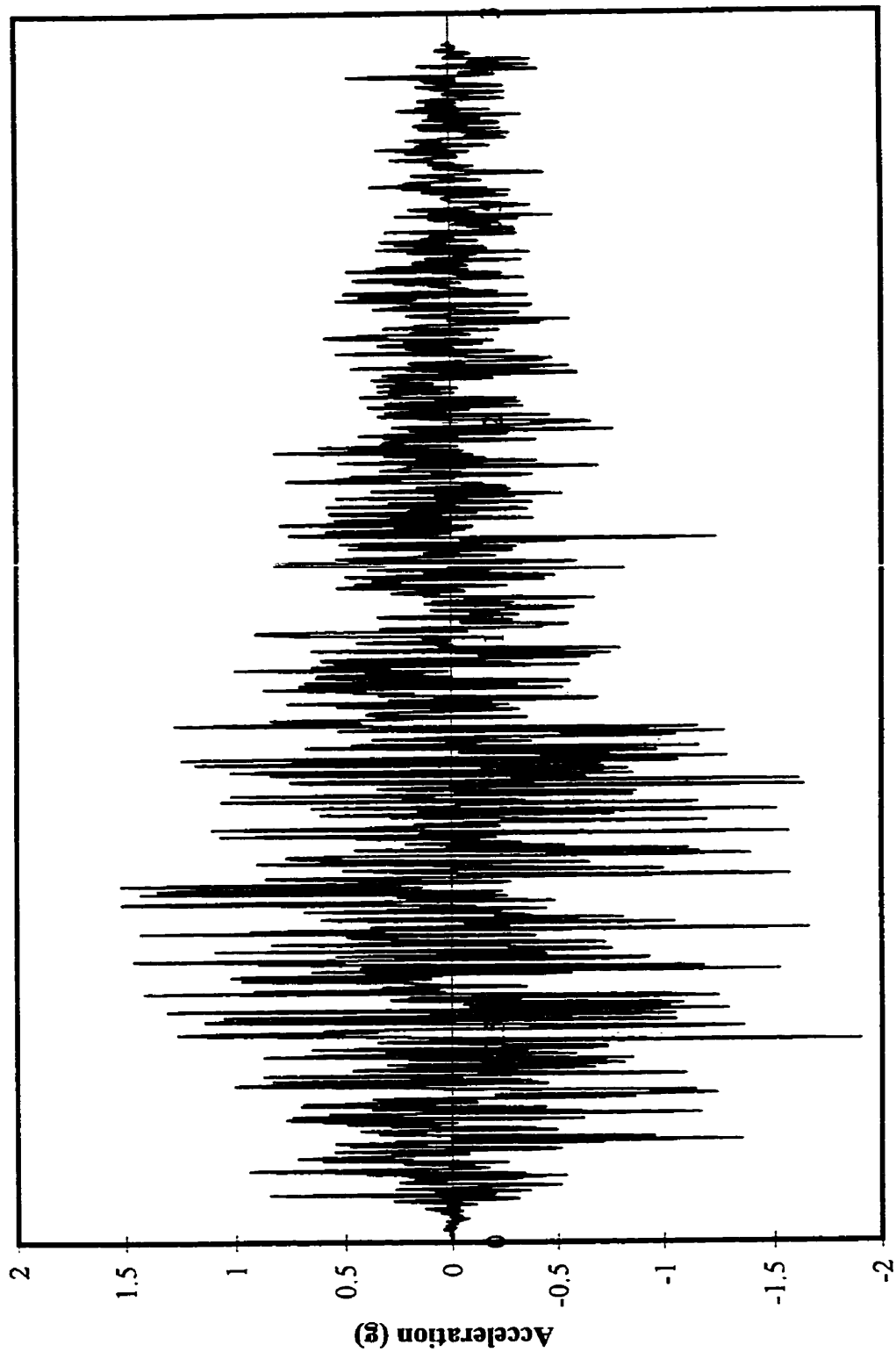

Figure A.7 Ground Motion Accelerogram for Atkinson M=7 @ 20 km - Scaled at 3.65

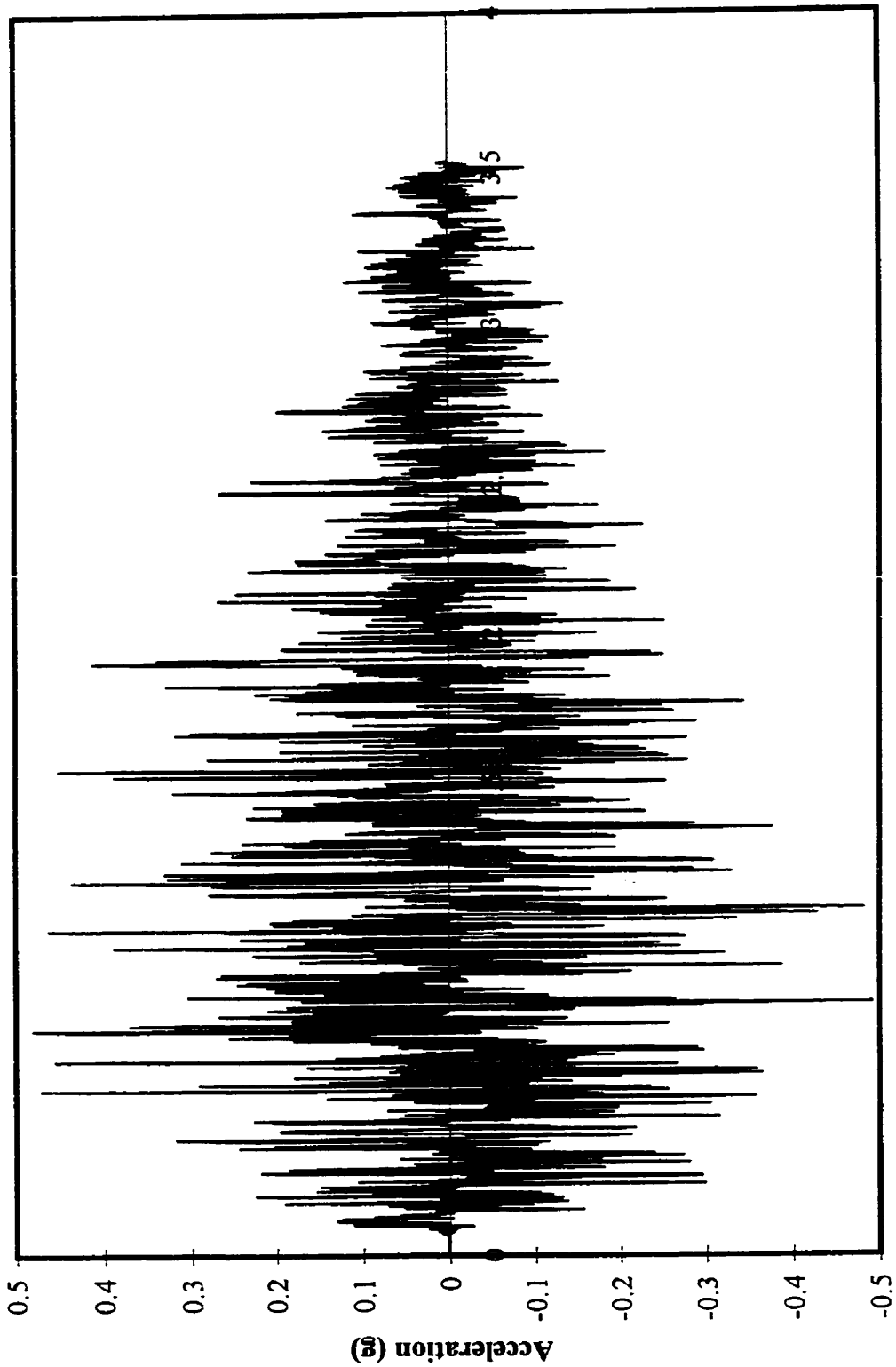

Figure A.8 Ground Motion Accelerogram for Atkinson M=7 @ 50 km - Scaled at 3.65

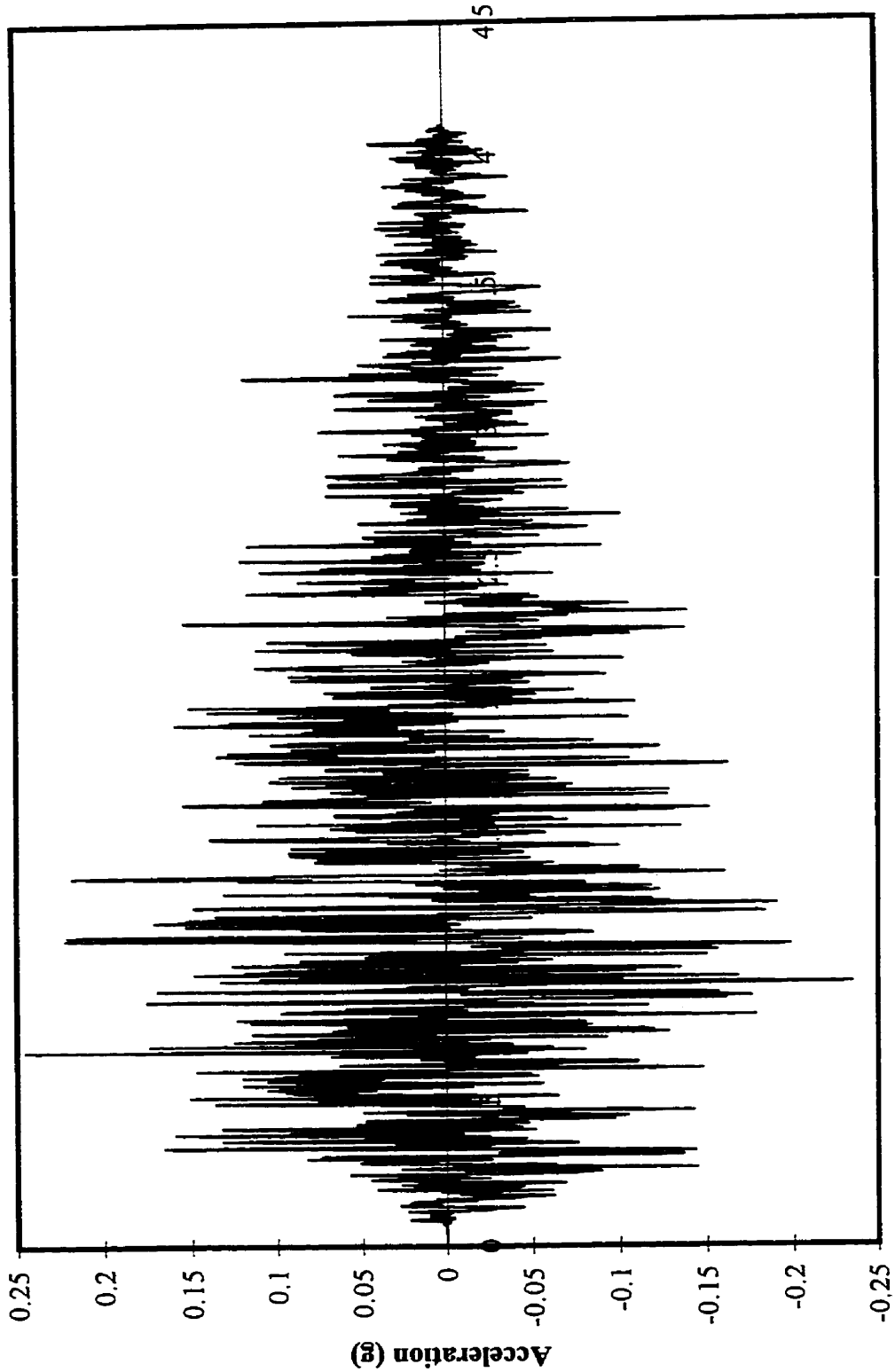

Figure A.9 Ground Motion Accelerogram for Atkinson M=7 @ 80 km - Scaled at 3.65

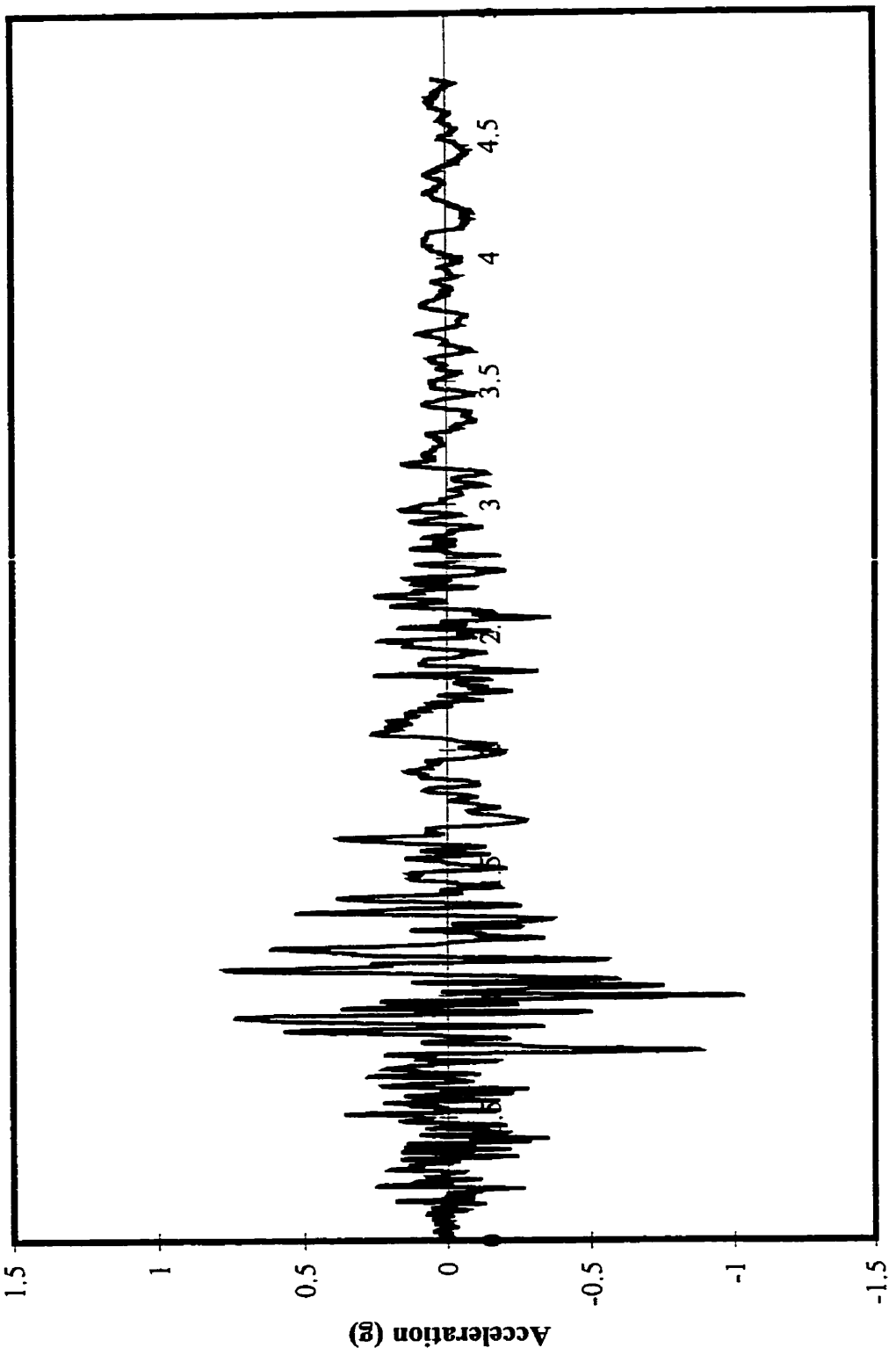

Figure A.10 Ground Motion Accelerogram for Coalinga Aftershock, 1983 - Scaled at 3.65

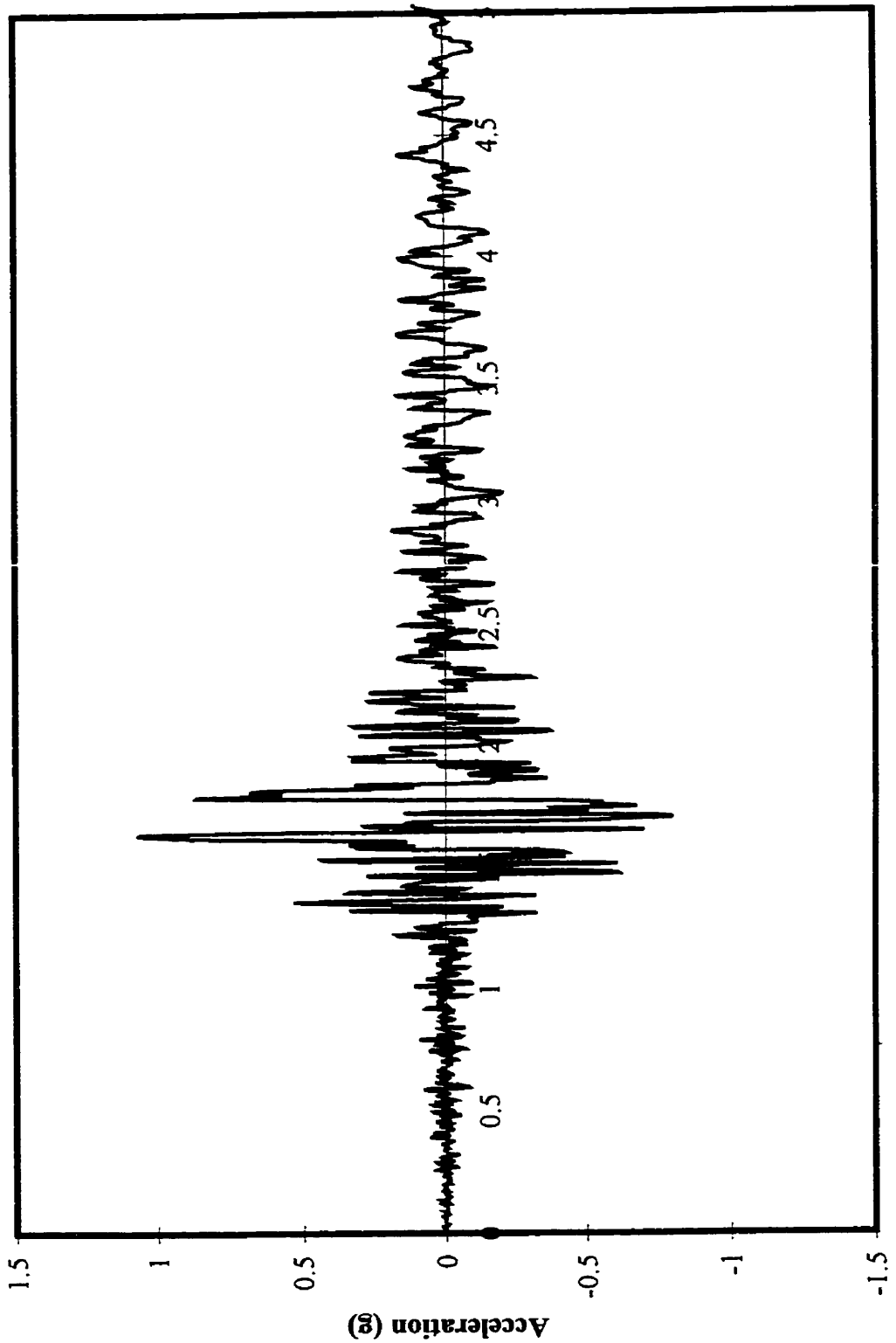

Figure A.11 Groud Motion Accelerogram for Whittier 1987, Union Oil Yard - Scaled at 3.65

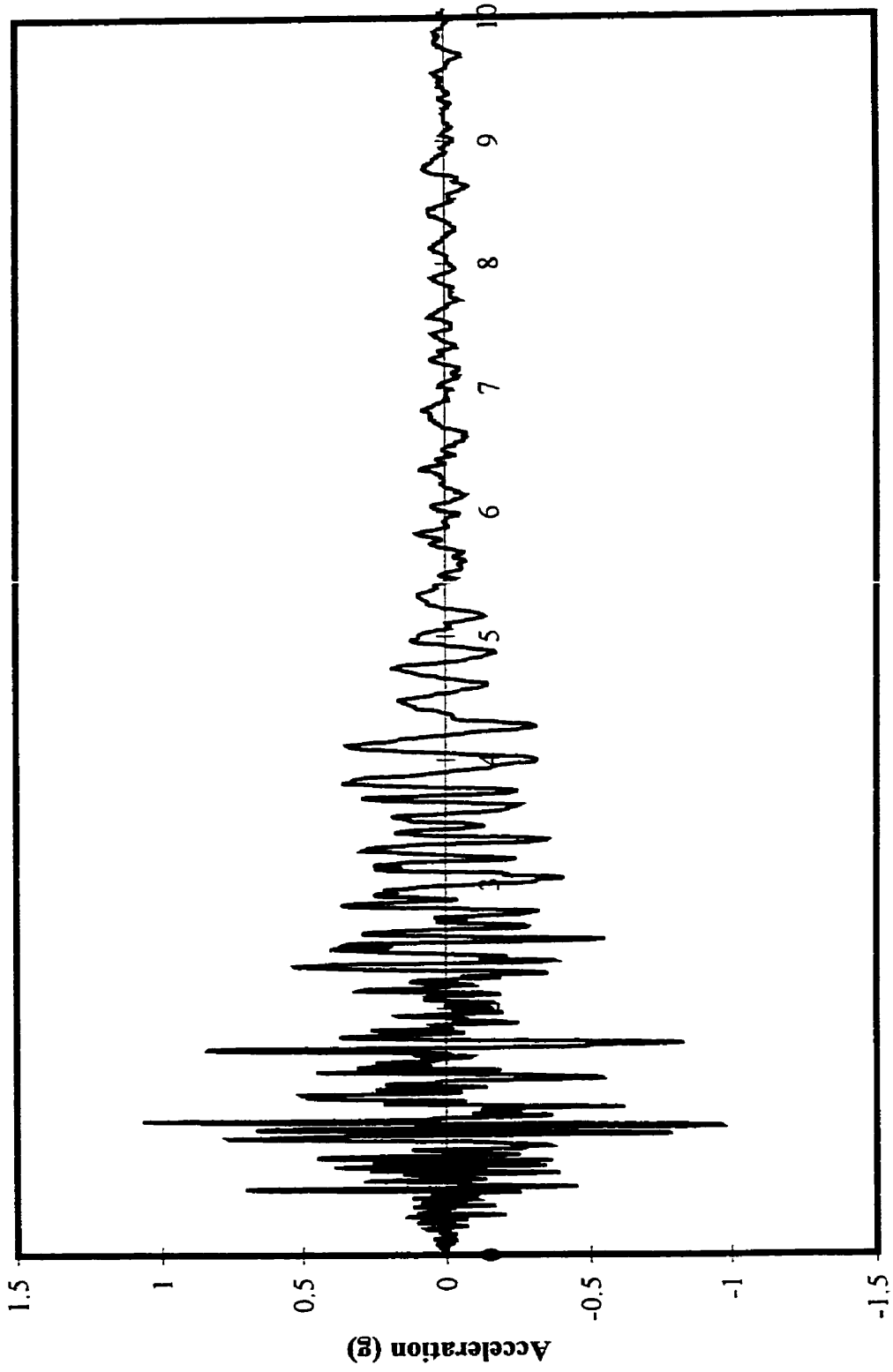

Figure A.12 Ground Motion Accelerogram for Morgan Hill, 1984 - Scaled at 3.65

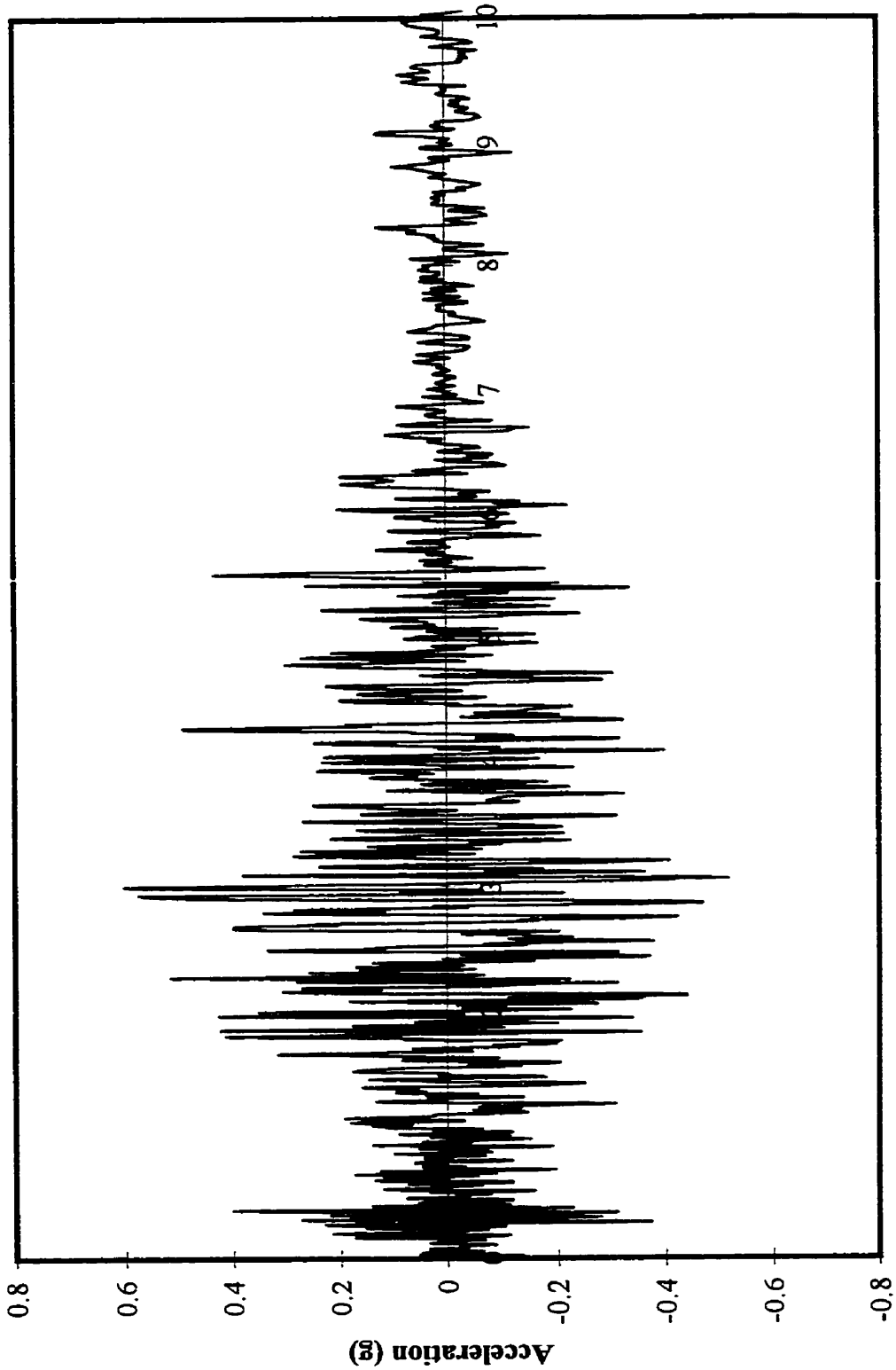

Figure A.13 Ground Motion Accelerogram for Puget Sound, 1949 - Scaled at 3.65

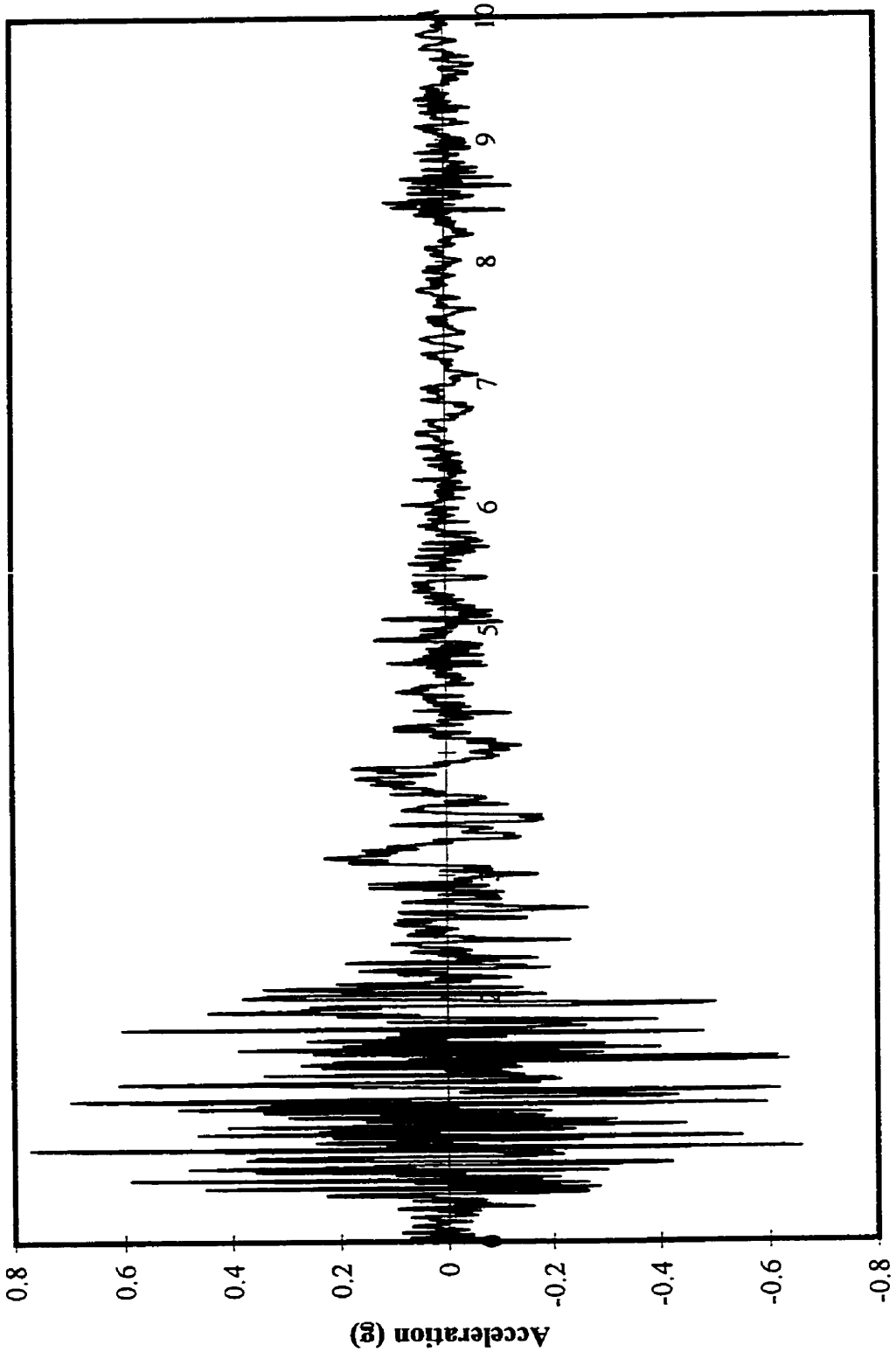

Figure A.14 Ground Motion Accelerogram fro San Fernando, 1971 S00W - Scaled at 3.65

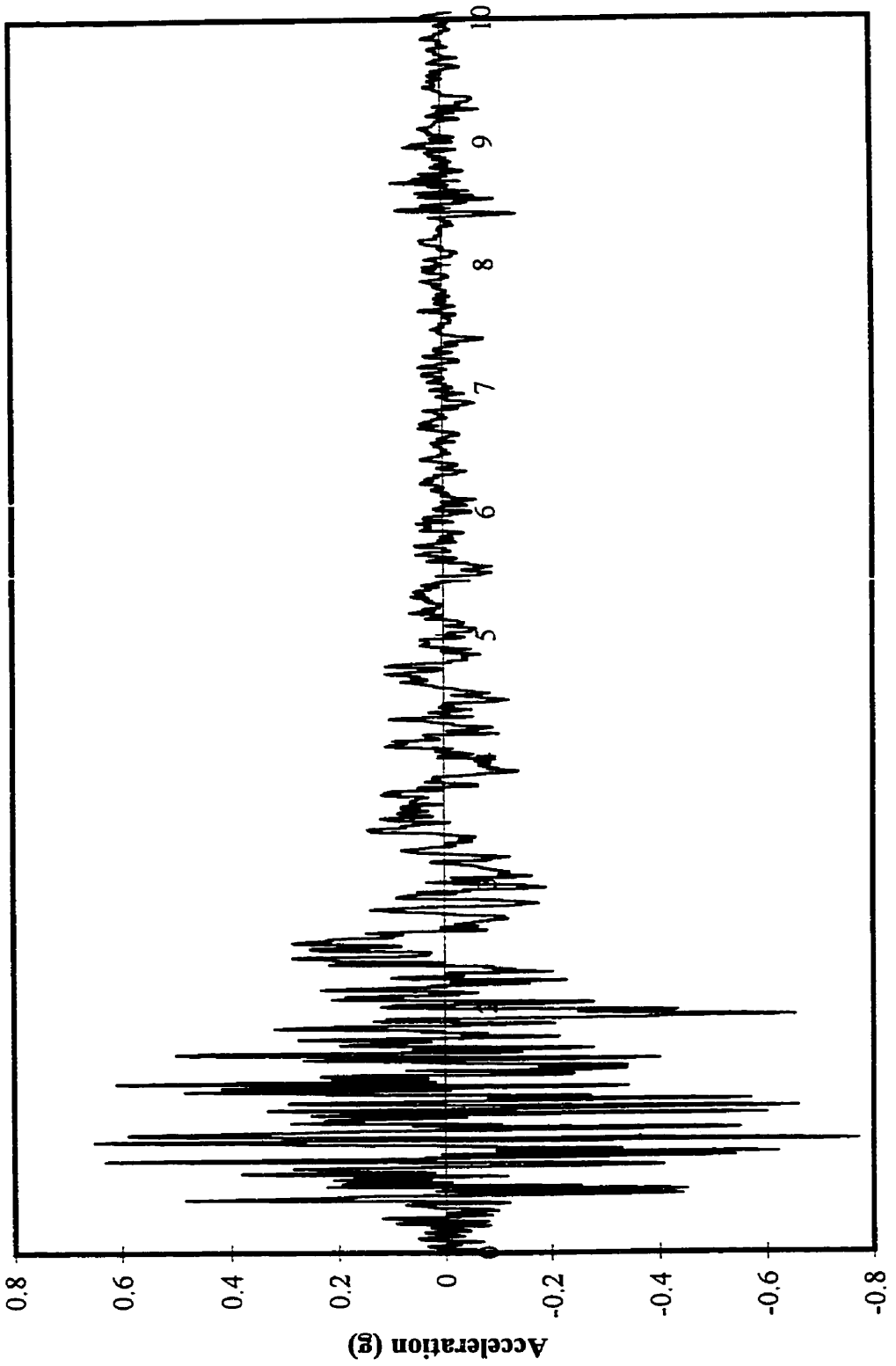

Figure A.15 Ground Motion Accelerogram for San Fernando, 1971 N90E - Scaled at 3.65

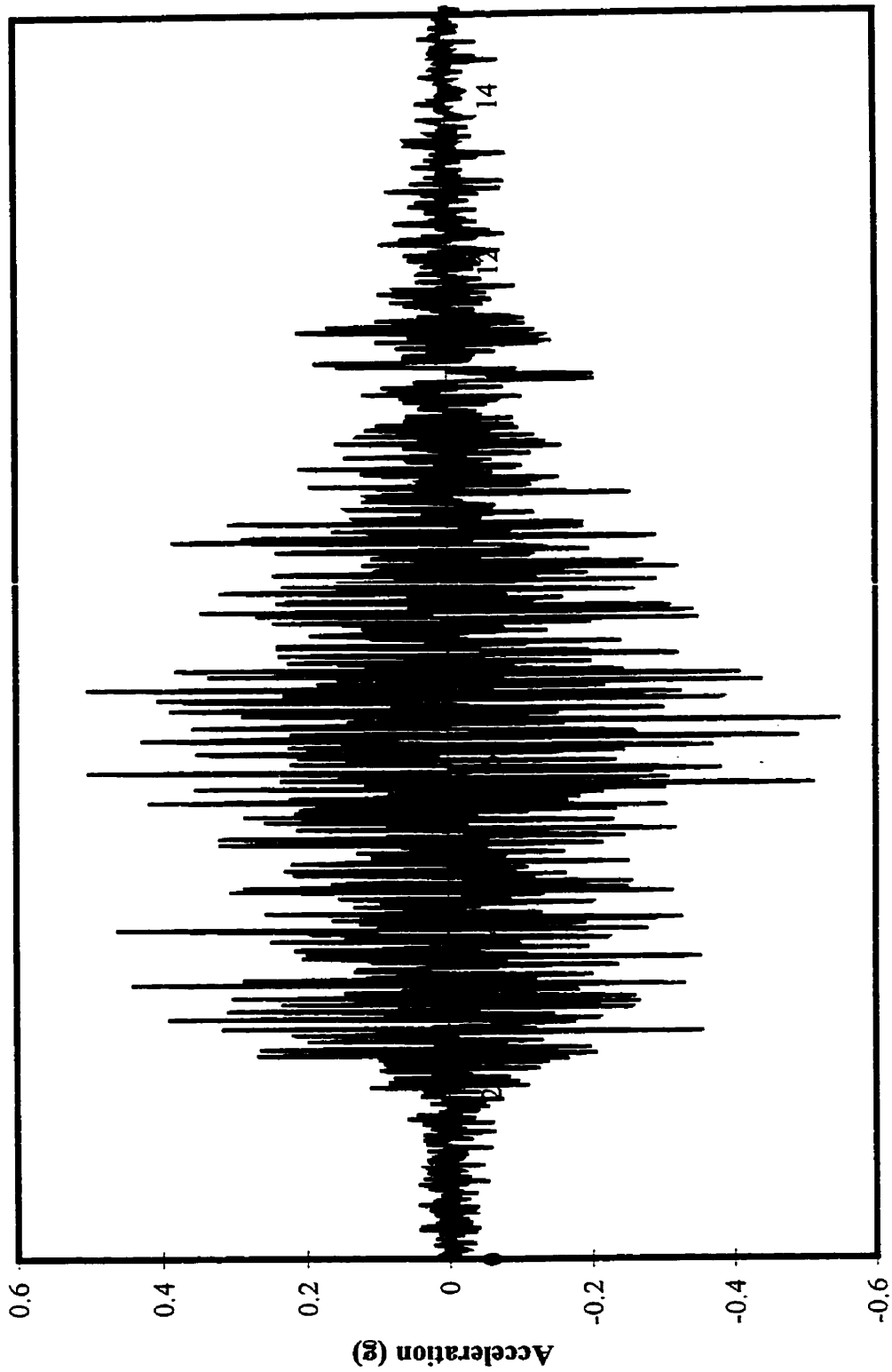

Figure A.16 Ground Motion Accelerogram for Mexico City, 1985 - Scaled at 3.65

APPENDIX B

POWER SPECTRAL DENSITY

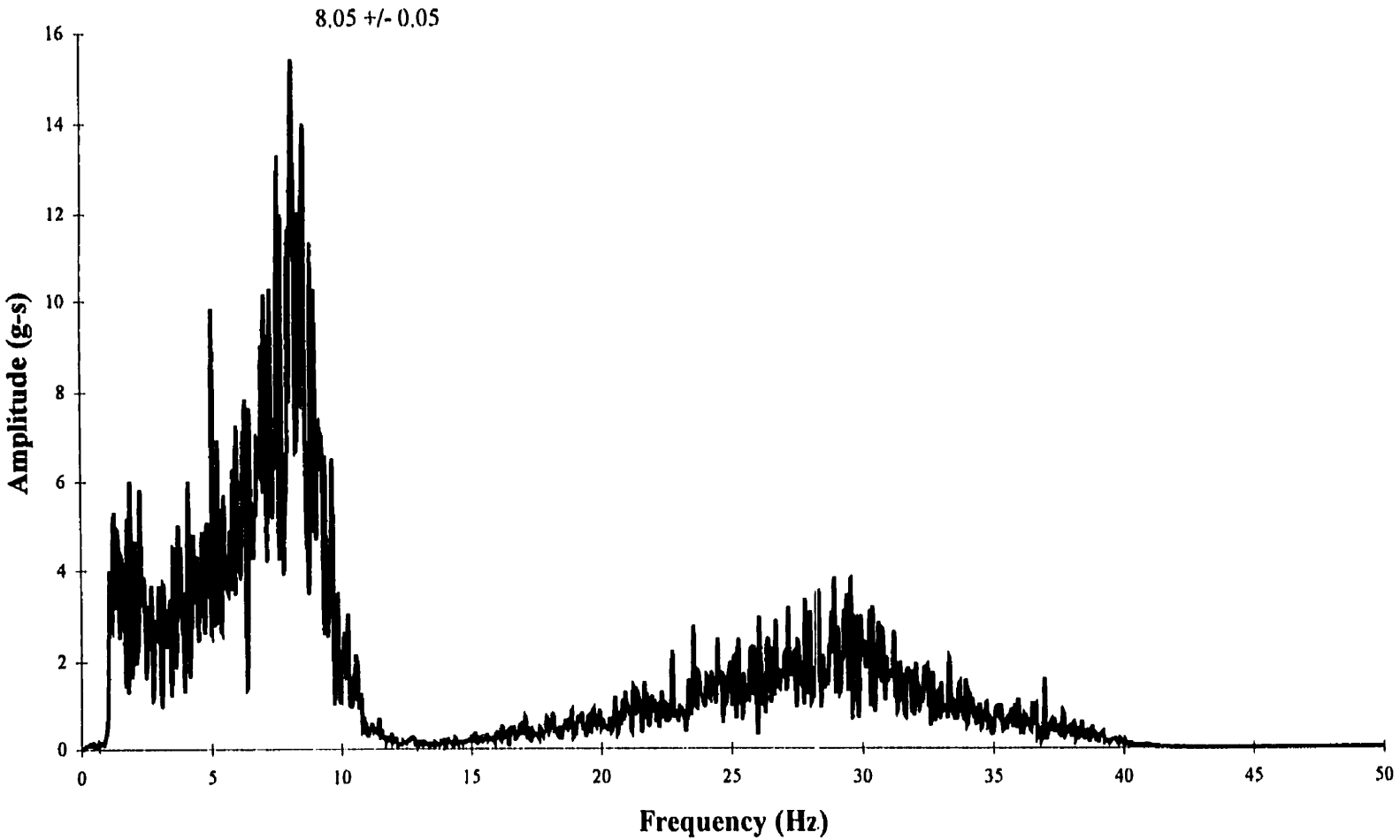

Figure B.1 Power Spectral Density - Specimen No.2 - before 100% Adak

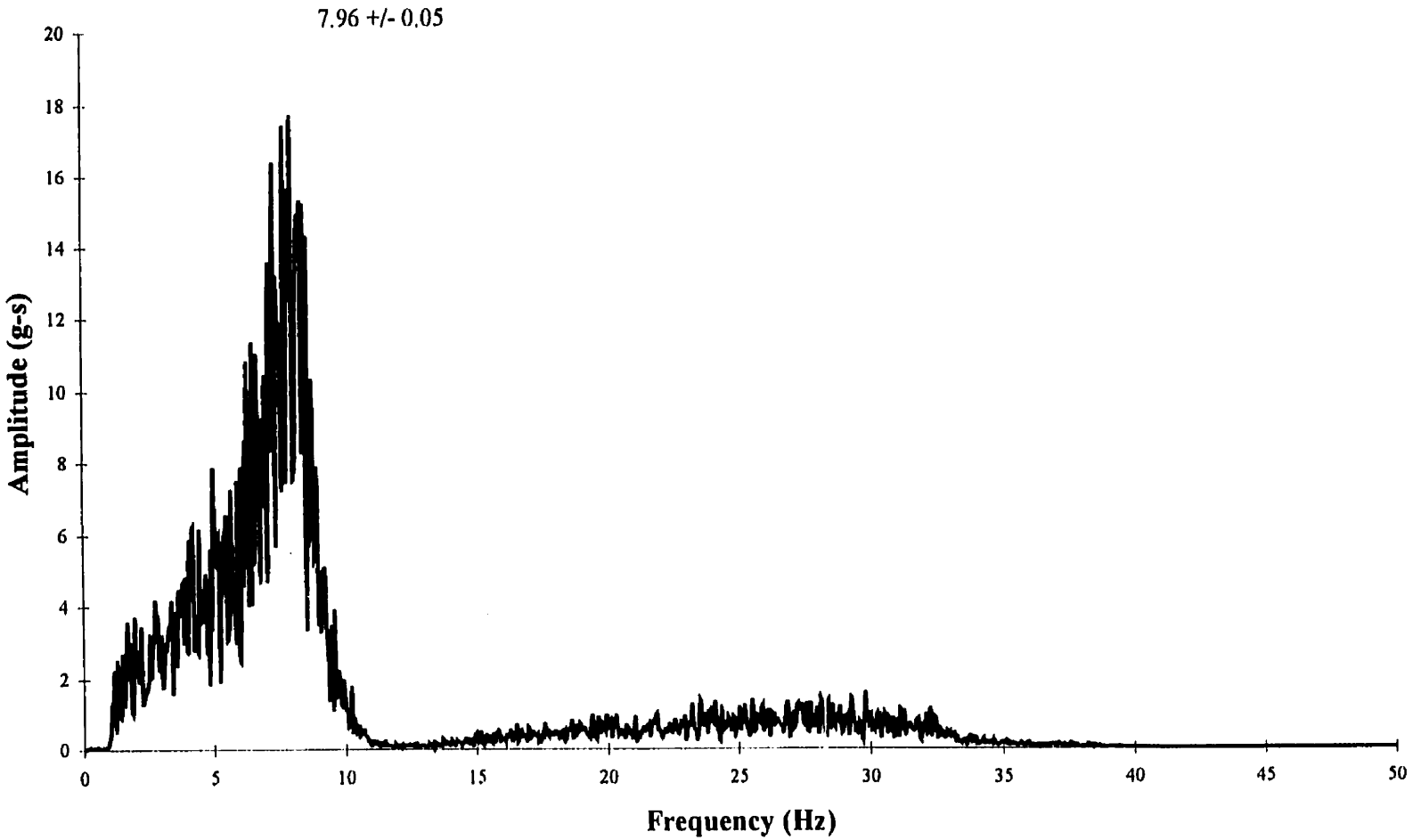

Figure B.2 Power Spectral Density - Specimen No.2 - after 100% Adak

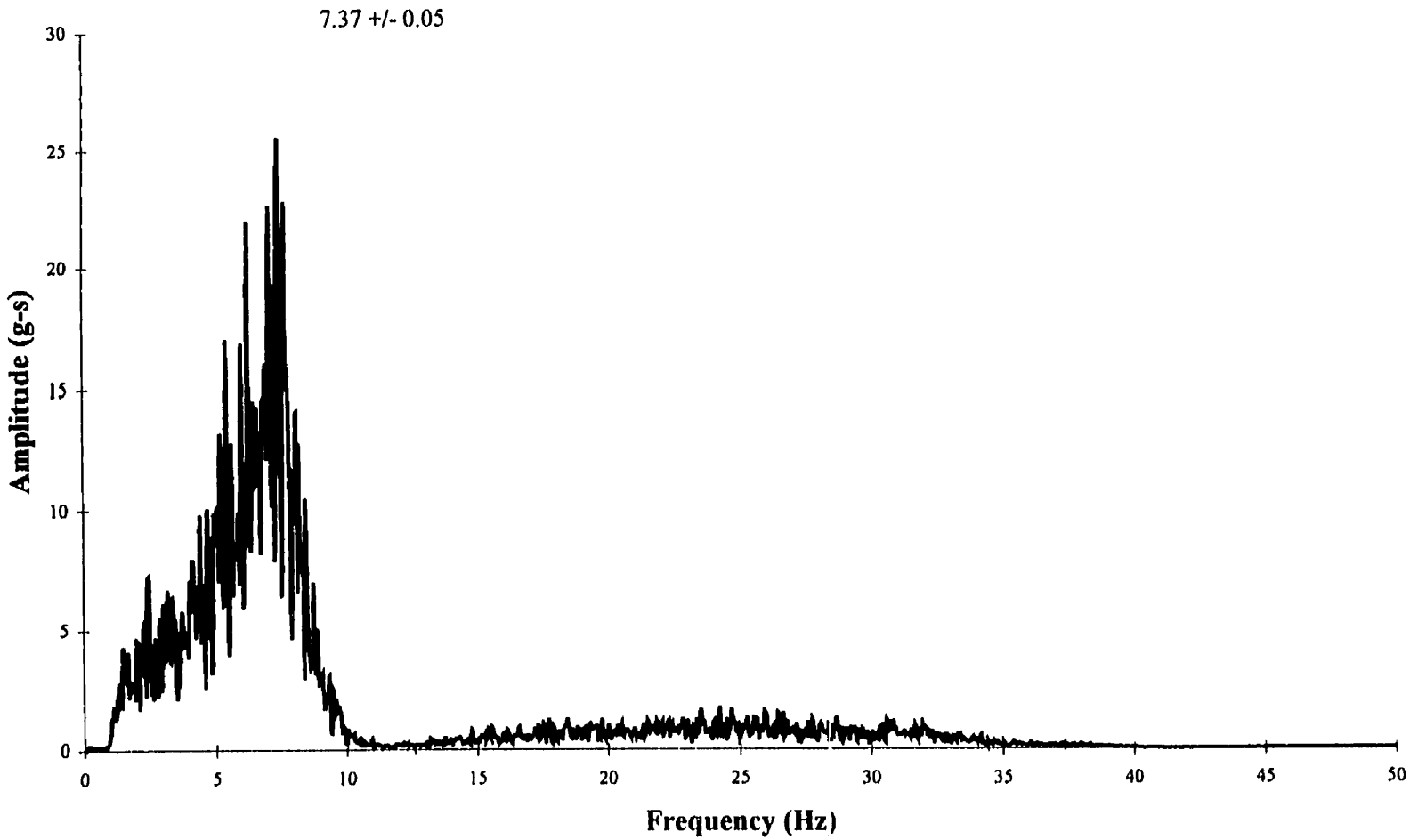

Figure B.3 Power Spectral Density - Specimen No.2 - after 200% Adak

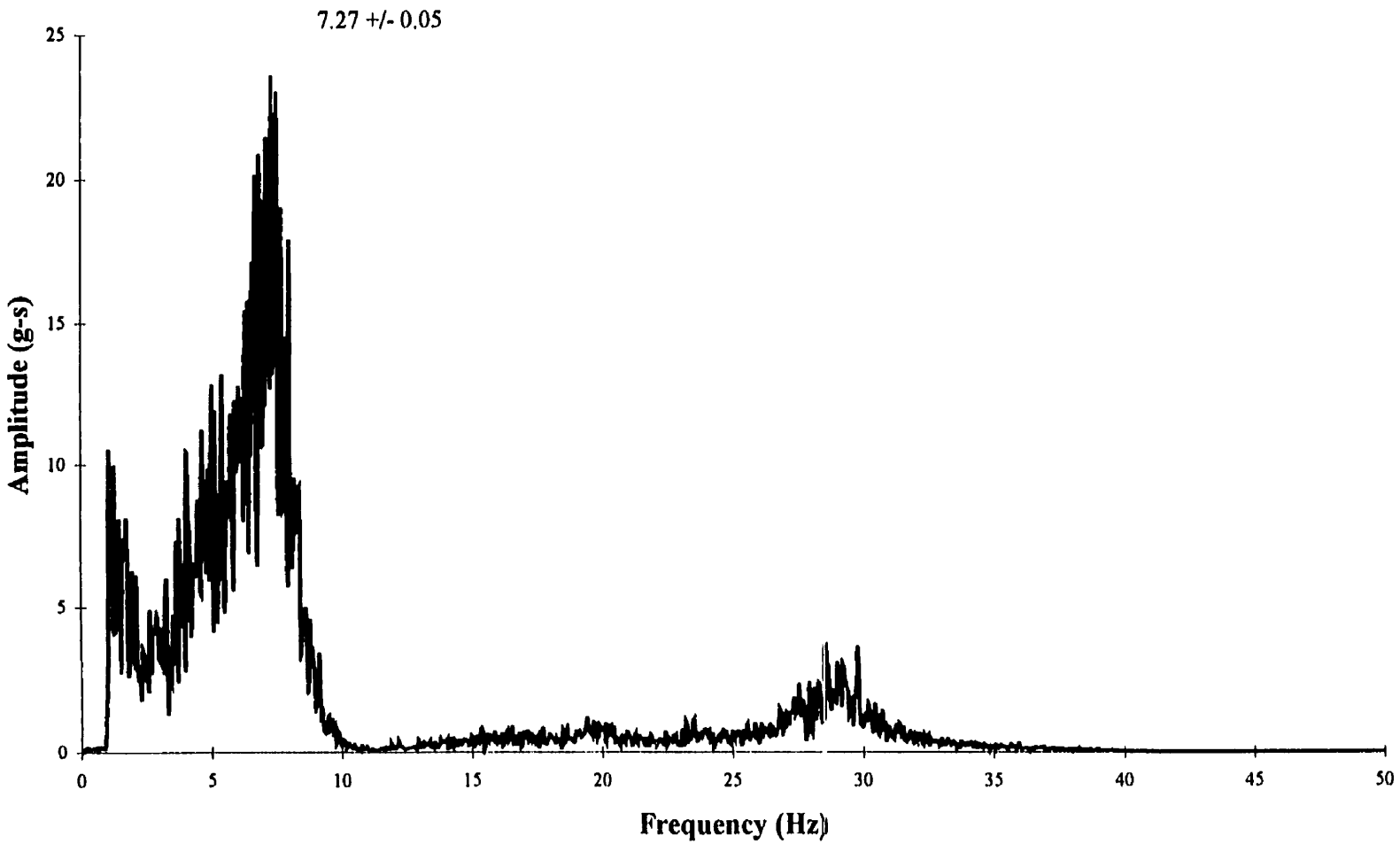

Figure B.4 Power Spectral Density - Specimen No.2 - after 100% Morgan Hill

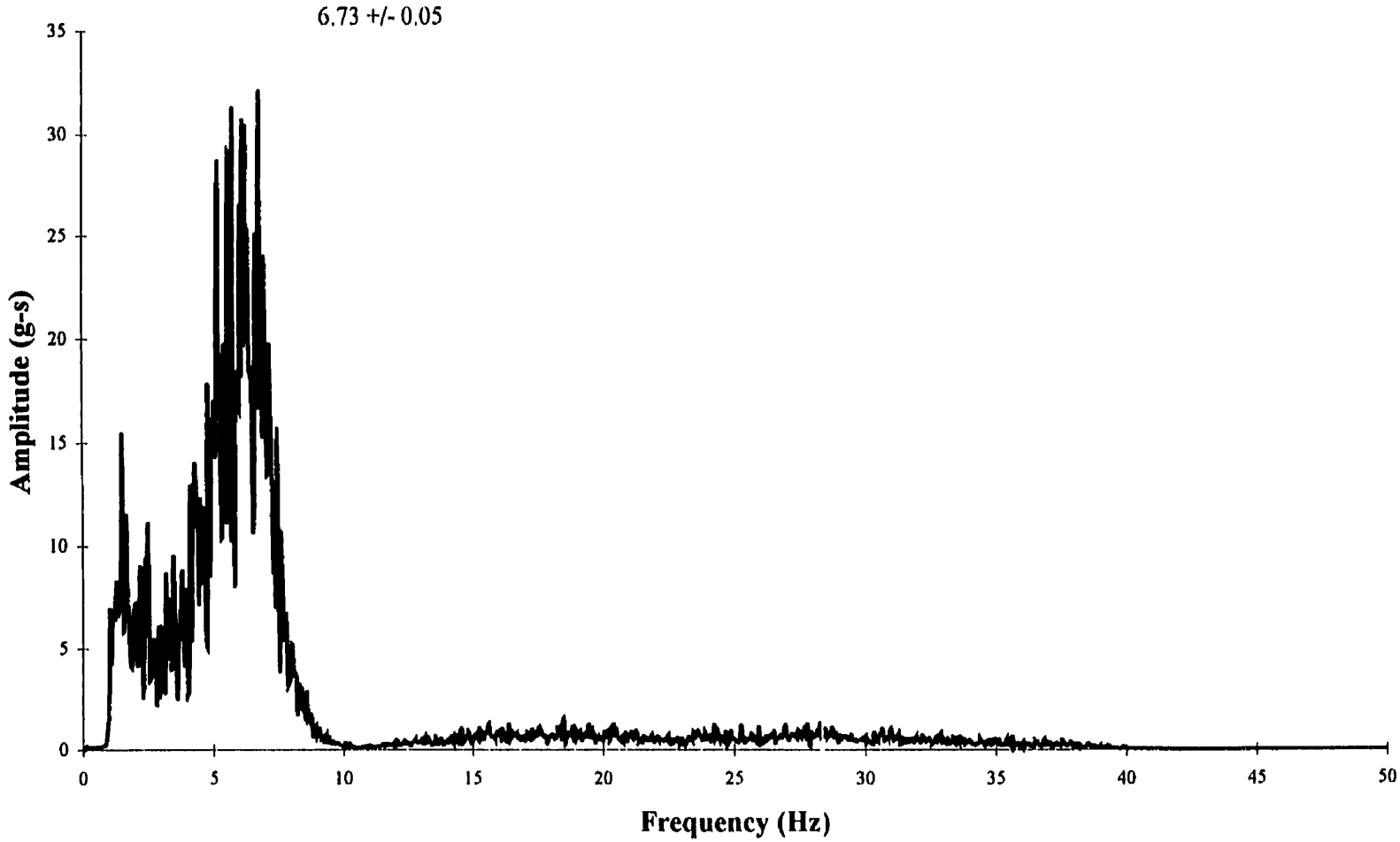

Figure B.5 Power Spectra Density - Specimen No.2 - after 200% Morgan Hill

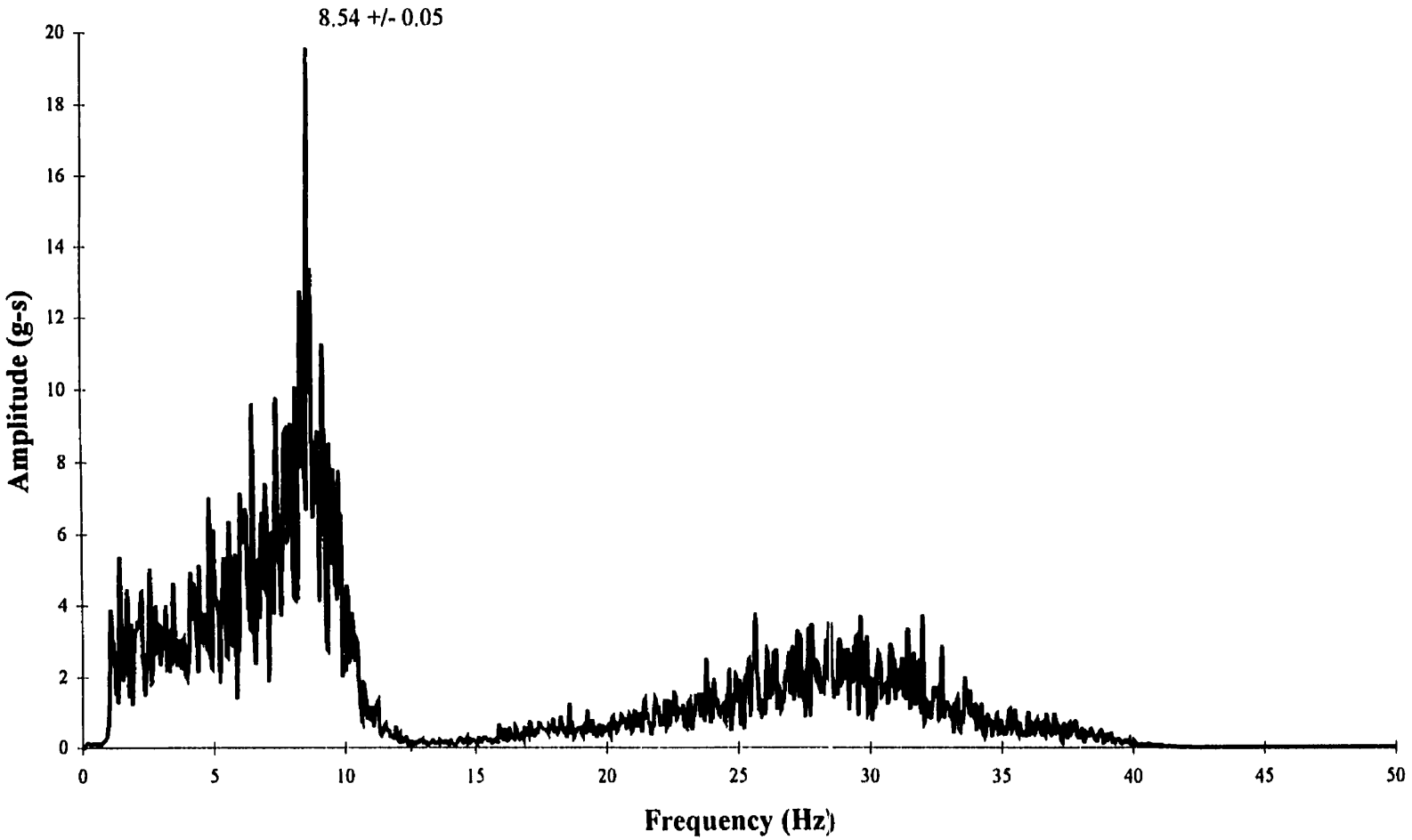

Figure B.6 Power Spectral Density - Specimen No.3 - before 100% Atkinson

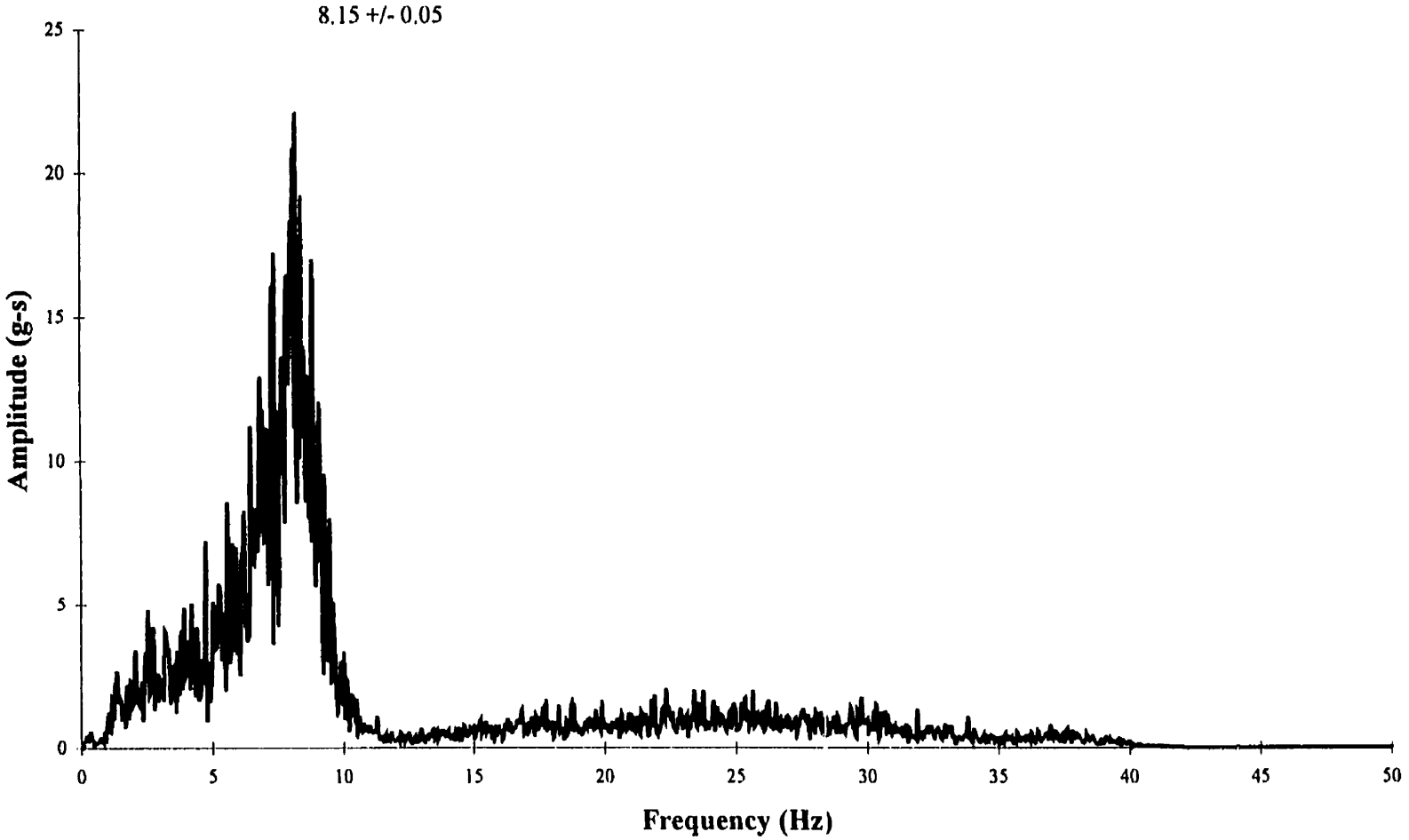

Figure B.7 Power Spectral Density - Specimen No. 3 - after 100% Atkinson

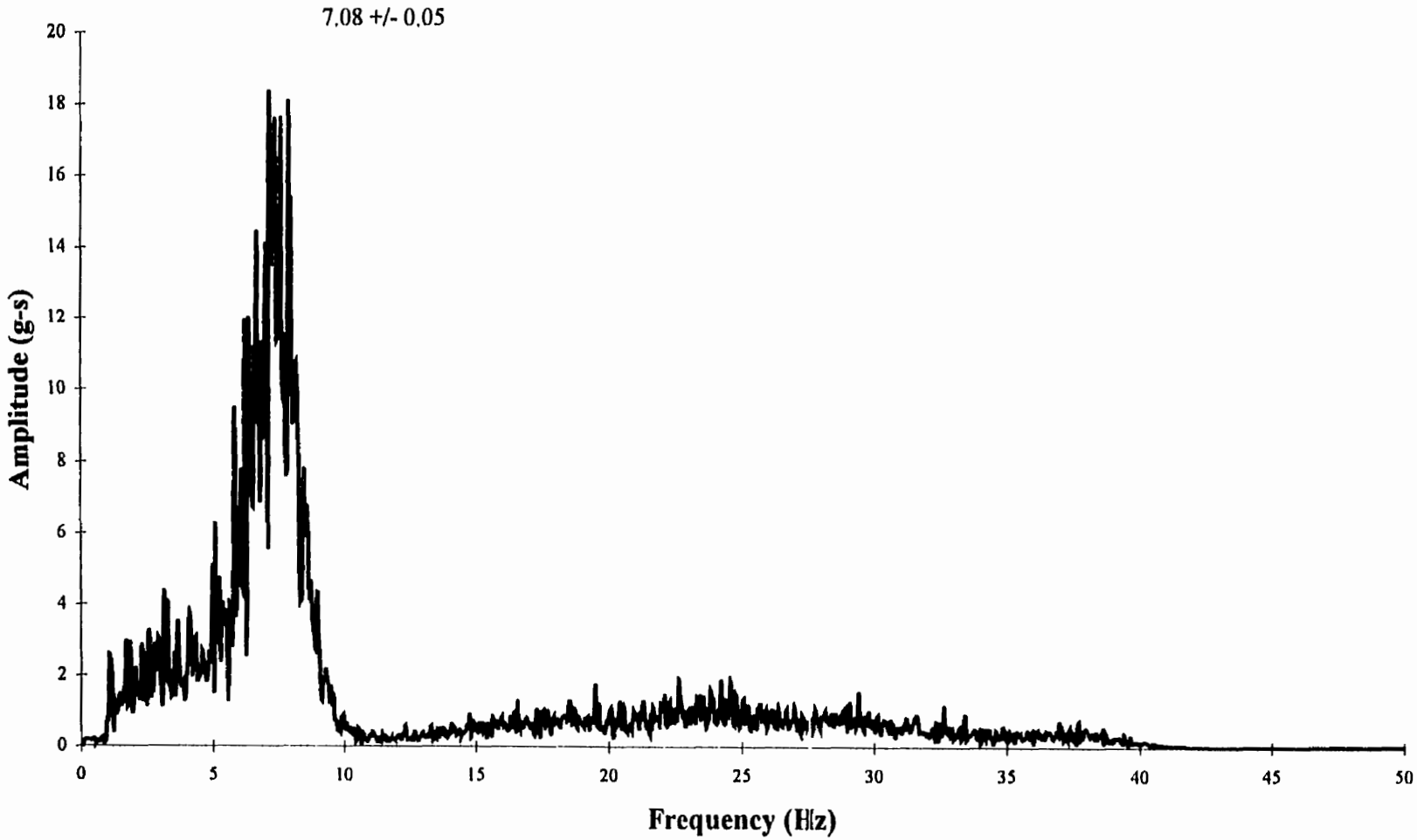

Figure B.8 Power Spectral Density - Specimen No.3 - after 200% Atkinson

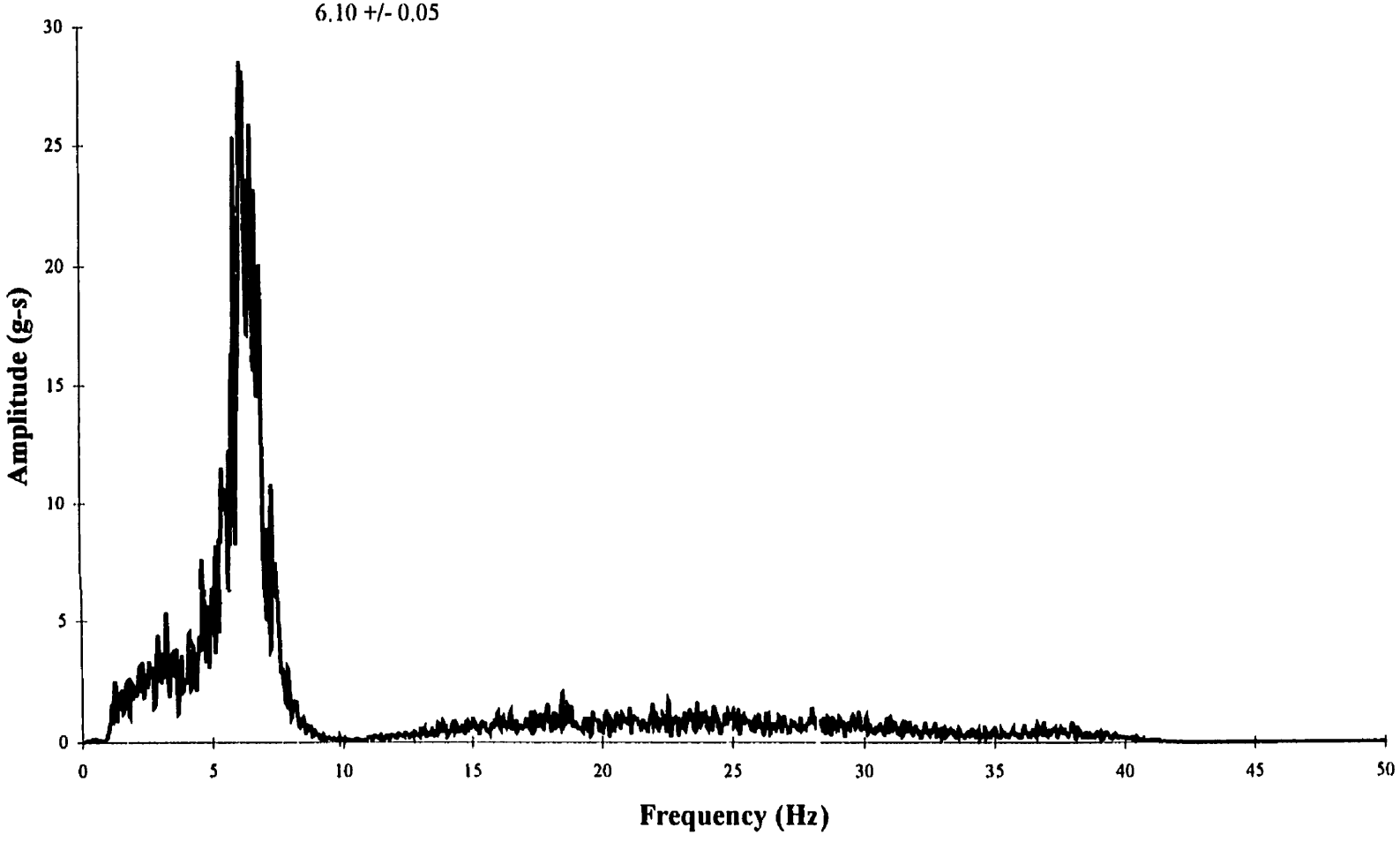

Figure B.9 Power Spectral Density - Specimen No.3 - after 300% Atkinson

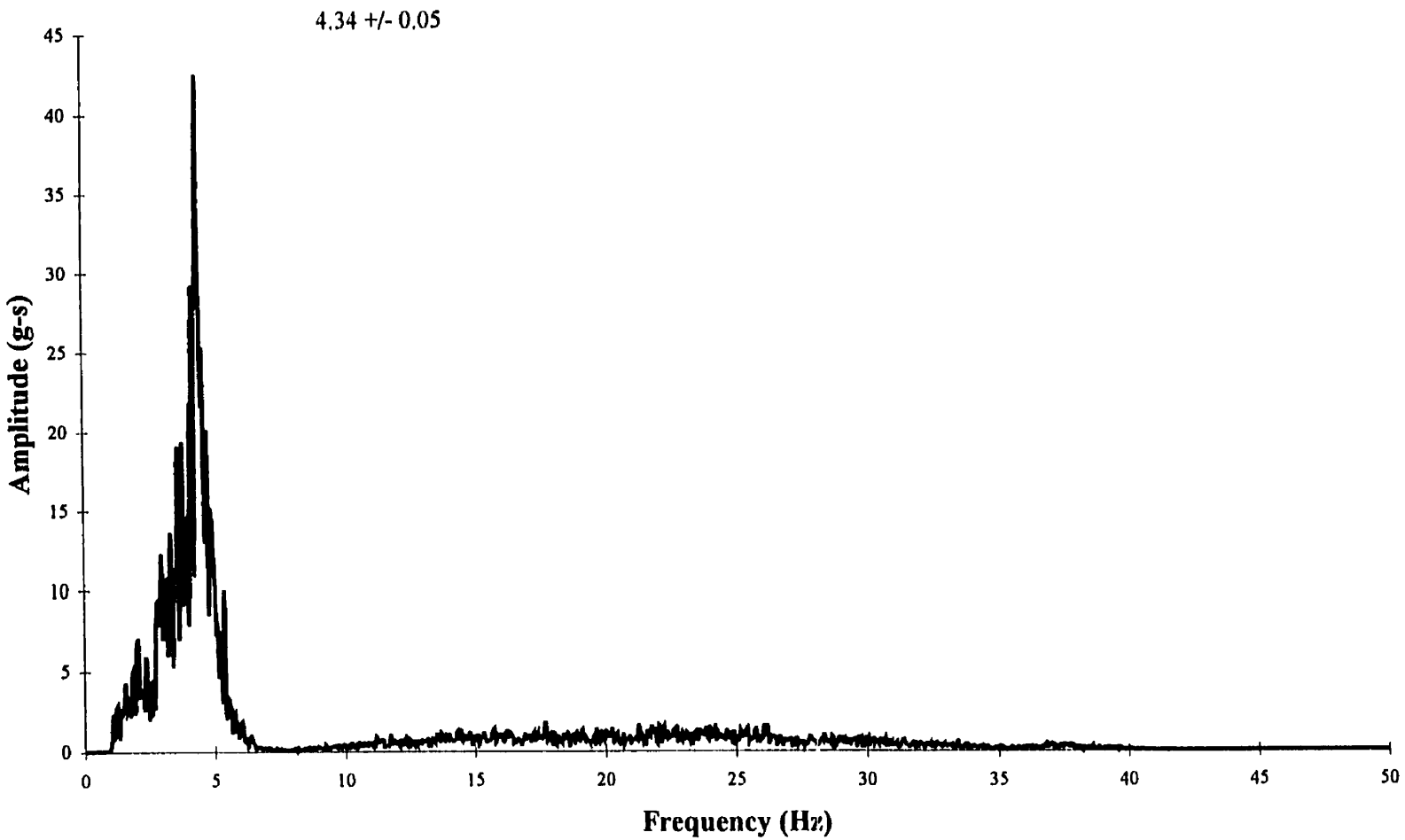

Figure B.10 Power Spectral Density - Specimen No.3 - after 400% Atkinson

APPENDIX C

EVALUATION OF DAMPING

Damping Tests - before 100% Adak
Specimen No. 2

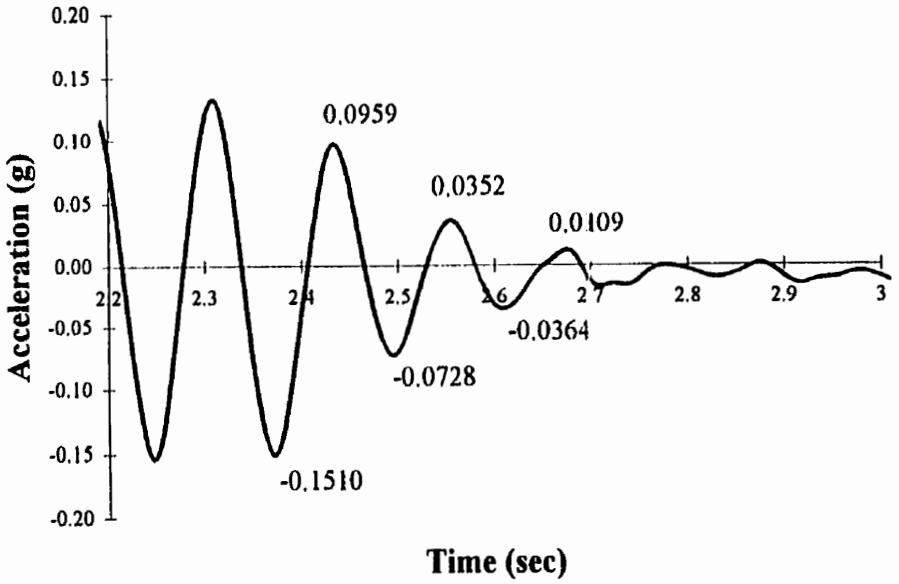

Double Cycle No.	Peak to-peak Amplitude (g)		δ=ln(cycle 1/cycle 2)	$\zeta=\delta/2\pi$
	Cycle 1	Cycle 2		
1	0.2469	0.1080	0.8269	0.132
2	0.1080	0.0473	0.8256	0.131

Mean= 13.2 %

Figure C.1 Evaluation of Damping, Specimen No.2 - before 100% Adak

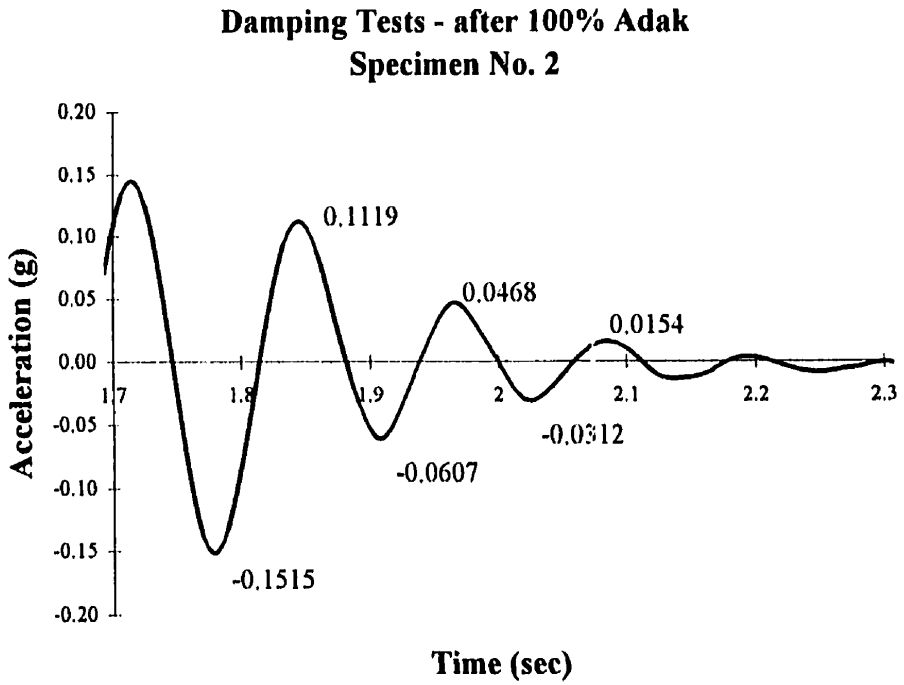

Double Cycle No.	Peak to-peak Amplitude (g)		δ=ln(cycle 1/cycle 2)	ζ=δ/2π
	Cycle 1	Cycle 2		
1	0.2634	0.1075	0.8962	0.142
2	0.1075	0.0466	0.8359	0.133

Mean= 13.8%

Figure C.2 Evaluation of Damping, Specimen No.2 - after 100% Adak

Damping Tests - after 200% Adak
Specimen No. 2

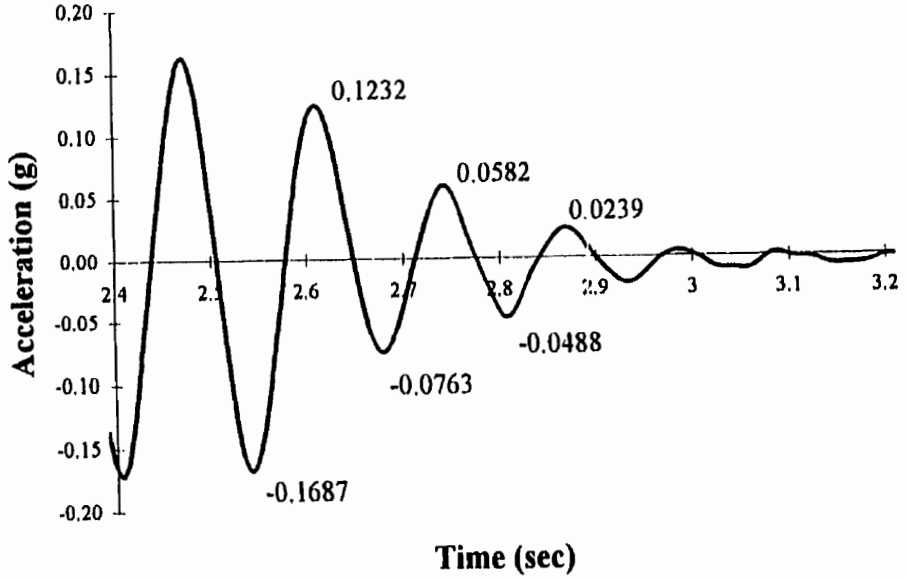

Double Cycle No.	Peak to-peak Amplitude (g)		δ=ln(cycle 1/cycle 2)	ζ=δ/2π
	Cycle 1	Cycle 2		
1	0.2919	0.1345	0.7748	0.123
2	0.1345	0.0727	0.6152	0.098

Mean= 11.1%

Figure C.3 Evaluation of Damping, Specimen No.2 - after 200% Adak

Damping Tests - after 100% Morgan Hill
Specimen No. 2

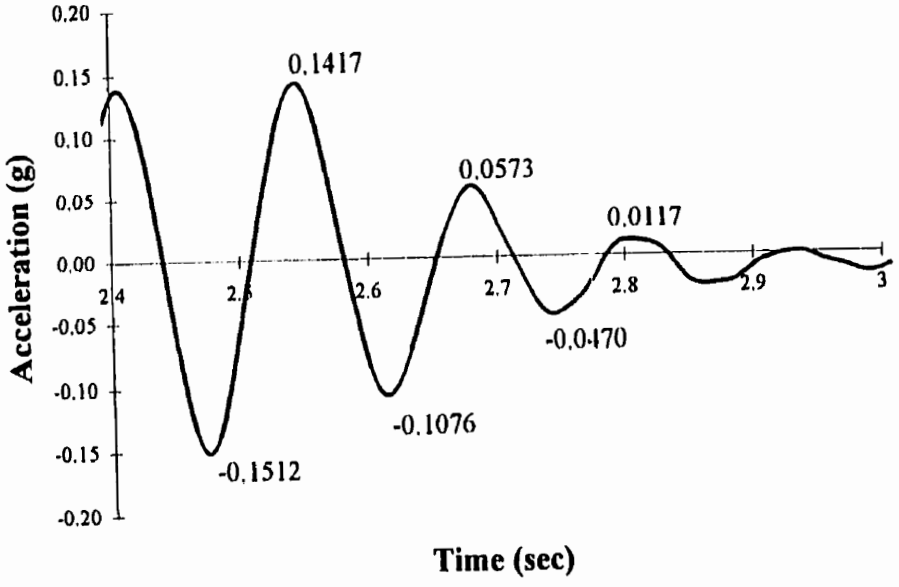

Double Cycle No.	Peak to-peak Amplitude (g)		δ=ln(cycle 1/cycle 2)	ζ=δ/2π
	Cycle 1	Cycle 2		
1	0.2929	0.1649	0.5745	0.091
2	0.1649	0.0587	1.0329	0.164

Mean= 12.8%

Figure C.4 Evaluation of Damping, Specimen No.2 - after 100% Morgan Hill

Damping Tests - after 200% Morgan Hill
Specimen No. 2

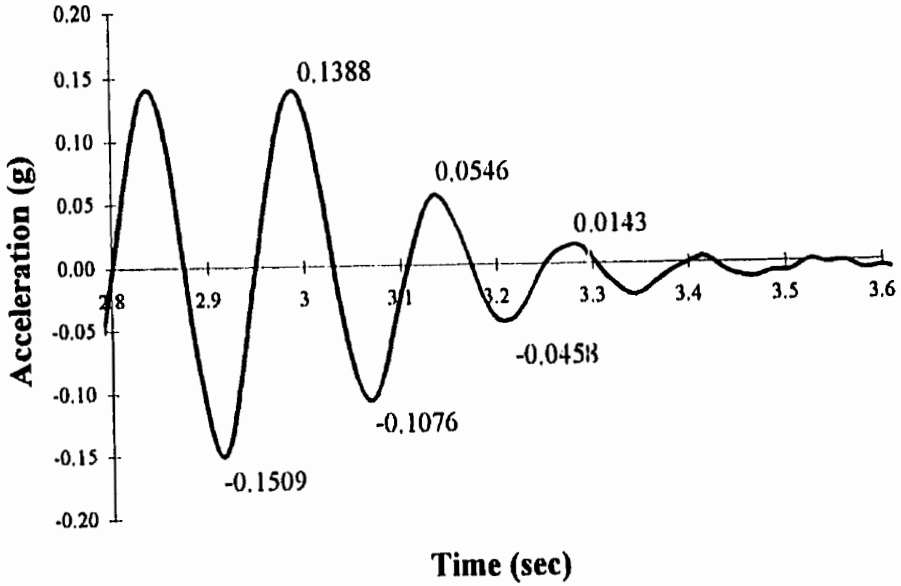

Double Cycle No.	Peak to-peak Amplitude (g)		δ=ln(cycle 1/cycle 2)	ζ=δ/2π
	Cycle 1	Cycle 2		
1	0.2897	0.1622	0.5800	0.092
2	0.1622	0.0601	0.9928	0.158

Mean= 12.5%

Figure C.5 Evaluation of Damping, Specimen No.2 - after 200% Morgan Hill

Damping Tests - before 100% Atkinson
Specimen No. 3

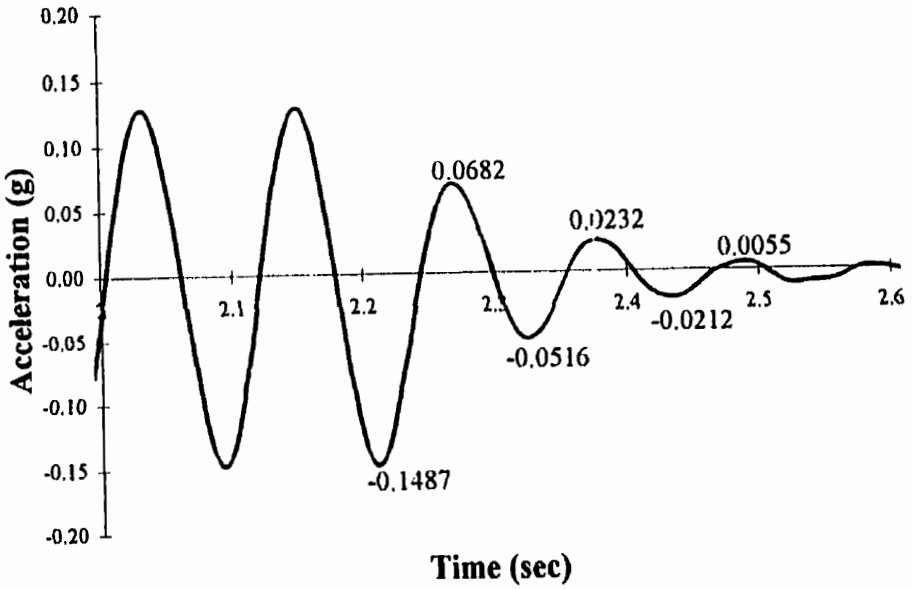

Double Cycle No.	Peak to-peak Amplitude (g)		δ=ln(cycle 1/cycle 2)	ζ=δ/2π
	Cycle 1	Cycle 2		
1	0.2169	0.0748	1.0646	0.169
2	0.0748	0.0267	1.0302	0.164

Mean= 16.7%

Figure C.6 Evaluation of Damping, Specimen No.3 - before 100% Atkinson

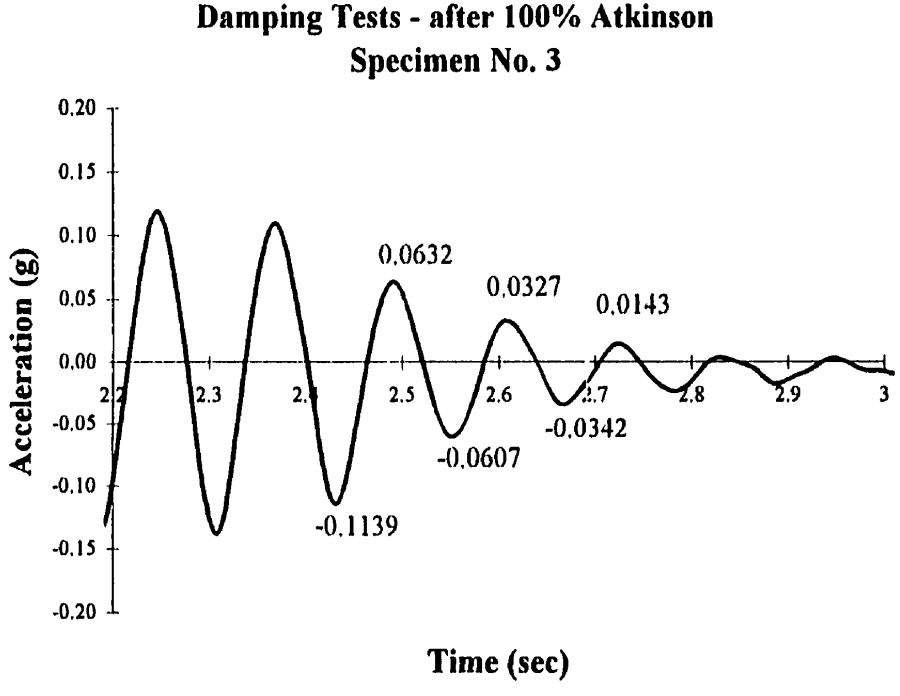

Double Cycle No.	Peak to-peak Amplitude (g)		δ=ln(cycle 1/cycle 2)	ζ=δ/2π
	Cycle 1	Cycle 2		
1	0.1771	0.0934	0.6398	0.102
2	0.0934	0.0485	0.6553	0.104

Mean= 10.3%

Figure C.7 Evaluation of Damping, Specimen No.3 - after 100% Atkinson

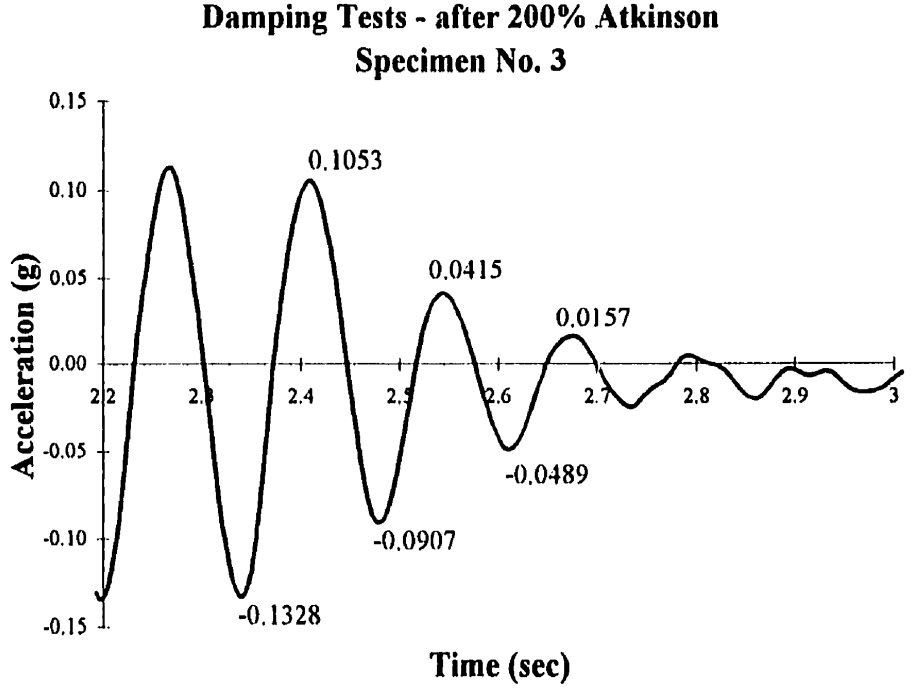

Double Cycle No.	Peak to-peak Amplitude (g)		δ=ln(cycle 1/cycle 2)	ζ=δ/2π
	Cycle 1	Cycle 2		
1	0.2381	0.1322	0.5884	0.094
2	0.1322	0.0646	0.7161	0.114

Mean= 10.4%

Figure C.8 Evaluation of Damping, Specimen No.3 - after 200% Atkinson

Damping Tests - after 300% Atkinson
Specimen No. 3

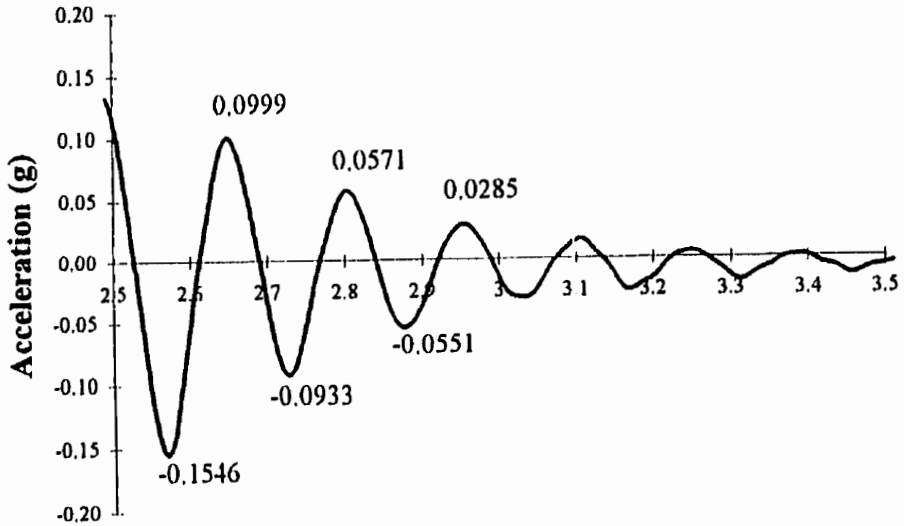

Double Cycle No.	Peak to-peak Amplitude (g)		δ=ln(cycle 1/cycle 2)	ζ=δ/2π
	Cycle 1	Cycle 2		
1	0.2545	0.1504	0.5260	0.084
2	0.1504	0.0836	0.5873	0.093

Mean= 8.9%

Figure C.9 Evaluation of Damping, Specimen No.3 - after 300% Atkinson

Damping Tests - after 400% Atkinson
Specimen No. 3

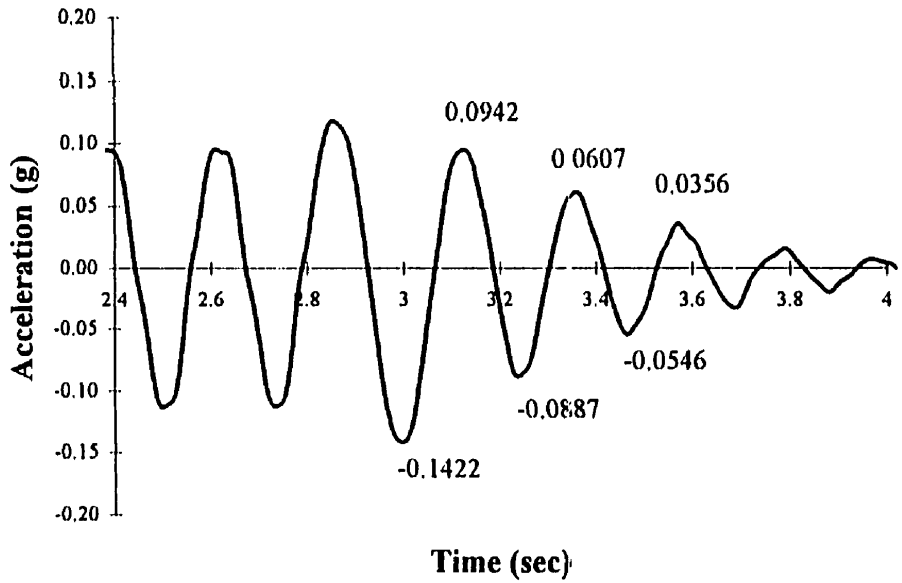

Double Cycle No.	Peak to-peak Amplitude (g)		δ=ln(cycle 1/cycle 2)	ζ=δ/2π
	Cycle 1	Cycle 2		
1	0.2364	0.1494	0.4589	0.073
2	0.1494	0.0902	0.5045	0.080

Mean= 7.7%

Figure C.10 Evaluation of Damping, Specimen No.3 - after 400% Atkinson

APPENDIX D

MEASURED SEISMIC TIME HISTORIES

Table D.1 Envelope of Values for Seismic Tests at +20°C

Test No.	Specimen No.	Ground Motion	Relative Displacement (mm)		Pin Acceleration (g)		Table Acceleration (g)		Base Shear (kN)	
			(+ve)	(-ve)	(+ve)	(-ve)	(+ve)	(-ve)	(+ve)	(-ve)
T10-3	2	Adak 100%	2.19	-2.33	0.566	-0.691	0.790	-0.663	33.9	-41.4
T10-6	2	Adak 200%	4.37	-3.55	0.933	-0.958	1.32	-1.43	59.6	-57.5
T11-1	2	Morgan Hill 100%	5.38	-3.67	0.950	-0.926	0.938	-0.631	57.0	-55.6
T11-4	2	Morgan Hill 200%	7.38	-6.37	2.11	-1.73	1.70	-1.25	126.8	-103.7
T11-7	2	Morgan Hill 400%	54.3	-61.2	3.67	-2.01	3.14	-2.17	220.5	-120.7
T12-3	3	Atkinson 100%	2.17	-3.41	0.770	-0.660	0.709	-0.501	47.2	-39.8
T12-6	3	Atkinson 200%	3.48	-5.02	1.01	-1.05	1.53	-1.14	60.6	-63.0
T12-9	3	Atkinson 300%	6.81	-10.3	1.57	-1.61	1.55	-1.35	93.9	-96.5
T12-12	3	Atkinson 400%	39.3	-26.7	1.59	-1.64	2.14	-2.54	95.6	-98.7

Table D.1 Envelope of Values for Seismic Tests at +20°C (cont.)

Test No.	Specimen No.	Ground Motion	Curvature (section 1) (rad/km)		Curvature (section 2) (rad/km)		Curvature (section 3) (rad/km)	
			(+ve)	(-ve)	(+ve)	(-ve)	(+ve)	(-ve)
T10-3	2	Adak 100%	4.4×10^{-5}	-4.1×10^{-5}	3.6×10^{-6}	-2.1×10^{-6}	2.3×10^{-6}	-1.2×10^{-6}
T10-6	2	Adak 200%	10.2×10^{-5}	-7.4×10^{-5}	4.6×10^{-6}	-3.5×10^{-6}	4.0×10^{-6}	-1.5×10^{-6}
T11-1	2	Morgan Hill 100%	12.9×10^{-5}	-7.2×10^{-5}	4.2×10^{-6}	-3.9×10^{-6}	3.9×10^{-6}	-1.6×10^{-6}
T11-4	2	Morgan Hill 200%	17.9×10^{-5}	-14.0×10^{-5}	4.7×10^{-6}	-4.7×10^{-6}	5.1×10^{-6}	-2.8×10^{-6}
T11-7	2	Morgan Hill 400%	235×10^{-5}	-138×10^{-5}	41.3×10^{-6}	-45.8×10^{-6}	27.3×10^{-6}	-468×10^{-6}
T12-3	3	Atkinson 100%	5.4×10^{-5}	-5.0×10^{-5}	2.8×10^{-6}	-2.2×10^{-6}	2.3×10^{-6}	-1.5×10^{-6}
T12-6	3	Atkinson 200%	9.1×10^{-5}	-9.9×10^{-5}	3.4×10^{-6}	-2.9×10^{-6}	3.5×10^{-6}	-2.9×10^{-6}
T12-9	3	Atkinson 300%	20.1×10^{-5}	-29.2×10^{-5}	3.1×10^{-6}	-4.4×10^{-6}	9.2×10^{-6}	-4.2×10^{-6}
T12-12	3	Atkinson 400%	173×10^{-5}	-105×10^{-5}	21.4×10^{-6}	-17.0×10^{-6}	13.6×10^{-6}	-15.3×10^{-6}

Table D.1 Envelope of Values for Seismic Tests at +20°C (cont.)

Test No.	Specimen No.	Ground Motion	Max Strain Starter Bar (section 1) (με)		Max Strain Starter Bar (section 2) (με)		Max Strain Starter Bar (section 3) (με)	
			(+ve)	(-ve)	(+ve)	(-ve)	(+ve)	(-ve)
T10-3	2	Adak 100%	49.9	-27.9	42.4	-23.8	44.7	-25.5
T10-6	2	Adak 200%	106.8	-50.6	71.1	-43.0	73.0	-46.8
T11-1	2	Morgan Hill 100%	133.5	-53.8	69.9	-45.2	71.0	-49.2
T11-4	2	Morgan Hill 200%	227.3	-59.2	155.9	-58.3	119	-62.3
T11-7	2	Morgan Hill 400%	5546	-156.6	5574	-878	5717	-410.6
T12-3	3	Atkinson 100%	77.7	-31.4	15.0	-4.4	0	0
T12-6	3	Atkinson 200%	123.5	-51.3	30.3	-9.8	99.7	-40.2
T12-9	3	Atkinson 300%	296.8	-48.5	44.1	-30.2	186	-52.4
T12-12	3	Atkinson 400%	4511	-155	4582	-86.4	4580	550

Table D.1 Envelope of Values for Seismic Tests at +20°C (cont.)

Test No.	Specimen No.	Ground Motion	Max Strain Stirrup Bar (section 1) (με)		Max Strain Stirrup Bar (section 2) (με)	
			(+ve)	(-ve)	(-ve)	(+ve)
T10-3	2	Adak 100%	0	0	0	0
T10-6	2	Adak 200%	0	0	0	0
T11-1	2	Morgan Hill 100%	0	0	0	0
T11-4	2	Morgan Hill 200%	30.5	-28.4	11.3	-2.9
T11-7	2	Morgan Hill 400%	120.8	-2.4	2.7	-2.0
T12-3	3	Atkinson 100%	16.7	-7.2	0	0
T12-6	3	Atkinson 200%	31.2	-9.8	1.9	-2.2
T12-9	3	Atkinson 300%	38.5	-34.0	3.0	-2.7
T12-12	3	Atkinson 400%	4472	-58.5	27.0	-59.4

Table D.2 Envelope of Values for Seismic Tests at -40°C

Test No.	Specimen No.	Ground Motion	Relative Displacement (mm)		Pin Acceleration (g)		Table Acceleration (g)		Base Shear (kN)	
			(+ve)	(-ve)	(+ve)	(-ve)	(+ve)	(-ve)	(+ve)	(-ve)
T13-1	4	Adak 100%	1.15	-1.48	3.69	-0.813	1.47	-1.51	221.1	-48.8
T13-2	4	Adak 200%	2.70	-2.67	3.35	-0.960	1.21	-1.07	201.0	-57.7
T14-1	4	Atkinson 100%	1.83	-2.20	3.47	-1.23	0.837	-0.669	208.3	-74.0
T14-3	4	Atkinson 300%	5.62	-6.20	2.76	-1.65	1.64	-1.61	165.9	-99.5
T14-4	4	Atkinson 400%	5.48	-5.88	2.81	-1.80	2.58	-1.93	168.5	-107.8
T14-5	4	Atkinson 500%	10.06	-9.79	3.50	-2.38	2.83	-2.41	210.0	-142.7
T14-6	4	Atkinson 600%	15.06	-10.74	4.44	-1.93	3.77	-2.23	266.4	-115.9

Table D.2 Envelope of Values for Seismic Tests at -40°C (cont.)

Test No.	Specimen No.	Ground Motion	Curvature (section 1) (rad/km)		Curvature (section 2) (rad/km)		Curvature (section 3) (rad/km)	
			(+ve)	(-ve)	(+ve)	(-ve)	(+ve)	(-ve)
T13-1	4	Adak 100%	2.8×10^{-5}	-4.0×10^{-5}	2.1×10^{-6}	-3.3×10^{-6}	0.5×10^{-6}	-1.8×10^{-6}
T13-2	4	Adak 200%	8.8×10^{-5}	-7.6×10^{-5}	5.8×10^{-6}	-2.8×10^{-6}	1.4×10^{-6}	-2.7×10^{-6}
T14-1	4	Atkinson 100%	4.5×10^{-5}	-4.7×10^{-5}	3.5×10^{-6}	-1.3×10^{-6}	2.0×10^{-6}	-0.0×10^{-6}
T14-3	4	Atkinson 300%	21.1×10^{-5}	-8.7×10^{-5}	0.0×10^{-6}	-1.8×10^{-6}	0.5×10^{-6}	-1.1×10^{-6}
T14-4	4	Atkinson 400%	22.2×10^{-5}	-9.6×10^{-5}	0.0×10^{-6}	-17.0×10^{-6}	22.3×10^{-6}	-0.0×10^{-6}
T14-5	4	Atkinson 500%	36.5×10^{-5}	-22.3×10^{-5}	0.0×10^{-6}	-16.1×10^{-6}	22.8×10^{-6}	-0.0×10^{-6}
T14-6	4	Atkinson 600%	51.1×10^{-5}	-23.4×10^{-5}	0.0×10^{-6}	-15.3×10^{-6}	43.9×10^{-6}	-1.7×10^{-6}

Table D.2 Envelope of Values for Seismic Tests at -40°C (cont.)

Test No.	Specimen No.	Ground Motion	Max Strain Starter Bar (section 1) (με)		Max Strain Starter Bar (section 2) (με)		Max Strain Starter Bar (section 3) (με)	
			(+ve)	(-ve)	(+ve)	(-ve)	(+ve)	(-ve)
T13-1	4	Adak 100%	57.3	-31.5	26.1	-28.5	21.7	-23.6
T13-2	4	Adak 200%	134.7	-50.2	99.5	-42.9	72.6	-34.5
T14-1	4	Atkinson 100%	100.5	-202.7	36.8	-28.4	31.0	-27.3
T14-3	4	Atkinson 300%	275.6	-64.2	130.8	-67.7	113.7	-63.9
T14-4	4	Atkinson 400%	228.3	-74.8	132.8	-88.7	116.7	-78.9
T14-5	4	Atkinson 500%	667.3	-77.1	238.6	-97.9	237.3	-83.4
T14-6	4	Atkinson 600%	1247	-4068	4583	-133.9	290.7	-107.7

Table D.2 Envelope of Values for Seismic Tests at -40°C (cont.)

Test No.	Specimen No.	Ground Motion	Max Strain Stirrup Bar (section 1) (με)		Max Strain Stirrup Bar (section 2) (με)	
			(+ve)	(-ve)	(-ve)	(+ve)
T13-1	4	Adak 100%	5.8	-24.1	0	-0
T13-2	4	Adak 200%	2.8	-2.6	0	-0
T14-1	4	Atkinson 100%	0	-0	0	-0
T14-3	4	Atkinson 300%	6.6	-2.0	4.0	-2.2
T14-4	4	Atkinson 400%	7.3	-22.3	2.8	-11.8
T14-5	4	Atkinson 500%	7.1	-2.0	7.4	-2.4
T14-6	4	Atkinson 600%	26.2	-6.4	8.6	-1.0

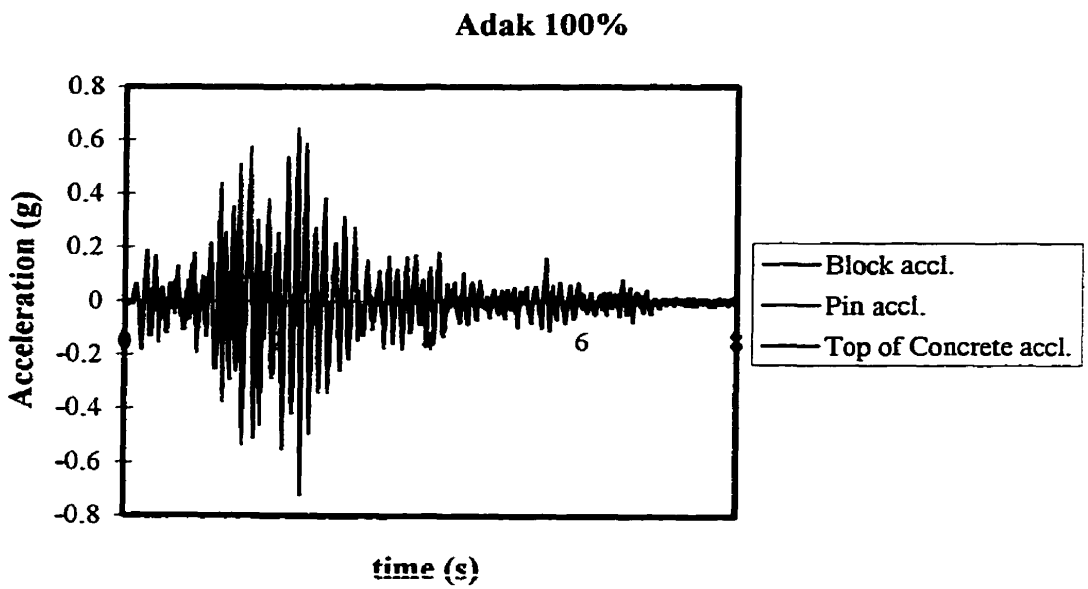

Figure D.1 Measured Acceleration of Block, Pin and Top of Concrete for Adak 100%

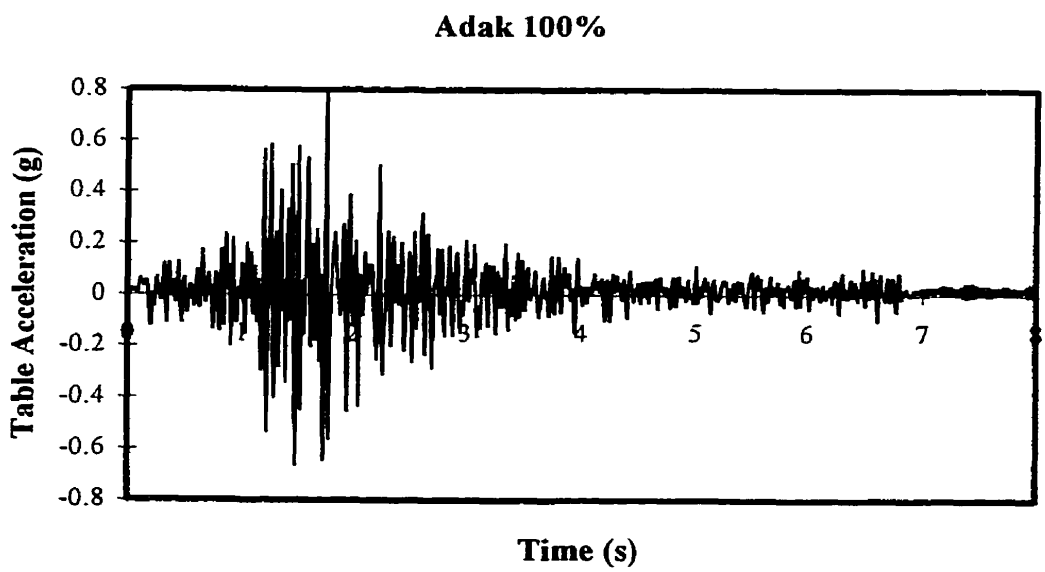

Figure D.2 Measured Table Acceleration for Adak 100%

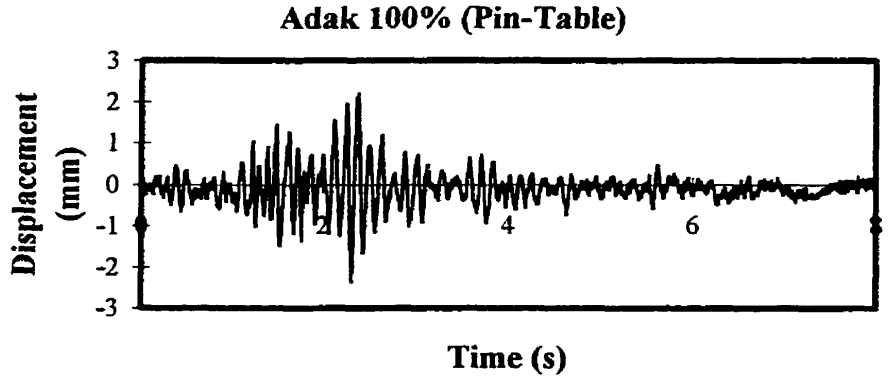

Figure D.3 Relative Displacement (Pin-Table) for Adak 100%

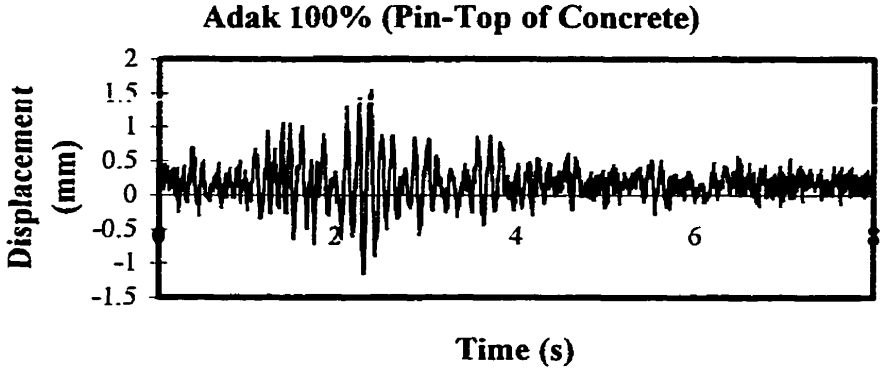

Figure D.4 Relative Displacement (Pin-Top of Concrete) for Adak 100%

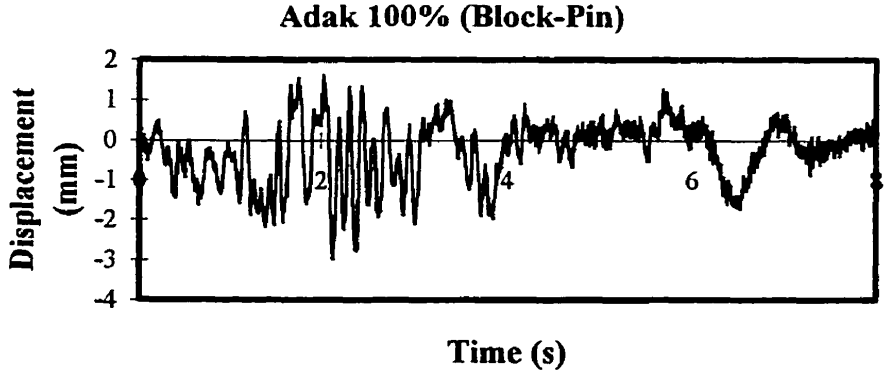

Figure D.5 Relative Displacement (Block-Pin) for Adak 100%

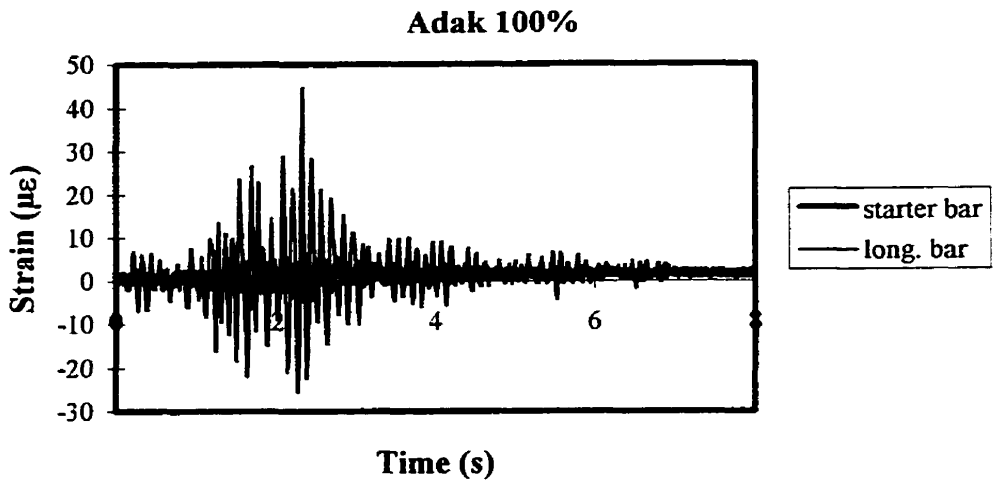

Figure D.6 Measured Strains from Starter and Longitudinal Bars (165 mm from the base) for Adak 100%

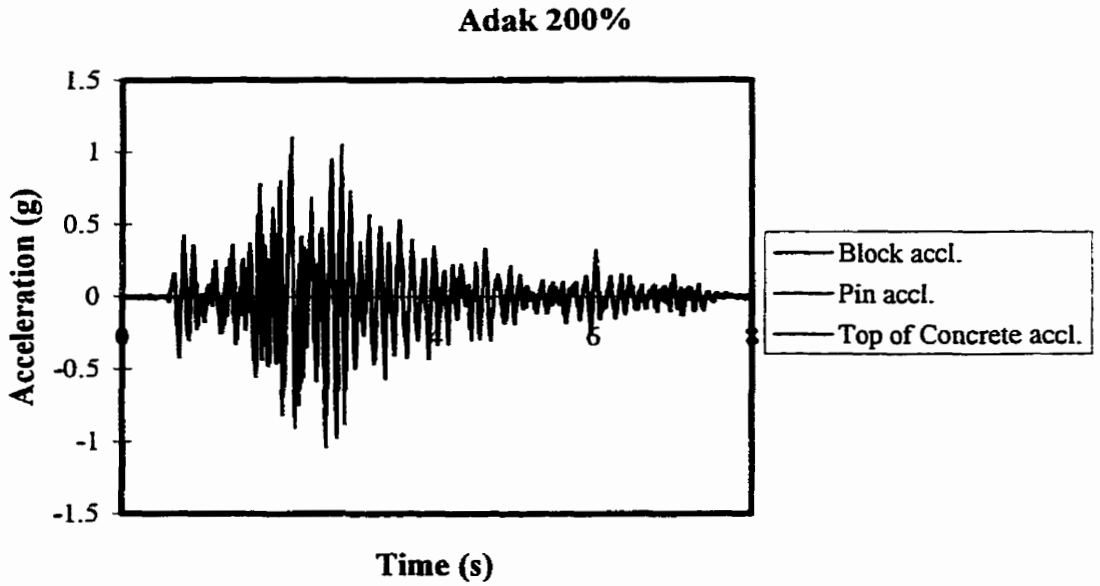

Figure D.7 Measured Acceleration of Block, Pin and Top of Concrete for Adak 200%

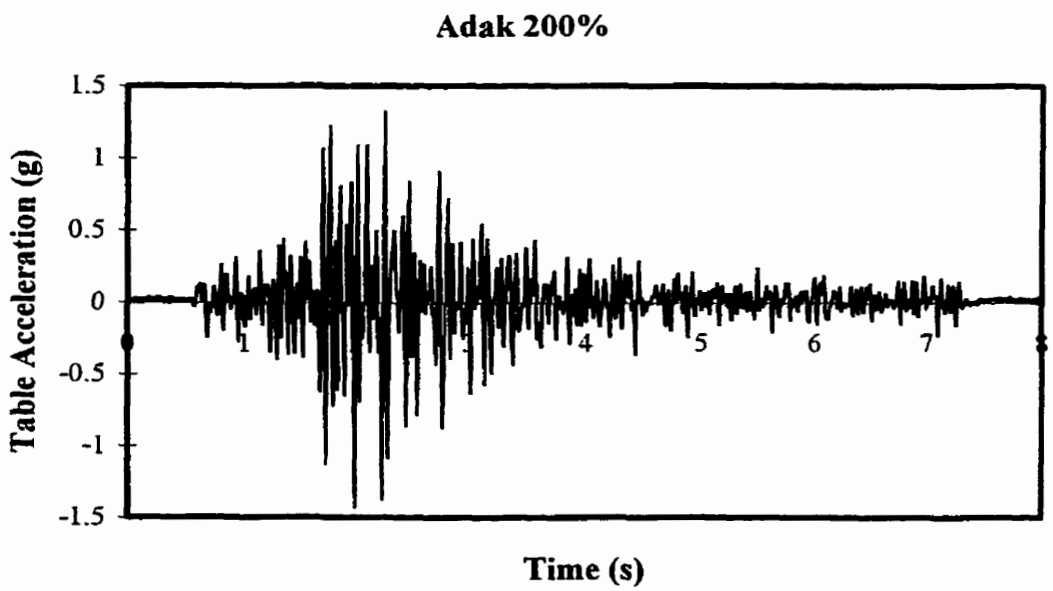

Figure D.8 Measured Table Acceleration for Adak 200%

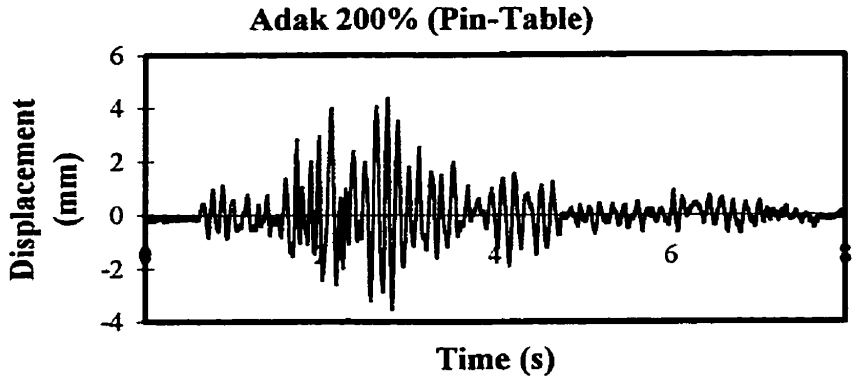

Figure D.9 Relative Displacement (Pin-Table) for Adak 200%

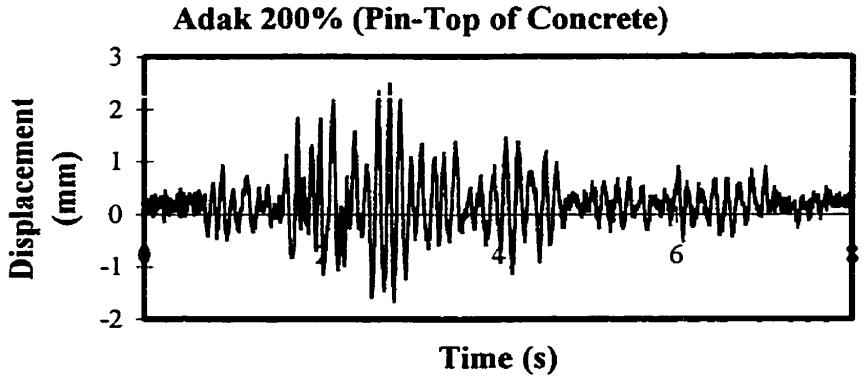

Figure D.10 Relative Displacement (Pin-Top of Concrete) for Adak 200%

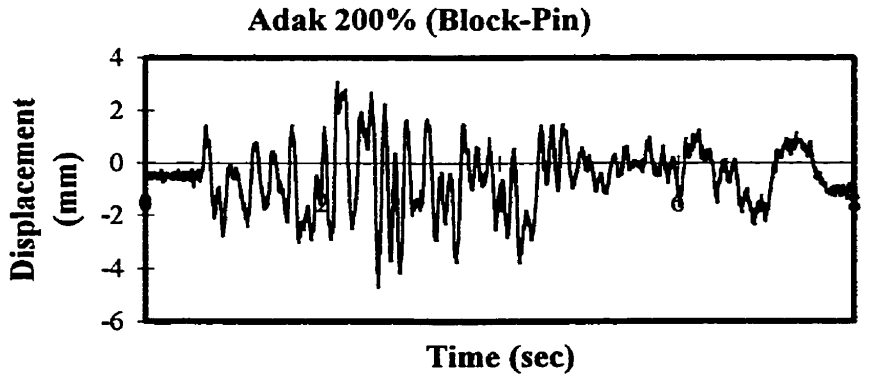

Figure D.11 Relative Displacement (Block-Pin) for Adak 200%

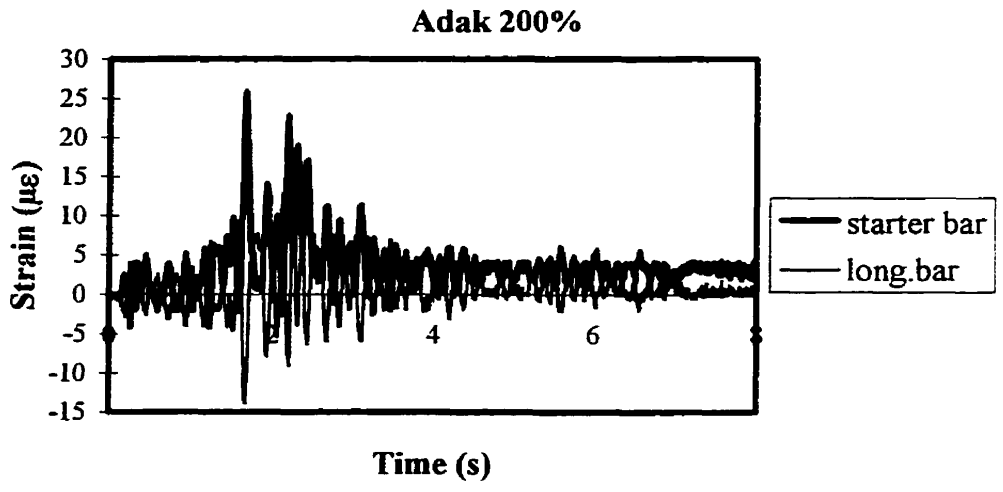

Figure D.12 Measured Strains from Starter and Longitudinal Bars (165 mm from the base) for Adak 200%

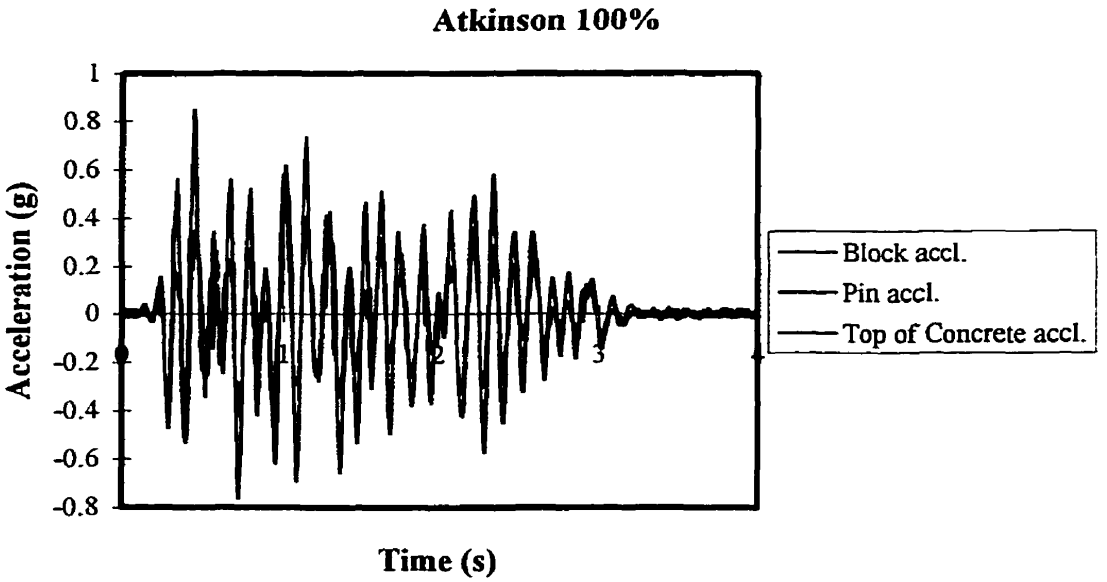

Figure D.13 Measured Acceleration of Block, Pin and Top of Concrete for Atkinson 100%

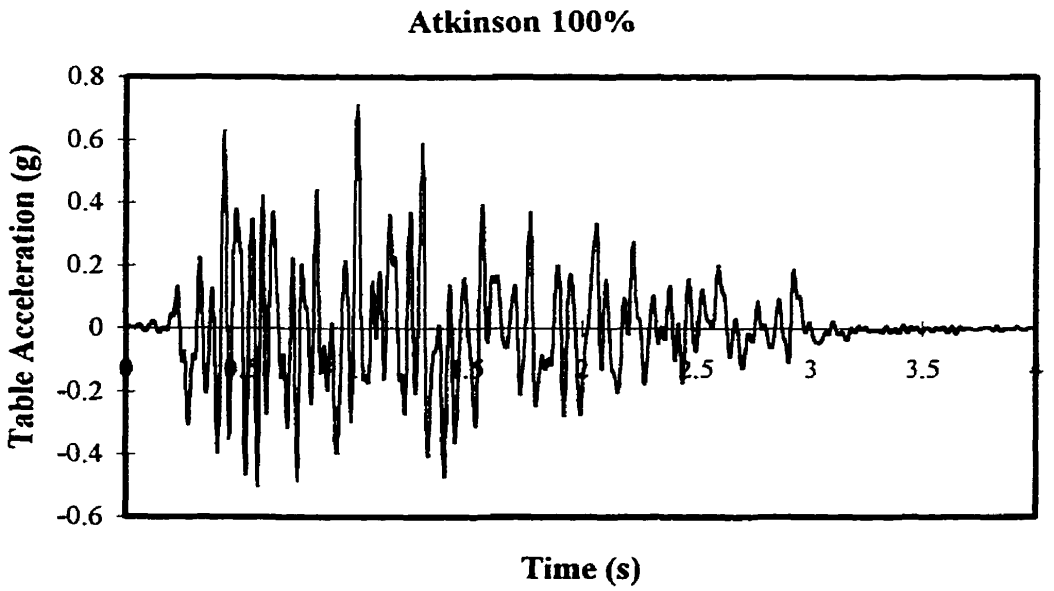

Figure D.14 Measured Table Acceleration for Atkinson 100%

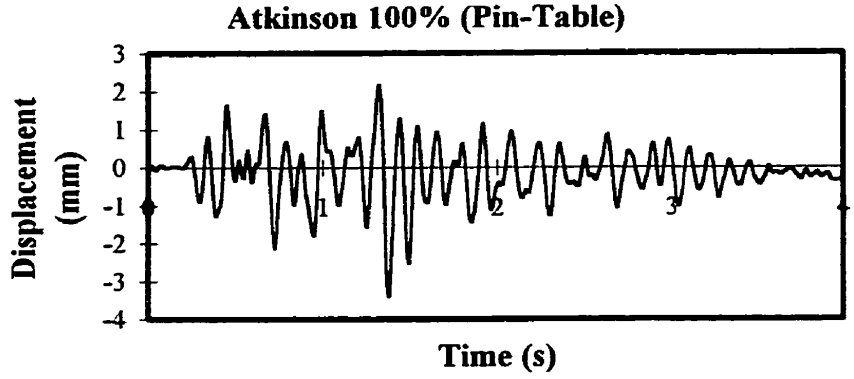

Figure D.15 Relative Displacement (Pin-Table) for Atkinson 100%

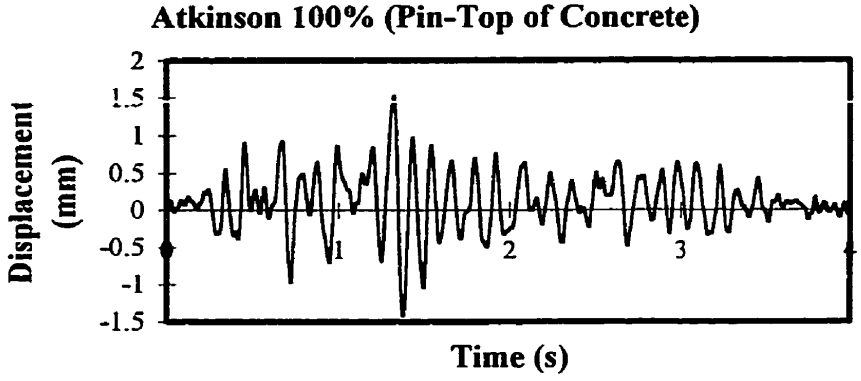

Figure D.16 Relative Displacement (Pin-Top of Concrete) for Atkinson 100%

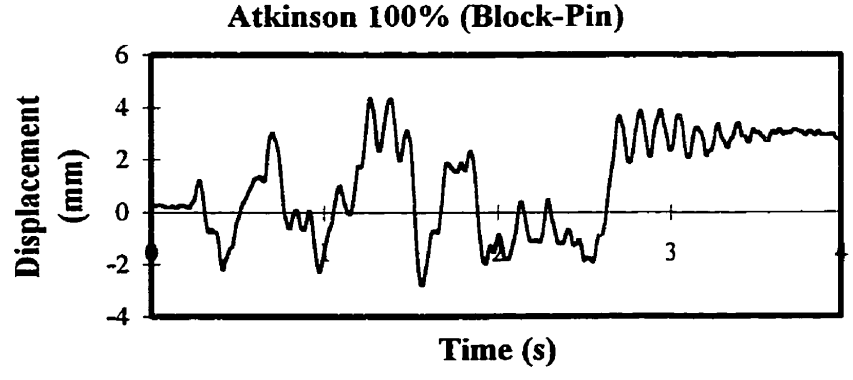

Figure D.17 Relative Displacement (Block-Pin) for Atkinson 100%

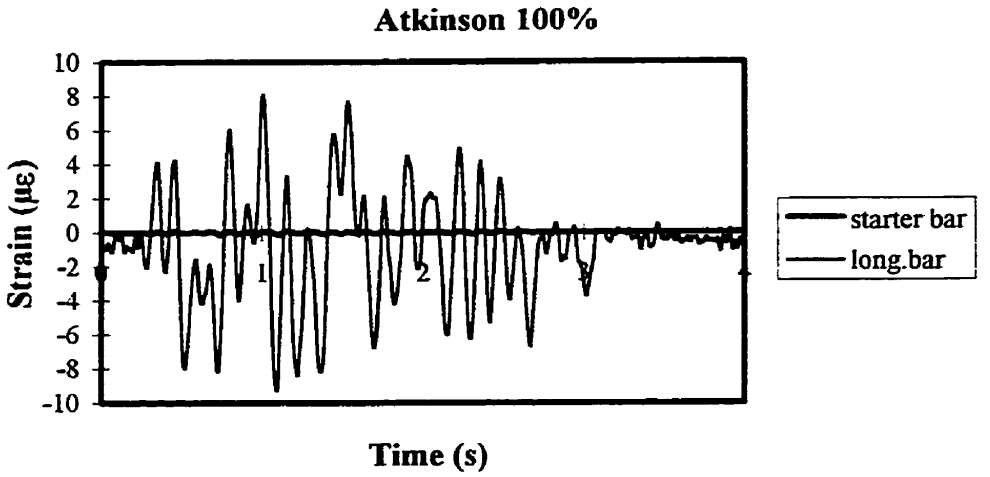

Figure D.18 Measured Strains from Starter and Longitudinal Bars (165 mm from the base) for Atkinson 100%

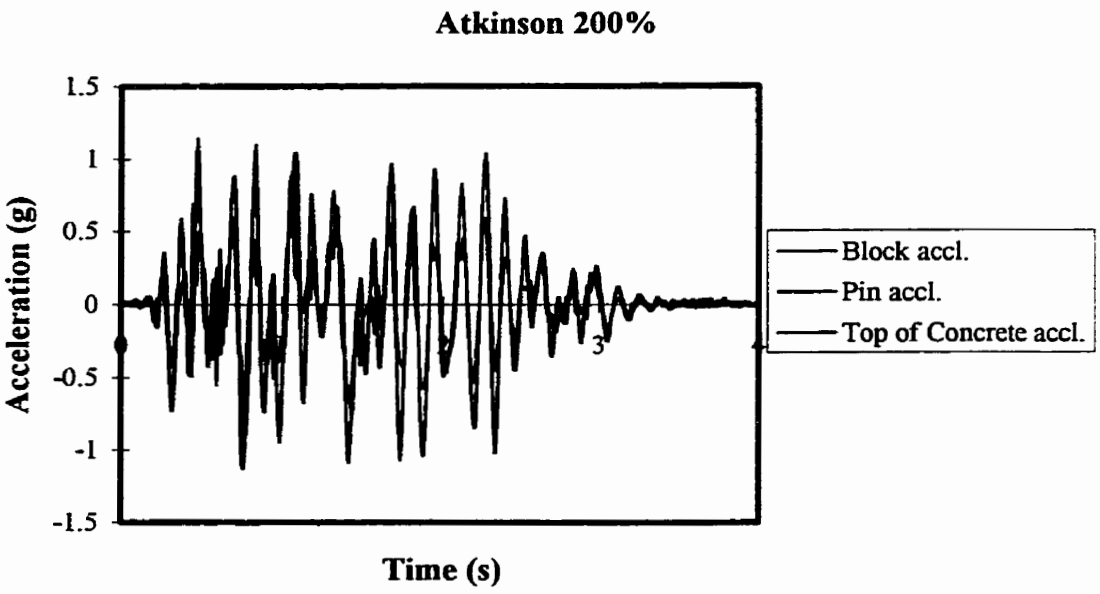

Figure D.19 Measured Acceleration of Block, Pin and Top of Concrete for Atkinson 200%

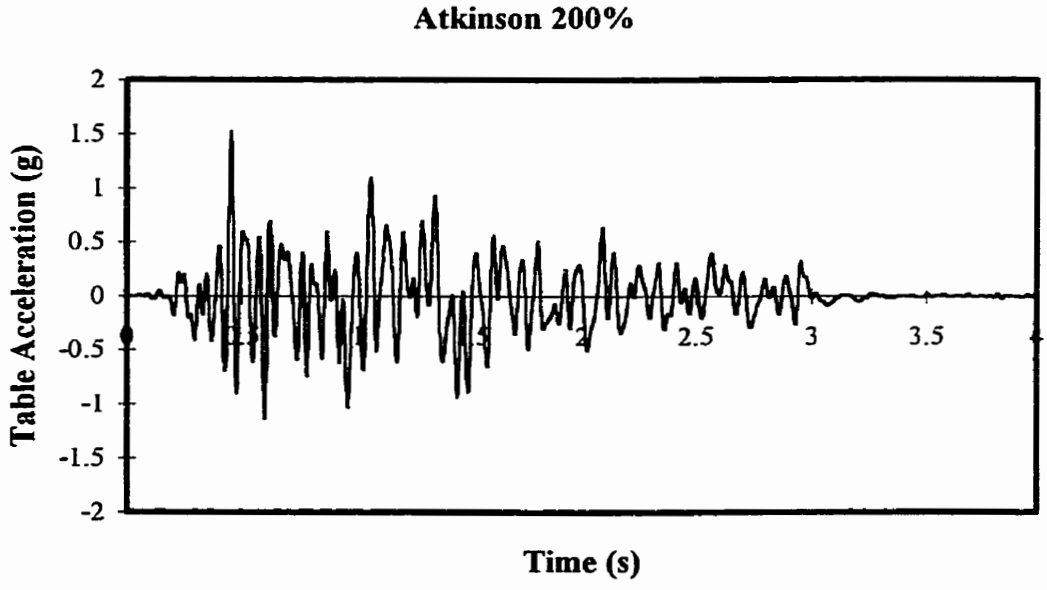

Figure D.20 Measured Table Acceleration for Atkinson 200%

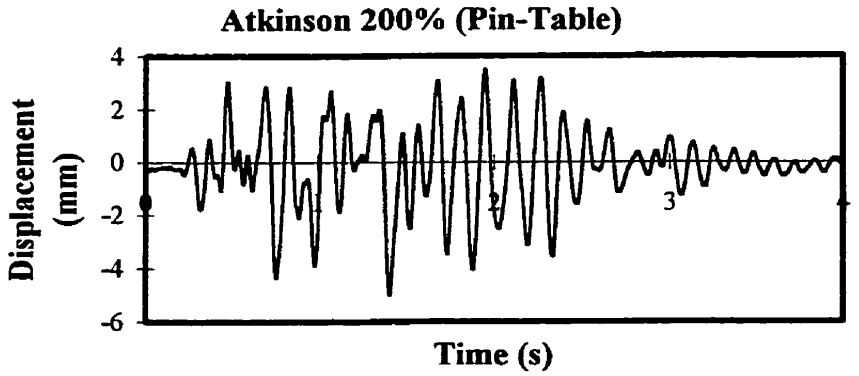

Figure D.21 Relative Displacement (Pin-Table) for Atkinson 200%

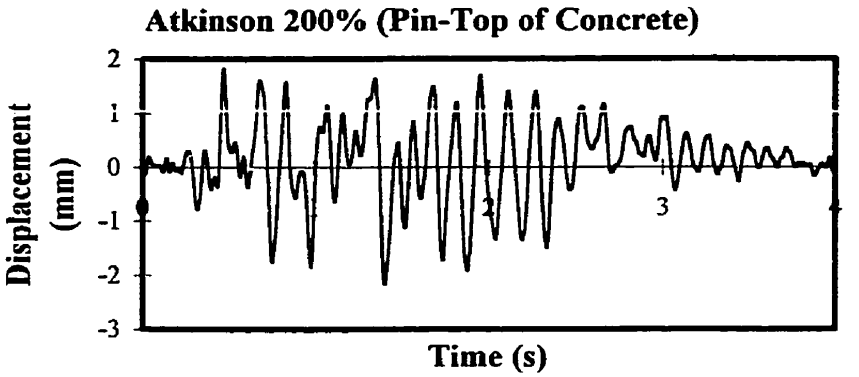

Figure D.22 Relative Displacement (Pin-Top of Concrete) for Atkinson 200%

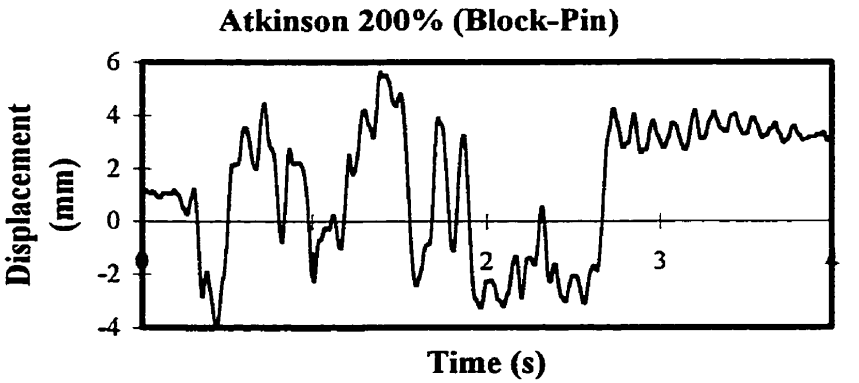

Figure D.23 Relative Displacement (Block-Pin) for Atkinson 200%

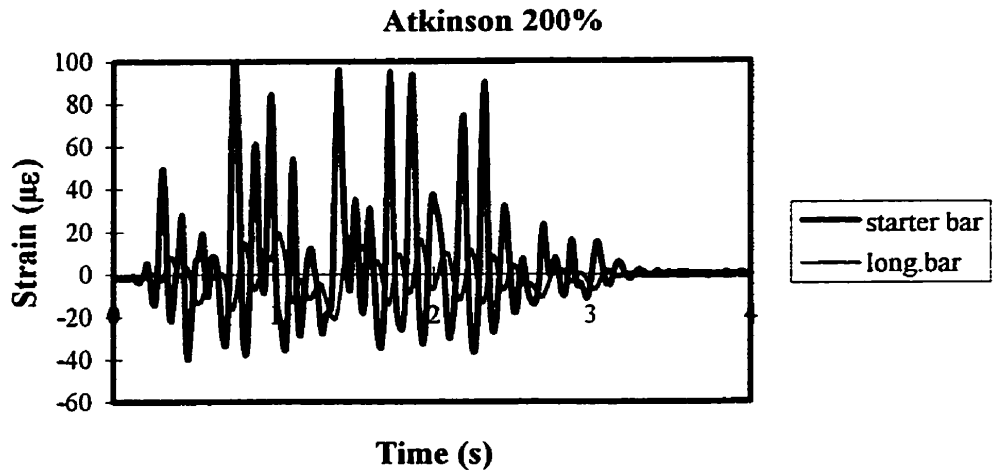

Figure D.24 Measured Strains from Starter and Longitudinal Bars (165 mm from the base) for Atkinson 200%

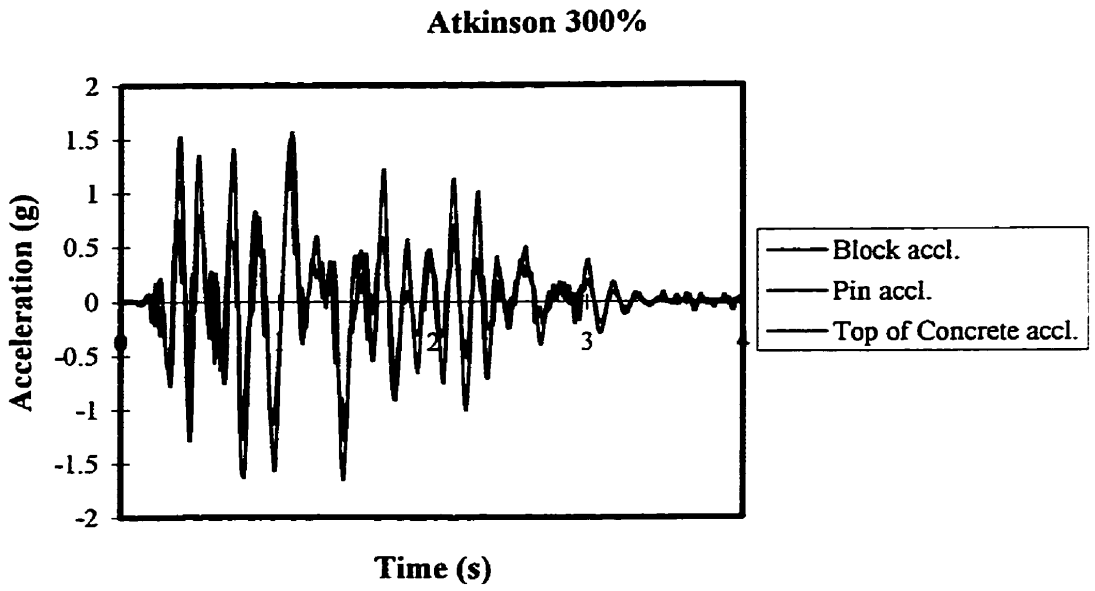

Figure D.25 Measured Acceleration of Block, Pin and Top of Concrete for Atkinson 300%

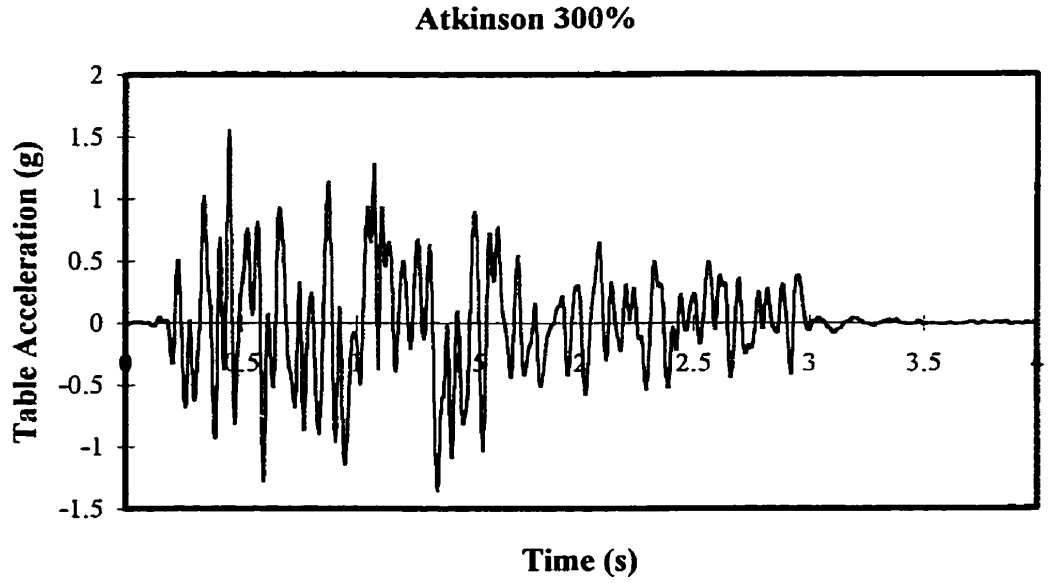

Figure D.26 Measured Table Acceleration for Atkinson 300%

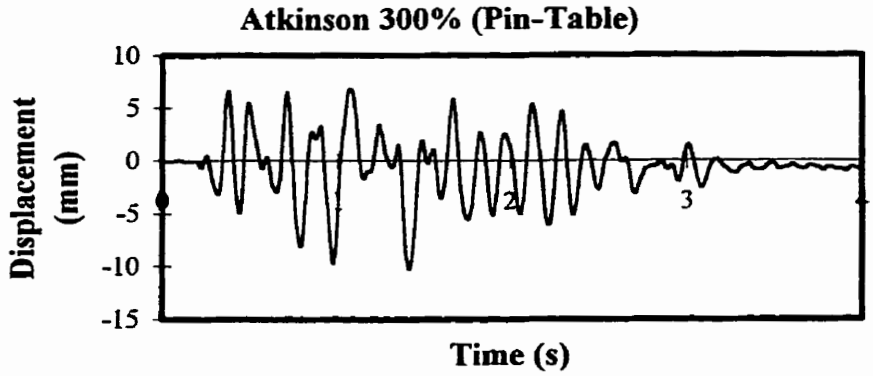

Figure D.27 Relative Displacement (Pin-Table) for Atkinson 300%

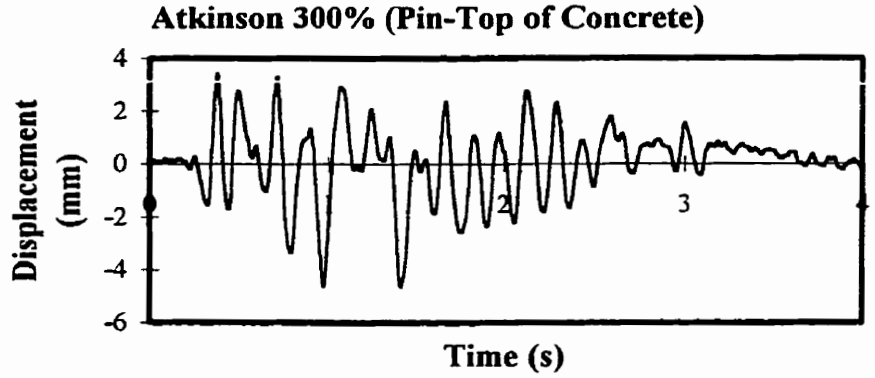

Figure D.28 Relative Displacement (Pin-Top of Concrete) for Atkinson 300%

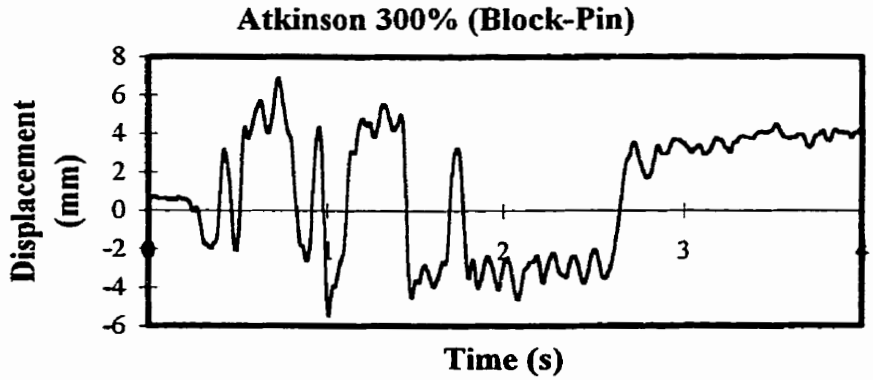

Figure D.29 Relative Displacement (Block-Pin) for Atkinson 300%

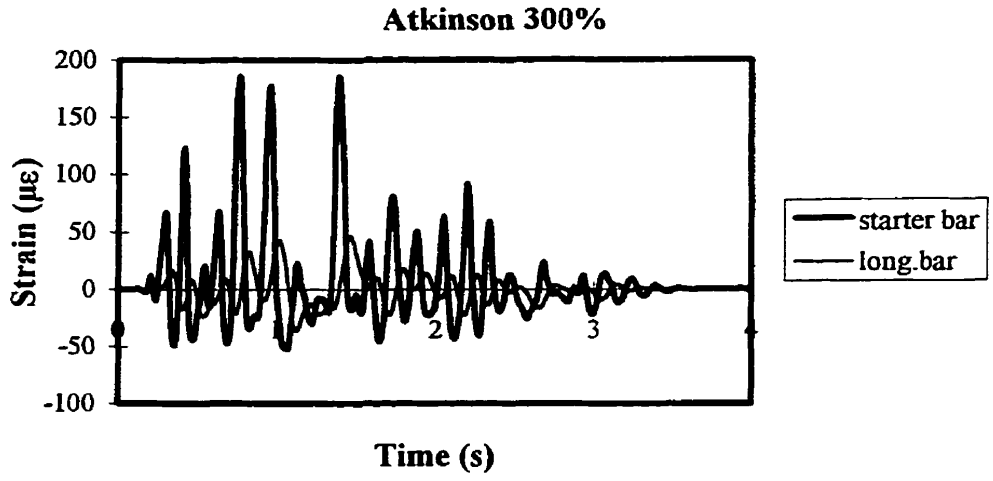

Figure D.30 Measured Strains from Starter and Longitudinal Bars (165 mm from the base) for Atkinson 300%

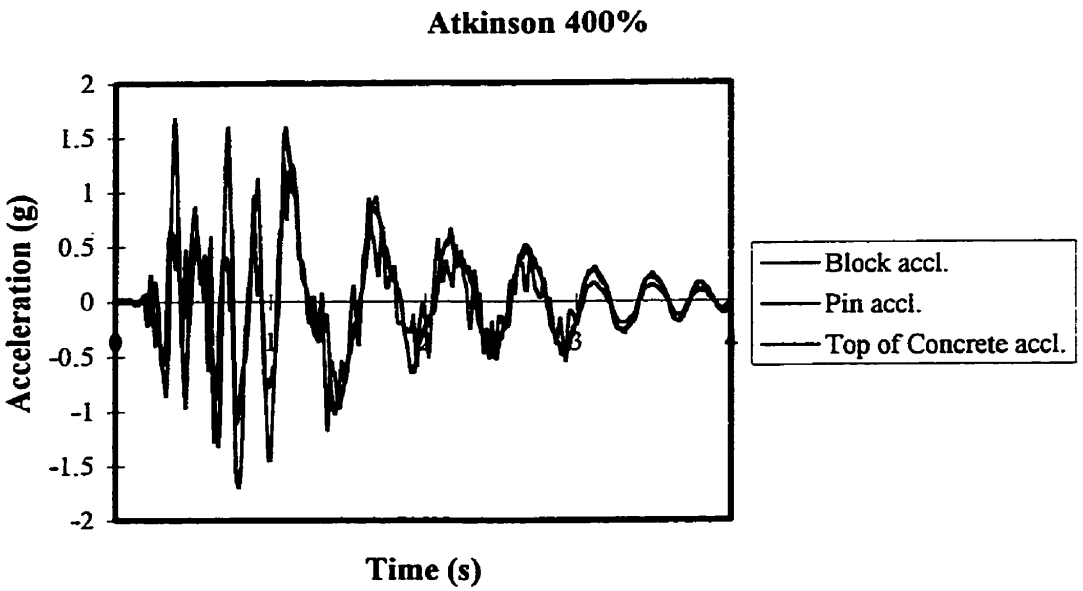

Figure D.31 Measured Acceleration of Block, Pin and Top of Concrete for Atkinson 400%

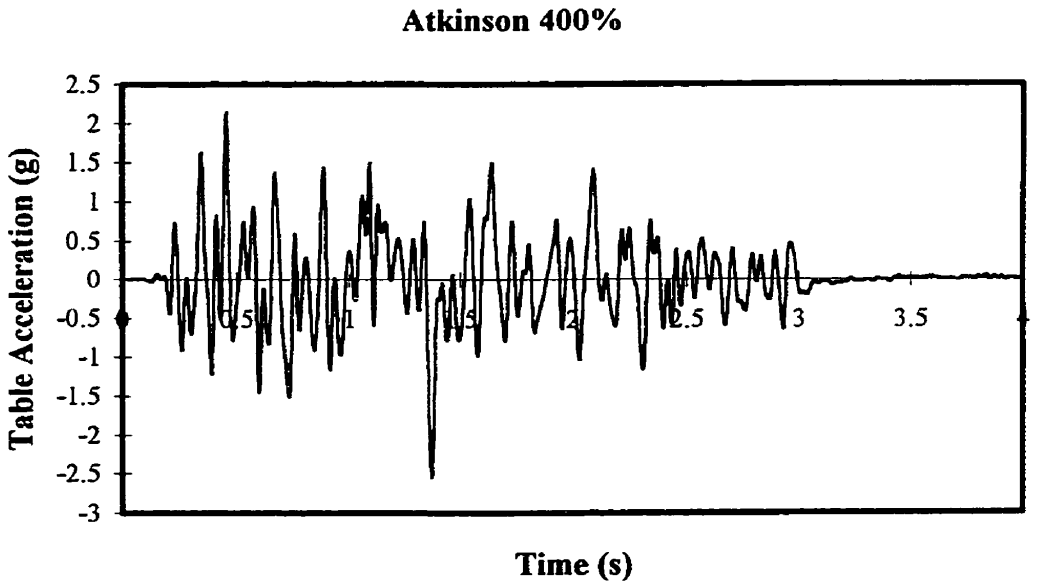

Figure D.32 Measured Table Acceleration for Atkinson 400%

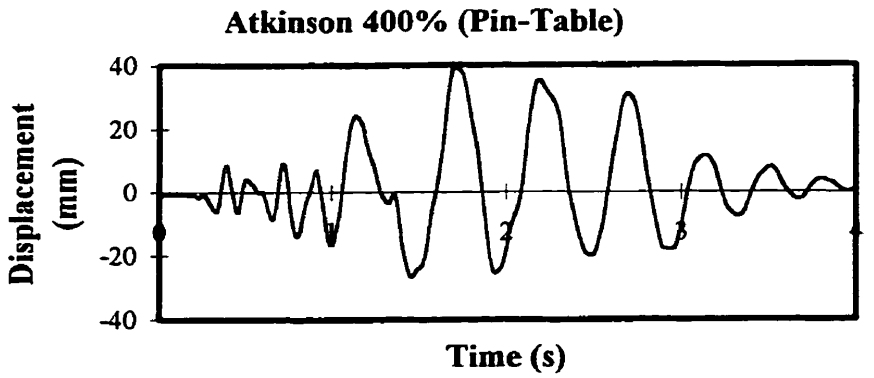

Figure D.33 Relative Displacement (Pin-Table) for Atkinson 400%

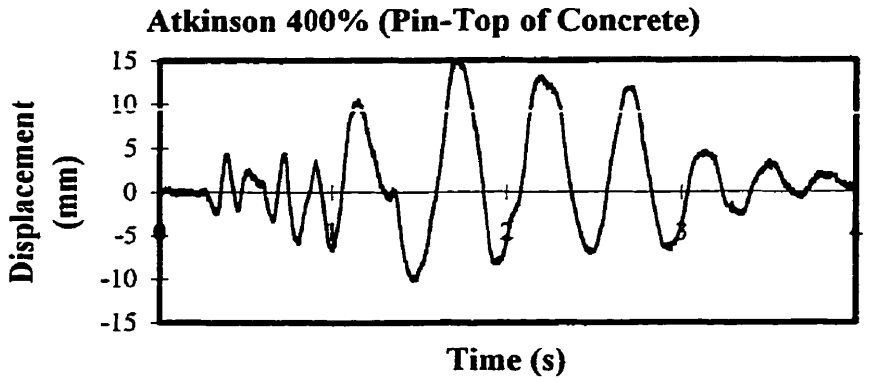

Figure D.34 Relative Displacement (Pin-Top of Concrete) for Atkinson 400%

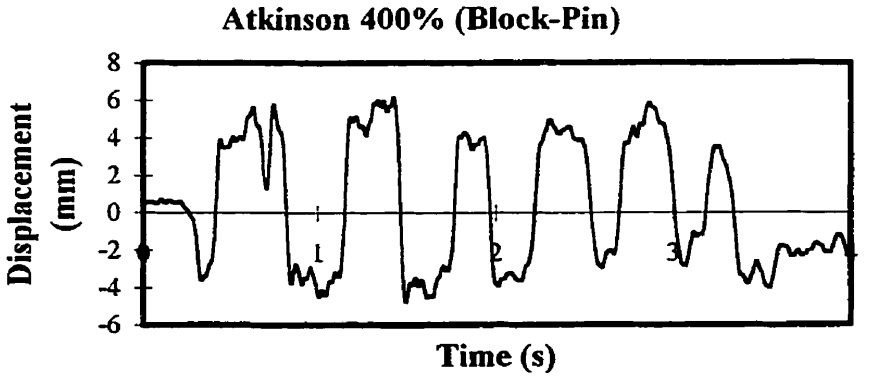

Figure D.35 Relative Displacement (Block-Pin) for Atkinson 400%

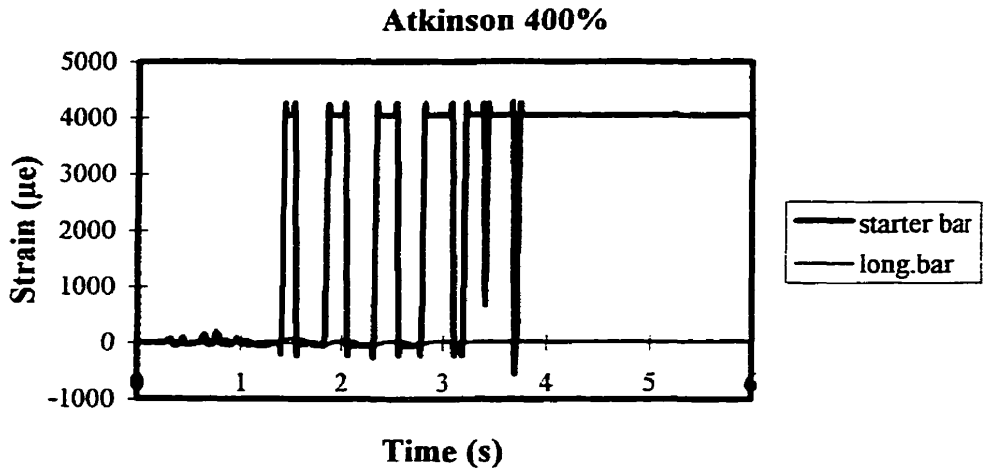

Figure D.36 Measured Strains from Starter and Longitudinal Bars (165 mm from the base) for Atkinson 400%

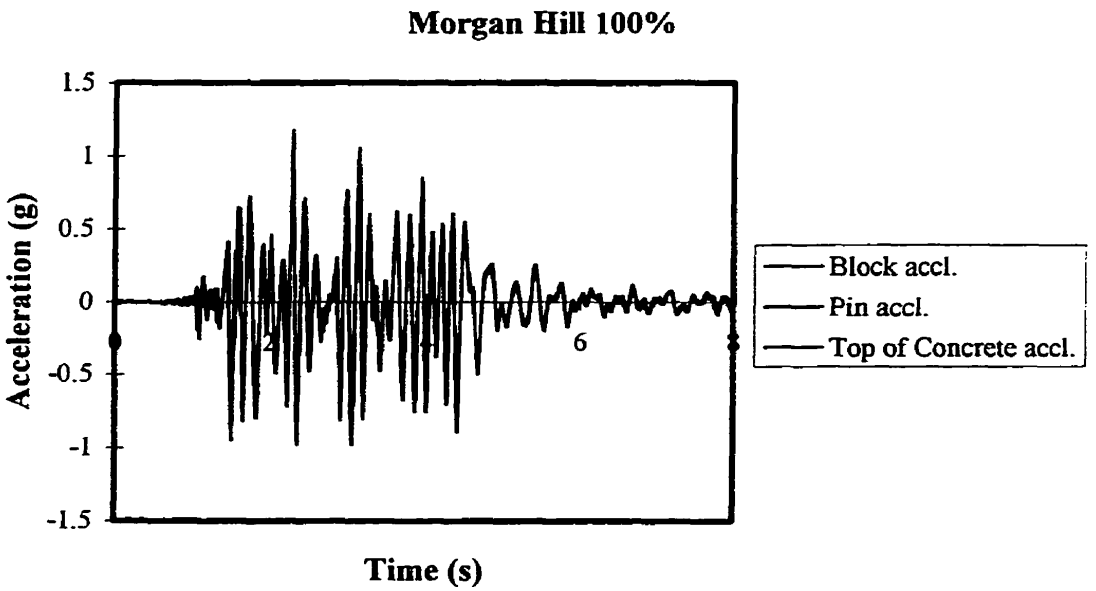

Figure D.37 Measured Acceleration of Block, Pin and Top of Concrete for Morgan Hill 100%

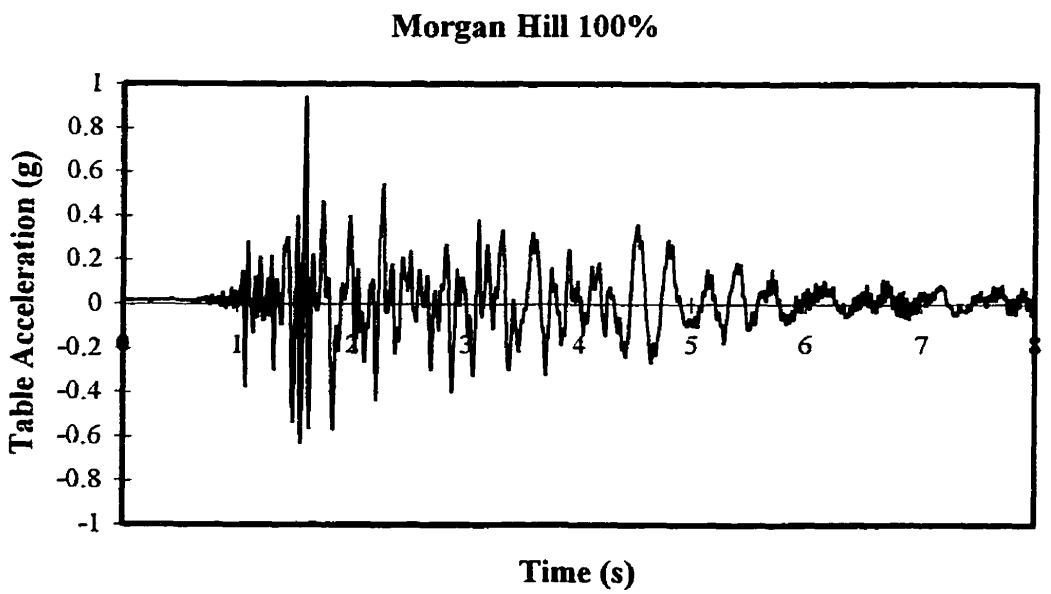

Figure D.38 Measured Table Acceleration for Morgan Hill 100%

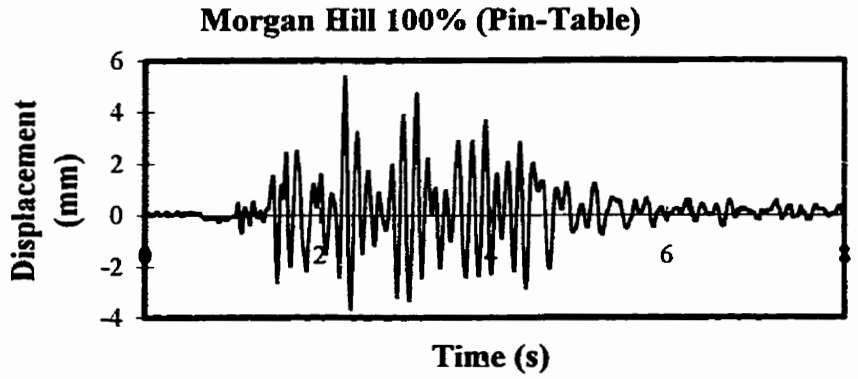

Figure D.39 Relative Displacement (Pin-Table) for Morgan Hill 100%

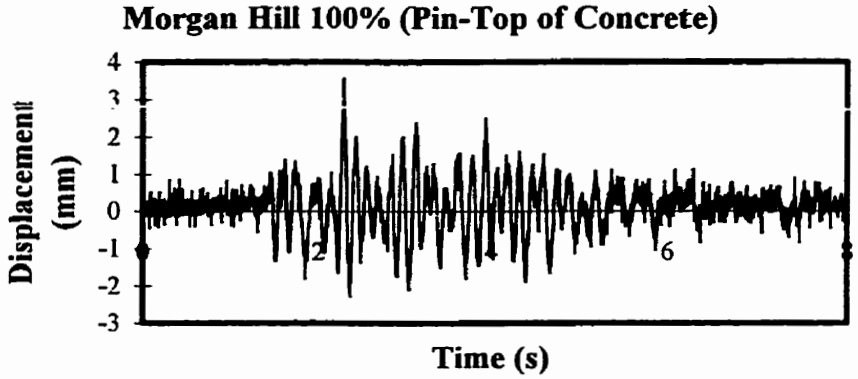

Figure D.40 Relative Displacement (Pin-Top of Concrete) for Morgan Hill 100%

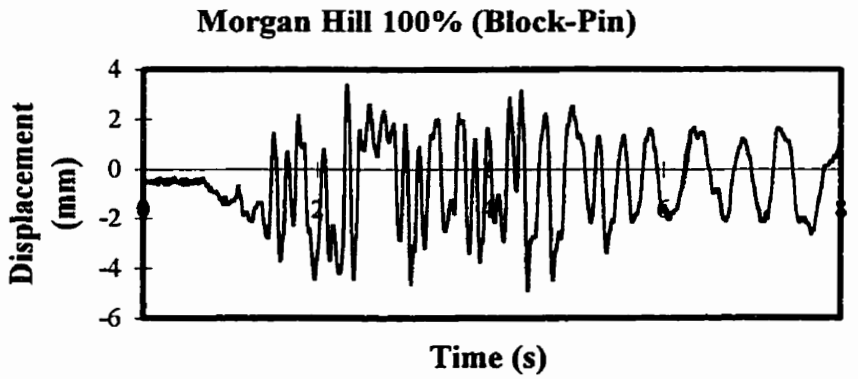

Figure D.41 Relative Displacement (Block-Pin) for Morgan Hill 100%

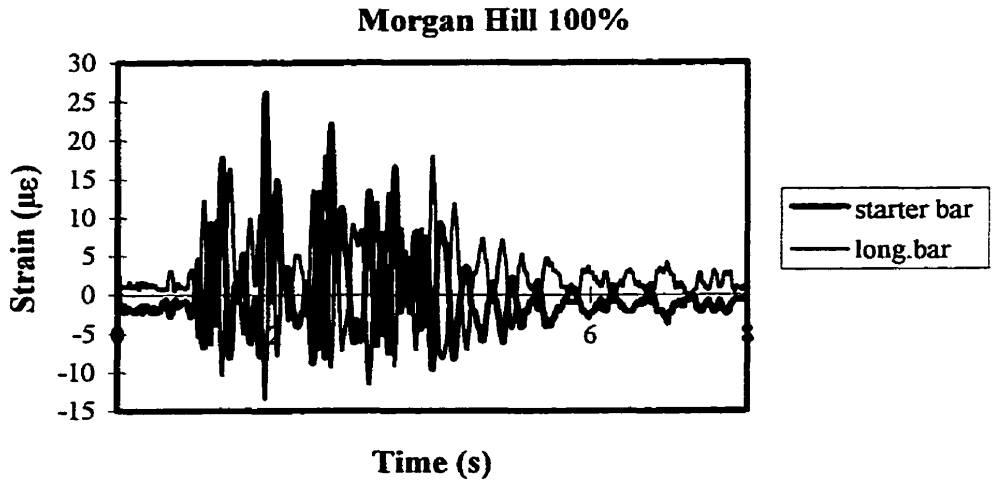

Figure D.42 Measured Strains from Starter and Longitudinal Bars (165 mm from the base) for Morgan Hill 100%

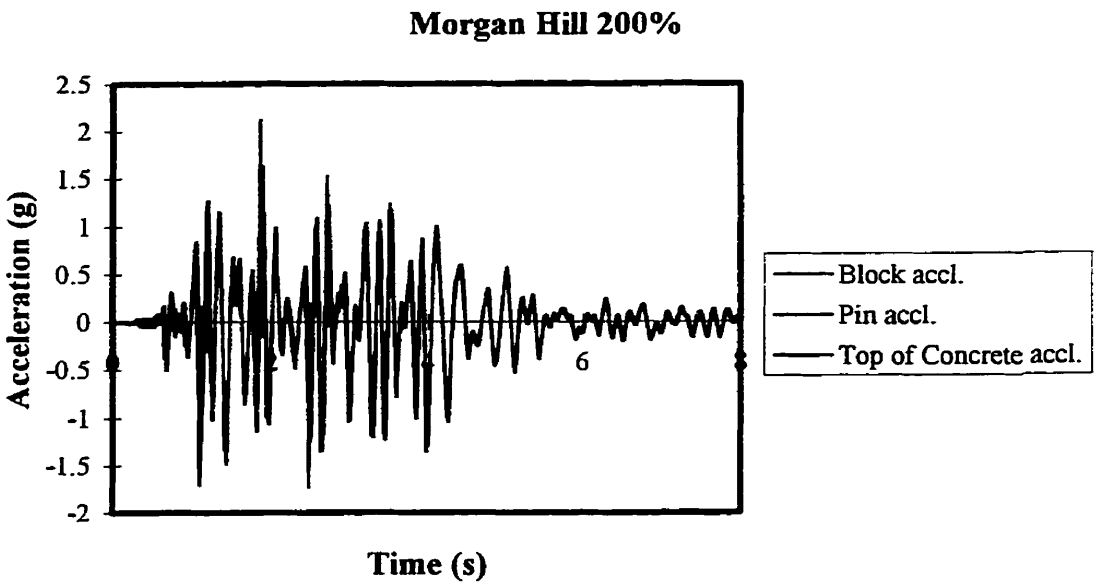

Figure D.43 Measured Acceleration of Block, Pin and Top of Concrete for Morgan Hill 200%

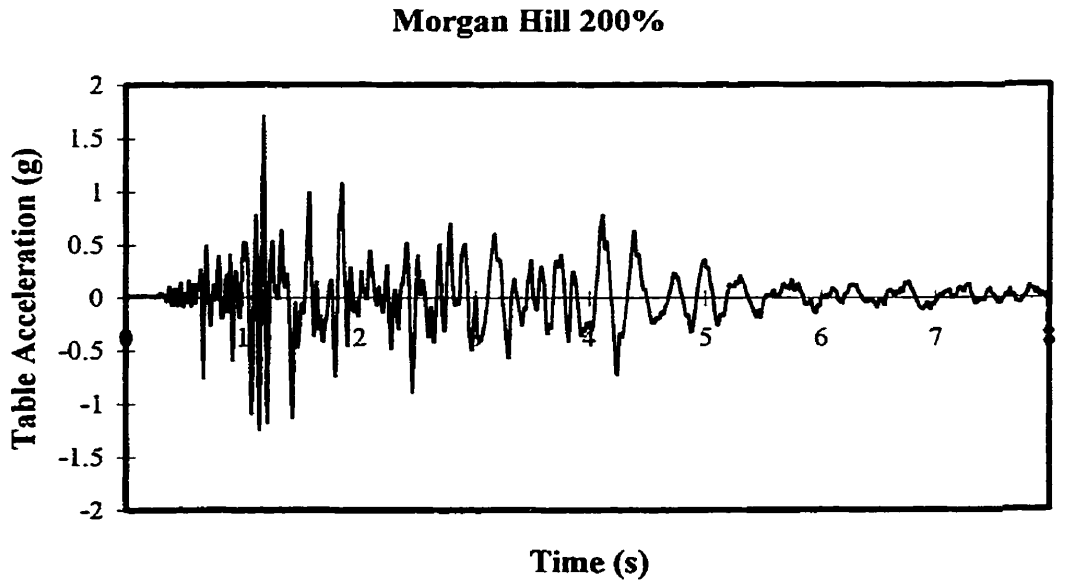

Figure D.44 Measured Table Acceleration for Morgan Hill 200%

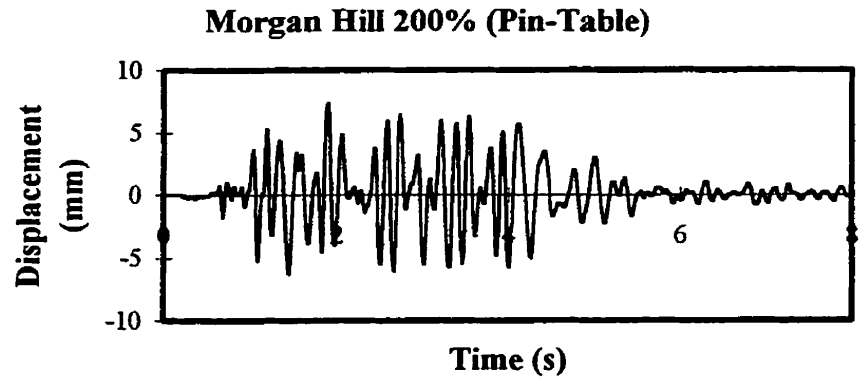

Figure D.45 Relative Displacement (Pin-Table) for Morgan Hill 200%

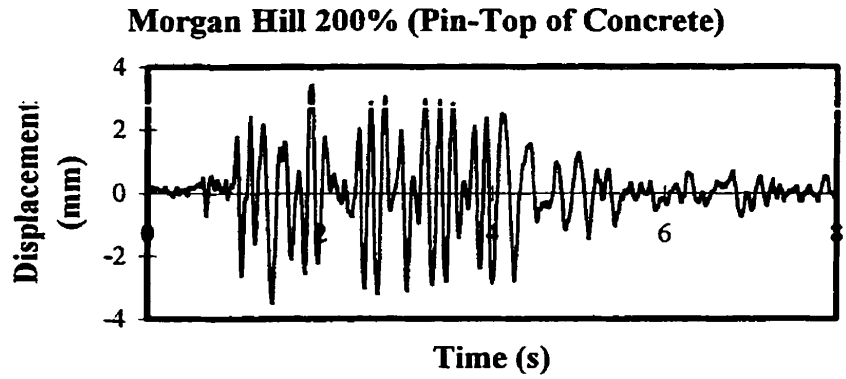

Figure D.46 Relative Displacement (Pin-Top of Concrete) for Morgan Hill 200%

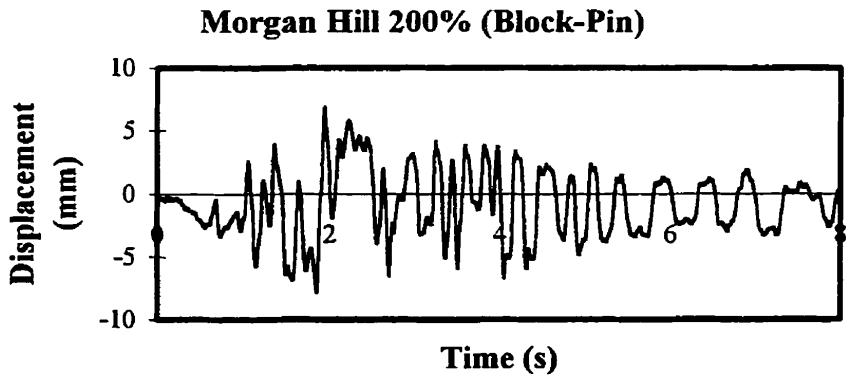

Figure D.47 Relative Displacement (Block-Pin) for Morgan Hill 200%

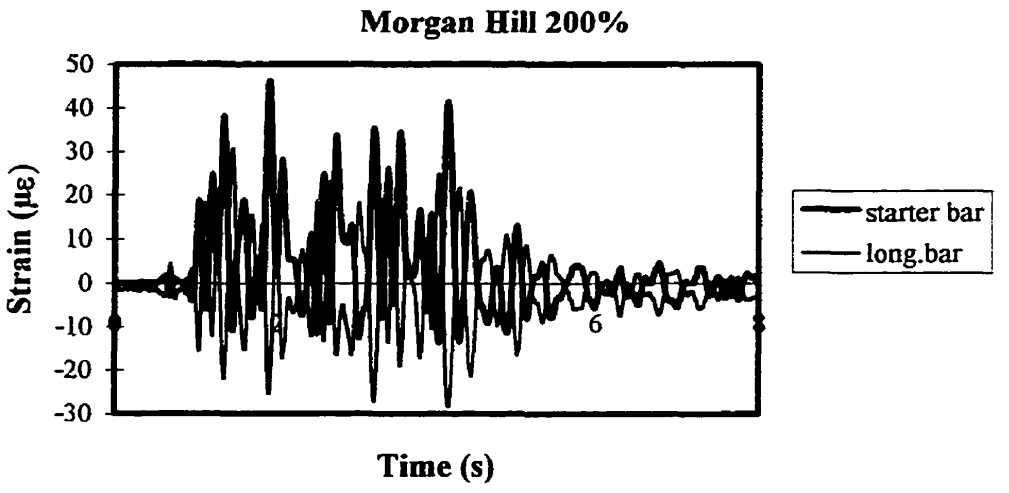

Figure D.48 Measured Strains from Starter and Longitudinal Bars (165 mm from the base) for Morgan Hill 200%

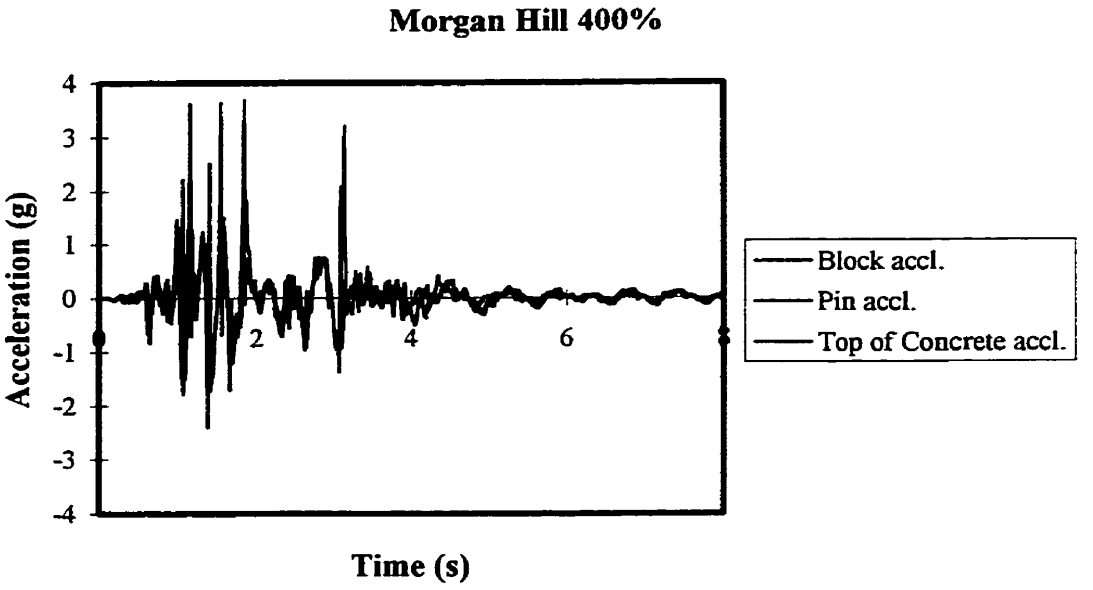

Figure D.49 Measured Acceleration of Block, Pin and Top of Concrete for Morgan Hill 400%

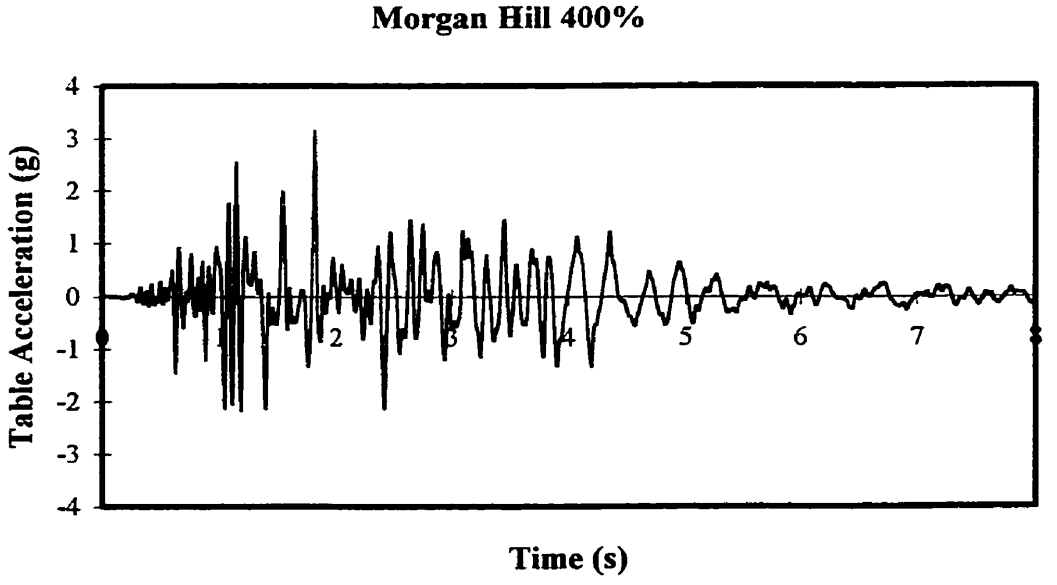

Figure D.50 Measured Table Acceleration for Morgan Hill 400%

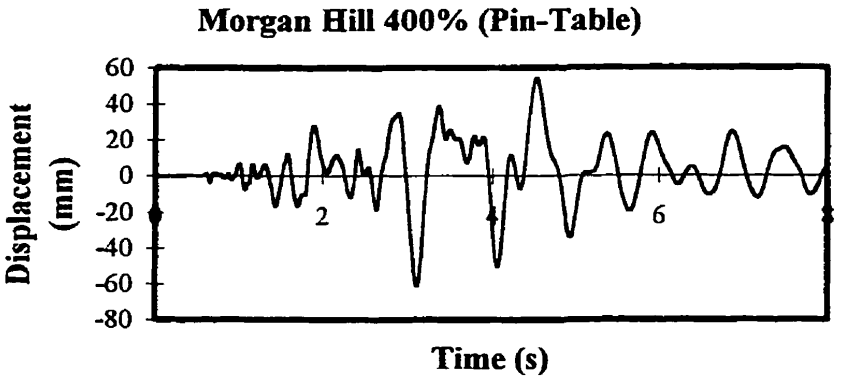

Figure D.51 Relative Displacement (Pin-Table) for Morgan Hill 400%

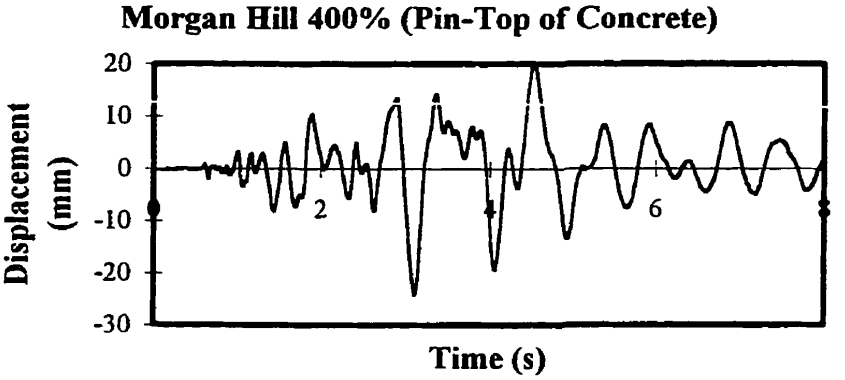

Figure D.52 Relative Displacement (Pin-Top of Concrete) for Morgan Hill 400%

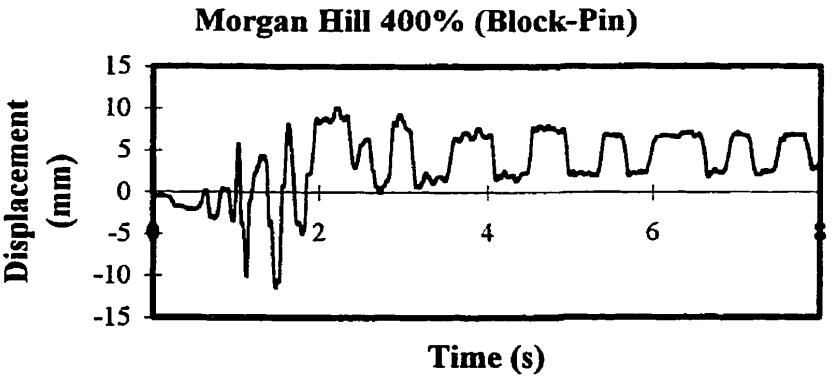

Figure D.53 Relative Displacement (Block-Pin) for Morgan Hill 400%

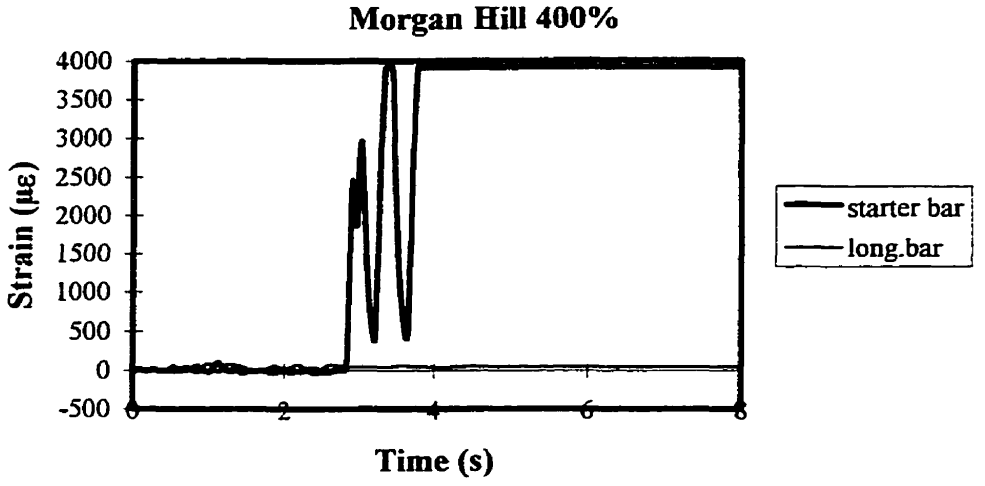

Figure D.54 Measured Strains from Starter and Longitudinal Bars (165 mm from the base) for Morgan Hill 400%

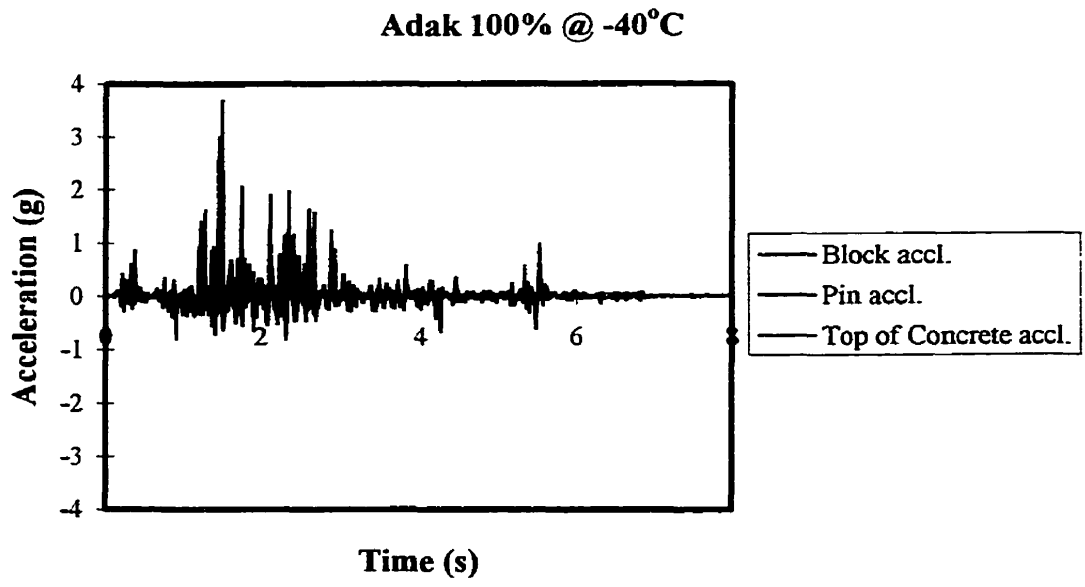

Figure D.55 Measured Acceleration of Block, Pin and Top of Concrete for Adak 100% at -40°C

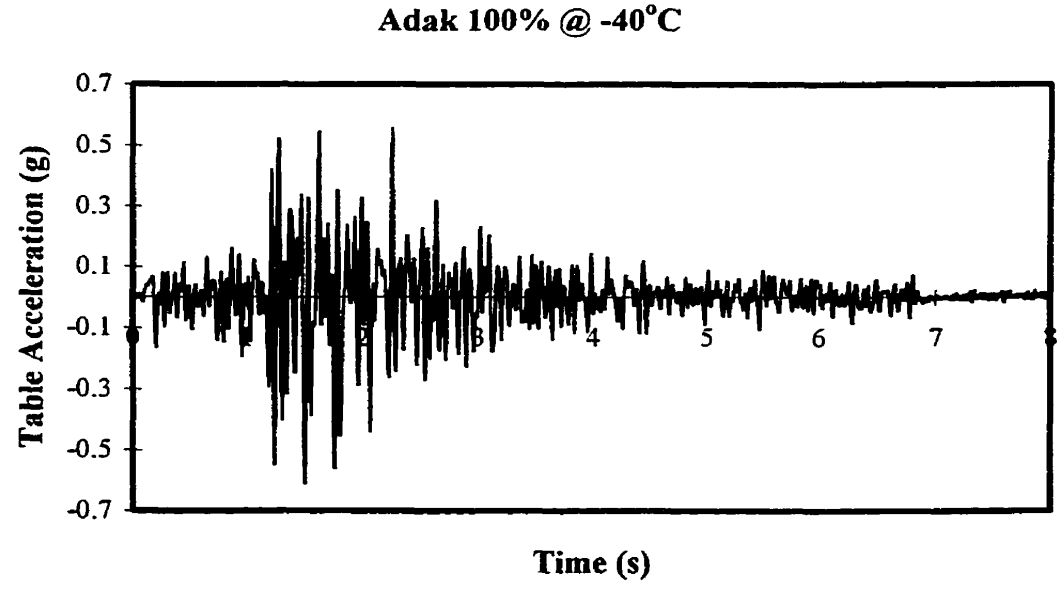

Figure D.56 Measured Table Acceleration for Adak 100% at -40°C

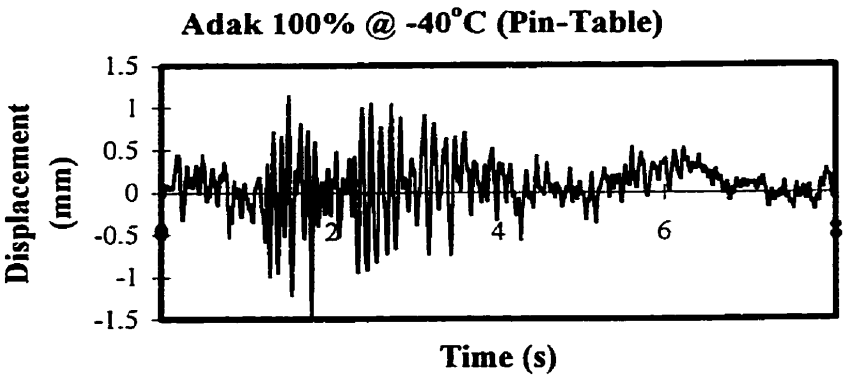

Figure D.57 Relative Displacement (Pin-Table) for Adak 100% at -40°C

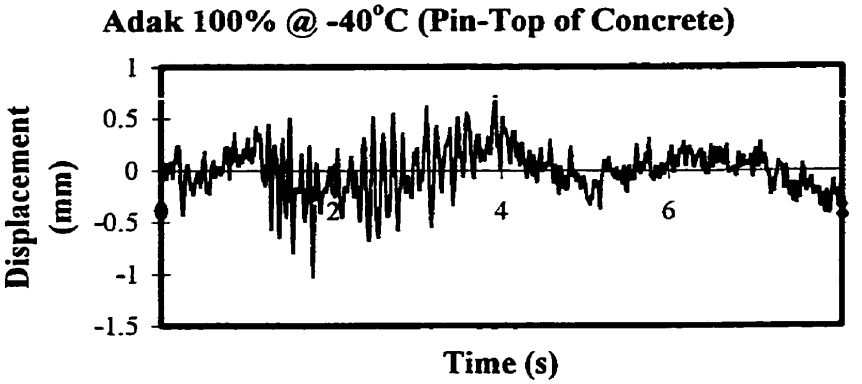

Figure D.58 Relative Displacement (Pin-Top of Concrete) for Adak 100% at -40°C

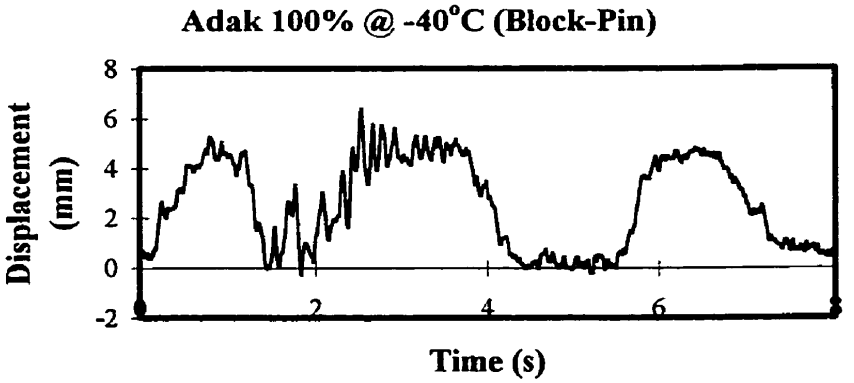

Figure D.59 Relative Displacement (Block Pin) for Adak 100% at -40°C

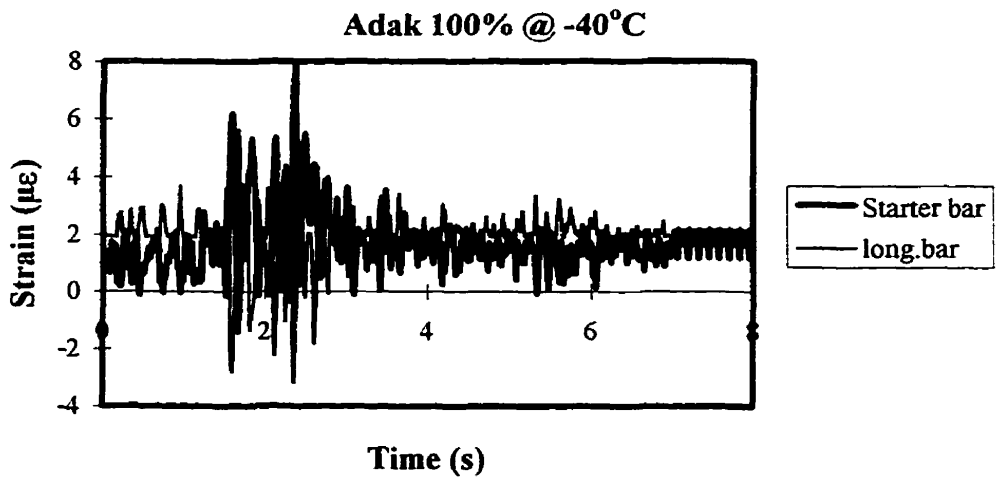

Figure D.60 Measured Strains from Starter and Longitudinal Bars (165 mm from the base) for Adak 100% @ -40°C

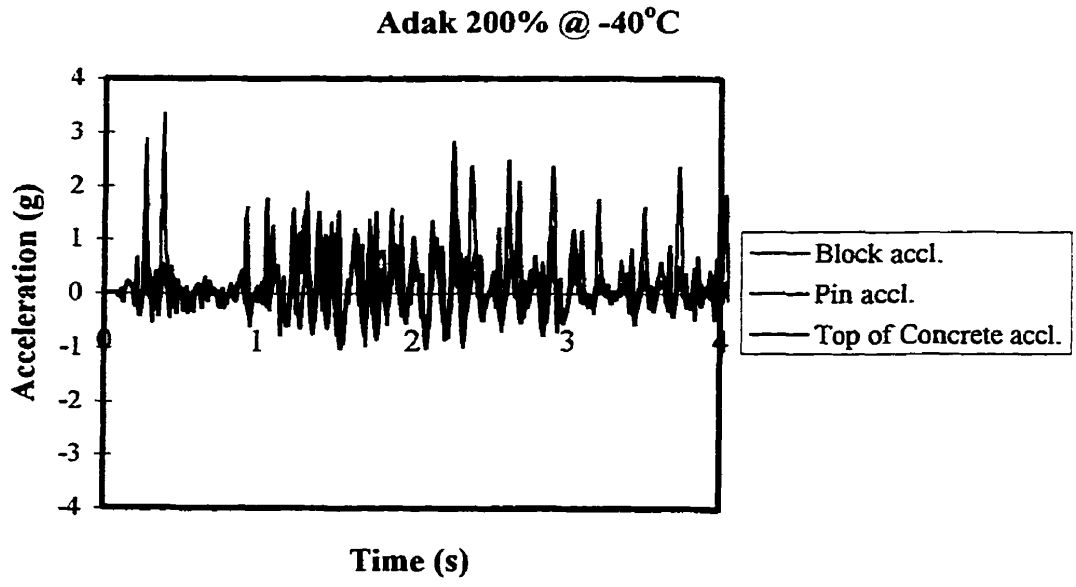

Figure D.61 Measured Acceleration of Block, Pin and Top of Concrete for Adak 200% at -40°C

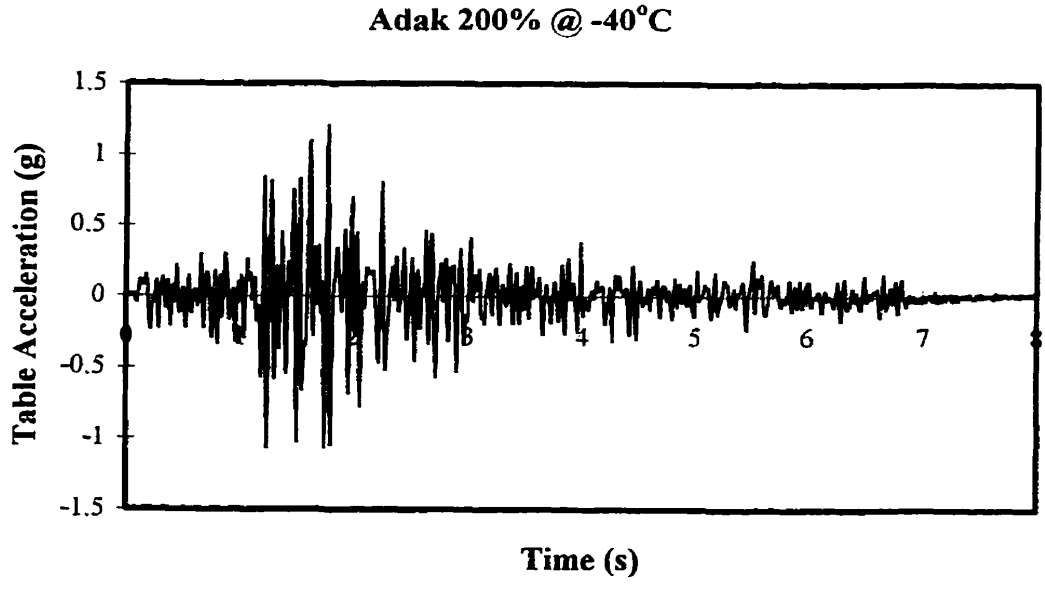

Figure D.62 Measured Table Acceleration for Adak 200% at -40°C

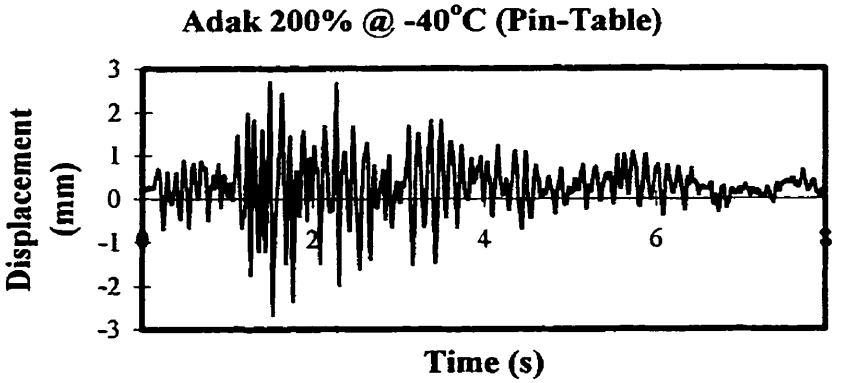

Figure D.63 Relative Displacement (Pin-Table) for Adak 200% at -40°C

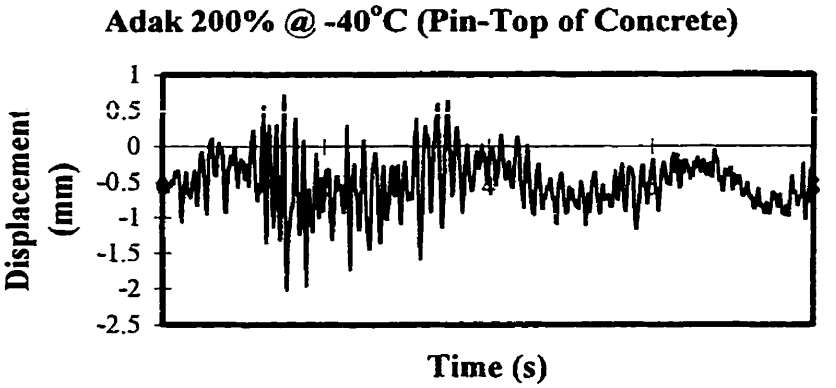

Figure D.64 Relative Displacement (Pin-Top of Concrete) for Adak 200% at -40°C

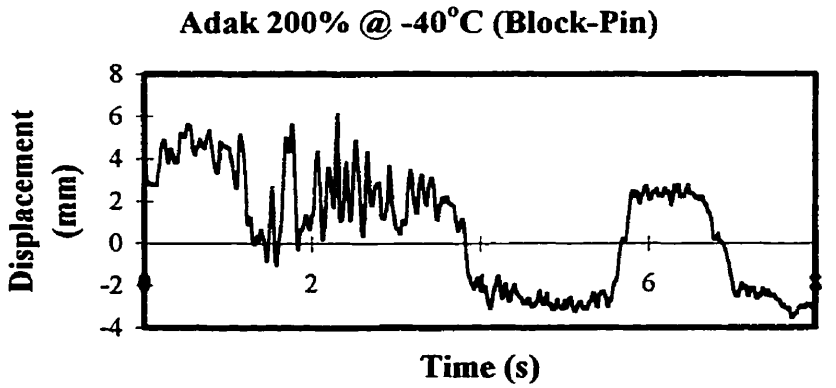

Figure D.65 Relative Displacement (Block-Pin) for Adak 200% at -40°C

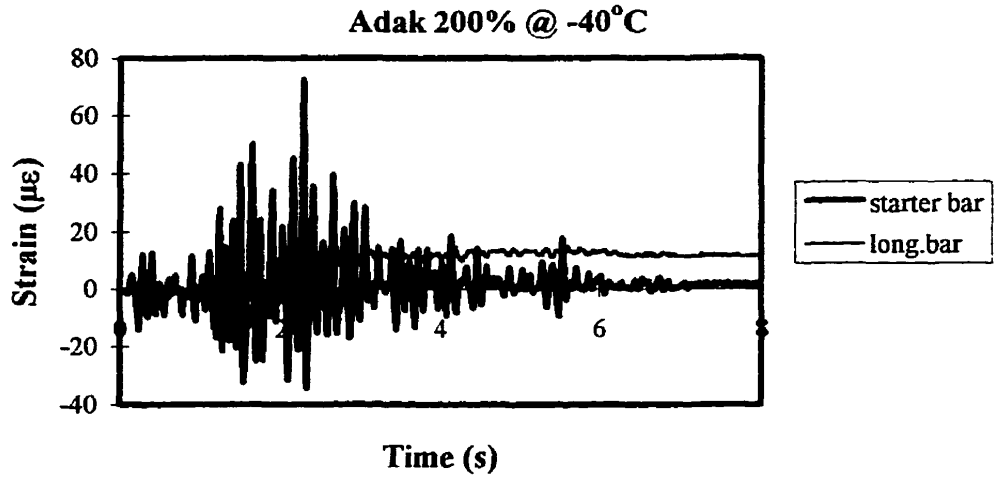

Figure D.66 Measured Strains from Starter and Longitudinal Bars (165 mm from the base) for Adak 200% @ -40°C

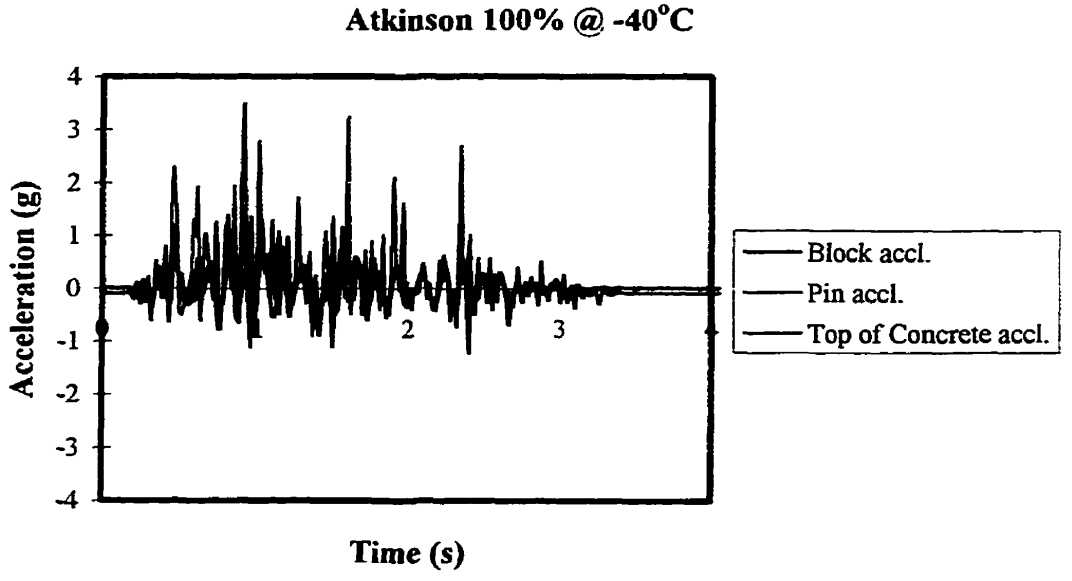

Figure D.67 Measured Acceleration of Block, Pin and Top of Concrete for Atkinson 100% at -40°C

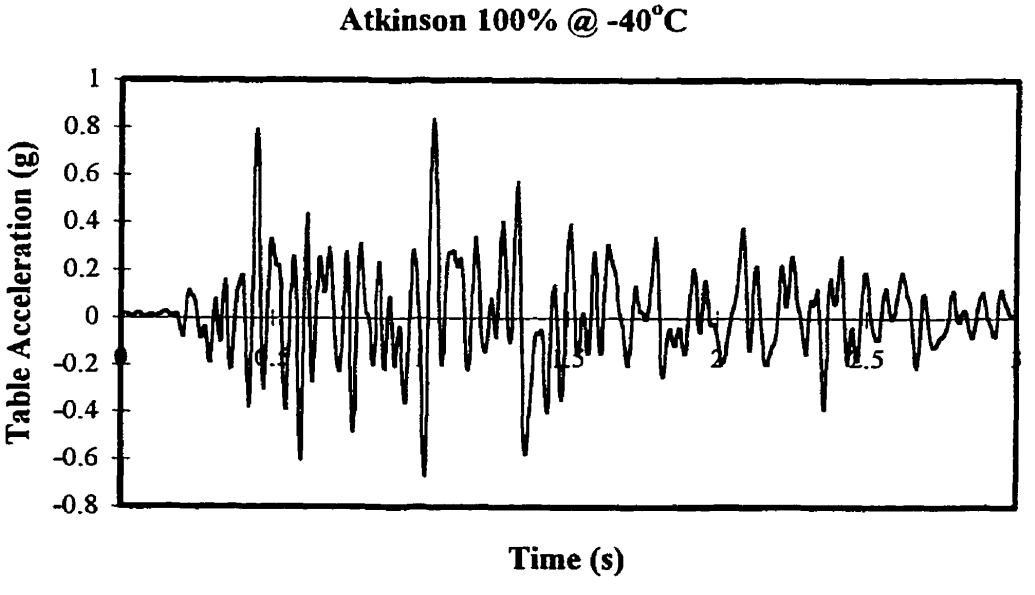

Figure D.68 Measured Table Acceleration for Atkinson 100% at -40°C

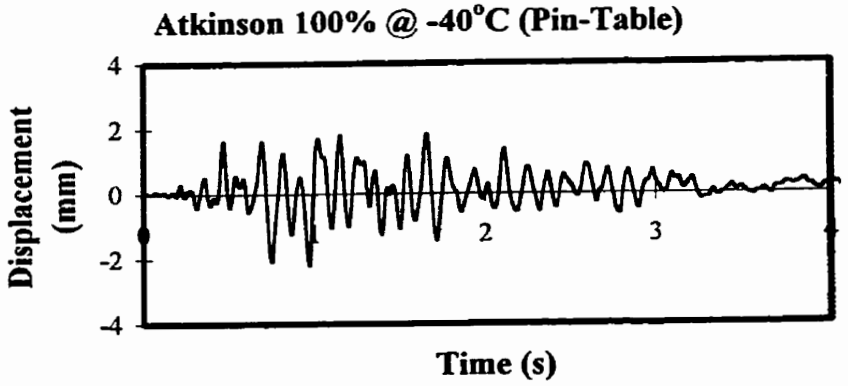

Figure D.69 Relative Displacement (Pin-Table) for Atkinson 100% at -40°C

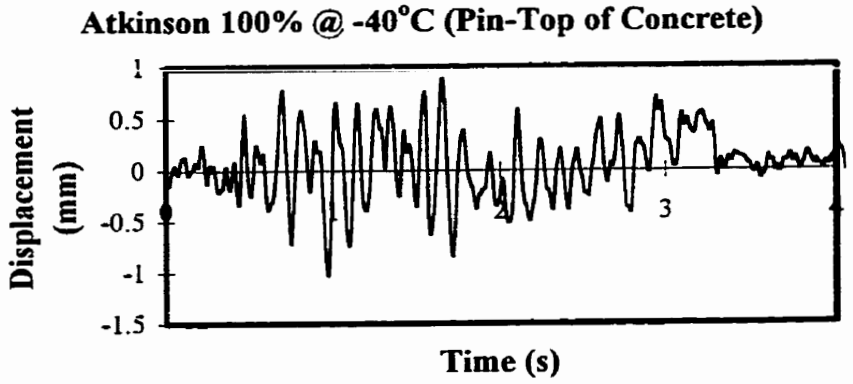

Figure D.70 Relative Displacement (Pin-Top Concrete) for Atkinson 100% at -40°C

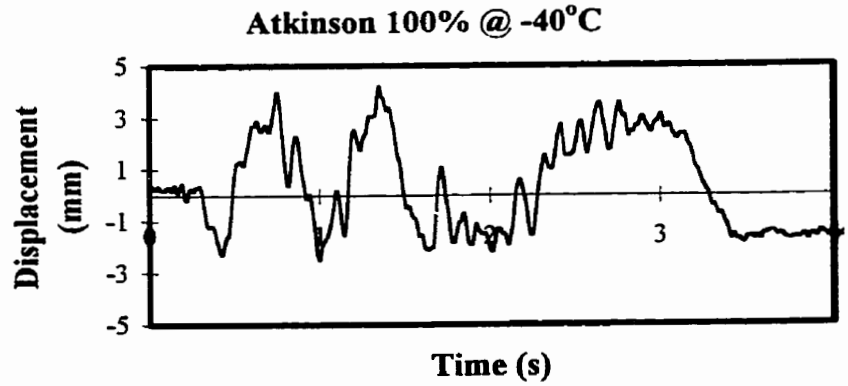

Figure D.71 Relative Displacement (Block-Pin) for Atkinson 100% at -40°C

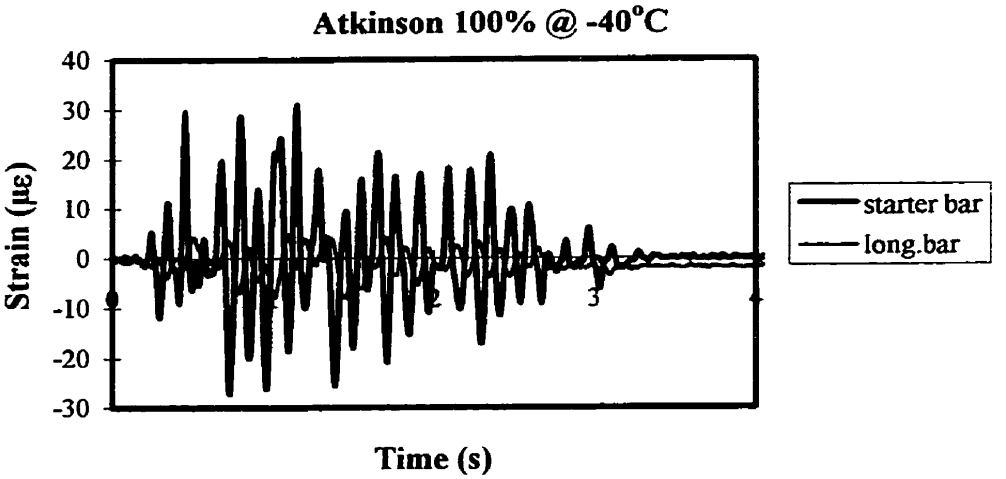

Figure D.72 Measured Strains from Starter and Longitudinal Bars (165 mm from the base) for Atkinson 100% @ -40°C

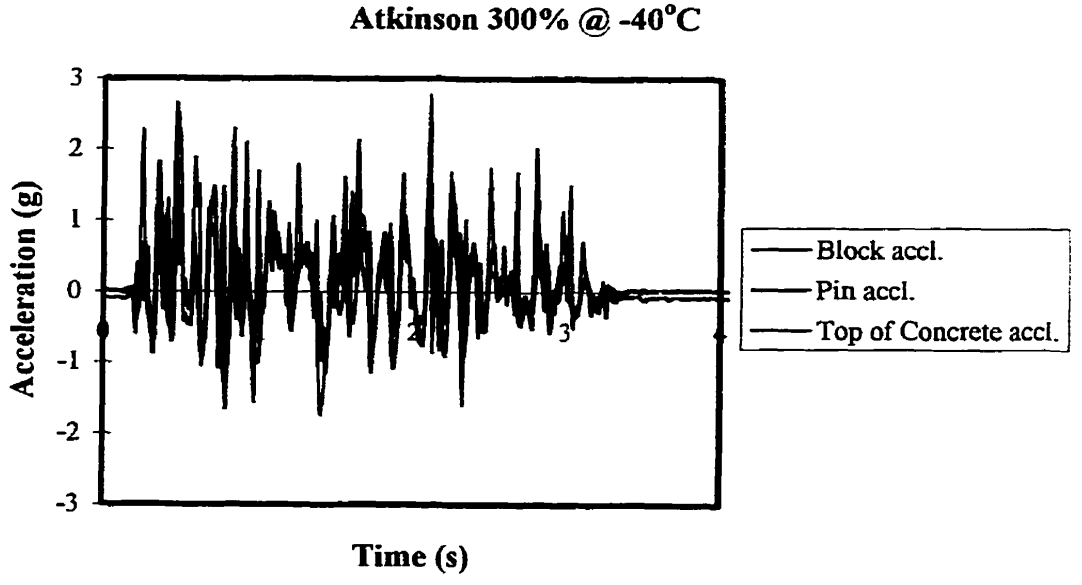

Figure D.73 Measured Acceleration of Block, Pin and Top of Concrete for Atkinson 300% at -40°C

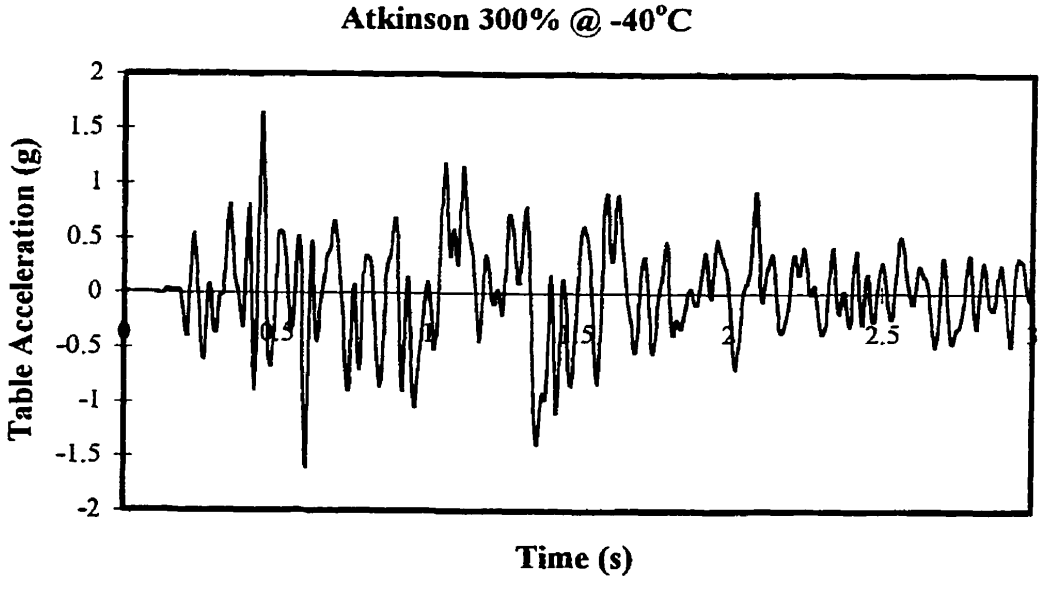

Figure D.74 Measured Table Acceleration for Atkinson 300% at -40°C

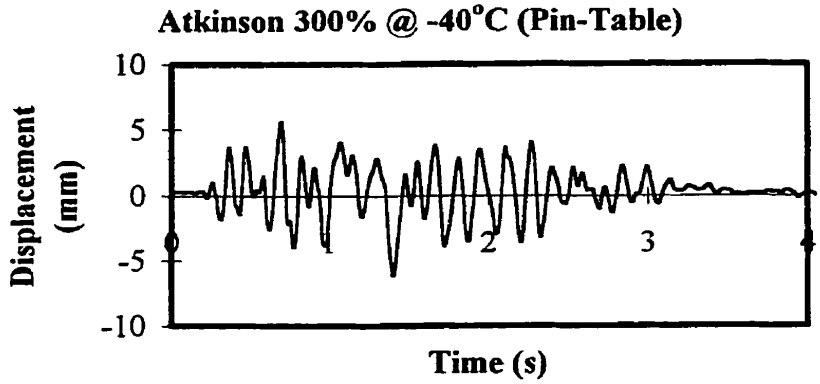

Figure D.75 Relative Displacement (Pin-Table) for Atkinson 300% at -40°C

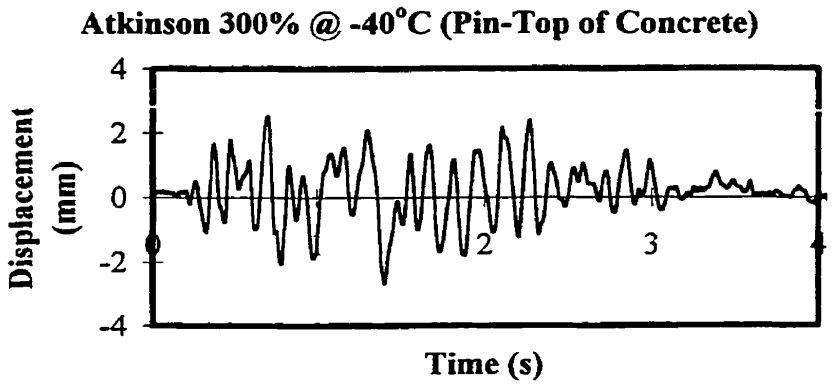

Figure D.76 Relative Displacement (Pin-Top Concrete) for Atkinson 300% at -40°C

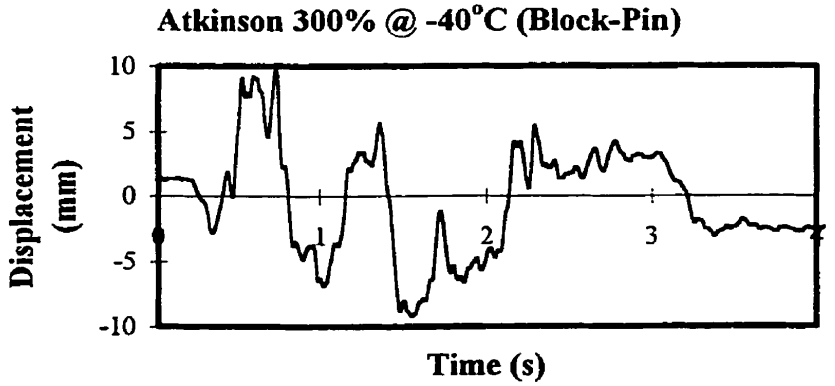

Figure D.77 Relative Displacement (Block-Pin) for Atkinson 300% at -40°C

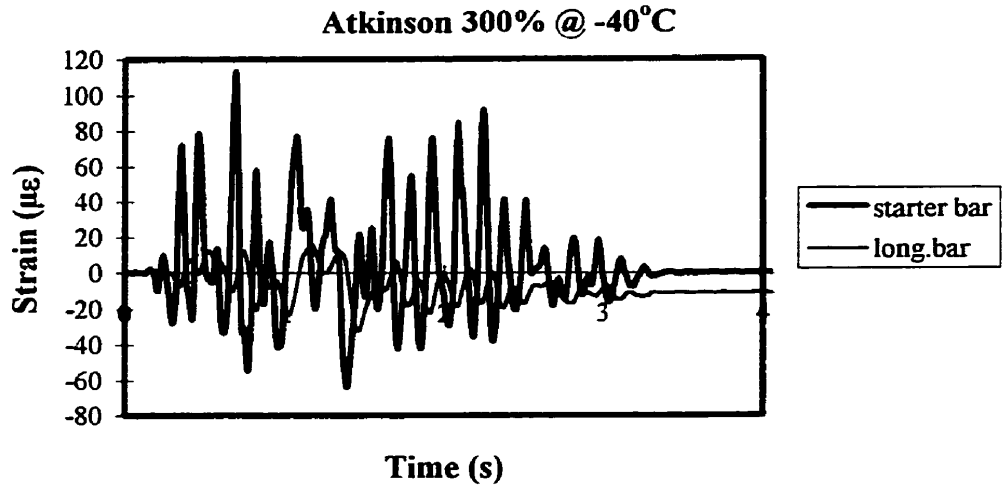

Figure D.78 Measured Strains from Starter and Longitudinal Bars (165 mm from the base) for Atkinson 300% @ -40°C

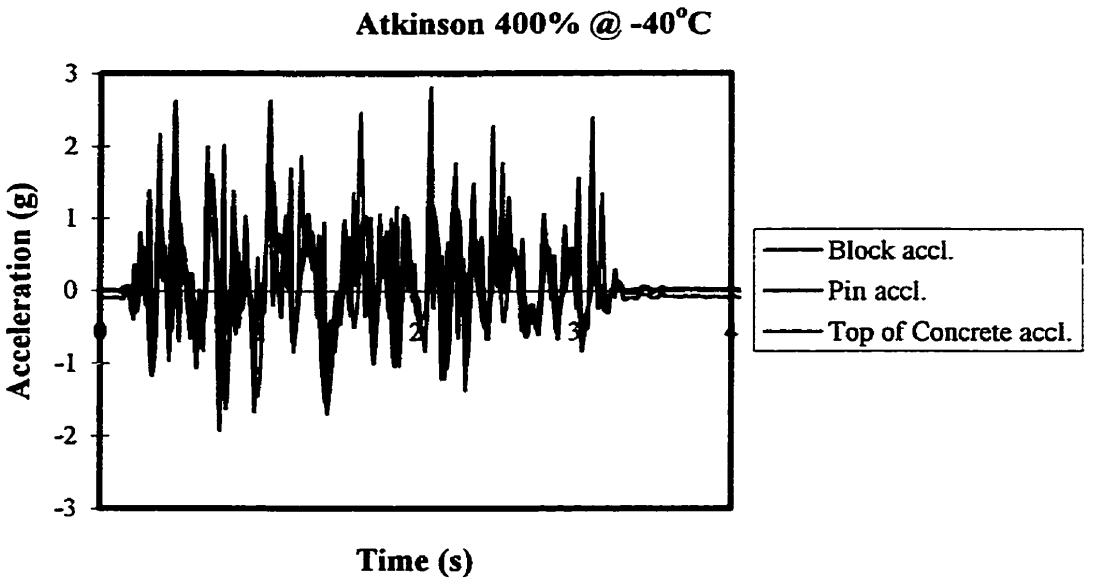

Figure D.79 Measured Acceleration of Block, Pin and Top of Concrete for Atkinson 400% at -40°C

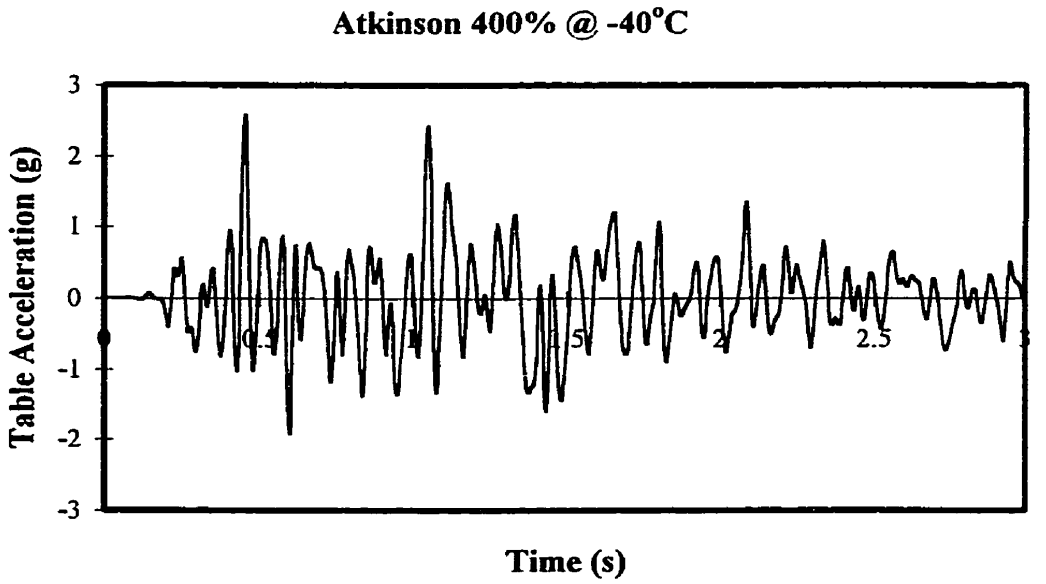

Figure D.80 Measured Table Acceleration for Atkinson 400% at -40°C

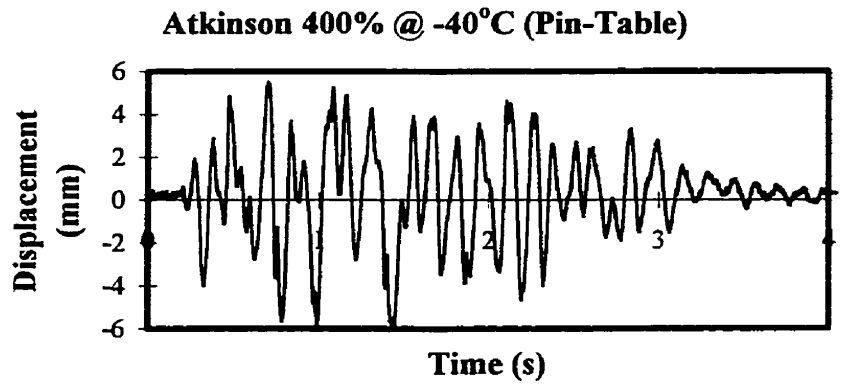

Figure D.81 Relative Displacement (Pin-Table) for Atkinson 400% at -40°C

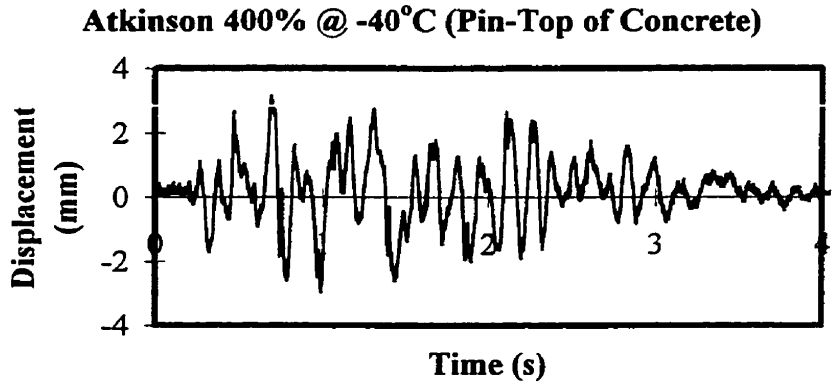

Figure D.82 Relative Displacement (Pin-Top Concrete) for Atkinson 400% at -40°C

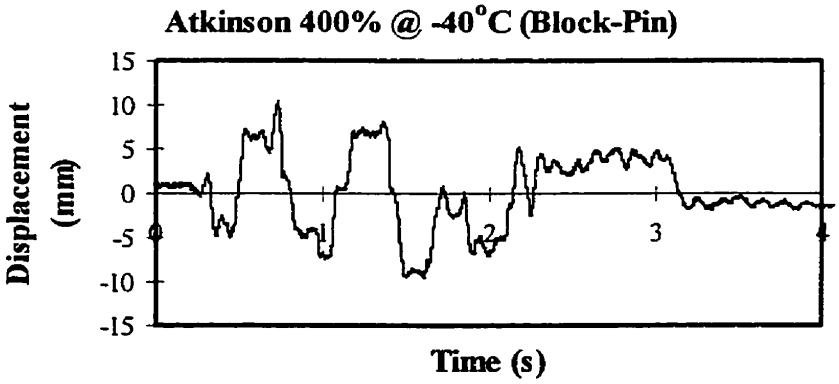

Figure D.83 Relative Displacement (Block-Pin) for Atkinson 400% at -40°C

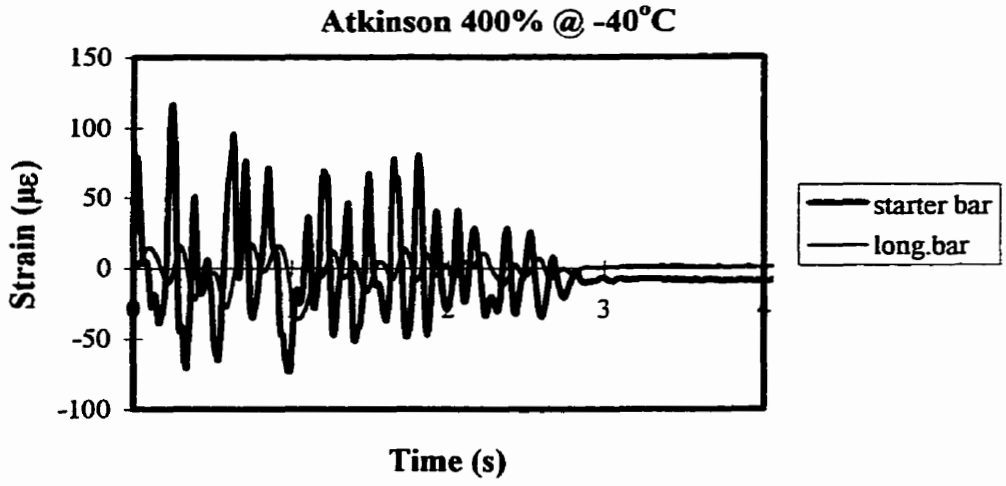

Figure D.84 Measured Strains from Starter and Longitudinal Bars (165 mm from the base) for Atkinson 400% @ -40°C

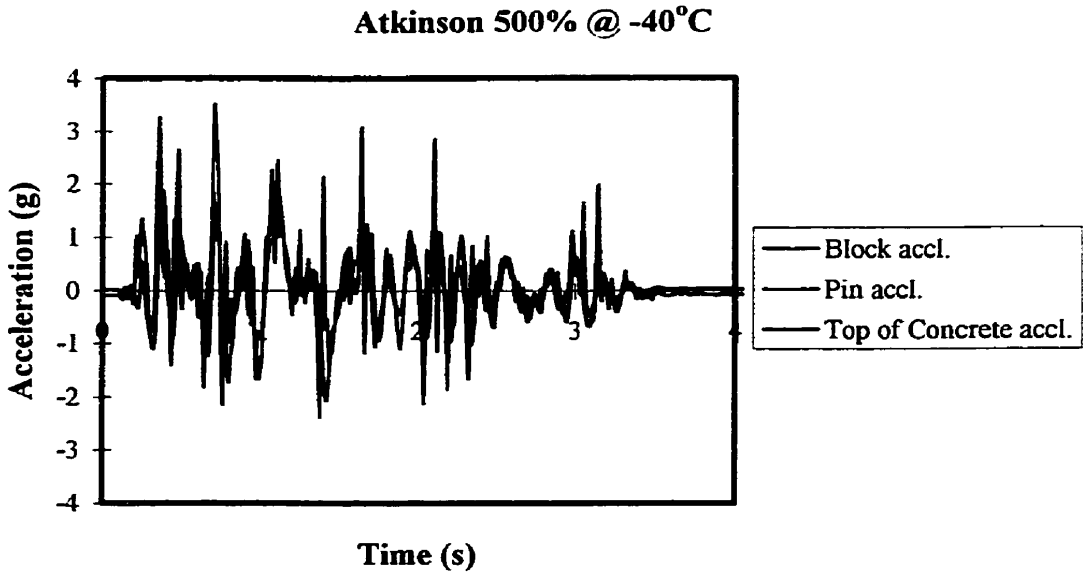

Figure D.85 Measured Acceleration of Block, Pin and Top of Concrete for Atkinson 500% at -40°C

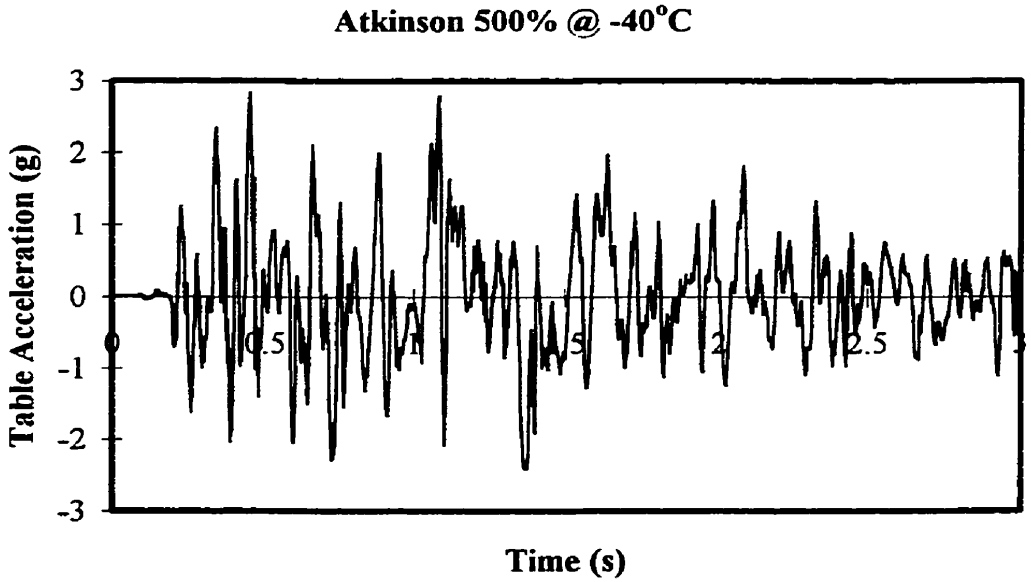

Figure D.86 Measured Table Acceleration for Atkinson 500% at -40°C

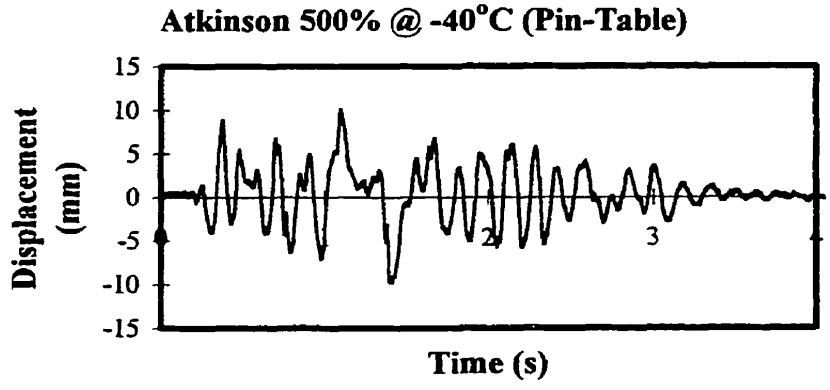

Figure D.87 Relative Displacement (Pin-Table) for Atkinson 500% at -40°C

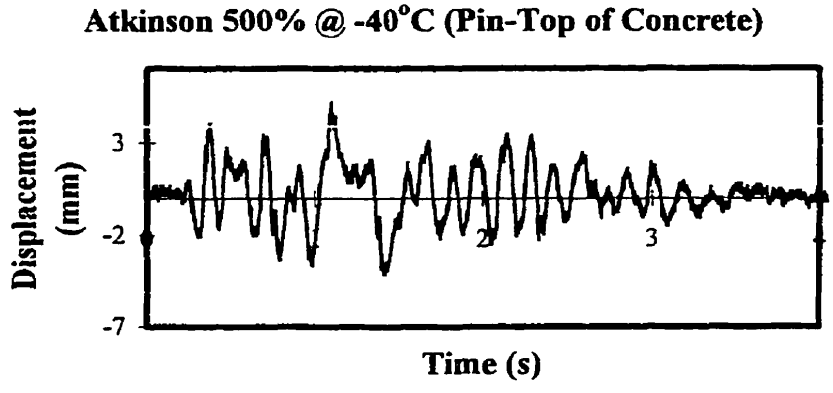

Figure D.88 Relative Displacement (Pin-Top Concrete) for Atkinson 500% at -40°C

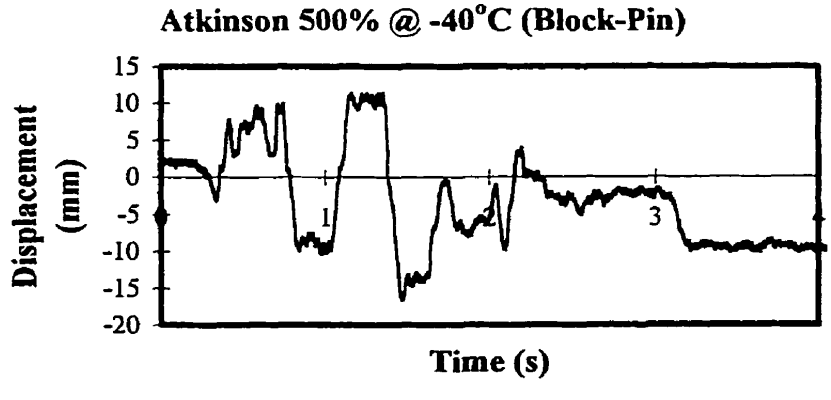

Figure D.89 Relative Displacement (Block-Pin) for Atkinson 500% at -40°C

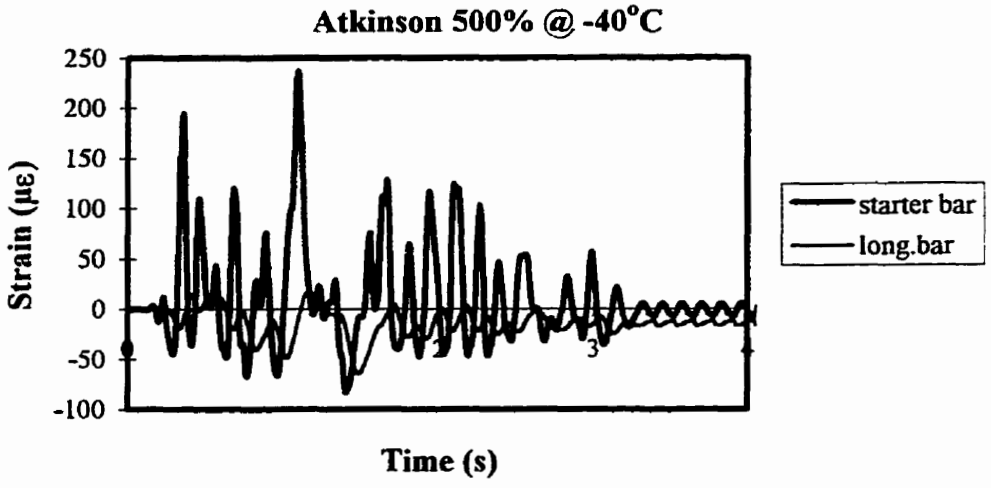

Figure D.90 Measured Strains from Starter and Longitudinal Bars (165 mm from the base) for Atkinson 500% @ -40°C

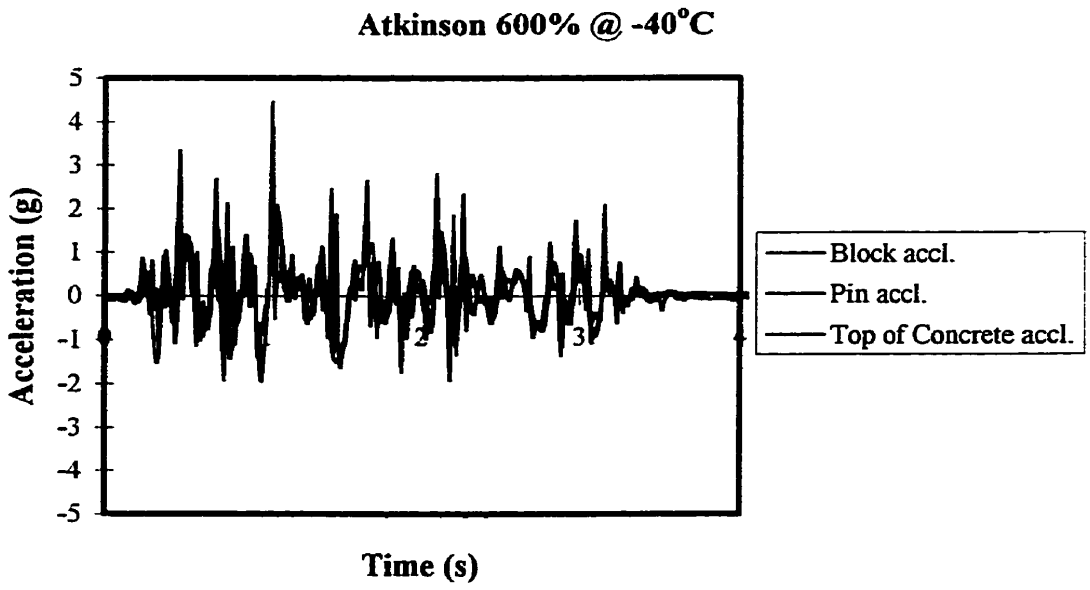

Figure D.91 Measured Acceleration of Block, Pin and Top of Concrete for Atkinson 600% at -40°C

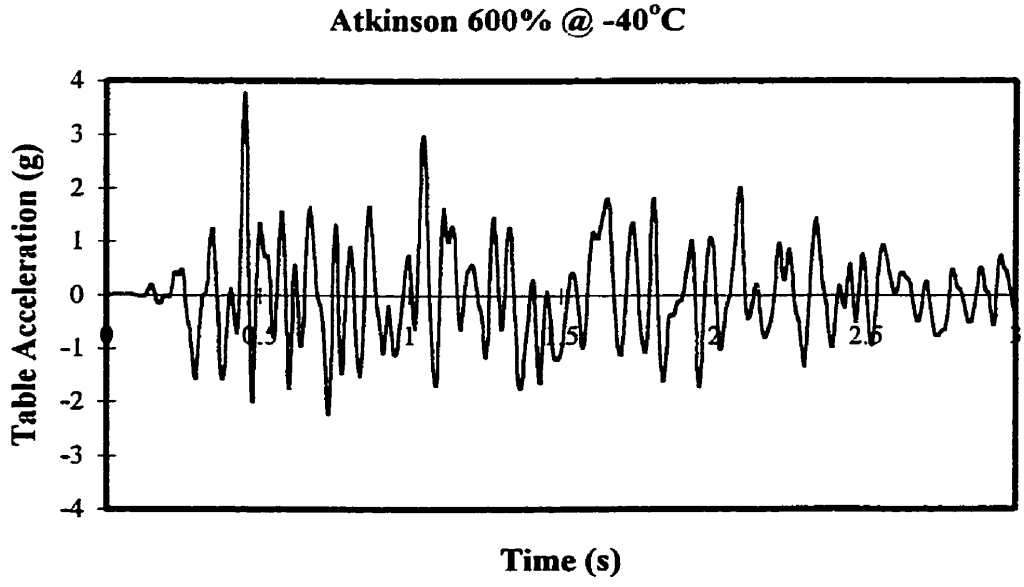

Figure D.92 Measured Table Acceleration for Atkinson 600% at -40°C

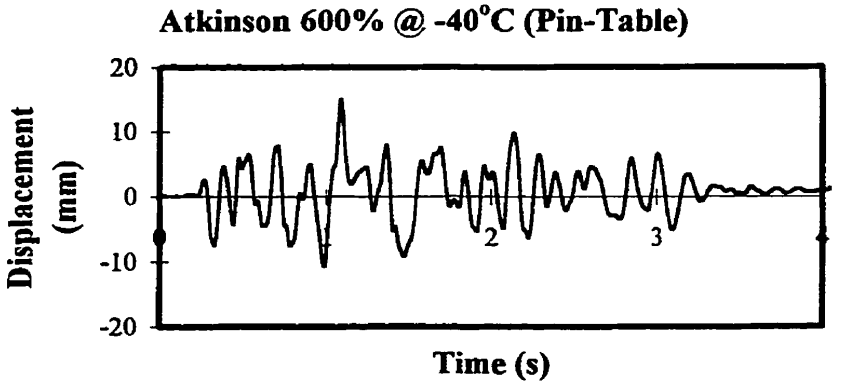

Figure D.93 Relative Displacement (Pin-Table) for Atkinson 600% at -40°C

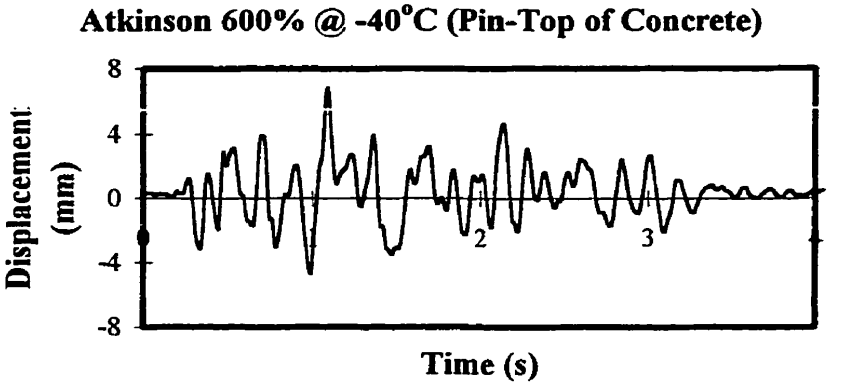

Figure D.94 Relative Displacement (Pin-Top Concrete) for Atkinson 600% at -40°C

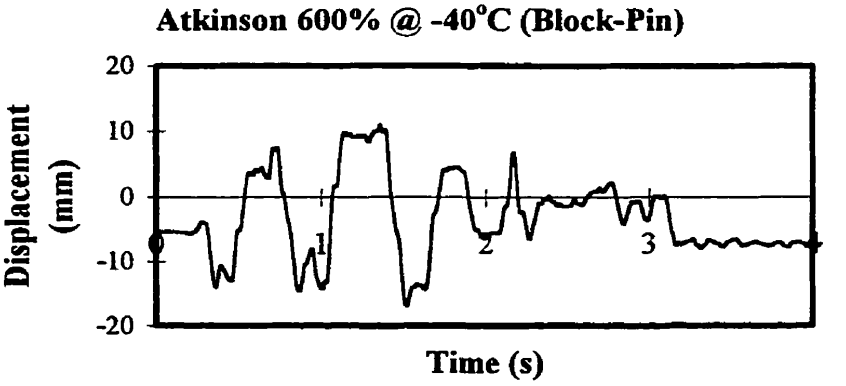

Figure D.95 Relative Displacement (Block-Pin) for Atkinson 600% at -40°C

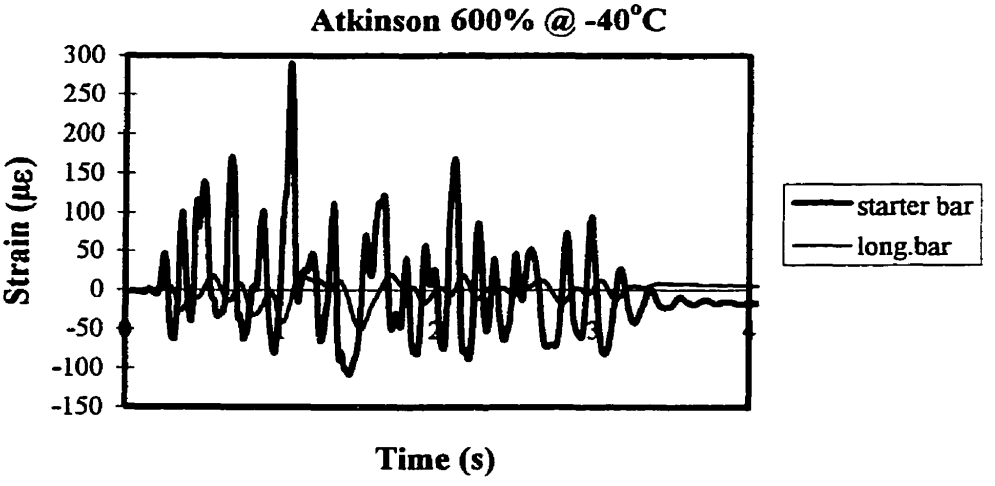

Figure D.96 Measured Strains from Starter and Longitudinal Bars (165 mm from the base) for Atkinson 600% @ -40°C